Entwicklungen und Untersuchungen zur Bildgebung der Schilddrüse: ^{124}Iod-PET/CT, 3D-Ultraschall und nuklearmedizinisch-sonographische Bildfusion

Habilitationsschrift
vorgelegt am 11.02.2014
dem Rat der Medizinischen Fakultät
der Friedrich-Schiller-Universität

von
Dr. med. Martin Freesmeyer
aus Jena

Gutachter

1. Prof. Dr. med. Dietmar Gottschild, Jena
2. Prof. Dr. med. Jörg Kotzerke, Dresden
3. Prof. Dr. med. Dr. rer. nat. Andreas Bockisch, Essen

Erteilung Lehrbefähigung am 09.09.2014

Abkürzungsverzeichnis

Abb.	Abbildung
bzw.	beziehungsweise
3D	dreidimensional
3D-US	dreidimensionaler Ultraschall
3D-sn-US	sensornavigierter dreidimensionaler Ultraschall
3D-ms-US	mechanisch geschwenkter dreidimensionaler Ultraschall
ca.	zirka
cm	Zentimeter
CT	Computertomographie
DGN	Deutsche Gesellschaft für Nuklearmedizin
DICOM	Digital Imaging and Communications in Medicine
DMSA	2,3-Dimercaptosuccinsäure
em *oder* EM	Ellipsoidmodell
et al.	et alii
EUSV	Enhandced Ultrasound Storage Volume
^{18}F	^{18}F-Fluorid
^{18}F-FDG	^{18}F-Fluor-Fluorodesoxyglucose
fhSPECT	freehand Single-photon emission computed tomography
^{68}Ga	^{68}Ga-Gallium
^{68}Ga-DOTATOC	^{68}Ga-Gallium-(DOTA(0)-Phe(1)-Tyr(3))octreotid
keV	Kiloelektronenvolt
kBq	Kilobequerel
ldCT	Niedrigdosis-Computertomographie
MBq	Megabequerel
MC	manually contoured
MHz	Megahertz
mAs	Milliamperesekunden
min	Minute
mm	Millimeter
MRT	Magnetresonanztomographie
mSv	Millisievert
mt	manually traced
PACS	Picture Archiving and Communication System
PET	Positronenemissionstomographie
S.	Seite
SD	Standardabweichung
SPECT	Single-photon emission computed tomography
Suppl.	Supplement
Tab.	Tabelle
^{99m}Tc	metastabiles ^{99m}Technetium
$^{99m}TcO_4$	metastabiles ^{99m} Technetium-Pertechnetat
TcTU	thyreoidaler Technetium-Uptake
TSH	Thyreotropin: Thyreoidea-stimulierendes Hormon
US	Ultraschall
VOI	Volume of interest
z.B.	zum Beispiel

Das ist es, was ich den anatomischen Gedanken in der Medizin nenne.

Ich behaupte, dass kein Arzt ordnungsgemäß

über einen krankhaften Vorgang zu denken vermag,

wenn er nicht imstande ist, ihm einen Ort im Körper anzuweisen.

Rudolf Virchow (1821 - 1902)

Inhaltsverzeichnis

1. Einleitung

1.1. Nuklearmedizinische Bildgebung und Hybridbildgebung

Das Wesen nuklearmedizinischer Bildgebung besteht in der Fähigkeit, auf molekularer Ebene metabolisch-funktionelle Prozesse darstellen zu können. Die Stoffwechselinformationen sollen zwar räumlich zugeordnet werden, jedoch ist die Abbildung eines exakten anatomischen Kontextes limitiert.

Zum Zwecke nuklearmedizinischer Untersuchungen werden schwach radioaktive Marker (Synonyma: Radiotracer oder Radiopharmaka) in den Körper eingebracht, deren Weg und/oder Verteilung berührungsfrei mit hochempfindlichen Bildgebungseinrichtungen auf der Grundlage von Szintillationsdetektoren gemessen und dargestellt werden können. Ziel ist es, physiologische und pathologische funktionelle Phänomene möglichst sensitiv und spezifisch zu diagnostizieren.

Die Einführung der Schnittbildverfahren (Tomographie) in die nuklearmedizinische Bildgebung eröffnete die Möglichkeit der überlagerungsfreien Darstellung krankhafter Prozesse. Bereits in den frühen 1960er Jahren stellte David E. Kuhl den ersten transversalen Emissionstomographen vor. In der Nuklearmedizin werden heute zwei emissionstomographische Verfahren unterschieden:

- Die Einzel(Single)-Photonen-Emissions-Tomographie (SPECT) ist eine Form der Schnittbildgebung, bei der zunächst Rohdaten (Projektionsbilder) während der Rotation der Detektorköpfe einer Gammakamera um den Patienten aufgezeichnet und danach SPECT-Bildstapel in frei wählbarer Orientierung rekonstruiert werden. Bei dieser tomographischen Technik werden die im Rahmen des Gammazerfalls (einzeln) entstehenden Photonen detektiert. Die erzielbare Ortsauflösung der erzeugten Tomogramme beträgt 1 bis 1,5 cm. Seit einigen Jahren steht ein System zur handgeführten SPECT zur Verfügung (declipseSPECT, SurgicEye GmbH, München, Deutschland). Diese als freehand SPECT bezeichnete Technik dient der intraoperativen Visualisierung von radioaktiv markierten Lymphknoten im Rahmen des Wächterlymphknoten-Konzeptes *(Wendler et al. 2007, Wendler et al. 2009)*.
- Die Positronen-Emissions-Tomographie (PET) hingegen wird mit Detektoren durchgeführt, die in einem geschlossenen Ringdesign räumlich fixiert angeordnet sind. Hierbei kommen Positronenemitter zum Einsatz. Bei der Vereinigung der sehr kurzlebigen Positronen mit Elektronen (Annihilation) entstehen zeitgleich zwei Gammaquanten, die in entgegengesetzter Richtung (180°) emittiert werden. Das (nahezu) gleichzeitige Eintreffen der beiden Photonen am Detektorring wird für die Ortung der Zerfallsereignisse genutzt (Koinzidenzschaltung). Die PET ist der SPECT

hinsichtlich der Detektions- und Abbildungsgüte deutlich überlegen. Dies betrifft beispielsweise die generelle Empfindlichkeit, die Quantifizierung und die bessere Ortsauflösung von ca. 4 mm.

Die anatomisch korrekte Zuordnung von Befunden ist jedoch bei beiden Methoden ungenügend. Dieses grundlegende Problem der emissionstomographischen Techniken hat folgerichtig zum Konzept der multimodalen Bildgebung (Hybridbildgebung) geführt, bei dem nuklearmedizinisch-funktionelle und radiologisch-morphologische Schnittbildtechnik in einem Gerät kombiniert werden.

Um die Jahrtausendwende wurde zunächst PET/CT, kurze Zeit später SPECT/CT in die klinische Praxis eingeführt *(Kinahan et al. 1998, Beyer et al. 2000)*. In den letzten Jahren sind erste PET/MR-Geräte installiert worden *(Schlemmer et al. 2008, Torwarth et al. 2011, Quick et al. 2013, Drzezga et al. 2013, Platzek et al. 2013).* Trotz der apparativen Vereinigung der Geräte in einem gemeinsamen Gehäuse erfolgen die Untersuchungen in der Regel (unmittelbar) sequentiell, bei allerdings identischer Lagerung des Patienten auf dem gleichen Untersuchungstisch. In den letzten Jahren ist eine PET-Detektor-Technologie verfügbar geworden, die erstmals die simultane Akquisition von PET- und MRT-Daten erlaubt *(Judenhöfer et al. 2008, Pichler et al. 2008)*.

Die Vorteile der hybriden Methoden liegen nicht nur in der besseren anatomischen Korrelation nuklearmedizinischer Befunde bzw. der konsekutiv höheren diagnostischen Genauigkeit. Bei der PET/CT-Diagnostik hat der Ersatz der zeitaufwendigen quellenbasierten Schwächungskorrektur herkömmlicher (Stand-alone-)PET-Geräte durch die CT-basierte Technik darüber hinaus zu einer erheblichen Verkürzung der Untersuchungsdauer geführt *(Kinahan et al. 1998)*. Die zeitliche Optimierung des klinischen Workflow sowie die Steigerung des Patientenkomforts sind weitere bedeutsame Aspekte.

Die erfolgreiche klinische Einführung der Hybridgeräte hat gezeigt, dass nuklearmedizinische und radiologische Verfahren in vielen Bereichen nicht kompetitiv, sondern komplementär zu betrachten sind und dass durch deren (nahezu) simultane Nutzung und die korrelierte Auswertung der Modalitäten große Vorteile entstehen.

Limitierend hinsichtlich der flächendeckenden Einführung hybrider Bildgebungssysteme in alle ambulanten und stationären Leistungsbereiche wirken die sehr hohen Beschaffungs- und Unterhaltungskosten sowie die begrenzten Erstattungsmöglichkeiten durch die Kostenträger insbesondere in Deutschland. Mithin ist die Entwicklung preisgünstigerer Technologien wünschenswert.

Die Einbeziehung der Sonographie in das Konzept der Hybridbildgebung war bisher nur sporadisch Gegenstand wissenschaftlicher und technischer Publikationen, wobei zur räumlichen Ortung (Positionsbestimmung) der Ultraschallbilder verschiedene

Trackingmethoden zum Einsatz kamen. Es wurden drei unterschiedliche Herangehensweisen berichtet:

A. Eine chilenisch-französische Arbeitsgruppe hat eine Vorgehensweise in drei sequentiellen Arbeitsschritten untersucht, bei dem in einem ersten und zweiten Schritt separat ^{99m}Tc-DMSA-SPECT-Daten der Nieren sowie optisch sensornavigierte 3D-Ultraschall-Daten (sogenannte 2.5D-Ultraschall) akquiriert werden, die mit Hilfe einer Workstation in einem dritten Schritt erfolgreich automatisch segmentiert, koregistriert, bewegungskorrigiert und fusioniert werden *(Galdames et al. 2011)*.

B. Ein weiteres Konzept, das unter Beteiligung dieser Arbeitsgruppe entwickelt wurde, nutzt in einem Procedere mit zwei Arbeitsschritten ebenfalls die optische Sensornavigation *(Bucki et al. 2007)*. Im Vorfeld ist hier die räumliche Kalibrierung des Ultraschallsystems mit dem Untersuchungstisch einer SPECT-Kamera notwendig, wobei Ultraschallkopf und SPECT-Untersuchungstisch jeweils mit optischen Markern ausgestattet sind. In einem ersten Arbeitsschritt erfolgt zunächst die SPECT-Untersuchung, nach der deren Abschluss Patient unverändert liegen bleiben muss. Die automatisch segmentierten ^{99m}Tc-DMSA-SPECT-Daten der Nieren werden in einem zweiten Arbeitsschritt in einer optisch navigierten Ultraschall-Untersuchung „live“ überlagert und als Fusionsbild dargestellt.

C. Auch ein drittes Konzept, das ebenfalls zwei Arbeitsschritte erfordert, basiert auf dem Tracking (Sensornavigation) handelsüblicher Ultraschallköpfe, wobei häufig die magnetische und nur selten die optische Navigationstechnik zum Einsatz kommt. Hierfür werden handelsübliche Ultraschallsonden mit Magnetfeldsensoren ausgerüstet und in einem lokal erzeugten elektromagnetischen Feld geortet. Durch die Bestimmung der exakten Position des Schallkopfes kann die räumliche Lage der sonographischen Bildebene in Echtzeit ermittelt werden. Vor einer Untersuchung werden in einem ersten Schritt bereits akquirierte Schnittbilddaten auf das Gerät transferiert und in einem zweiten anhand anatomischer Landmarken manuell koregistriert. Danach wird der zu überlagernde Schnittbilddatensatz automatisch je nach Schallkopfposition reorientiert und der jeweilige Bildausschnitt entweder neben dem korrespondierenden Ultraschallbild angezeigt oder passgenau dem Ultraschallbild überlagert. Diese Bildfusion erfolgt in Echtzeit während des Untersuchungsvorganges, wobei das Mischungsverhältnis und die „Fensterung“ der Bildinformationen im angezeigten Fusionsbild frei wählbar sind. Die magnetisch sensornavigierte Ultraschallfusionstechnik wurde seit dem Beginn des letzten Jahrzehntes von verschiedenen Firmen als kommerzielles Produkt etabliert (GE, Volume Navigation; Esaote, Virtual Navigator; Hitachi, Real-Time Virtual Sonography; Philips, PercuNav; Siemens, eSie Fusion). Ursprünglich wurde die Technologie entwickelt, um MRT- und

CT-Daten registrieren und während der Ultraschalluntersuchung im Sinne einer Bildfusion in Echtzeit überlagern zu können, wobei bei *allen* bisherigen Arbeiten die Schnittbildführung bei bioptisch-interventionellen Maßnahmen im Ultraschall im Fokus steht. Dieses Image-Guidance-Konzept wurde insbesondere bei Prostatabiopsien *(Kaplan et al. 2002, Singh et al. 2008, Xu et al. 2008, Miyagawa et al. 2010, Ukimura 2010, Hadaschik et al. 2011, Natarajan et al. 2011)* und Lebererkrankungen *(Minami et al. 2007, Crocetti et al. 2008, Jung et al. 2009, Hakime et al. 2010, Rennert et al. 2011, Clevert et al. 2012)* angewendet. Erst in neueren Arbeiten wurde die PET/CT in das Konzept der Schnittbildführung bei Ultraschall-Interventionen im Sinne einer PET/US-Fusionsbildgebung übertragen *(Ewertsen 2010, Ewertsen et al. 2011, Venkatesan et al. 2011, Di Mauro et al. 2013, Futamura et al. 2013)*. Zwischenzeitlich ist neben der manuellen die Option der automatischen Koregistrierung während des Untersuchungsvorganges möglich *(Wein et al. 2007, Wein et al. 2008)*.

Alle drei genannten technischen Umsetzungen einer sonographisch-nuklearmedizinischen Bildfusion wurden bisher nicht im Kontext der Schilddrüsenbildgebung untersucht.

Die dargestellten Prinzipien sind im aktuell verfügbaren Entwicklungsstand mit unterschiedlichen Nachteilen und Limitationen verbunden:

- Erstens ist das Vorgehen in mehreren Arbeitsschritten (zeitliche Trennung von nuklearmedizinischer Schnittbildakquisition und Koregistrierung/Bildfusion mit Ultraschall) mit einem bedeutenden logistischen Aufwand für Patient und Untersucher verbunden.
- Zweitens ist zwischen den Arbeitsschritten Schnittbilddatenakquisition und Ultraschalluntersuchung in der Regel die erneute Lagerung bzw. die Umlagerung des Patienten notwendig, sodass Fehlregistrierungen aufgrund unterschiedlicher Positionierung kaum zu vermeiden sind. Zwar ist die Durchführung der Bildfusion bei Herangehensweise B und C grundsätzlich auch auf der Untersuchungsliege des SPECT-Gerätes, also ohne erneute Lagerung des Patienten, möglich. Allerdings sind leichte unwillkürliche Patientenbewegungen auch bei diesem Procedere unvermeidlich. Dem kann vor allem im Kopf-Hals-Bereich durch geeignete Fixierungsmaßnahmen des Kopfes teilweise entgegengewirkt werden, wobei diese Fixierungen wiederum den freien Zugang zum Untersuchungsbereich erschweren.
- Drittens kommt es bei der Durchführung von Ultraschalluntersuchungen durch den Kontakt des Schallkopfes zu den Weichteilen regelhaft zu einer leichten Verformung des Gewebes. Konsekutiv kann es bei der Überlagerung mit den berührungs- und dadurch deformierungsfrei akquirierten nuklearmedizinischen Bildern zu Inkongruenzen der anatomischen Grenzen und zu Fehlregistrierungen kommen.

Die genannten Limitationen haben dazu beigetragen, dass die Methoden bisher kaum Eingang in die klinische Routine gefunden haben.

Die Gesamtheit der methodischen Probleme wäre nur durch ein neues Detektorkonzept zu überwinden, das die simultane Akquisition der sonographischen und nuklearmedizinischen Daten mit einem kompakten, beide Modalitäten kombinierenden, hybriden Detektor erlaubt (Hardwareintegration).

1.2. Dreidimensionale Ultraschalldiagnostik (3D-US)

Ultraschall-Bildgebung (US) ist ein Standard-Diagnoseverfahren, das durch den sehr guten Weichteilkontrast und die hohe Ortsauflösung einen großen Stellenwert insbesondere in der Diagnostik von Weichteilen und parenchymatösen Organe erlangt hat *(Sheth 2010)*. Dies gilt beispielsweise für die Schilddrüse und die Halsweichteile *(Hegedüs 2004)*.

Obwohl US faktisch eine tomographische Bildgebungstechnik ist *(Struve 1982)*, werden im Gegensatz zur PET, SPECT, MRT und CT die untersuchten Körperregionen nicht lückenlos dokumentiert bzw. nicht vollständig im digitalen Praxis- oder Krankenhaus-Archiv gespeichert. In der Routinediagnostik beschränkt man sich auf die Archivierung ausgewählter zweidimensionaler Bilder der untersuchten Organe sowie von (erkannten) pathologischen Befunden. Zudem werden die Bilder in der Regel nicht digital gespeichert, sondern als Hardcopy ausgedruckt und archiviert *(Sholosh et Borhani 2011)*. Diese historisch gewachsene klinische Praxis führt zu verschiedenen Nachteilen:

- Vom Untersucher nicht erkannte/übersehene Befunde werden nicht dokumentiert, was zur hohen Interobservervariabilität beiträgt und insbesondere bei weniger erfahrenen Untersuchern bedeutsam erscheint *(Andermann et al. 2007)*.
- Die bei allen anderen Schnittbildverfahren übliche, nachträgliche kritische Überprüfung von Untersuchung und Befund durch einen anderen, in der Regel erfahreneren Arzt (Oberarzt, Chefarzt) im Sinne einer Nachbefundung (Second Reading) ist nicht möglich, da die Bildinformationen der untersuchten Region nicht mehr vollständig für die retrospektive Analyse und Bewertung zur Verfügung steht.
- Nachträgliche Messungen von Abständen und Volumina sind kaum möglich.
- Die Bewertung/Befundung ist an die Präsenz des Patienten im jeweiligen Arbeitsbereich gebunden.
- Nur wenn Unplausibilitäten rechtzeitig nach der Untersuchung erkannt werden, kann diese wiederholt werden, was allerdings nur bei Verfügbarkeit des Patienten möglich ist und zu logistischen Problemen führen kann.

- Die Delegation an wenig erfahrene Ärzte (oder gar an medizinisches Assistenzpersonal) ist ohne direkte Supervision nicht möglich. Mithin wird unter Umständen die Arbeitskraft gut ausgebildeter Ärzte zu ungünstigen Zeiten des Arbeitsablaufes gebunden.

Zur Lösung der vorgenannten Probleme kann der dreidimensionale Ultraschall (3D-US) beitragen, der seit den 70er Jahren erforscht und Ende der 80er Jahre erstmals kommerziell verfügbar wurde *(Woo)*. Faktisch haben sich jedoch initiale Erwartungen einer schnellen und breiten klinischen Einführung nicht erfüllt. Die klinischen Routine-Applikationen erstrecken sich auf wenige, eng begrenzte Teilbereiche, insbesondere die Pränataldiagnostik. Als Ursache sind die vorhandenen technischen Unzulänglichkeiten, der derzeit noch hohe zeitliche Aufwand in der Anwendung, die Inkompatibilität mit bestehenden Systemen für die Auswertung und Archivierung von Schnittbilddaten sowie die allgemein geringe Vergütung von Ultraschallleistungen anzusehen.

Allerdings wurden in den vergangenen Jahren erhebliche technische Fortschritte auf dem Gebiet des 3D-US erzielt *(Prager et al. 2010)*. Zwei Verfahren werden besonders häufig angewandt:

- Mechanische 3D-Sonographie:
    - Mit Hilfe sogenannter Volumensonden wird die 3D-Aufnahme durch ein im Schallkopfgehäuse (automatisch) *mechanisch geschwenktes* herkömmliches Array realisiert. Während des Aufnahmevorgangs wird der Ultraschallkopf nicht bewegt, sondern manuell fixiert. Das Scanvolumen entspricht den äußeren (lateralen) Grenzen des herkömmlichen sonographischen Scanfeldes einerseits und dem beim Schwenk abgedeckten Raumwinkel andererseits. Diese Methode wurde bereits 1989 erstmals vorgestellt *(Woo)*. Es stehen lineare und konvexe Designs zur Verfügung.
    - Eine Sonderform der mechanischen 3D-Sonographie stellt die *lineare Verschiebung* (ca. 15 cm) eines langen 2D-Detektors (ca. 10 cm) innerhalb eines Gehäuses dar *(Duric et al. 2005, Duric et al 2007, Duric et al. 2013)*. Diese Methode wird seit einiger Zeit kommerziell für die 3D-Sonographie der Mamma angeboten.
- Sensornavigierte 3D-Sonographie: Dabei werden handelsübliche Ultraschallsonden mit Ortssensoren ausgerüstet und deren Position bzw. Bewegung registriert (Tracking/Sensornavigation). Während der Untersuchung wird die exakte Position des Schallkopfes fortwährend zusammen mit dem 2D-US-Bild gespeichert. Daraus

kann ein 3D-Datensatz berechnet werden. Als Ortssensoren kommen zumeist Magnetfeldsensoren oder seltener optische Sensoren zum Einsatz.

Tatsächlich ist die Einführung des 3D-US in die klinische Praxis hinter den ursprünglichen Erwartungen zurückgeblieben *(Prager et al. 2010)*. Beigetragen dazu hat, dass die dargestellten Techniken in dem aktuell verfügbaren Entwicklungsstand Limitationen ausweisen:

- Mechanische 3D-Sonographie:
    - begrenzt großes Scanvolumen, insbesondere bei höher frequenten Sonden mit linearem Design
- Sensornavigierte 3D-Sonographie:
    - Notwendiges Trackingsystem
        - Platzbedarf an der US-Sonde
        - Störungen des Ortungssystems durch Metall (Magnetfeldsensoren) oder Verdeckung (optische Sensoren)
        - schon durch leichte Druckänderungen während des Scans können die 3D-US-Daten verzerrt dargestellt werden
        - Zeitbedarf für Rekonstruktion der 3D-Daten
- Allgemein:
    - Selbst bei den kommerziell verfügbaren Technologien können 3D-US-Datensätze in der Regel nur auf dem Ultraschallgerät selbst bzw. auf einer dedizierten 3D-US-Workstation gespeichert und weiterverarbeitet werden (vgl. 1.1.).
    - Keine routinetaugliche Archivierung im Praxis- oder Klinikarchiv
    - Keine Weiterverarbeitung auf Standard-Workstations für Schnittbildgebung

Wünschenswert ist jedoch die Möglichkeit des Exportes der 3D-US-Daten in einem ubiquitär kompatiblen Datenformat. Ziel ist die Archivierung im digitalen Praxis- oder Klinik-Archiv (PACS) sowie die Nachbetrachtung und -verarbeitung mit üblicher Schnittbild-Software. Vor einigen Jahren ist der DICOM-Standard Enhanced Ultrasound Volume Storage (EUVS) vorgestellt worden *(National Electrical Manufacturers Association, 2008)*. Dieser erlaubt es grundsätzlich erstmals, DICOM-Datensätze zu generieren, die auf handelsüblichen, multimodalen Workstations mit 3D-Standardsoftware betrachtet und nachverarbeitet werden können. Bedauerlicherweise ist dessen Implementierung auf den Ultraschallgeräten selbst sowie auf Schnittbild-Workstations bislang sehr gering.

Bisher wurden einige Studien veröffentlicht, die das klinische Potential des 3D-US in der Organvolumetrie beleuchten *(Schlögl et al. 2001, Schögl et al. 2006, Lyshchik et al. 2004, van Isselt et al. 2003)* (vgl. 1.3.). Diese Daten konnten - wie oben beschrieben - allerdings nur auf den Ultraschallgeräten selbst bzw. mit Hilfe dedizierter, gerätegebundener und kostenintensiver Workstations ausgewertet werden (vgl. 1.1.), was eine Verbreitung der Technik limitiert und einer spätere Auswertung der Datensätze auf Standard-Schnittbild-Workstations unmöglich macht.

1.3. Bildgebende Diagnostik der Schilddrüse

Die Schilddrüse des Menschen zeigt häufig Abweichungen von der Norm hinsichtlich Form, Größe und Funktion. Etwa 35 % der Bevölkerung weisen eine Vergrößerung und/oder knotige Veränderungen der Schilddrüse auf. Schilddrüsenknoten sind gehäuft in Regionen mit Iod-Mangelversorgung anzutreffen *(Munoz und Bernal 1997, Koc et al. 2002)*. Die Inzidenz knotiger Schilddrüsenveränderungen steigt mit dem Lebensalter *(Aghini-Lombardi et al. 1999, Polyzos et al. 2008)*.

Die Vergrößerung der Schilddrüse (Struma) kann zu zervikalem Globusgefühl, Schluckstörungen und mithin zu erheblichem individuellem Leidensdruck führen. Aber auch wenn der Patient beschwerdefrei ist, kann sich schleichend eine klinisch relevante Trachealkompression entwickeln.

Die Symptome einer Überfunktion der Schilddrüse sind mannigfaltig und variieren in ihrer Ausprägung beträchtlich. Subjektiv werden zum Beispiel innere Unruhe, Nervosität, Schlafstörungen und Hyperhidrosis wahrgenommen. Darüber hinaus bestehen auch unabhängig von der subjektiv wahrgenommenen Symptomatik erhöhte kardiovaskuläre Risiken, wie Herzrhythmusstörungen, Myokardinfarkt und plötzlicher Herztod *(Tuschy 2004)*. Zudem wird der Abbau von mineralisiertem Knochen begünstigt.

Auf Grund der vorgenannten morphologischen und funktionellen Veränderungen entsteht hoher Diagnostik- und Therapiebedarf der Schilddrüse.

Die morphologische Bildgebung der ersten Wahl in der Diagnostik von Schilddrüsenerkrankungen ist der zweidimensionale Ultraschall *(Lucas 2000, Ying et al. 2008)*. Die Sonographie ist einfach durchzuführen, gut verfügbar, kostengünstig und verursacht keine Strahlenexposition *(Reinartz et al. 2002)*.

Faktisch handelt es sich aufgrund der schichtweisen Abtastung und Darstellung um ein Schnittbildverfahren (Tomographie), wobei Bilderzeugung und Präsentation in Echtzeit ablaufen. Die hohe Ortsauflösung und der Weichteilkontrast ermöglichen eine subtile Beurteilung des Drüsenparenchyms und der Nachbarstrukturen (Lymphknoten, Gefäße).

Gashaltige und verkalkte Strukturen (z.B. Larynx, Trachea, Wirbelsäule) sind allerdings nur randständig zugänglich. Neben dieser morphologisch-orientierten B-Mode-Sonographie steht die farbkodierte Dopplersonographie (FKDS) zur Beurteilung der Durchblutungsverhältnisse zur Verfügung. Neuerdings ist auch die Elastographie Gegenstand wissenschaftlicher Untersuchungen, mit der die visko-elastischen Eigenschaften von Parenchym und Knoten evaluiert werden können *(Cantisani et al. 2013)*.

Seit Einführung der Ultraschalldiagnostik werden häufig klinisch asymptomatische Knoten diagnostiziert *(Hegedüs 2004)*. Dies geschieht einerseits bei der expliziten Schilddrüsensonographie und andererseits als Zufallsbefund zum Beispiel bei einer Untersuchung der Halsgefäße. Auf diese Tatsache scheint die ansteigende Inzidenz kleiner papillärer Schilddrüsenkarzinome bei gleichbleibender Mortalität zurückzuführen zu sein *(Brito et al. 2013)*.

Andere morphologisch orientierte Bildgebungsverfahren spielen in der Schilddrüsendarstellung eine untergeordnete Rolle. Die CT erlaubt die Beurteilung der Größe eines retrosternalen oder intrathorakalen Anteils sowie die Beurteilung von Nachbarstrukturen wie Trachea und Ösophagus *(Weber et al. 2000, Anders et al. 1998)*. Die MRT kommt vor allem bei lokal fortgeschrittenen Schilddrüsenkarzinomrezidiven bzw. bei metastasierten Stadien des Schilddrüsenkarzinoms zum Einsatz *(Hoang et al. 2013),* ist allerdings wegen der Schluckbewegungen und der von den benachbarten Arterien ausgehenden Pulsationen artefaktanfällig.

Die exakte Bestimmung des Organvolumens ist von großer klinischer Bedeutung, da sich die Entscheidung, ob und welche Therapie angewandt wird, zu einem relevanten Teil auf die Größe des Organs gründet. Darüber hinaus kommt der Änderung des Organvolumens im Rahmen der Verlaufskontrolle und somit in der Beurteilung des Therapieerfolges eine entscheidende Bedeutung zu *(van Isselt et al. 2003, Reinartz et al. 2002)*.

Die Standardmethode zur Bestimmung des Schilddrüsenvolumens ist der Ultraschall. Bei der herkömmlichen 2D-Sonographie erfolgt die seitengetrennte Vermessung der beiden Schilddrüsenlappen. Das vereinfachte mathematische Modell zur Berechnung basiert auf der Annahme, dass jeder Seitenlappen einem Rotationsellipsoid entspricht *(Brunn et al. 1981)*. Bei diesem Ellipsoidmodell (em) werden die beiden Lappenvolumina jeweils mit der Formel [$Länge_{max}$ x $Breite_{max}$ x $Tiefe_{max}$ x f] berechnet und zum Gesamtvolumen addiert. Für f werden als Korrekturfaktor unterschiedliche Werte vorgeschlagen *(Reinartz et al. 2002, Ying et al. 2008, Knudsen et al. 1999, Brunn et al. 1981)*, wobei in der Praxis meist der Faktor 0,5 verwendet wird. Bei der Anwendung des Ellipsoidmodells (em) in der Volumetrie kommt es jedoch zu einer relativ hohen Intra- und Interobservervariabilität *(Ozgen et al. 1999, Rago et al. 2006)*. Insbesondere bei knotigen Strumen kann es zu irregulären Abweichungen der Gestalt der

Schilddrüse, konkret zur Deformierung der Seitenlappen und/oder zur Verdickung des Isthmus kommen, sodass bei der Volumetrie mittels 2D-Sonographie große Ungenauigkeiten auftreten können *(Rago et al. 2006)*.

Verschiedene Autoren haben 3D-US-Verfahren für die Volumetrie evaluiert *(Tong et al. 1998)*. Wie bereits in Kapitel 1.2. geschildert, wird die Auswertung dabei in der Regel auf dem Ultraschallgerät selbst bzw. einer dedizierten, mit dem Ultraschallgerät verbundenen Workstation durchgeführt (Andermann et al. 2007, Kot et al. 2009). Da der Datenexport in einem ubiquitär kompatiblen DICOM-Format bisher nicht möglich war, konnte keine Auswertung mittels Standard-Schnittbildsoftware erfolgen.

Der Vorteile der 3D-US-basierten Organ-Volumetrie im Vergleich zur 2D-Technik besteht in einer höheren Genauigkeit *(Schlögl et al. 2001).* Andererseits sind die Intra- sowie Interobservervariabilität wesentlich geringer *(Lyshchik et al. 2004, Ng et al. 2004)*.

Als Alternative zur Volumenberechnung mittels Ellipsoidformel besteht für dreidimensionale Schnittbild-Datensätze die Möglichkeit, das Organvolumen in parallelen Schnitten von den umliegenden Geweben manuell abzugrenzen (manually traced borders = mt; manual contouring = MC). Diese Methode ist wesentlich weniger untersucherabhängig und wurde in einigen Arbeiten als Goldstandard genutzt *(van Isselt et al. 2003, Reinartz et al. 2002)*. Allerdings ist das Verfahren mit einem deutlich höheren Zeitaufwand verbunden.

In fast allen Studien über 3D-US-Volumetrie wurde der sensornavigierte 3D-US genutzt (vgl. 1.2.). Nur in einer Arbeit erfolgte zusätzlich der Vergleich zum mechanisch geschwenkten 3D-US *(Kot et al. 2009)*.

Hinsichtlich der funktionellen Bildgebung ist die ^{99m}Tc-Pertechnetat-Szintigraphie ($^{99m}TcO_4$) als Standardmethode auf dem Gebiet der Nuklearmedizin etabliert und ermöglicht eine rationelle Funktionstopographie sowie quantitative Analysen bei geringer Strahlenexposition. $^{99m}TcO_4$ ist als Generator-Radionuklid flächendeckend verfügbar *(Luster et al. 2010)*. Für den normalgewichtigen Erwachsenen wird die intravenöse Applikation von 37 bis 74 MBq $^{99m}TcO_4$ empfohlen *(Dietlein et al. 2007A)*. Die Strahlenexposition der Schilddrüse beträgt pro Untersuchung etwa 0,9 mSv (bei 70 MBq), wobei die Knochenmark- und Gonadendosis unter 0,1 mSv liegt *(Schicha und Schober 2013)*.

$^{99m}TcO_4$ weist eine ähnliche Molekülgröße wie Iodid auf und wird über den Natriumjodidsymporter *(Spitzweg et Morris 2002)* aktiv aus der Blutbahn in die Thyreozyten aufgenommen *(Wolff 1998)*. Im Gegensatz zum Iod wird es nicht in die Tyrosinreste des Thyreoglobulins eingebaut.

20 bis 30 Minuten nach der intravenösen Verabreichung des Tracers wird an einer speziellen Schilddrüsenkamera ein planares Szintigramm aufgezeichnet. Darüber hinaus erfolgt die

Quantifizierung der Aktivitätsaufnahme der Schilddrüse, die in Prozent als thyreoidaler Technetium-Uptake (TcTU) angegeben wird *(Franken et al. 2010, Dietlein et al. 2007A)*.

Der TcTU beträgt im Normalkollektiv 0,5 bis 2 % *(Mahlstedt et al. 1989, Schicha et Schober 2013)*. Iodmangel, thyreostatische Therapie mit schwefelhaltigen Verbindungen sowie die Autoimmunerkrankung Morbus Basedow gehen mit einem erhöhten TcTU einher *(Atkins 1971)*. Ein erniedrigter Uptake kann auf eine Hypothyreose, eine stattgehabte Iodexposition bzw. auf eine Medikation mit Perchlorat oder Levothyroxin hindeuten. Auch die Autoimmunthyreopathie Typ Hashimoto ist in der Regel durch einen geringen thyreoidalen Uptake gekennzeichnet *(Atkins 1971)*.

Auch bei der Schilddrüsenszintigraphie bestehen die typischen Limitationen nuklearmedizinischer Verfahren, insbesondere im Hinblick auf die begrenzte Ortsauflösung von ca. 1 cm sowie die fehlende direkte morphologische Korrelation der Befunde. Daneben besteht eine Abhängigkeit der ermittelten quantitativen Parameter vom Abstand des Patienten zum Kameradetektor.

Die Szintigraphie stellt eine Projektions- bzw. Summationsdarstellung der Schilddrüse in frontaler Ansicht dar. Die Abbildung als Schnittbilddatensatz (SPECT) ist vor allem wissenschaftlichen Fragestellungen vorbehalten und erfolgt nur selten in der klinischen Routine. Anhaltspunkte für die räumliche Zuordnung geben lediglich eine vom medizinischen Assistenzpersonal vorgenommene, als Kreuz auf dem Szintigramm abgebildete Markierung des Jugulums sowie die in der Regel schwach erkennbaren Unterkieferspeicheldrüsen (Gll. submandibulares).

Ein weiteres Problem besteht in der limitierten Darstellung retrosternaler und intrathorakaler Anteile der Schilddrüse infolge der Strahlenabsorption durch das Sternum *(Dietlein et al. 2007A)*.

Eine Folge der begrenzten Ortsauflösung ist, dass sich Knoten, die einen Durchmesser kleiner als 1 cm aufweisen, dem szintigraphischen Nachweis entziehen können. Darüber hinaus bilden sich anatomische Besonderheiten der Schilddrüse, wie beispielsweise der im Ultraschall erschwert darstellbare Lobus pyramidalis, im Szintigramm häufig nicht ab.

Die korrelative Bewertung von Ultraschall und Szintigraphie erfolgt derzeit durch den side-by-side Vergleich beider Verfahren, wobei der räumlichen Vorstellungskraft und der Erfahrung des Untersuchers große Bedeutung zukommt. Hierbei wird das szintigraphische, frontal orientierte Projektions- bzw. Summationsbild mit den sonographischen, transversal oder sagittal ausgerichteten Schnittbildern korreliert. Ein kommerziell verfügbares, hybrides Bildgebungsverfahren, das in Analogie zur PET/CT, SPECT/CT und PET/MRT die eindeutige räumliche Verknüpfung und Überlagerung der nuklearmedizinisch-funktionellen

mit der morphologisch-sonographischen Information erlaubt, steht bisher nicht zur Verfügung.

Das Radioisotop ^{124}Iod ist ein Zyklotronprodukt und kann in hoher radiochemischer und radionukleärer Reinheit hergestellt werden *(Knust et al. 2000)*. Der Anteil der Positronenzerfälle an der emittierten Gesamtstrahlung wird mit 22,8 % angeben. Im Gegensatz zu vielen anderen in der PET verwendeten Radioisotopen ermöglicht die relativ lange Halbwertszeit von 4,2 Tagen den Transport über große Distanzen.

Der Einsatz der PET ermöglicht eine exakte Quantifizierung der Aufnahme eines PET-Tracers mit einer hohen räumlichen Auflösung. In der Kombination mit der Computertomographie als PET/CT wird eine exakte intrinsische Koregistrierung von funktionellen und anatomischen Zusammenhängen ermöglicht *(Beyer et al. 2000)*.

Bei Untersuchungen mit ^{124}Iod an verschiedenen PET-Systemen hat sich gezeigt, dass die höhere Positronenenergie (max. 2138 keV/mittlere 819 keV) und der damit größere „positron range effect“ im Vergleich zum häufig angewandten Nuklid ^{18}F (Halbwertszeit: 110 min, Positronenanteil 96,7 %, maximale Energie: 634 keV, mittlere Energie 243 keV) zu einer um ca. 1mm geringeren räumlichen Auflösung führt *(Herzog et al. 2002, Jentzen et al. 2008B, Pentlow et al. 1991, Robinson et al. 2004)*. Klinisch wird diesem Phänomen jedoch keine große Bedeutung beigemessen *(Jentzen et al. 2008B)*.

Die vorhandenen Publikationen zur klinischen Anwendung von ^{124}Iod widmen sich nahezu ausschließlich der Bildgebung des differenzierten Schilddrüsenkarzinoms mit der PET oder der PET/CT *(Sgouros et al. 2004, Lubberink et al. 2008, Kolbert et al. 2007, Jentzen et al. 2008A, Jentzen et al. 2010, Hobbs et al. 2009, Herzog et al. 2002, Jentzen et al. 2008B, Freudenberg et al. 2004A, Freudenberg et al. 2007A, Freudenberg et al. 2007B, Freudenberg et al. 2010B, Freudenberg et al. 2010A)*. Die Anwendung dieses Isotops erlaubt eine exaktere Bestimmung der prätherapeutischen Dosimetrie im Vergleich zum herkömmlich angewandten Radionuklid ^{131}Iod und kann daher zur individualisierten Planung der ablativen Radiojodtherapie eingesetzt werden.

Bisher wurde nur eine Studie publiziert, die sich (in Anteilen) mit der Anwendung von ^{124}Iod-PET/CT bei gutartigen Schilddrüsenerkrankungen beschäftigt *(Eschmann et al. 2002)*. Hierbei konnte das Konzept einer PET-basierten intratherapeutischen Dosimetrie bei simultaner Verabreichung von ^{124}Iod (30 bis 40 MBq) und ^{131}Iod (526 bis 1237 MBq) im Rahmen der Radiojodtherapie demonstriert werden.

In der Zusammenschau aller vorgenannten Fakten und Argumente lässt sich für die etablierte Schilddrüsendiagnostik feststellen, dass trotz des hohen klinischen Standards folgende Limitationen bestehen:

- geringe Ortsauflösung (Szintigraphie)

- Darstellbarkeit von retrosternalem und intrathorakalem Schilddrüsengewebe nur partiell möglich (Sonographie und Szintigraphie)
- Korrelation zwischen Anatomie und Funktion unzureichend
    - innerhalb der Schilddrüse: mangelnde räumliche Verknüpfung funktioneller und morphologischer Befunde (Szintigraphie vs. Sonographie)
    - zwischen Schilddrüse und Nachbarorganen (Szintigraphie)
    - keine Präsentation als überlagertes Fusionsbild
- Darstellung und Beurteilung kalk- oder gashaltiger Nachbarstrukturen der Schilddrüse insuffizient (Sonographie und Szintigraphie)
- Volumetrie (Sonographie):
    - Ungenauigkeit des etablierten Ellipsoidmodells bei Abweichungen der Form der Schilddrüsenlappen von der Norm
    - erhebliche Inter- und Intraobservervariabilität
- Lückenhafte Dokumentation und mangelnde Archivierbarkeit des Untersuchungsvolumens
    - Nachbefundung (Second Reading) unmöglich
    - nachträgliche Messungen unmöglich

Den genannten begrenzenden Faktoren kommt angesichts der Häufigkeit und der therapeutischen Relevanz von Schilddrüsenerkrankungen große klinische Bedeutung zu.

2. Aufgaben- und Zielstellungen der Arbeit

Die Ziele der vorliegenden Arbeit bestehen in der Entwicklung neuer Methoden der Schilddrüsendiagnostik und deren initialer klinischer Bewertung. Dabei werden drei Hauptthemenfelder bearbeitet, die sich inhaltlich teilweise überschneiden, jedoch zur besseren Übersicht in getrennten Kapiteln dargestellt werden:

- ^{124}Iod-Niedrigaktivitäts-PET/Niedrigdosis-CT (^{124}Iod-PET/CT)
- Dreidimensionale Sonographie (3D-US)
- Nuklearmedizinisch-sonographische Fusionsbildgebung

^{124}Iod-Niedrigaktivitäts-PET/Niedrigdosis-CT (^{124}Iod-PET/CT)

Das klinische Potential der ^{124}Iod-PET/CT-Diagnostik soll unter Verwendung von 1 MBq ^{124}Iod überprüft werden.

- Klinische Untersuchung zur Funktionstopographie mit ^{124}Iod-PET/CT im Vergleich zu planarer $^{99m}TcO_4$-Szintigraphie und $^{99m}TcO_4$-SPECT *(adressiert in Publikation 3.1.1., S. 17)*.
  - Werden alle szintigraphisch diagnostizierten Befunde in der ^{124}Iod-PET gesehen?
  - Werden über die planare Szintigraphie hinaus mittels SPECT und ^{124}Iod-PET zusätzliche Befunde erhoben?
  - Lassen sich durch ^{124}Iod-PET/CT anatomische Details (Lobus pyramidalis) und pathologische Besonderheiten (retrosternaler Anteil) besser erfassen?
  - Kommt es bei multifokalen Schilddrüsenautonomien durch die in der ^{124}Iod-PET zusätzlich ermittelten Befunde zur Änderung des therapeutischen Volumens?
- Klinische Untersuchung zur prätherapeutischen Dosimetrie: Vergleich des Uptakes beim herkömmlichen Radiojodtest (3 MBq ^{131}Iod) mit der Niedrigaktivitäts-PET/CT (1 MBq ^{124}Iod) 30 Stunden nach Applikation *(adressiert in Manuskript 3.1.2., S. 26)*.
  - Ist eine prätherapeutische Uptake-Messung mit 1 MBq ^{124}Iod-PET möglich?
  - Wie hoch ist die Übereinstimmung zwischen den ^{124}Iod-PET-Uptake-Werten und den ^{131}Iod-Messungen an einem Szintillationssonden-Messplatz?
  - Wie groß ist die Abhängigkeit der ermittelten ^{124}Iod-Uptake-Werte vom untersuchten Volumen? Wie hoch ist der Anteil extrathyreoidaler Aktivität? Vergleich von Messungen (a) des gesamten Halses, (b) eines schwellwertbasierten Isokontur-Volumens und (c) eines an den anatomischen Organgrenzen auf der Grundlage der CT konturierten Volumens

- Entwicklung eines einfachen und zeiteffizienten, auf möglichst viele Patienten anwendbaren mathematischen Modells zur Schilddrüsenvolumetrie auf der Grundlage schwellwertbasierter Isokontur-Volumina in ^{124}Iod-Niedrigaktivitäts-PET-Datensätzen *(adressiert in Manuskript 3.1.3., S. 40)*.
    - Ist mit isokonturbasierten Volumetrieverfahren in der PET das Schilddrüsenvolumen einfach und zeiteffizient mit einer Abweichung < 10 % gegenüber einer zeitaufwendigen manuellen Konturierung im ldCT bestimmbar?
    - Lässt sich bei einem sehr niedrigen Isokontur-Schwellenwert ein mathematisches Modell entwickeln, mit dessen Hilfe (a) eine Anwendbarkeit auf > 90 % der Patienten sowie (b) eine Abweichung der Volumetrieergebnisse < 10 % gegenüber der Referenz möglich ist?

Dreidimensionale Sonographie (3D-US)

Die Anwendbarkeit und das klinische Potential des 3D-US bei Schilddrüsenerkrankungen sollen untersucht werden:

- DICOM-Export und -Archivierung von 3D-US-Daten der Schilddrüse *(adressiert in Publikation 3.2.1., S. 52)*
    - Wie häufig lässt sich im Patientenkollektiv, das zur Planung einer Radiojodtherapie vorgestellt wird, die Schilddrüse mit einem kommerziell verfügbaren konvexen 3D-US-Schallkopf komplett erfassen?
    - Welche digitalen Modifikationen exportierter 3D-US-Datensätze sind für die weitere Verarbeitung und die Archivierung in einem Klinik-PACS notwendig?
- Multimodale Phantomuntersuchung zur Volumetrie der Schilddrüse unter Einbeziehung von CT, MRT, 2D-US sowie sensornavigiertem und mechanisch geschwenktem 3D-US *(adressiert in Manuskript 3.2.2.1., S. 60)* .
    - Welchen Einfluss hat die Form der Schilddrüse auf das bestimmte Volumen?
    - Wie unterscheiden sich dabei die Ergebnisse der nach dem Ellipsoidmodell bestimmten Volumina von denen der manuell konturierten Methode?
    - Sind die Ergebnisse der beiden 3D-US-Volumetrieverfahren vergleichbar mit denen der anderen Schnittbildverfahren?
- Klinische Untersuchung zur Volumetrie der Schilddrüse: Vergleich Niedrigdosis-CT und mechanisch geschwenkter 3D-US *(adressiert in Publikation 3.2.2.2., S. 75)*.
    - Wie hoch ist die Übereinstimmung der Volumetrie-Ergebnisse von 3D-US und Niedrigdosis-CT bei Auswertung nach dem Ellipsoid-Model, respektive mit der manuell konturierten Methode?
    - Stellt 3D-US eine potentielle Alternative zur Niedrigdosis-CT dar?

Nuklearmedizinisch-sonographische Fusionsbildgebung

Vorgestellt wird die Entwicklung und Erprobung verschiedener Methoden der nuklearmedizinisch-sonographischen Fusionsbildgebung.

- Softwarebasierte (offline) nuklearmedizinisch-sonographische Fusionsbildgebung (adressiert in Posterpräsentation 3.3.1., S. 82)
  - Ist die softwarebasierte Bildfusion grundsätzlich durchführbar?
  - Worin bestehen technische und klinische Limitationen?
- Sensornavigierte nuklearmedizinisch-sonographische Fusionsbildgebung (adressiert in den 7 Publikationen und Manuskripten der Kapitel 3.3.2.1. und 3.3.2.2, S. 84 und 101)
  - Ist die sensornavigierte nuklearmedizinisch-sonographische Fusionsbildgebung durchführbar und anwendbar?
  - Welche ersten klinischen Erfahrungen können in der onkologischen Bildgebung, bei Fremdkörpern/Implantaten und in der Schilddrüsenbildgebung gesammelt werden?
  - Wo liegen potentielle Anwendungsgebiete der Methode, welche weiterführenden klinischen Studien sind sinnvoll?
  - Worin bestehen technische und klinische Limitationen? Welche Weiterentwicklungen sind notwendig?
- Integriert-sequentielles Prinzip der nuklearmedizinisch-sonographischen Fusionsbildgebung: Kombination von freehand SPECT und sensornavigierter Sonographie (adressiert in Publikation 3.3.3.1., S. 110)
  - Ist das neu entwickelte, integriert-sequentielle Prinzip klinisch anwendbar?
  - Welche technischen und klinischen Limitationen sind vorhanden, welche Weiterentwicklungen sind notwendig?
- Integriert-simultanes Prinzip der nuklearmedizinisch-sonographischen Fusionsbildgebung: Kombination von real-time handheld Emission Spot Allocator (rthESA) und 2D-Sonographie (adressiert in Manuskript 3.3.3.2., S. 117)
  - Ist das neu entwickelte Prinzip am Phantom erfolgreich anwendbar?
  - Welche technischen Limitationen sind vorhanden?

3. Publikationen und Manuskripte zur kumulativen Habilitation

3.1. ^{124}Iod-Niedrigaktivitäts-PET/Niedrigdosis-CT (^{124}Iod-PET/CT) der Schilddrüse

3.1.1. Funktionstopographie der Schilddrüse mit ^{124}Iod-PET/CT

Low-Activity ^{124}I-PET/Low-Dose CT Versus ^{99m}Tc-Pertechnetate Planar Scintigraphy or ^{99m}Tc-Pertechnetate Single-Photon Emission Computed Tomography of the Thyroid: A Pilot Comparison

Publikation 2013 in CLINICAL NUCLEAR MEDICINE

Low-Activity ^{124}I-PET/Low-Dose CT Versus ^{99m}Tc-Pertechnetate Planar Scintigraphy or ^{99m}Tc-Pertechnetate Single-Photon Emission Computed Tomography of the Thyroid

A Pilot Comparison

Andreas M. Darr, MD, Thomas Opfermann, PhD,* Tobias Niksch, PhD,* Dominik Driesch, PhD,† Robert J. Marlowe, BA,‡ and Martin Freesmeyer, MD**

Purpose of the Report: The standard thyroid functional imaging method, ^{99m}Tc-pertechnetate (^{99m}Tc-PT) planar scintigraphy, has technical drawbacks decreasing its sensitivity in detecting nodules or anatomical pathology. ^{124}I-PET, lacking these disadvantages and allowing simultaneous CT, may have greater sensitivity for these purposes. We performed a blinded pilot comparison of ^{124}I-PET(/CT) versus ^{99m}Tc-PT planar scintigraphy or its cross-sectional enhancement, ^{99m}Tc-PT single-photon emission CT (SPECT), in characterizing the thyroid gland with benign disease.

Patients and Methods: Twenty-one consecutive adults with goiter underwent low-activity (1 MBq/0.027 mCi) ^{124}I-PET/low-dose (30 mAs) CT, ^{99m}Tc-PT planar scintigraphy, and ^{99m}Tc-PT-SPECT. Endpoints included the numbers of "hot spots" with/without central photopenia and "cold spots" detected, the proportion of these lesions with morphological correlates, the mean volume and diameter of visualized nodules, and the number of cases of lobus pyramidalis or retrosternal thyroid tissue identified.

Results: ^{124}I-PET detected significantly more "hot spots" with/without central photopenia ($P < 0.001$), significantly more nodules ($P < 0.001$), and more "cold spots" than did ^{99m}Tc-PT planar scintigraphy or ^{99m}Tc-PT-SPECT, including all lesions seen on the ^{99m}Tc-PT modalities. Ultrasonographic correlates were found for all nodules visualized on all 3 modalities and 92.5% of nodules seen only on ^{124}I-PET. Nodules discernible only on ^{124}I-PET had significantly smaller mean volume or diameter ($P < 0.001$) than did those visualized on ^{99m}Tc-PT planar scintigraphy or ^{99m}Tc-PT-SPECT. ^{124}I-PET(/CT) identified significantly more patients with a lobus pyramidalis ($P < 0.001$) or retrosternal thyroid tissue ($P < 0.05$).

Conclusions: ^{124}I-PET(/CT) may provide superior imaging of benign thyroid disease compared to planar or cross-sectional ^{99m}Tc-PT scintigraphy.

Key Words: ^{124}I-PET/CT, ^{99m}Tc-pertechnetate planar scintigraphy, ^{99m}Tc-pertechnetate single-photon emission computed tomography, thyroid gland, benign thyroid diseases, goiter

(*Clin Nucl Med* 2013;38: 770–777)

Since the 1970s, planar scintigraphy with ^{99m}Tc-pertechnetate has been the standard imaging method to assess thyroid functional topography.[1,2]

However, this modality has several deficiencies regarding sensitivity and informativeness. Low specific ^{99m}Tc-pertechnetate thyroid uptake limits spatial resolution to ~10 mm,[3] although scan quality can be somewhat improved by ^{99m}Tc-pertechnetate single-photon emission computed tomography (SPECT),[3,4] which allows examination of 3-dimensional (3D) cross-sections without superposition. Additionally, the low gamma radiation energy of ^{99m}Tc-pertechnetate causes high absorption in the sternum and thus insufficient imaging of retrosternal and intrathoracic thyroid tissue and inadequate quantification of tracer uptake in such structures.[1–2,4,6] Furthermore, ^{99m}Tc-pertechnetate planar scintigraphy carries a relatively high risk of measurement errors caused by fluctuations in the patient's distance from the gamma camera. Moreover, to date, planar scintigraphic imaging cannot be carried out simultaneously with morphological imaging and thus does not allow direct (and therefore easy and accurate) functional-morphological comparison. With ^{99m}Tc-pertechnetate planar scintigraphy, side-by-side comparison with a separately obtained sonogram or CT scan is necessary,[1] although where a requisite scanner is available, hybrid imaging is of course possible with ^{99m}Tc-pertechnetate-SPECT.

At least theoretically, PET with ^{124}I (^{124}I-PET) may avoid some limitations of ^{99m}Tc-pertechnetate scintigraphy in thyroid imaging.[3] PET scanners have high spatial resolutions (≥4 mm) and allow more precise tracer uptake quantification. Additionally, they can simultaneously perform CT, enabling exact functional-anatomic coregistration.[7] The high photon energy of the PET tracer and the transmission correction by the low-dose CT compensate for the effects of self-attenuation.[7] Another CT benefit is reliable retrosternal thyroid tissue detection.[8]

However, to our knowledge, published ^{124}I-PET(/CT) studies to date have focused almost exclusively on pretherapeutic dosimetry to plan radioiodine treatment of metastases or ablation of thyroid residues in (near) totally thyroidectomized differential thyroid carcinoma patients.[9–22] Only 1 work has dealt with ^{124}I-PET in nonmalignant thyroid disease, and that only in a small subgroup (n = 12).[17] The investigation compared the uptake of 30-40 MBq (0.81-1.08 mCi) of ^{124}I versus that of 526-1237 MBq (14.21-33.43 mCi) of therapeutic ^{131}I administered at the same time; ^{124}I-PET scan quality was not analyzed or compared with that of standard imaging methods.

More accurate functional imaging of benign thyroid disease and morphological imaging of the thyroid could enable selection of more appropriate therapeutic radioiodine activities and lead to more selective and accurate application of surgery. The present pilot investigation was therefore performed to compare ^{124}I-PET, ^{99m}Tc-pertechnetate planar scintigraphy, and ^{99m}Tc-pertechnetate-SPECT in functional imaging of the intact thyroid in patients with benign thyroid disorders. We also compared the ability of ^{124}I-PET/CT and the ^{99m}Tc-pertechnetate modalities to detect anatomical and pathological details of the thyroid.

PATIENTS AND METHODS

Patients

The study included 21 consecutive adults with benign thyroid disorders referred to our clinic for radioiodine therapy. The

Received for publication December 4, 2012; and revision accepted June 25, 2013.

From the *Clinic of Nuclear Medicine, Jena University Hospital, and †BioControl Jena, Data Analysis and Process Optimization, Jena, Germany; and ‡Spencer-Fontayne Corporation, Jersey City, NJ.

Conflicts of interest and sources of funding: none declared.

Reprints: Martin Freesmeyer, MD, Clinic of Nuclear Medicine, Jena University Hospital, Bachstr. 18, 07740 Jena, Germany. E-mail: Martin.Freesmeyer@med.uni-jena.de.

Portions of this work were presented as a German-language abstract at the 2012 Annual Meeting of the Deutsche Gesellschaft für Nuklearmedizin, Bremen, April 2012.

ISSN: 0363-9762/13/3810–0770

TABLE 1. Patient Characteristics

Characteristic	Value
Age, yr	
Median (minimum-maximum)	66 (51–76)
Mean ± SD	63.0 ± 9.4
Female, n (%)	16 (76%)
Thyroid disorder, n (%)	
Goiter	
Uninodular	10 (48%)
Multinodular	7 (33%)
Without nodules	4 (19%)
Toxic*	17 (81%)
Serum thyrotropin, mIU/L (normal range: 0.25–4.04 mIU/L)	
Median (minimum-maximum)	0.07 (0.01–0.72)
Mean ± SD	0.17 ± 0.21

SD indicates standard deviation.

*Goiter was considered to be toxic when serum thyrotropin was <0.25 mIU/L.

diagnoses were confirmed through routine laboratory testing of thyroid function and autoimmunity, as well as routine imaging including ^{99m}Tc-pertechnetate planar scintigraphy, used to determine the therapeutic radioiodine activity. Selected cohort characteristics are shown in Table 1.

Study Design, Endpoints, and Ethics

The study was a blinded comparison of ^{124}I-PET(/CT), ^{99m}Tc-pertechnetate planar scintigraphy, and ^{99m}Tc-pertechnetate-SPECT. No comparison was made with ^{99m}Tc-pertechnetate-SPECT/CT because that modality is not available at our center. The study endpoints comprised numbers of "hot spots," defined as areas of intense radioisotope uptake relative to adjacent tissue, "cold spots," defined as areas of low radioisotope uptake, ie, photopenia, relative to adjacent tissue, and "hot spots" with a central photopenic region, leading to a ring-like appearance on the functional image. Additional endpoints included the proportion of such focal findings with morphologic correlates on 2-dimensional (2D) ultrasonography (acquired routinely), 3D ultrasonography (performed for a separate clinical study),[23] and the (low-dose) CT component of the ^{124}I-PET/CT, as well as the mean volume and diameter on ultrasonography of visualized nodules. ^{124}I-PET/CT and the ^{99m}Tc-pertechnetate modalities were also compared with respect to the number of cases of lobus pyramidalis or retrosternal thyroid tissue that they identified.

Each patient provided written informed consent for all examinations.

Comparisons were made jointly by 2 nuclear medicine specialists experienced in thyroidology, who were unaware of any patient data beyond those related to the studied nuclear medicine methods, ultrasonography, and CT. The ^{124}I-PET/CT images and 3D ultrasonography datasets were evaluated using TrueD software on the syngo MultiModality workstation (Siemens, Erlangen, Germany). The ^{124}I-PET and ^{99m}Tc-pertechnetate-SPECT images were previewed as Maximum Intensity Projections and thoroughly analyzed in all 3 standard planes.

Comparison of the functional images with sonograms was made side by side. The 2D ultrasonography data comprised the representative capture images of each thyroid lobe and nodule stored in a Picture Archiving and Communication System at the discretion of the operator, and the routine written report on overall findings. The 3D ultrasonography images encompassed the entire thyroid in all cases. For ultrasonographic correlates with functional imaging focal findings, nodule volume was determined by measuring nodule length, width, and depth on 2 perpendicular planes and using the formula length × width × depth/2.

The search for CT correlates of focal findings used a hybrid representation on a multimodal analysis panel in the case of ^{124}I-PET and was carried out side-by-side in the case of the ^{99m}Tc-pertechnetate scintigraphic modalities.

^{124}I-PET/CT

^{124}I-PET/CT images were acquired using a Biograph mcT 40 system (Siemens). Scanning occurred 13.6 ± 8.6 hours after oral administration of 1 MBq (0.027 mCi) of commercially obtained ^{124}I, an activity chosen based on phantom studies (unpublished data). Patients were scanned in supine position with 1 bed position measured during 10 minutes. The scan region included the whole neck and the upper thorax so that any retrosternal thyroid tissue could be imaged. Anatomic coregistration and attenuation correction were performed using CT at its lowest tube setting (30 mAs), with a 120-kV tube voltage, 3-mm scan slice width, and 1.2 pitch, without contrast agent. Images were reconstructed with a 3-mm slice thickness and a 1.5-mm increment. The radiation exposure attributable to the CT was only ~0.3 mSv.

^{99m}Tc-Pertechnetate Planar Scintigraphy and ^{99m}Tc-Pertechnetate-SPECT

^{99m}Tc-pertechnetate planar scintigraphy was performed using a Nucline TH-22 gamma camera with an LETH: KT 060000-0029V0 collimator (MEDISO Medical Imaging Systems, Budapest, Hungary). A mean activity of 61.9 ± 5.4 MBq (1.67 ± 0.15 mCi) ^{99m}Tc-pertechnetate was injected intravenously, and recording was performed ~22 minutes later with the patient seated. Planar scanning duration was ~5 minutes.

Immediately after planar scintigraphy, SPECT images were acquired using the Symbia S double-headed gamma camera (Siemens); the images were reconstructed using a 3D iterative method (3D-Flash; Siemens). Total SPECT scanning time was ~22 minutes.

Ultrasonography

All neck ultrasonography was performed by 1 of 3 physicians experienced in this procedure, using linear probes (LOGIQ 9 system, 7L and M12L probes; GE Healthcare, Milwaukee, WI, USA) for the 2D examination and convex probe (Voluson E8 system, RAB4-8-D, 2–8 MHz probe; GE Healthcare) for the 3D examination.

Statistics

No sample size calculations were performed for this pilot comparison. To assess the significance of differences among nuclear medicine methods, we used the binomial test for numbers of detected nodules and of patients with pathological anatomy, and analysis of variance followed by the 2-sided Mann-Whitney test for the maximum ultrasonographic diameter and volume of the detected nodules. $P < 0.05$ was deemed to show significance. All statistical calculations were performed using R software, 2011 edition (R Foundation, Vienna, Austria).

RESULTS

As seen in Table 2, significantly more "hot spots" with/without central photopenia and significantly more total focal findings were noted on ^{124}I-PET than with the ^{99m}Tc-pertechnetate modalities. More "cold spots" were visualized on ^{124}I-PET, but this difference was not significant. All "cold spots" detectable by ultrasonography, ie, those greater than or equal to 1 cm in diameter, were subjected to ultrasonography-guided fine-needle aspiration cytology; none revealed signs of malignancy.

TABLE 2. Focal Findings in 21 Patients With Benign Thyroid Disease on ^{124}I-PET, ^{99m}Tc-Pertechnetate Planar Scintigraphy, and ^{99m}Tc-Pertechnetate-SPECT

	^{124}I-PET	^{99m}Tc-Pertechnetate Planar Scintigraphy	^{99m}Tc-Pertechnetate-SPECT	Statistical Comparison
"Hot spots"	83	25	33	*†‡
With central photopenia	17	3	5	*†
Without central photopenia	66	22	28	*†‡
"Cold spots"	9	5	6	NS
Total focal findings	92	30	39	*†‡

NS indicates no significant differences among the methods; PET, positron emission tomography; SPECT, single-photon emission computed tomography.
*^{124}I-PET vs. ^{99m}Tc-pertechnetate planar scintigraphy: $P < 0.001$.
†^{124}I-PET vs. ^{99m}Tc-pertechnetate-SPECT: $P < 0.001$.
‡^{99m}Tc-pertechnetate-SPECT vs. ^{99m}Tc-pertechnetate planar scintigraphy: $P < 0.05$.

^{99m}Tc-pertechnetate-SPECT detected significantly more "hot spots" and total focal findings, and greater numbers of "hot spots" with central photopenia and of "cold spots" than did ^{99m}Tc-pertechnetate planar scintigraphy. All focal findings on ^{99m}Tc-pertechnetate planar scintigraphy were evident on ^{99m}Tc-pertechnetate-SPECT and ^{124}I-PET, and all focal findings seen on ^{99m}Tc-pertechnetate-SPECT but not on ^{99m}Tc-pertechnetate planar scintigraphy were also noted on ^{124}I-PET (Table 2, Figs. 1–3).

As seen in Table 3, all focal findings noted on the ^{99m}Tc-pertechnetate modalities and the vast majority of focal findings apparent only on ^{124}I-PET had ultrasonographic correlates. However, nearly 18% of focal findings on ^{99m}Tc-pertechnetate planar scintigraphy, more than a third of focal findings on ^{99m}Tc-pertechnetate-SPECT, more than half of all focal findings on ^{124}I-PET, and almost two thirds of focal findings seen only on ^{124}I-PET lacked CT correlates.

As shown in Table 3 and Figure 4, on average, ^{124}I-PET visualized smaller nodules than did ^{99m}Tc-pertechnetate-SPECT, and ^{99m}Tc-pertechnetate-SPECT in turn visualized smaller nodules than did ^{99m}Tc-pertechnetate planar scintigraphy. The nodules seen on ^{124}I-PET were somewhat above half the mean volume and under three quarters of the mean maximal diameter of those shown on ^{99m}Tc-pertechnetate-SPECT, which were on average around 20% smaller in volume and 10% smaller in maximal diameter than those seen on ^{99m}Tc-pertechnetate planar scintigraphy. The nodules visualized only on ^{124}I-PET were significantly smaller in mean volume and mean maximal diameter than were those also visualized on the ^{99m}Tc-pertechnetate modalities. Nodules seen on ^{99m}Tc-pertechnetate-SPECT but not ^{99m}Tc-pertechnetate planar scintigraphy were significantly smaller in both respects than were the nodules discernible on both ^{99m}Tc-pertechnetate modalities.

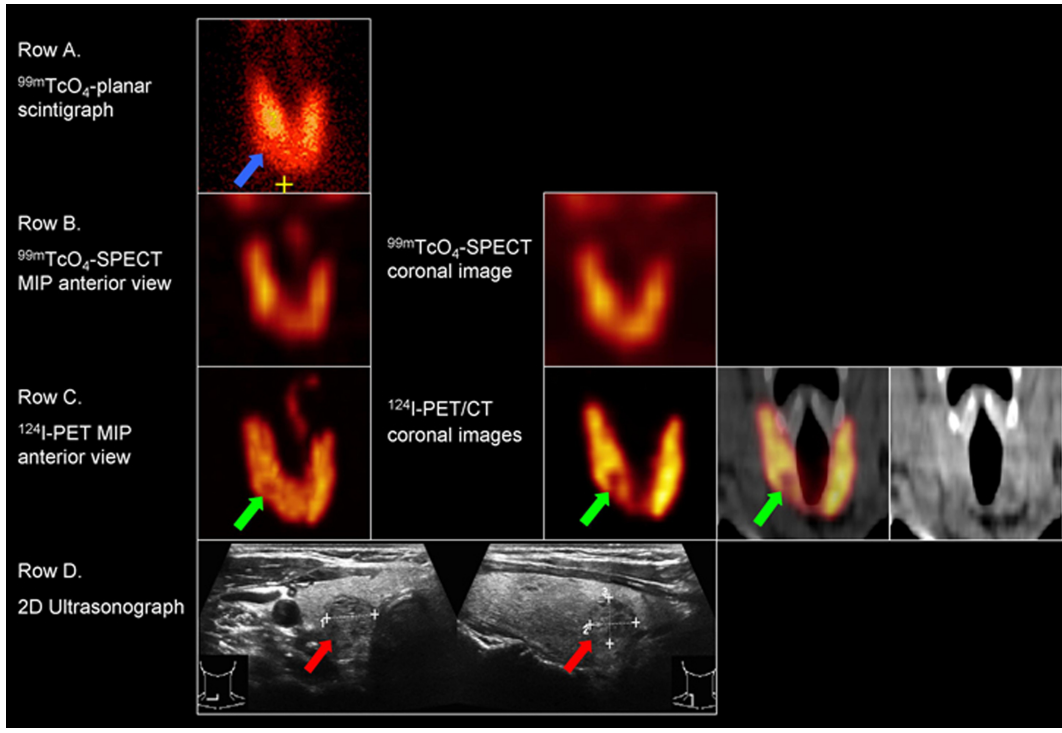

FIGURE 1. Comparison of ^{99m}Tc-pertechnetate planar scintigraphy (Row A), ^{99m}Tc-pertechnetate-SPECT (Row B), ^{124}I-PET and ^{124}I-PET/CT (Row C), and 2D ultrasonography (Row D) in a 51-year-old female patient with nodular goiter (dimensions 1.0 × 1.0 × 0.9 cm; volume 24 mL; TSH 0.72 mIU/L, no pharmacotherapy). An area of possible moderate hypofunction in the ^{99m}Tc-pertechnetate planar scan (*blue arrow*) is clearly shown in the ^{124}I-PET and ^{124}I-PET/CT (*green arrows*). This lesion corresponds to the small nodule in the caudal right thyroid lobe on the 2D sonogram (*red arrows*).

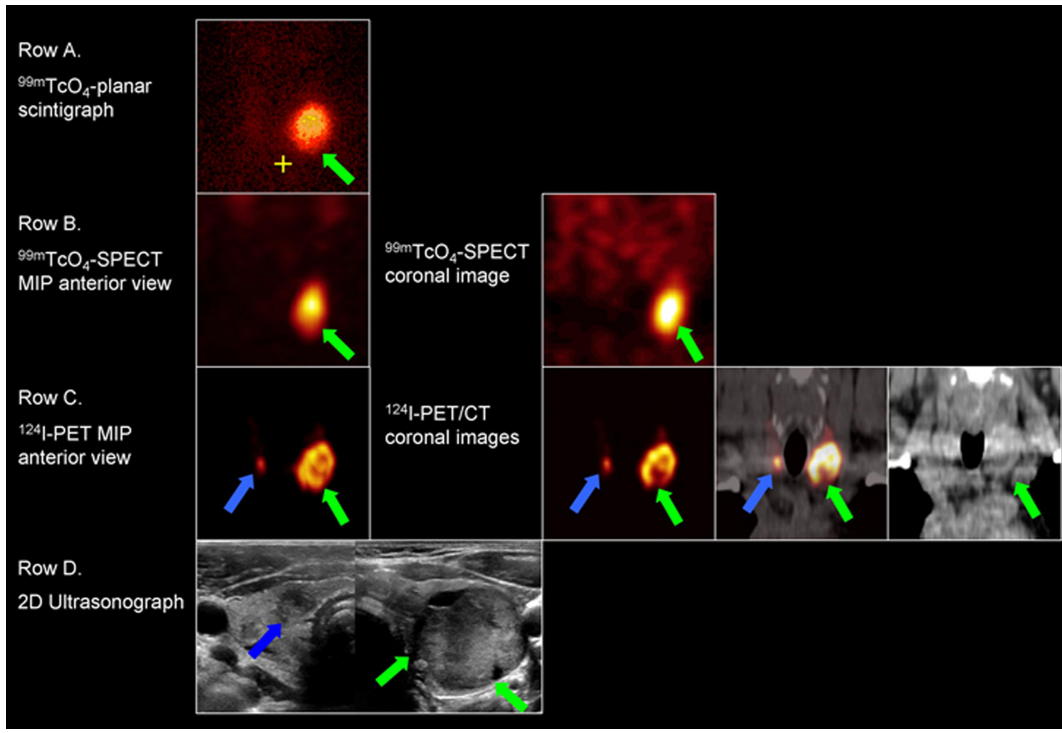

FIGURE 2. Comparison of ^{99m}Tc-pertechnetate planar scintigraphy (Row A), ^{99m}Tc-pertechnetate-SPECT (Row B), ^{124}I-PET and ^{124}I-PET/CT (Row C), and 2D ultrasonography (Row D) in a 52-year-old male patient with toxic nodular goiter (volume 42 mL, TSH <0.01 mIU/L, no pharmacotherapy). The first 3 modalities show an autonomous adenoma in the left thyroid lobe (*green arrows*). A central photopenic region and a small adenoma caudally in the right thyroid lobe (*blue arrows*) are visible only on ^{124}I-PET and ^{124}I-PET/CT. A morphological correlate of both nodules is evident in the 2D sonogram.

^{124}I-PET visualized the lobus pyramidalis in the patient in whom this site was visualized on the ^{99m}Tc-pertechnetate modalities and in significantly more patients overall (Table 4). The low-dose CT carried out in conjunction with ^{124}I-PET defined the retrosternal portion of the thyroid gland in the patient in whom this structure could be defined by marking the jugulum in the ^{99m}Tc-pertechnetate modalities and in significantly more patients overall (Table 4, Fig. 5).

In the 17 patients with thyrotropin suppression, the mean volume of autonomous nodules was greater on ^{124}I-PET than on ^{99m}Tc-pertechnetate planar scintigraphy/SPECT: 7.4 ± 4.7 mL versus 6.4 ± 4.4 mL, corresponding to an average absolute difference of 0.9 ± 0.7 mL. The mean relative difference between the modalities was 21.9% ± 18.4%, while the median (minimum-maximum) relative difference was 19.3% (3.9%-32.0%).

DISCUSSION

The present pilot investigation is, to our knowledge, the first published study comparing the value of ^{124}I-PET, performed with a low activity (1 MBq/0.027 mCi) together with low-dose CT, against that of the current standard imaging procedure, ^{99m}Tc-pertechnetate planar scintigraphy, or that of ^{99m}Tc-pertechnetate-SPECT in thyroid gland diagnostics. This work was initially based on 3 assumptions: (1) the positron emitter ^{124}I would provide higher image quality due to superior spatial resolution and image contrast, (2) the higher energy of ^{124}I and the CT transmission correction would result in fewer absorption effects, and (3) minimal ^{124}I activities would suffice for adequate imaging due to the high specific tracer uptake and the high measuring sensitivity of PET. The present observations largely justify these assumptions.

Our main finding was that, relative to ^{99m}Tc-pertechnetate planar scintigraphy or its cross-sectional enhancement, ^{99m}Tc-pertechnetate-SPECT, ^{124}I-PET was associated with information gains—almost all statistically significant—regarding all tested variables. ^{124}I-PET identified significantly more "hot spots" with/without central photopenia and significantly more focal findings overall (Table 2), and defined the lobus pyramidalis (Table 4) in significantly more patients than did the 2 ^{99m}Tc-pertechnetate modalities. The CT component of the ^{124}I-PET/CT procedure also identified a retrosternal portion of the thyroid gland in significantly more patients than did ^{99m}Tc-pertechnetate scintigraphy (Table 4). Further, ^{124}I-PET detected more "cold spots" than did its functional imaging comparators, but perhaps because of the limited number of such lesions, the difference did not attain statistical significance. On the other hand, the use of ^{124}I-PET did not reduce informativeness in any of the patients because this modality revealed all focal findings seen on ^{99m}Tc-pertechnetate planar scintigraphy or ^{99m}Tc-pertechnetate-SPECT, and defined the lobus pyramidalis and retrosternal thyroid tissue in all patients in whom the ^{99m}Tc-pertechnetate modalities did.

Because the nodules registered only on ^{124}I-PET had significantly smaller volumes and diameters than did those seen on the ^{99m}Tc-pertechnetate modalities (Table 3), the higher sensitivity of ^{124}I-PET for focal findings was at least partly attributable to the greater spatial resolution of PET. Our data do not allow an analysis of the extent to which the improved image contrast of PET also contributed to this advantage.

An important aspect of our study was to determine if the incremental focal findings seen on ^{124}I-PET corresponded to actual thyroid gland pathologies or if they were false positive. We therefore sought morphological correlates for all functional imaging focal

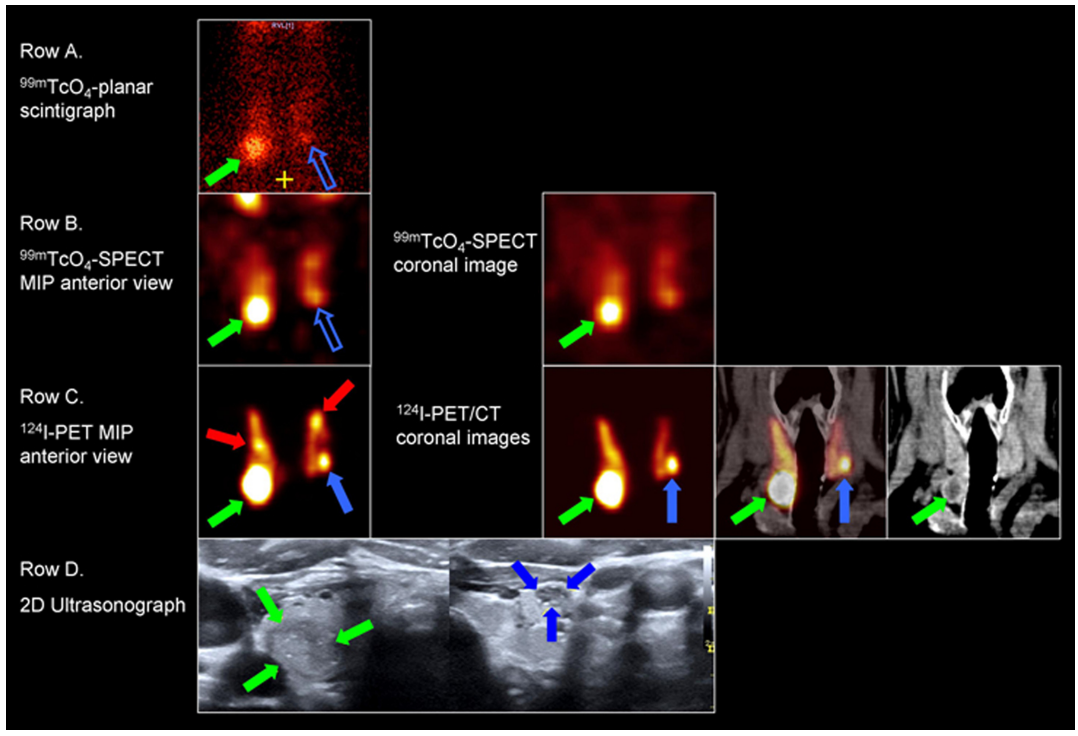

FIGURE 3. Comparison of ^{99m}Tc-pertechnetate planar scintigraphy (Row A), ^{99m}Tc-pertechnetate-SPECT (Row B), ^{124}I-PET and ^{124}I-PET/CT (Row C), and 2D ultrasonography (Row D) in a 71-year-old female patient with goiter (volume 14 mL, TSH 0.09 mIU/L, treatment with levothyroxine, 150 μg/d). An autonomous adenoma caudally in the right thyroid lobe is visible in all 3 nuclear medicine modalities and a correlate is seen on 2D ultrasonography (*green arrows*). However, 3 additional ''hot spots'' (*red arrows* and *solid blue arrows*) are clearly detectable in the ^{124}I-PET and ^{124}I-PET/CT images, but only dimly detectable in the ^{99m}Tc-pertechnetate scans (*hollow blue arrows*).

findings. Whereas focal findings common to the ^{99m}Tc-pertechnetate modalities as well as ^{124}I-PET always had an ultrasonographic correlate, the incremental ^{124}I-PET findings had such a correlate in about 92% of cases (Table 3). This observation suggests that the additional ^{124}I-PET focal findings indeed almost always corresponded to thyroid gland structural changes and therefore provided a diagnostic benefit.

It could not be determined whether the 8% of incremental focal findings lacking an ultrasonographic correlate were artifacts or

TABLE 3. Correlation Between Focal Findings on Studied Nuclear Medicine Modalities and on Morphologic Imaging Modalities Nodule* Volume and Diameter According to Detectability by the Given Modalities

Diagnostic Category	# of Focal Findings	n (%) of Focal Findings With Correlate on:		Mean ± SD Nodule Volume on Ultrasonography, mL	Mean ± SD Maximal Nodule Diameter, cm
		Ultrasonography	CT		
^{99m}Tc-pertechnetate planar scintigraphy, all focal findings	30	30 (100%)	25 (83.3%)	5.5 ± 4.3	2.1 ± 0.6
^{99m}Tc-pertechnetate-SPECT, all focal findings	39	39 (100%)	25 (64.2%)	4.5 ± 4.3	1.9 ± 0.7
^{99m}Tc-pertechnetate-SPECT focal findings not seen on ^{99m}Tc-pertechnetate planar scintigraphy	9	9 (100%)		0.9 ± 0.8†	1.2 ± 0.3†
^{124}I-PET, all focal findings	92	88 (95.7%)	44 (47.8%)	2.5 ± 3.7	1.4 ± 0.7
^{124}I-PET focal findings not seen on ^{99m}Tc-pertechnetate planar scintigraphy or ^{99m}Tc-pertechnetate-SPECT	53	49 (92.5%)	15 (35.9%)	0.4 ± 0.3‡	0.9 ± 0.3‡

CT indicates computed tomography; PET, positron emission tomography; SPECT, single-photon emission computed tomography.

*Includes both "hot" and "cold" nodules.

†Statistically significant difference at $P < 0.05$ between nodules seen on ^{99m}Tc-pertechnetate-SPECT but not ^{99m}Tc-pertechnetate planar scintigraphy (n = 9) vs. nodules seen on both these modalities (n = 30).

‡Statistically significant difference at $P < 0.001$ between nodules seen only on ^{124}I-PET (n = 53) vs. nodules seen on one or both of ^{99m}Tc-pertechnetate planar scintigraphy or ^{99m}Tc-pertechnetate-SPECT as well as on ^{124}I-PET (n = 39).

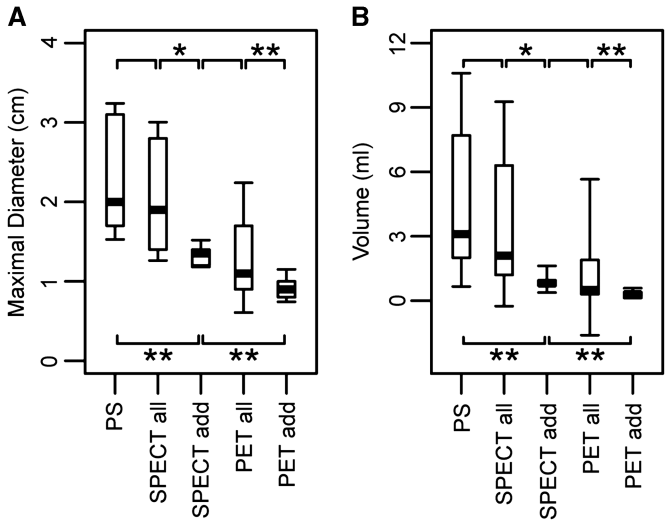

FIGURE 4. Mean maximal diameter in centimeters (**A**) and mean volume in milliliters (**B**), as determined by ultrasonography, of nodules corresponding to focal findings on nuclear imaging modalities. *Statistically significant at $P < 0.05$; **statistically significant at $P < 0.001$. PET indicates positron emission tomography; PET add, nodules corresponding to focal findings on ^{124}I-PET, but not on ^{99m}Tc-pertechnetate scintigraphy; PET all, all nodules corresponding to focal findings on ^{124}I-PET; PS, ^{99m}Tc-pertechnetate planar scintigraphy; SPECT, single-photon emission computed tomography; SPECT add, nodules corresponding to focal findings on ^{99m}Tc-pertechnetate-SPECT, but not ^{99m}Tc-pertechnetate planar scintigraphy; SPECT all, all nodules corresponding to focal findings on both ^{99m}Tc-pertechnetate-SPECT and ^{99m}Tc-pertechnetate planar scintigraphy; ^{99m}Tc, ^{99m}Tc-pertechnetate.

comprised nodules too small to be detected by 2D or 3D ultrasonography or to have been considered sufficiently clinically relevant to be documented in 2D "capture images" in everyday practice. Where 2D ultrasonographic image archiving was incomplete, the ultrasonographic comparison relied on experimental 3D ultrasonography acquired using a mechanically swept convex probe array,[23] which was diagnostically inferior to the routine, guideline-based 2D procedure with high-frequency linear probes. Of interest, magnetic navigated real-time ultrasonography fusion with ^{124}I-PET in another cohort suggests that ultrasonographic correlates of ^{124}I focal findings are almost always found if the images are well-registered (unpublished data). Future ^{124}I-PET validation should include careful, state-of-the-art ultrasonography performed promptly after the ^{124}I-PET.

Due to its limited ability to differentiate among soft tissues, non–contrast-enhanced CT of the thyroid gland is less sensitive than is routine ultrasonography.[24,25] Accordingly, we could not find a CT correlate for more than half of focal findings (Table 3), and absence of such a correlate was especially common in noncystic or noncalcified nodules. Unsurprisingly, CT did not deliver further information about the 8% of ^{124}I-PET findings lacking an ultrasonographic correlate. Our functional-morphological correlation results suggest the necessity for thyroid gland ultrasonography even when ^{124}I-PET or ^{99m}Tc-pertechnatate-SPECT is performed together with CT.

Despite the limited clinical utility of the visualization of small nodules, the present findings of superior sensitivity of ^{124}I-PET compared to the ^{99m}Tc-pertechnetate modalities may be clinically relevant in at least 4 ways, especially in centers, such as ours, that lack ^{99m}Tc-SPECT/CT scanners and, hence, the ability to obtain hybrid images other than with PET. Firstly, our observation of an average 21.9% enlargement in autonomous thyroid tissue volume when estimated by ^{124}I-PET in patients with laboratory signs of hyperthyroidism as well as focal autonomy findings (n = 17) suggests that use of ^{99m}Tc-pertechnetate planar scintigraphy or ^{99m}Tc-pertechnetate-SPECT may be associated with moderate underestimation of therapeutic ^{131}I-activity requirements because calculation of such activities using the Marinelli formula is linearly related to the autonomous volume.[17,26] Secondly, the superiority of ^{124}I-PET in detecting central photopenic areas of focal "hot spots"—whether or not the morphological correlate was partially cystic or completely solid—might enhance the ability to track a nodule's natural history, eg, the cystic transformation. Additionally, in large adenomas, photopenic regions might be substantial enough to permit reduction of planned therapeutic activities. Thirdly, the significantly greater ability of ^{124}I-PET to define the lobus pyramidalis could provide important hints. The lobus pyramidalis may be a locus of pathologic alterations,[27] including benign nodular changes and—albeit rarely—thyroid cancer. Moreover, we occasionally see remarkably large postsurgical remnants of the lobus pyramidalis when this anatomical detail is poorly visualized preoperatively on scintigraphy and therefore overlooked by the surgeon.

Lastly, the greater ability of the CT component of ^{124}I-PET/CT to ensure the diagnosis of retrosternal thyroid tissue could more definitively rule in/rule out surgery, the first-line therapy when such tissue is distended.[6,28–30] Nonetheless, these benefits remain theoretical until they are prospectively evaluated in outcome studies. Moreover, ^{124}I-PET/CT and ^{99m}Tc-pertechnetate-SPECT/CT should be compared to clarify their roles where both are available or one or the other could be added.

Further, 2 drawbacks of ^{124}I-PET(/CT) relative to ^{99m}Tc-pertechnetate scintigraphy should be noted. For one, even a very small ^{124}I activity (1 MBq/0.027 mCi) is substantially costlier than are standard activities of ^{99m}Tc-pertechnetate. This factor may limit ^{124}I-PET(/CT) usage. Secondly, the total patient radiation exposure of our ^{124}I-PET/CT protocol was more than eightfold that of ^{99m}Tc-pertechnetate. Assuming 25% thyroid uptake of 1 MBq (0.027 mCi)

TABLE 4. Detectability of the Lobus Pyramidalis or Retrosternal Portion of the Thyroid Gland According to Nuclear Medicine Modality in 21 Patients With Benign Thyroid Diseases

Anatomic Site	Number of Patients With Defined Site by:		*P*
	^{99m}Tc-pertechnetate planar scintigraphy or ^{99m}Tc-pertechnetate-SPECT	^{124}I-PET(/CT)	
Lobus pyramidalis	1	12	<0.001
Retrosternal portion of thyroid*	1	7	<0.05

*Based on the CT image in the case of the ^{124}I-PET(/CT); based on marking the jugulum in the case of the ^{99m}Tc-pertechnetate modalities.

CT, computed tomography; PET, positron emission tomography; SPECT, single-photon emission computed tomography.

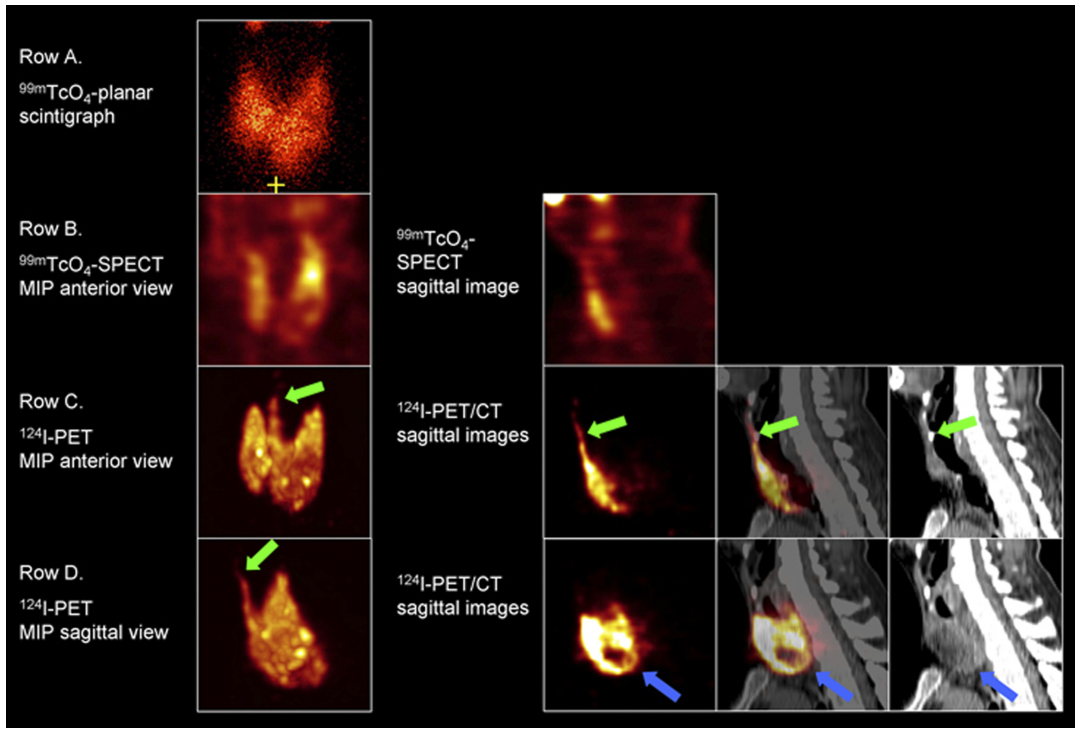

FIGURE 5. Comparison of ^{99m}Tc-pertechnetate planar scintigraphy (Row A), ^{99m}Tc-pertechnetate-SPECT (Row B), ^{124}I-PET and ^{124}I-PET/CT (Row C), and 2D ultrasonography (Row D) in a 62-year-old male patient with nontoxic nodular goiter (volume 120 mL, TSH 0.60 mIU/L, no pharmacotherapy). The lobus pyramidalis or the retrosternal portion of the thyroid gland are not clearly depicted on the ^{99m}Tc-pertechnetate planar scintigraphy or ^{99m}Tc-pertechnetate-SPECT scans, but are well defined on ^{124}I-PET and ^{124}I-PET/CT images (*green* and *blue arrows*, respectively).

^{124}I, the exposure is ~6.5 mSv for the PET procedure, while the low-dose CT component contributes ~0.3 mSv, for a total of ~6.8 mSv. Assuming less than 3% thyroid uptake of 60 MBq (1.62 mCi) ^{99m}Tc-pertechnetate, scintigraphy with that isotope would entail ~0.8 mSv/procedure of radiation exposure. This difference may limit the applicability of ^{124}I-PET/CT in benign thyroid diseases. ^{124}I-PET/CT should probably be reserved for cases with ambiguous ^{99m}Tc-pertechnetate scintigraphic findings, or for patients scheduled for radioiodine therapy. In this latter setting, the ~6.8 mSv ^{124}I-PET/CT dose would provide negligible incremental radiation exposure. However, increased accuracy in measuring the area targeted for therapy could either increase the likelihood of selecting a sufficient activity or avoid over-treatment. Indeed, prevention of an excessive therapeutic activity could achieve a net reduction of radiation exposure despite use of ^{124}I-PET/CT.

This study has certain limitations, most notably the relatively small cohort, the lack of sample size calculation, and the fact that the ^{124}I-PET/CT and 3D ultrasonography were performed prospectively in relation to clinical studies and the ^{99m}Tc-pertechnetate-SPECT was performed additionally for special assessment, but the ^{99m}Tc-pertechnetate planar scintigraphy and 2D ultrasonography were performed routinely. A clinical study without these limitations is needed to confirm the present results.

Additionally, as noted earlier, the present comparison did not include ^{99m}Tc-pertechnetate-SPECT/CT, which is not yet widely available in Europe. Regarding detection of retrosternal thyroid tissue, the lack of simultaneous morphological imaging with ^{99m}Tc-pertechnetate-SPECT may have biased our findings towards ^{124}I-PET.

Our comparison also did not include ^{123}I scintigraphy. The use of this modality to image thyroid nodules is not recommended in German guidelines,[3,26] and relative to ^{124}I, ^{123}I has the disadvantages of a much shorter half-life (~13 hours vs. ~4 days), complicating logistics, and greater cost (~21 euros/administration vs. ~9–~14 euros/administration at our clinic).

In conclusion, this pilot comparison suggests that low-activity ^{124}I-PET performed together with (low-dose) CT has superior sensitivity to that of ^{99m}Tc-pertechnetate planar scintigraphy or ^{99m}Tc-pertechnetate-SPECT in functional thyroid imaging in patients with benign thyroid disorders. ^{124}I-PET detected significantly more total focal findings ("hot spots" plus "cold spots") and visualized significantly smaller nodules, although the clinical relevance of the latter is uncertain. In patients with biochemical hyperthyroidism and functional focal findings, ^{124}I-PET/CT identified a greater autonomous area and anatomical pathology in significantly more patients. A confirmatory comparative study is warranted.

Ultimately, ^{124}I-PET/CT may provide clinical benefit in benign thyroid disorders, albeit less extensively than in thyroid cancer. These benefits would include more accurate planning of radioiodine therapy activities and a more exact diagnosis of retrosternal extension when ^{123}I-SPECT/CT is unavailable. Moreover, the low-dose CT component may allow evaluation of adjacent structures, eg, the trachea and esophagus.

REFERENCES

1. Luster M, Verburg FA, Scheidhauer K. Diagnostic imaging work up in multinodular goiter. *Minerva Endocrinol*. 2010;35:153–159.
2. Giovanella L, Ceriani L, Ghelfo A. Second-generation thyrotropin receptor antibodies assay and quantitative thyroid scintigraphy in autoimmune hyperthyroidism. *Horm Metab Res*. 2008;40:484–486.

3. Garcia EV. Physical attributes, limitations, and future potential for PET and SPECT. *J Nucl Cardiol*. 2011;19(suppl 1):S19–S29.
4. Zaidi H. Comparative methods for quantifying thyroid volume using planar imaging and SPECT. *J Nucl Med*. 1996;37:1421–1426.
5. Franken PR, Guglielmi J, Vanhove C, et al. Distribution and dynamics of (99m)Tc-pertechnetate uptake in the thyroid and other organs assessed by single-photon emission computed tomography in living mice. *Thyroid*. 2010; 20:519–526.
6. Shah PJ, Bright T, Singh SS, et al. Large retrosternal goitre: a diagnostic and management dilemma. *Heart Lung Circ*. 2006;15:151–152.
7. Beyer T, Townsend DW, Brun T, et al. A combined PET/CT scanner for clinical oncology. *J Nucl Med*. 2000;41:1369–1379.
8. Hegedus L. Clinical practice. The thyroid nodule. *N Engl J Med*. 2004;351: 1764–1771.
9. Freudenberg L, Jentzen W, Goerges R, et al. 124I-PET dosimetry in advanced differentiated thyroid cancer. Therapeutic impact. *Nuklearmedizin*. 2007;46: 121–128.
10. Freudenberg LS, Jentzen W, Marlowe RJ, et al. 124-iodine positron emission tomography/computed tomography dosimetry in pediatric patients with differentiated thyroid cancer. *Exp Clin Endocrinol Diabetes*. 2007;115:690–693.
11. Sgouros G, Kolbert KS, Sheikh A, et al. Patient-specific dosimetry for 131I thyroid cancer therapy using 124I PET and 3-dimensional-internal dosimetry (3D-ID) software. *J Nucl Med*. 2004;45:1366–1372.
12. Lubberink M, Abdul Fatah S, Brans B, et al. The role of (124)I-PET in diagnosis and treatment of thyroid carcinoma. *Q J Nucl Med Mol Imaging* 2008;52:30–36.
13. Kolbert KS, Pentlow KS, Pearson JR, et al. Prediction of absorbed dose to normal organs in thyroid cancer patients treated with 131I by use of 124I PET and 3-dimensional internal dosimetry software. *J Nucl Med*. 2007;48: 143–149.
14. Jentzen W, Freudenberg L, Eising EG, et al. Optimized 124I PET dosimetry protocol for radioiodine therapy of differentiated thyroid cancer. *J Nucl Med*. 2008;49:1017–1023.
15. Jentzen W, Hobbs RF, Stahl A, et al. Pre-therapeutic (124)I PET(/CT) dosimetry confirms low average absorbed doses per administered (131)I activity to the salivary glands in radioiodine therapy of differentiated thyroid cancer. *Eur J Nucl Med Mol Imaging*. 2010;37:884–895.
16. Hobbs RF, Wahl RL, Lodge MA, et al. 124I PET-based 3D-RD dosimetry for a pediatric thyroid cancer patient: real-time treatment planning and methodologic comparison. *J Nucl Med*. 2009;50:1844–1847.
17. Eschmann SM, Reischl G, Bilger K, et al. Evaluation of dosimetry of radioiodine therapy in benign and malignant thyroid disorders by means of iodine-124 and PET. *Eur J Nucl Med Mol Imaging* 2002;29:760–767.
18. Herzog H, Tellman L, Qaim SM, et al. PET quantitation and imaging of the non-pure positron-emitting iodine isotope 124I. *Appl Radiat Isot*. 2002;56: 673–679.
19. Jentzen W, Weise R, Kupferschlager J, et al. Iodine-124 PET dosimetry in differentiated thyroid cancer: recovery coefficient in 2D and 3D modes for PET(/CT) systems. *Eur J Nucl Med Mol Imaging*. 2008;35:611–623.
20. Freudenberg LS, Antoch G, Jentzen W, et al. Value of (124)I-PET/CT in staging of patients with differentiated thyroid cancer. *Eur Radiol*. 2004;14: 2092–2098.
21. Freudenberg LS, Fromke C, Petrich T, et al. Thyroid remnant dose: 124I-PET/CT dosimetric comparison of rhTSH versus thyroid hormone withholding before radioiodine remnant ablation in differentiated thyroid cancer. *Exp Clin Endocrinol Diabetes*. 2010;118:393–399.
22. Freudenberg LS, Jentzen W, Petrich T, et al. Lesion dose in differentiated thyroid carcinoma metastases after rhTSH or thyroid hormone withdrawal: (124)I PET/CT dosimetric comparisons. *Eur J Nucl Med Mol Imaging*. 2010; 37:2267–2276.
23. Freesmeyer M, Darr A, Schierz JH, et al. 3D ultrasound DICOM data of the thyroid gland. First experiences in exporting, archiving, second reading and 3D processing. *Nuklearmedizin*. 2012;51:73–78.
24. Shetty SK, Maher MM, Hahn PF, et al. Significance of incidental thyroid lesions detected on CT: correlation among CT, sonography, and pathology. *AJR Am J Roentgenol*. 2006;187:1349–1356.
25. Nygaard B, Nygaard T, Court-Payen M, et al. Thyroid volume measured by ultrasonography and CT. *Acta Radiol*. 2002;43:269–274.
26. Dietlein M, Dressler J, Grunwald F, et al. [Guideline for radioiodine therapy for benign thyroid diseases (version 4)]. *Nuklearmedizin*. 2007;46:220–223.
27. Spencer RP, Scholl RJ, Erbay N. Tc-99m pertechnetate thyroid images in hyperthyroidism. Size, distribution, and presence of a pyramidal lobe. *Clin Nucl Med*. 1997;22:519–522.
28. Machado NO, Grant CS, Sharma AK, et al. Large posterior mediastinal retrosternal goiter managed by a transcervical and lateral thoracotomy approach. *Gen Thorac Cardiovasc Surg*. 2011;59:507–511.
29. Kilic D, Findikcioglu A, Ekici Y, et al. When is transthoracic approach indicated in retrosternal goiters? *Ann Thorac Cardiovasc Surg*. 2011;17:250–253.
30. Kadhim AL, Sheahan P, Timon C. Management of life-threatening airway obstruction caused by benign thyroid disease. *J Laryngol Otol*. 2006;120: 1038–1041.

3.1. ^{124}Iod-Niedrigaktivitäts-PET/Niedrigdosis-CT (^{124}Iod-PET/CT) der Schilddrüse

3.1.2. Prätherapeutische Bestimmung der Iodaufnahme mit ^{124}Iod-PET

Low-activity ^{124}I-PET/low-dose CT versus ^{131}I Probe Measurements in Pretherapy Assessment of Radioiodine Uptake in Benign Thyroid Diseases

Publikation in JOURNAL OF CLINICAL ENDOCRINOLOGY AND METABOLISM 2014

Low-activity ^{124}I-PET/low-dose CT versus ^{131}I probe measurements in pretherapy assessment of radioiodine uptake in benign thyroid diseases

Julian G Westphal[1], Thomas Winkens[1], Christian Kühnel[1,2], Martin Freesmeyer[1]

[1] Clinic of Nuclear Medicine, Jena University Hospital, Friedrich Schiller University of Jena, Jena, Germany and [2] Ernst-Abbe-Fachhochschule Jena, University of Applied Sciences, Jena, Germany

[*]*Corresponding author:*

Dr. Martin Freesmeyer, Clinic of Nuclear Medicine, Jena University Hospital

Bachstrasse. 18, 07740 Jena, Germany

Phone: +49-3641-933220; Fax: +49-3641-933244

E-Mail: martin.freesmeyer@med.uni-jena.de

Abstract

Context Radioiodine therapy of benign thyroid diseases requires pretherapy assessment of radioactive iodine uptake (RAIU) for reliable therapy planning.

Objective To assess RAIU by low-activity ^{124}I-Positron Emission Tomography/low-dose Computed Tomography (^{124}I-PET/CT) in comparison with standard ^{131}I probe measurements.

Design/Setting Prospective comparative study, conducted at the Jena University Hospital, Jena, Germany in a referral center setting.

Patients 79 Patients with benign thyroid diseases were screened, 40 of whom met the inclusion criteria (stable TSH, fT3, fT4 levels; no thyroid specific medication, no iodine contamination) and 24 of whom agreed to participate by signing an informed consent.

Interventions All patients received the standard ^{131}I scintillation probe uptake test 30 hours after administration of 3 MBq ^{131}I. Seven days later all patients were subjected to ^{124}I-PET/CT uptake measurement 30 hours after administration of 1 MBq ^{124}I.

Main Outcome Measures The decay-corrected uptake values of both techniques were compared. Additionally three different Volume-of-Interest based evaluation methods in PET/CT (whole neck [WN], automatic isocontour [IC], and manually contoured [MC]) were evaluated.

Results The ^{131}I probe measurement and ^{124}I-PET.WN method provided very similar mean RAIUs (30.7±10.3%; 31.7±8.9%), resulting in a significant positive correlation ($r=0.93$, $p<0.001$). Compared to ^{124}I-PET.WN, the ^{124}I-PET.IC (29.8±8.6%) and the ^{124}I-PET.MC (24.5±7.1%) demonstrate lower uptake values.

Conclusions Using activities as low as 1 MBq, the ^{124}I-PET.WN method shows a good correlation with conventional ^{131}I probe measurement. Thus, ^{124}I-PET/CT is a suitable alternative for pretherapy RAIU evaluations. This may offer potential additional benefits like PET/US fusion imaging and CT volumetry.

Introduction

Benign thyroid diseases are very common worldwide (1) and radiotherapy with ^{131}I is an established method for their treatment. However, the fractional radioactive iodine uptake (RAIU) (measured activity / applied activity) and the elimination of the stored iodine considerably vary from patient to patient. Therefore a pretherapy assessment of individual iodine kinetics is very important to avoid overexposure or under-treatment (2-4).

Pretherapy RAIU measurements are typically performed with 3 MBq ^{131}I(4). Several methods have been recommended with regard to procedures, timing, and activity measurements (5). For example, a single measurement of neck activity is possible via ^{131}I scintillation probe or gamma camera, and empirically derived standard half-lives can be used to calculate the therapeutic activity. Alternatively, repeated activity measurements can be performed within 2 days or longer. In this case, the therapeutic activity can be calculated on the basis of the approximate maximal thyroid uptake and effective half-lives (*5*). Limitations of the standard method with ^{131}I are the dependence from the measuring distance between patient and detector, as well as the impossibility to correct for the attenuation of neck tissues.

The feasibility of accurate quantitative RAIU evaluations via ^{124}I-Positron Emission Tomography (PET) has previously been described (6, 7). Studies on pretherapy or intratherapy dosimetry with ^{124}I-PET/Computed Tomography (CT) are also available, however they are limited to differentiated thyroid carcinoma (8-12). To the best of our knowledge, to date only one study has investigated ^{124}I-PET dosimetry in benign thyroid diseases (13).

PET/CT measurements have several advantages compared to conventional assessments with ^{131}I and scintillation probe or gamma camera, i.e., higher sensitivity, superior spatial resolution, simple quantitation, anatomic correlation, and the possibility to limit the effects of attenuation. These aspects concur to indicate that pretherapy dosimetry with ^{124}I-PET/CT is a potential alternative for RAIU assessments, particularly in centers without Single-photon Emission Computed Tomography /CT facilities.

The aim of this prospective, pilot study was to assess the feasibility of pretherapy RAIU determination via low-activity-^{124}I-PET/low-dose-CT, in comparison with established ^{131}I probe measurements

Materials and methods

Phantom study

Prior to the study, a phantom examination investigated whether the residual ^{131}I had an influence on the quantification of ^{124}I in the PET/CT setup. For this purpose a 200-ml plastic cylinder was filled with a low activity of 250 kBq ^{124}I, placed in a larger tank filled with water, and subsequently measured in the PET/CT scanner. Afterwards the larger tank was filled with a solution that contained an activity of 200 MBq ^{131}I and measured accordingly.

Patients and ethics

Patients with benign thyroid diseases referred to our institution in March/April 2012 in preparation for radiotherapy were included in the study. This was designed as a pilot subgroup analysis within a larger study approved by the local ethics committee and the German Federal Office of Radiation Protection. All participants signed a written informed consent.

Study protocol

Screening

The initial screening was performed according to currently valid guidelines (anamnesis; measurement of thyroid-stimulating hormone [TSH], free triiodothyronine [fT3], and free thyroxin [fT4]; neck ultrasound; and planar ^{99m}Tc-pertechnetate scintigraphy) (14).

Inclusion and exclusion criteria

Criteria for inclusion were the diagnosis of a benign thyroid disease potentially requiring treatment, the absence of thyroid-specific treatment, and a proven stability of thyroid metabolism, whereas variability of TSH <0.2 mU/l, fT3 <1.5 pmol/l, or fT4 <2.0 pmol/l were considered acceptable.

Patients were excluded if they had received thyroid-specific treatment within the previous 12 weeks; if their anamnesis was positive for iodine contamination; or if a relevant change in thyroid metabolism (as assessed by TSH levels) occurred between the investigations.

Dosimetry schedule

Patients underwent first a standard dosimetry with ^{131}I probe measurement 30 hours after oral administration of 3 MBq ^{131}I (0.08 mCi). Dosimetry with ^{124}I PET/CT was performed 30 hours after oral administration of 1 MBq ^{124}I (0.027 mCi), 7 days after standard dosimetry. Thyroid parameters were checked prior to the oral administration of the radiopharmaceuticals.

Tracer preparation and administration

^{131}I-NaI tracer solution was obtained from GE Healthcare Buchler GmbH & Co KG (Braunschweig, Germany). ^{124}I-NaI tracer solution, produced by proton irradiation of ^{124}Te-enriched tellurium, was obtained from IBA molecular (BV Cyclotron VU, Amsterdam, The Netherlands). Both fluid tracers were filled into identical capsules (HGK, size 3; GE Healthcare Buchler GmbH & Co KG) onto a crystalline sodium-phosphate carrier. The filling was performed under sterile conditions. The tracer activity of the test capsules was measured using a dose calibrator (Isomed 2010, MED Nuklear-Medizintechnik Dresden GmbH, Dresden, Germany).

Scan modalities

^{131}I probe measurements

The activity in patients was measured using a Thyroid Uptake Counter ISOMED 2162 (MED Nuklear-Medizintechnik Dresden GmbH). The measuring distance between detector and neck was kept at 45 cm using a spacer. The detector was fitted with a collimator NZ-136-01 (MED Nuklear-Medizintechnik Dresden GmbH). The NaI crystal detector had dimensions of 5x5 cm and was connected to a multichannel analyzer through a photomultiplier tube. For quality assurance purposes, each measurement was preceded by a check of the energy spectrum using a ^{137}Cs test source, as well as by measurement of the background activity.

Low-activity ^{124}I–PET / low-dose CT

^{124}I-PET/CT scans were acquired according to an established protocol, using a Biograph mCT 40 system (Siemens, Erlangen, Germany) (15). Patients were scanned in supine position with one bed position measured during 10 min. The scan region included the whole neck and the upper thorax, thus including any retrosternal thyroid tissue. Anatomic co-registration and attenuation correction were performed using native CT at its lowest tube setting (30 mAs), with 120 kV tube voltage, 3-mm scan

slice width and 1.2 pitch. Images were reconstructed at 3-mm slice thickness and 1.5-mm increment. The radiation exposure attributable to CT was only ~0.3 mSv.

Quantitative analyses

^{131}I probe measurements

The computer-based assessment proceeded by means of the dedicated standard software UPT 2000 (MED Nuklear-Medizintechnik Dresden GmbH). The thyroid activity was calculated as ratio of counts measured in the patients field of view versus counts measured in a standard phantom, in both cases after subtraction of the background count rate.

Low-activity ^{124}I–PET / low-dose CT

The PET and CT data sets were fused using the software PMOD 3.407 (PMOD Technologies Ltd., Zurich, Switzerland) and quantified using the volume-of-interest (VOI) technique. Three methods were used for this purpose. First a VOI was placed on the whole neck (^{124}I-PET.WN), ensuring that any retrosternal parts were included. Second, a measurement took place using an automatic isocontour (^{124}I-PET.IC) VOI (limit 0.2 kBq/ml), whereas the automatism was set up to include intra-thyroid hypofunctional areas and exclude extra-thyroid artifacts. Third, VOIs were manually placed slice-by-slice in coronal data sets according to the thyroid contour (manually contoured; ^{124}I-PET.MC) (Fig. 1).

Data evaluation

In analogy to other studies, a correction of the measured activities based on the different decay of ^{124}I and ^{131}I was performed to allow a comparison of the activities of the two radionuclides (8) (Equation 1). Accordingly, all data and figures were shown as decay-corrected uptake (Upt).

$$UPT = \frac{A_{t_x}}{A_{t_0} \cdot e^{\frac{-ln(2) \cdot t_x}{t_{1/2}}}} \cdot 100\%$$

(Equation 1)

where A_{t_x} is the activity concentration at time t_x, A_{t0} the applied activity at t_0 and $t_{1/2}$ the half-life of the iodine isotope used.

Statistical analysis

Linear correlations analyses were performed using the Pearson product-moment correlation coefficient. Because correlation coefficients cannot fully demonstrate a correspondence of calculated and reference RAIUs, a slightly modified version of the Bland and Altman method was also applied (16). For this purpose, relative uptake differences were calculated for all measurements. Thus, all relative uptake differences were expressed as ratios varying from -1.0 to 1.0, allowing for calculation of the mean discrepancies between methods. In addition, the methods were compared using the limits of agreement recommended by Bland and Altman (16), which include 95% of all expected values.

To assess systematic errors, the 95% confidence intervals of the means were also calculated. If the confidence intervals did not include the zero value, the corresponding method had a significant systematic error (overestimation or underestimation).

Finally, an analysis of variance (ANOVA) was performed to verify that the RAIU results did not depend on the levels of uptake.

Results

Phantom Study

The measured activity of the ^{124}I phantom was 7.07 kBq, or 2.85% higher than the obtained activity after the ^{131}I background was added (Table 1).

Patients

Seventy-nine patients were screened, 40 of whom fulfilled the inclusion criteria and 24 of whom agreed to participate in the study (Table 2). All participants were fully examined according to protocol. The mean orally administered activities were 3.06±0.15 MBq for ^{131}I and 1.02±0.05 MBq for ^{124}I. The ^{131}I uptake measurements took place on average 30 h 1 min ± 6 min and the ^{124}I uptake measurements 30 h 5 min ± 8 min after oral administration of the tracer.

Comparison of conventional versus PET-based RAIU measurement

The mean decay-corrected RAIU at 30 hours was 30.7±10.3% for the ^{131}I probe measurement and 31.7±8.9% for the ^{124}I-PET.WN measurement, resulting in a significant positive correlation between the two methods ($r=0.93$, $p<0.001$). The modified Bland and Altman analysis included the zero value in the 95% confidence interval, thus suggesting no systematic overestimation or underestimation. The limits of agreement ranged from -0.21 to 0.29 (Table 3, Fig. 2). The median relative decay-corrected uptake difference was 9 %.

Comparison of different VOI procedures used for ^{124}I-PET/CT

The mean RAIUs provided by the ^{124}I-PET.IC procedure (29.8±8.6%) were lower (-1.9±0.6%) than those provided by the ^{124}I-PET.WN procedure (31.7%), resulting in a significant relative systematic underestimation (confidence interval -0.08 to -0.05; $p<0.001$) (Table 3, Fig. 3). The mean RAIU obtained with the ^{124}I-PET.MC (24.5±7.1%) showed an even clearer systematic relative underestimation (-7.2±2.4%) (confidence interval -0.28 to -0.23; $p<0.001$) (Table 3, Fig. 3) compared with ^{124}I-PET.WN (31.7±8.9%).

The above findings did not significantly depend on the levels of uptake ($p>0.05$) (Table 3).

Discussion

The superiority of low-activity ^{124}I-PET/low-dose CT in the functional-morphological assessment of the thyroid has been recently demonstrated (15) , however quantitative data concerning benign thyroid diseases are still limited. To date, only one small study has reported on intratherapy dosimetry with 30-40 MBq ^{124}I in patients undergoing radioiodine therapy (13). The present study, in contrast, was designed to assess the feasibility of ^{124}I–PET/CT in pretherapy dosimetry using a very limited dose of ^{124}I (1MBq), in comparison with conventional ^{131}I probe measurements.

In the present study, the mean percent iodine uptake 30 hours after administration of ^{131}I or ^{124}I was well comparable, at least with the ^{124}I–PET/CT.WN procedure, and showed moderate standard deviations. The results of the two methods (^{124}I–PET.WN and ^{131}I probe) were positively and significantly correlated, with no evidence of systematic over- or underestimations. Only in individual cases, however, there were noticeable relative deviations, possibly due to technical measurement errors, variable measuring distances, or insufficient attenuation correction in the case of ^{131}I measurements. Changes in thyroid status are also a possible explanation, although the lag between the measurements was short and the exclusion criteria were tightly checked. Although anamnestically ascertained, an iodine contamination also remains a possibility.

The intratherapy study of Eschmann et al. has found a similar positive correlation after simultaneous application of ^{124}I and ^{131}I (13). Furthermore the presented phantom study also showed that the influence of residual ^{131}I is marginal, especially since the activity of ^{131}I in the patients' thyroid 7 days after administration is considerably lower than 200 MBq of the phantom investigation.

Also, comparing pre- and intratherapy measurements with ^{131}I alone, Reinartz et al. have found a significant positive correlation between the ^{131}I uptake before and during radioiodine therapy, in both cases 24 and 48 hours after tracer administration (17).

An exact determination of the gland volume is of primary importance during the thyroid diagnostics and after radiotherapy (18, 19). Because PET and CT are both tomographic methods, their combination allows a VOI-based approach. Within this approach, a simultaneous assessment of partial volumes and corresponding activities is also possible, for example via threshold-based autocontour procedures (as the ^{124}I-PET.IC used in this study) or procedures based on manual contouring (as the ^{124}I-PET.MC used in this study).

Comparing the two contouring procedures (^{124}I-PET.IC and ^{124}I-PET.MC) with the whole-neck procedure (^{124}I-PET.WN), it became clear that ^{124}I-PET.IC and ^{124}I-PET.MC significantly underestimated the iodine uptake. The good correlation between the three procedures, on the other hand, is explained by the fact that the same data set was investigated.

The software used in this study (PMOD 3.407) allows a rapid and effective threshold-based contouring of tracer-enriched areas. In general, the isocontour assessments allow a clear delimitation of intra- and extra-thyroid activity, whereas probe measurements necessarily include neighboring structures, e.g. neck soft tissue and portions of the salivary glands. Accordingly, both the ^{124}I-PET.WN and the ^{131}I probe assessments resulted in higher RAIU levels, with a minimal relative overestimation possibly due to inclusion of extra-thyroid storage areas (Fig. 2).

Manual contouring of the thyroid along its anatomical boundaries in CT results in the calculation of correct volumes, however the time effort is considerable (20, 21). Nonetheless, CT-based volumetry is particularly meaningful in case of large goiters and/or retrosternal extensions not visible at sonography (20). An additional benefit is the simple and reliable assessment of neighboring structures, particularly the trachea (22).

Nuclear medicine imaging usually provides larger representations of the actual target areas, therefore contouring based on CT is expected to exclude a certain amount of activity. Accordingly, the present data show that the ^{124}I-PET.MC procedure systematically relatively underestimates the RAIU in comparison not only with the ^{131}I method but also with the ^{124}I-PET.WN and ^{124}I-PET.IC procedures. Thus, the ^{124}I-PET.MC procedure is suitable for valid volume estimation but insufficient for correct thyroid uptake determination.

According to the manufacture’s specifications the spatial resolution of the PET/CT scanner used in the present study was 7.5 mm for ^{124}I. The reasons for this performance are multiple, including not only the physical resolution of the PET but also the so-called positron range effect. Empiric data show that the mean positron range of ^{124}I in water is approximately 1.8-2.6 mm, clearly higher than for ^{18}F (0.6 mm) (6, 23-27). The differences in the positron range reside in the higher mean and maximal positron energy (603-1691 keV) of ^{124}I. In small target areas, the consecutively higher positron range can cause a decrease of measurement accuracy. For this reason, other investigators use the recovery coefficients (RC) as correction factor for tumor-like objects, e.g. metastases (28). Unpublished phantom investigations from our group, on the other hand, have shown that deviations are marginal in large volumes (20-200ml), thus a correction with RC was considered unnecessary in this study.

A relevant advantage of RAIU measurements via ^{124}I-PET/CT is the lower radiation exposure

compared with conventional ^{131}I probe measurement. In case of a thyroid uptake of 25%, the effective whole-body equivalent dose for 3 MBq ^{131}I is ~33 mSv and for 1 MBq ^{124}I only ~6.5 mSv (29). Also, only additional ~0.3 mSv derive from low-dose CT.

Although not a focus of this study, the use of ^{124}I-PET/CT for RAIU assessment in benign thyroid diseases has other potential advantages compared to conventional, independently performed ^{131}I probe measurement and neck ultrasound. First, the measuring distance does not substantially influence the measurement, and the simultaneously performed CT allows an accurate and reproducible attenuation correction (30). Second, the CT allows a parallel and reliable volumetry assessment – in contrast to ultrasound largely operator-independent – particularly useful in case of problematic anatomic variants (21). Third, the CT allows the inclusion of scintigraphically hypofunctional areas or retrosternal extensions, aspects that can largely influence the decision of whether radiotherapy or thyroidectomy is indicated (31). Finally, the ^{124}I-PET/CT allows also a fusion with ultrasound imaging, which – owing to a better soft-tissue contrast and higher resolution of the latter – can substantially contribute to the diagnosis (32). Even though these presented advantages are features of a number of available thyroid investigation techniques as well (e.g. ^{123}I-SPECT/CT, ultrasound plus planar scintigraphy) ^{124}I-PET/CT offers the possibility to combine all the above into one clinical workflow, thus reducing overall time effort.

The costs of pretherapy RAIU with ^{124}I-PET/CT seem at first high, especially if PET/CT technology is not already available at the site. If available, however, the costs can be substantially reduced by investigating several patients per day, since ^{124}I is usually obtained as a solution in larger quantities. At our institutions the price for ^{124}I per patient and investigation was 22 € (10 investigations with 1 MBq per day), compared to 17-19 € per patient for ^{131}I. Furthermore the ^{124}I-PET/CT scan itself requires little preparation, since the interval between administration and measurement is rather large in any scenario and the scan time is only 10 minutes. This allows a flexible time slot planning of short PET/CT investigations, especially in daytimes when PET/CT units are less frequented, e.g., early in the morning or late in the afternoon.

The present study has some clear limitations, first of all the small number of patients investigated. The second is the lack of comparison with intratherapy dosimetry, given the pilot intent of the investigations. Third, the results do not provide any kinetics information, since only one time point post tracer administration was investigated. A larger study with multiple time points and a valid intratherapy dosimetry are therefore warranted.

Conclusion

The present study shows that very low activities of ^{124}I – in addition to providing excellent diagnostic imaging – can be simply and efficiently used for pretherapy dosimetry in patients with benign thyroid disease. Also, ^{124}I-PET/CT allows the parallel assessment of RAIU and volume in one session, although none of the procedures applied in this study proved feasible in conveying both types of information. Other advantages can also be envisaged, for example higher measurement accuracy, volumetry of problematic anatomic variants, and fusion with ultrasound images. The present results need validation in a large prospective study, including fine correlation analyses with intratherapy dosimetry.

Acknowledgments

The authors thank GE Healthcare Buchler GmbH & Co KG for providing the test capsules. Furthermore we would like to thank Dr. Ernesta Palombo-Kinne for carefully and critically reviewing and translating the manuscript. Also we would like to extend our gratitude to Ms. Judith Biermann for her assistance in establishing the study protocol.

Figures

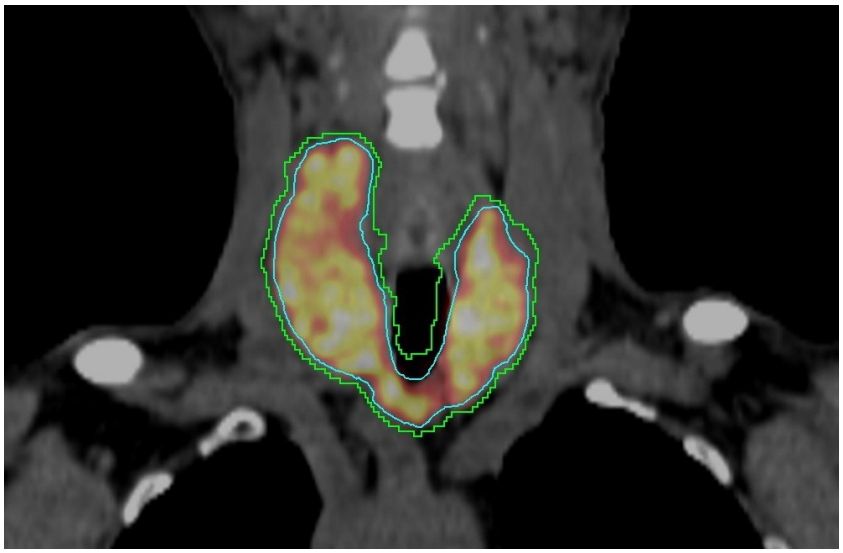

FIGURE 1. Screen capture of images obtained with the software PMOD (version 3.407) showing the ^{124}I-PET.WN (light blue) and the ^{124}I-PET.IC (green) procedures in a fused coronal reconstruction.

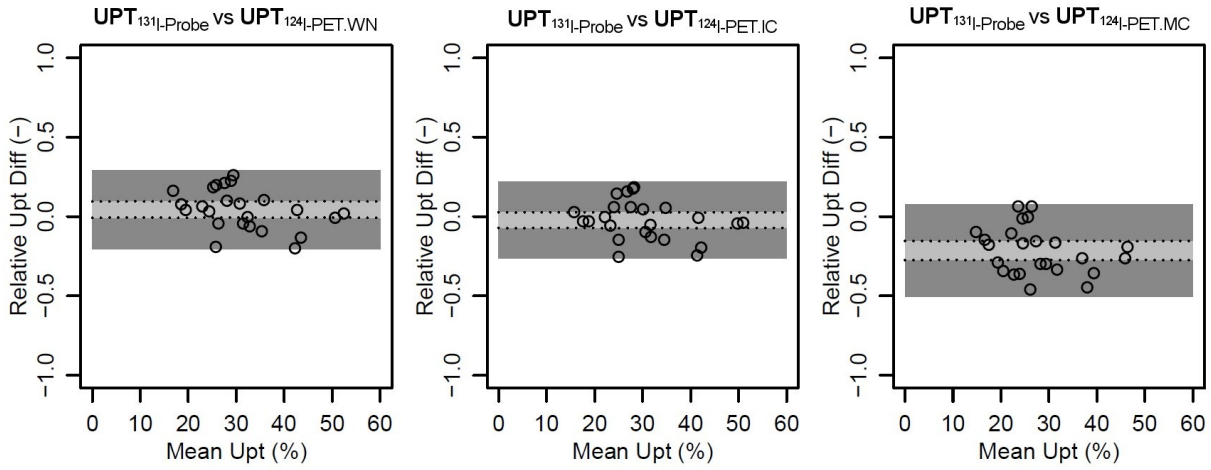

FIGURE 2. Modified Bland and Altman plots showing relative decay-corrected uptake (Upt) differences between conventional ^{131}I probe measurements and three ^{124}I-PET/CT volume-of-interest (VOI) procedures (^{124}I-PET.WN: whole neck; ^{124}I-PET.IC: isocontour; ^{124}I-PET.MC: manually contoured). The light grey areas indicate the 95% confidence interval of uptake differences. If the zero value is not included in the light grey area, the respective method shows a significant systematic overestimation or underestimation. Dark grey areas represent the limits of agreement (1.96-fold standard deviation) according to Bland and Altman.

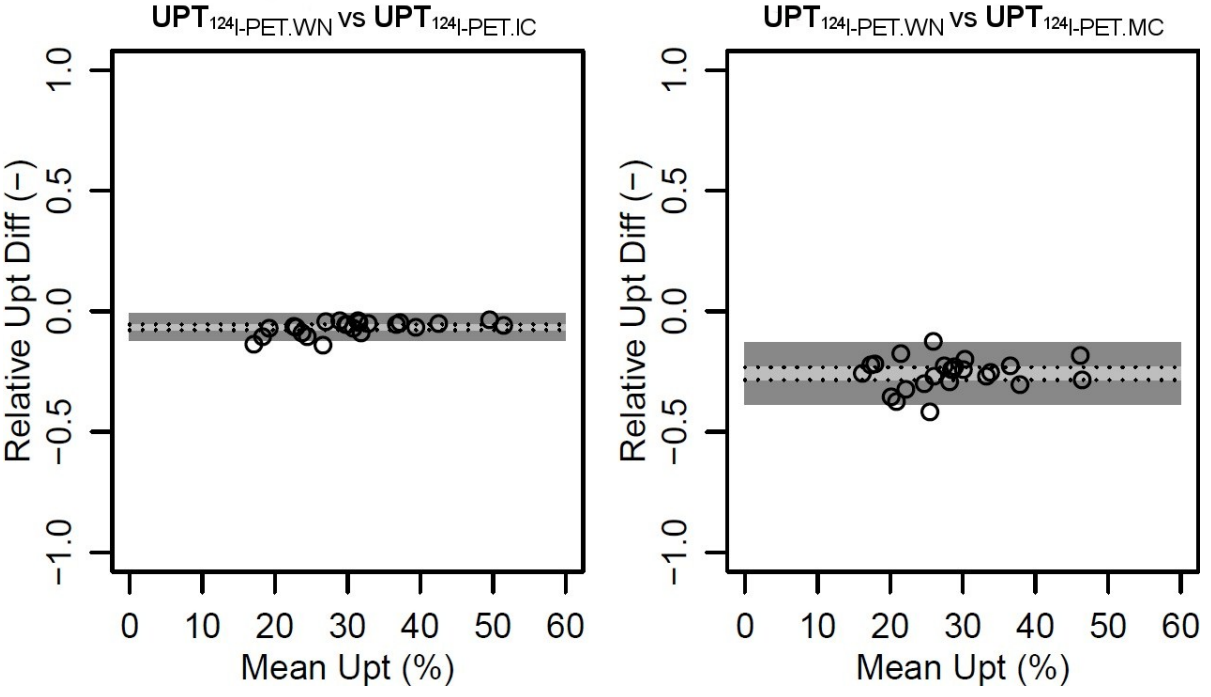

FIGURE 3. Modified Bland and Altman plots showing relative decay-corrected uptake (Upt) differences between three ^{124}I-PET/CT volume-of-interest (VOI) procedures (^{124}I-PET.WN: whole neck; ^{124}I-PET.IC: isocontour; ^{124}I-PET.MC: manually contoured). The light grey areas indicate the 95% confidence interval of mean uptake differences. If the zero value is not included in the light grey area, the respective method shows a significant systematic overestimation or underestimation. Dark grey areas represent the limits of agreement (1.96-fold standard deviation) according to Bland and Altmann.

Tables

TABLE 1 Phantom Study

Phantom	Measured ^{124}I Activity in kBq*	True ^{124}I Activity
^{131}I Background tank	11.91	0
^{124}I Cylinder	248.09	253.95
^{124}I Cylinder in ^{131}I background tank	241.02	253.04

*as measured in PET/CT, true activities were corrected for physical decay (4.176 days) between activimetric control and PET/CT scan

TABLE 2 Patient characteristics

Characteristic	Value	
Age, years	Median (range)	70 (49 - 77)
	Mean ± SD	69.0 ± 7.5
Females, n (%)		18 (75%)
Thyroid disorder, n (%)	Unifocal autonomy	4 (16.7%)
	Multifocal autonomy	13 (54.2%)
	Non-toxic goiter	7 (29.2%)
Thyroid volume, ml	Median (range)	68 (31 - 204)
	Mean ± SD	74 ± 37
TSH, mU/ml	Median (range)	
	before ^{131}I	0.33 (0.01-2.86)
	before ^{124}I	0.33 (0.01-2.71)
	Mean ± SD	
	before ^{131}I	0.46 ± 0.56
	before ^{124}I	0.47 ± 0.55

TABLE 3 Statistical analyses of relative decay-corrected uptake differences

	^{131}I probe vs ^{124}I-PET.WN†	^{131}I probe vs ^{124}I-PET.IC‡	^{131}I probe vs ^{124}I-PET.MC§	^{124}PET.WN vs ^{124}PET.IC	^{124}PET.WN vs ^{124}PET.MC
Upper limit of agreement	0.29	0.22	0.08	-0.01	-0.13
Upper limit of CI*	0.09	0.03	-0.15	-0.05	-0.23
Mean	0.04	-0.02	-0.21	-0.07	-0.26
Lower limit of CI	-0.01	-0.07	-0.27	-0.08	-0.28
Lower limit of agreement	-0.21	-0.26	-0.51	-0.12	-0.39
Median	0.04	-0.03	-0.23	-0.06	-0.25
Standard deviation	0.13	0.12	0.15	0.03	0.07
Correlation coefficient	0.93	0.93	0.90	1.00	0.98
p value (correlation)	<0.001	<0.001	<0.001	<0.001	<0.001
p value (ANOVA)	>0.05	>0.05	>0.05	>0.05	>0.05

*CI: confidence interval; †WN: whole neck; ‡IC: isocontour; §MC: manually contoured

References

1. Wang C, Crapo LM 1997 The epidemiology of thyroid disease and implications for screening. Endocrinol Metab Clin North Am 26:189-218

2. Silberstein EB, Alavi A, Balon HR, Clarke SE, Divgi C, Gelfand MJ, Goldsmith SJ, Jadvar H, Marcus CS, Martin WH, Parker JA, Royal HD, Sarkar SD, Stabin M, Waxman AD 2012 The SNMMI practice guideline for therapy of thyroid disease with 131I 3.0. J Nucl Med 53:1633-1651

3. Lassmann M, Chiesa C, Flux G, Bardies M 2011 EANM Dosimetry Committee guidance document: good practice of clinical dosimetry reporting. Eur J Nucl Med Mol Imaging 38:192-200

4. Dietlein M, Dressler J, Eschner W, Lassmann M, Leisner B, Reiners C, Schicha H, Deutsche Gesellschaft fur N, Deutsche Gesellschaft fur Medizinische P 2007 [Procedure guideline for radioiodine test (Version 3)]. Nuklearmedizin 46:198-202

5. Hanscheid H, Canzi C, Eschner W, Flux G, Luster M, Strigari L, Lassmann M 2013 EANM Dosimetry Committee Series on Standard Operational Procedures for Pre-Therapeutic Dosimetry II. Dosimetry prior to radioiodine therapy of benign thyroid diseases. Eur J Nucl Med Mol Imaging 40:1126-1134

6. Pentlow KS, Graham MC, Lambrecht RM, Daghighian F, Bacharach SL, Bendriem B, Finn RD, Jordan K, Kalaigian H, Karp JS, Robeson WR, Larson SM 1996 Quantitative imaging of iodine-124 with PET. J Nucl Med 37:1557-1562

7. Ott RJ, Batty V, Webb BS, Flower MA, Leach MO, Clack R, Marsden PK, McCready VR, Bateman JE, Sharma H, et al. 1987 Measurement of radiation dose to the thyroid using positron emission tomography. Br J Radiol 60:245-251

8. Sgouros G, Kolbert KS, Sheikh A, Pentlow KS, Mun EF, Barth A, Robbins RJ, Larson SM 2004 Patient-specific dosimetry for 131I thyroid cancer therapy using 124I PET and 3-dimensional-internal dosimetry (3D-ID) software. J Nucl Med 45:1366-1372

9. Phan H, Jager P, Paans A, Plukker J, Sturkenboom M, Sluiter W, Wolffenbuttel B, Dierckx R, Links T 2008 The diagnostic value of 124I-PET in patients with differentiated thyroid cancer. Eur J Nucl Med Mol Imaging 35:958-965-965

10. Jentzen W, Freudenberg L, Eising EG, Sonnenschein W, Knust J, Bockisch A 2008 Optimized 124I PET dosimetry protocol for radioiodine therapy of differentiated thyroid cancer. J Nucl Med 49:1017-1023

11. Hobbs RF, Wahl RL, Lodge MA, Javadi MS, Cho SY, Chien DT, Ewertz ME, Esaias CE, Ladenson PW, Sgouros G 2009 124I PET-based 3D-RD dosimetry for a pediatric thyroid cancer patient: real-time treatment planning and methodologic comparison. J Nucl Med 50:1844-1847

12. Freudenberg LS, Jentzen W, Stahl A, Bockisch A, Rosenbaum-Krumme SJ 2011 Clinical applications of 124I-PET/CT in patients with differentiated thyroid cancer. Eur J Nucl Med Mol Imaging 38 Suppl 1:S48-56

13. Eschmann SM, Reischl G, Bilger K, Kupferschlager J, Thelen MH, Dohmen BM, Besenfelder H, Bares R 2002 Evaluation of dosimetry of radioiodine therapy in benign and malignant thyroid disorders by means of iodine-124 and PET. Eur J Nucl Med Mol Imaging 29:760-767

14. Dietlein M, Dressler J, Grunwald F, Leisner B, Moser E, Reiners C, Schicha H, Schneider P, Schober O 2007 [Guideline for radioiodine therapy for benign thyroid diseases (version 4)]. Nuklearmedizin 46:220-223

15. Darr AM, Opfermann T, Niksch T, Driesch D, Marlowe RJ, Freesmeyer M 2013 Low-activity 124I-PET/low-dose CT versus 99mTc-pertechnetate planar scintigraphy or 99mTc-pertechnetate single-photon emission computed tomography of the thyroid: a pilot comparison. Clin Nucl Med 38:770-777

16. Bland JM, Altman DG 1986 Statistical methods for assessing agreement between two methods of clinical measurement. Lancet 1:307-310

17. Reinartz P, Zimny M, Schaefer W, Mueller B, Buell U, Sabri O 2003 Radioiodine therapy in patients with hyperthyroid disorder: standard versus dosimetric activity application. Nucl Med Commun 24:1247-1253

18. Reinartz P, Sabri O, Zimny M, Nowak B, Cremerius U, Setani K, Bull U 2002 Thyroid volume measurement in patients prior to radioiodine therapy: comparison between three-dimensional magnetic resonance imaging and ultrasonography. Thyroid 12:713-717

19. van Isselt JW, de Klerk JM, van Rijk PP, van Gils AP, Polman LJ, Kamphuis C, Meijer R, Beekman FJ 2003 Comparison of methods for thyroid volume estimation in patients with Graves' disease. Eur J Nucl Med Mol Imaging 30:525-531

20. Hermans R, Bouillon R, Laga K, Delaere PR, Foer BD, Marchal G, Baert AL 1997 Estimation of thyroid gland volume by spiral computed tomography. Eur Radiol 7:214-216

21. Nygaard B, Nygaard T, Court-Payen M, Jensen LI, Soe-Jensen P, Gerhard Nielsen K, Fugl M, Hegedus L 2002 Thyroid volume measured by ultrasonography and CT. Acta Radiol 43:269-274

22. Shin JJ, Grillo HC, Mathisen D, Katlic MR, Zurakowski D, Kamani D, Randolph GW 2011 The surgical management of goiter: Part I. Preoperative evaluation. The Laryngoscope 121:60-67

23. Gregory RA, Hooker CA, Partridge M, Flux GD 2009 Optimization and assessment of quantitative 124I imaging on a Philips Gemini dual GS PET/CT system. Eur J Nucl Med Mol Imaging 36:1037-1048

24. Herzog H, Tellman L, Qaim SM, Spellerberg S, Schmid A, Coenen HH 2002 PET quantitation and imaging of the non-pure positron-emitting iodine isotope 124I. Appl Radiat Isot 56:673-679

25. Jentzen W, Weise R, Kupferschlager J, Freudenberg L, Brandau W, Bares R, Burchert W, Bockisch A 2008 Iodine-124 PET dosimetry in differentiated thyroid cancer: recovery coefficient in 2D and 3D modes for PET(/CT) systems. Eur J Nucl Med Mol Imaging 35:611-623

26. Robinson S, Julyan PJ, Hastings DL, Zweit J 2004 Performance of a block detector PET scanner in imaging non-pure positron emitters--modelling and experimental validation with 124I. Phys Med Biol 49:5505-5528

27. Vandenberghe S 2006 Three-dimensional positron emission tomography imaging with 124I and 86Y. Nucl Med Commun 27:237-245

28. Jentzen W, Freudenberg L, Bockisch A 2011 Quantitative imaging of (124)I with PET/ CT in pretherapy lesion dosimetry. Effects impairing image quantification and their corrections. The quarterly journal of nuclear medicine and molecular imaging : official publication of the Italian Association of Nuclear Medicine 55:21-43

29. 1975 Summary of Current Radiation Dose Estimates to Humans from 123I, 124I, 125I, 126I, 130I, 131I, and 132I as Sodium Iodide. J Nucl Med 16:857-860

30. Kinahan PE, Townsend DW, Beyer T, Sashin D 1998 Attenuation correction for a combined 3D PET/CT scanner. Med Phys 25:2046-2053

31. Shah PJ, Bright T, Singh SS, Lang CM, Pyragius MD, Malycha P, Edwards JR 2006 Large retrosternal goitre: a diagnostic and management dilemma. Heart Lung Circ15:151-152

32. Guehne F, Winkens T, Mothes H, Freesmeyer M 2013 Differential Diagnosis of Thyroid Nodules via Real-time PET/Ultrasound (US) Fusion in a Case of Co-existing Medullary Thyroid Cancer and Adenoma. J Clin Endocr Metab

3.1. ^{124}Iod-Niedrigaktivitäts-PET/Niedrigdosis-CT (^{124}Iod-PET/CT) der Schilddrüse

3.1.3..Schwellwertbasierte Volumetrie der Schilddrüse mit ^{124}Iod-PET

Time Efficient Low-activity ^{124}I-PET Volumetry in Benign Thyroid Disorders by Automatic Isocontour Procedures: Mathematic Adjustment Using Manual Contoured Measurements in Low-dose CT

Publikation in ANNALS OF NUCLEAR MEDICINE, accepted 04.09.2014

Time Efficient Low-activity ^{124}I-PET Volumetry in Benign Thyroid Disorders by Automatic Isocontour Procedures: Mathematic Adjustment Using Manual Contoured Measurements in Low-dose CT

Julian G Westphal, Christian Kühnel, Martin Freesmeyer

From the Clinic of Nuclear Medicine, University Hospital of the University of Jena, Jena, Germany (J.G.W., C.K., M.F.); and Ernst-Abbe-Fachhochschule Jena, University of Applied Sciences, Jena, Germany (C.K.).

Corresponding author:

Dr. Martin Freesmeyer, Clinic of Nuclear Medicine, Jena University Hospital
Bachstrasse. 18, 07740 Jena, Germany
Phone: +49-3641-933220; Fax: +49-3641-933244
E-Mail: martin.freesmeyer@med.uni-jena.de

Type of Manuscript: Technical Developments

Acknowledgements:

The authors are grateful to Mr. Dominik Driesch (Biocontrol Jena, Jena, Germany) for statistical work, and careful examination of the data presented in this publication

Advances in knowledge

1. An automatic isocontour (IC) procedure has been developed for time efficient ^{124}I-PET volumetry in patients with benign thyroid disorders.
2. Using a low threshold (0.2 kBq/ml) makes the method applicable to over 90% of the patients examined.
3. In this patient population a median relative error of 9.0% from the reference occurred.

Implications for patient care

1. The methods will speed-up pre-therapeutic evaluation of thyroid gland volume in patients with benign thyroid disorders scheduled for radioiodine therapy.
2. In general, ^{124}I-PET/CT can not only provide dosimetric and morphological information of the thyroid, but also, largely, observer independent volumetric data from a single examination.
3. Radiation exposure is lower compared to standard ^{131}I evaluation methods, in pretherapeutic dosimetry.

Summary statement

We show that IC volumetry is a simple and rapid method for thyroid gland volume calculation, applicable to over 90% patients within a clinically acceptable error rate.

Abstract

Purpose

The aim of this study was to develop a simple and rapid threshold based isocontour delineation method for thyroid volumetry from Low-activity ^{124}Iodine Positron Emission Tomography/Low-dose Computed Tomography (^{124}I-PET/CT) data to speed up and simplify pre-therapy assessment of patients scheduled for radioiodine therapy.

Materials and Methods

^{124}I-PET/CT data from 45 patients (13 men and 32 women; mean age 67.6 ± 8.8) were analysed 30 hours after 1MBq ^{124}I administration. This was a pilot subgroup analysis of a larger study approved by the institutional review board and by the responsible authority of radiation protection. All participants signed a written informed consent. Anatomical reference volume was calculated using manually contoured (MC) data from low-dose CT images of the neck. In addition, we applied an automatic isocontour delineation method ($IC_{0.2/1.0}$), with two threshold values (0.2 and 1.0 kBq/ml), for volumetry of the PET data-set. Significant $IC_{0.2/1.0}$ shape aberrations from thyroid margins compared to low-dose CT e.g. due to cysts or calcifications lead to exclusion. Subsequently, a mathematical correlation ($mIC_{0.2/1.0}$), between $IC_{0.2/1.0}$ and MC, was established.

Results

Data from 41 patients ($IC_{0.2}$), and 32 patients ($IC_{1.0}$) were analysed. The mathematically calculated volume, mIC, showed a median deviation from MC, of ±9% (1%-54%) for $mIC_{0.2}$, and of ± 8.2% (1%-50%) for $mIC_{1.0.}$

Conclusion

Contour delineation with both, $mIC_{1.0}$ and $mIC_{0.2}$ gave rapid and reliable results. However, $mIC_{0.2}$ can be applied to significantly more patients (>90%).

Introduction

A recent study showed that Low-activity ^{124}Iodine Positron Emission Tomography/Low-dose Computer Tomography (^{124}I-PET/CT) provides more information when characterising internal structures, especially thyroid nodules, and analysing their spatial relationship with neighbouring structures, like trachea, or the gland's retrosternal portion (1). Furthermore, the possibility to use PET/Ultrasound fusion imaging, following ^{124}I-PET/CT, is advantageous as it expands diagnostic capability (2).

Precise thyroid volume estimation is a crucial step in pre-therapeutic evaluation since it helps select the therapeutic approach, and monitors treatment course (3, 4). Over the past decades, ultrasonography has become well established for thyroid imaging in the clinical routine. Thyroid lobe volume estimations are carried out using the ellipsoid model. However, pre-therapeutic evaluation results are inaccurate for drastically enlarged and/or abnormally shaped glands (5). Furthermore, accessibility to the gland's retrosternal portion is limited during sonography (6), and intra- and inter-observer variations are high (5, 7).

CT is an alternate method to estimate gland volume. However, patients are exposed to radiation (8). Apart from the ellipsoid model, volume can be estimated by extracting contours manually, slice-by-slice, using Low-dose CT (ldCT) and 3D-ultrasound data-sets (9). However, it is time consuming, and hardly compatible with routine clinical work (10). Although a software-based, time-saving, automatic contour delineation method was demonstrated for the thyroid gland, it is not routinely applicable, especially for abnormal glands containing cysts, calcifications or nodules with different sonographic characteristics (11). An alternative is PET, which allows automatic (metabolic) organ volume calculations, and identifying other pathologies using thresholding operations (isocontour delineation) (12-15). Applying this approach for ^{124}I thyroid gland examinations is potentially promising due to a regular high Target-Background-Ratio.

This study aimed to develop a simple and time-efficient algorithm for calculating thyroid volume from ^{124}I-PET/CT. For this, we formulated a mathematical model, correlating reference volume, of manually extracted contours from ldCT data-sets, with that derived from automatic, threshold-based isocontour delineation from ^{124}I-PET/CT data-sets.

Materials and Methods

Patients

Subjects included 45 patients with benign thyroid disease (See Table 1 for patient characteristic details). This was a pilot subgroup analysis of a larger study approved by the institutional review board and by the authority responsible for radiation protection. All participants signed a written informed consent.

Radionuclide preparation and administration

^{124}I-Sodium solution (IBA Molecular, BV Cyclotron VU, Amsterdam, The Netherlands), in a sodium-phosphate carrier, was pipetted into commercially available oral administration capsules, under sterile conditions (HGK, size 3; GE Healthcare, Buchler GmbH&CO KG). Capsule activity was measured

with a Dose Calibrator (Isomed 2010, MED Nuklear-Medizintechnik Dresden GmbH, Dresden, Germany). Patients fasted for ≥10 hours prior to oral capsule administration, and consumed 1L water within 2 hours. Food intake was allowed after 2 hours.

^{124}I-Low-Activity-PET/Low-Dose CT

^{124}I-PET/CT scan data was obtained following established protocols, on a Biograph mCT 40 scanner (Siemens, Erlangen, Germany) (1). For measurements, patients lay on their backs with a 21.6 cm cranio-caudal field-of-view. One PET scan bed position covered the entire neck region, the oral diaphragm and upper thorax. PET scan duration was 10 minutes. Low-dose CT (30 mA, 120 kV) was used for anatomical co-registration, and attenuation correction. All images were reconstructed with a slice thickness of 3mm. CT radiation exposure was ~ 0.3 mSv. All patients were imaged exactly 30 hours after radionuclide administration.

Data analysis

Data-sets were analysed using PMOD 3.407 software (PMOD Technologies Ltd., Zürich, Switzerland), case-by-case, supervised by a physician with 16 years radiology and 9 years nuclear medicine experience. Since a gold standard was not available, thyroid volume references were obtained by manual, slice-by-slice contoured measurements from the low-dose CT data-set. Manual contouring (MC) was done blinded, thrice, on different days to correct for intra-observer variation, and the average subsequently analysed.

Empirically found threshold values of 0.2 kBq/ml ($IC_{0.2}$) and 1 kBq/ml ($IC_{1.0}$), were used for automatic contouring from the PET data-set via a 3D-isocontour-VOI. The lower threshold value was established by measuring the parathyroid background value (average activity concentration: 0.089 ±0.042 kBq/ml). Approximately twice this activity concentration was chosen for reliably separating active thyroid tissue from surrounding tissue. The higher threshold value was defined as ~10-times the average background concentration (Fig.1). Using the 'No Inner Hole' and 'No Multi-Region' software options, prevented empty spaces caused by areas of low or no metabolism, and accidental artefact inclusion from either the scan edge, or unspecific extra-thyroidal activity. Due to the software's inability to recognise hypo-functional areas at the edge of the thyroid gland, special attention was paid to erroneous contouring of the affected areas; mostly depicted as concaves in the IC-VOI. For this, we visually compared the shapes in the ldCT and the PET/ldCT fusion image. A mismatch of more than 1.0 cm, between IC-contour and morphological CT-shape, in at least one of the three standard planes (coronal, axial, sagittal), was defined as the exclusion criterion. Finally, VOI activity (measured in kBq) was also determined.

Statistics

A multiple linear regression model (ANOVA), with step-wise, non-significant variable elimination, was applied to both IC variants. First, two independent variables (volume and activity), and the possibility of a y-axis variable intersection point were included. Second, volume data was fitted by eliminating the least significant variables until the remaining reached a significance of $p<0.05$. All statistical calculations were undertaken using R (R Development Core Team, R Foundation for Statistical Computing, Vienna Austria, 2013).

Results

^{124}I-PET scans were obtained, on average, 30.16 ±0.35 hours post nuclide administration. CT data volume was calculated for all 45 patients using MC, and a mean volume of 65.1 ±32.4 ml was found (Table 1). The derived 3D-VOIs had an average activity of 200.2 ±69.8 kBq. We found that peripheral hypo-functional areas (calcifications, cysts, nodules) were not included in the IC-VOI in 4 $IC_{0.2}$ patients and 13 $IC_{1.0}$ patients. Hence, IC analysis was undertaken in 41 $IC_{0.2}$ patients and 32 $IC_{1.0}$ patients. Mean metabolic thyroid volumes were 122.8 ±39.0 ml ($IC_{0.2}$) and 64.0 ±15.64 ml ($IC_{1.0}$), with an average activity of 242.4 ±69.1 kBq ($IC_{0.2}$) and 226.56 ±117.7 kBq ($IC_{1.0}$) (Table 2). Regression analysis of volumes (Fig. 2a/2c), gave coefficients (R) of 0.93 (MC versus $IC_{0.2}$) and 0.86 (MC versus $IC_{1.0}$). IC volumes were mathematically fitted based on the MC data ($mIC_{0.2/1.0}$) (Fig. 2b, d). $mIC_{1.0}$ data analysis showed that activity and IC volume had multifactorial influences on the calculated $mIC_{1.0}$ volume. In contrast, they did not influence $IC_{0.2}$ data, although associations with a significant offset value (Table 2) were seen. Fitted mIC volume regression analysis (Fig. 2b, d) gave R values of 0.93 (MC versus $mIC_{0.2}$) and 0.96 (MC versus $mIC_{1.0}$). The median relative deviations of the modified volumes from the MC volume were 9.0% (1%-54%) (MC versus $mIC_{0.2}$) and 8.2% (1%-50%) (MC versus $mIC_{1.0}$).

Discussion

A rapid and simple method to measure thyroid volume, using ^{124}I-PET data-sets, in benign thyroid disease patients can speed-up routine pre-therapeutic analysis, and make it observer independent. To address this, we developed an automatic isocontour delineation procedure that uses two different thresholds.

Automatic contouring of section image data sets is more time-efficient than manual contouring, in the clinical routine (14). However, in PET scan images, activity area contours are usually fuzzy. This phenomenon is particularly prominent in ^{124}I applications due to the high energy (1535 to 2138 keV) of emitted positrons, and their far range (1.8-2.6 mm). Furthermore, the complex decay of the isotope, with prompt gamma photon emission, and the resulting random coincidences play an important role(16).

Our results show that a high degree of equivalence, between the IC and reference volumes (ldCT), can be achieved with an isocontour threshold of 1.0 kBq/ml ($IC_{1.0}$). However, this was not applicable to 29% (13/45) patients with large, calcified, and/or cystic thyroid glands. This is because, in contrast to CT, low or no activity image areas were not included in the PET-$IC_{1.0}$ scan image isocontouring. For the method to be applicable to a majority of patients, selecting a low threshold was necessary. Our strategy to use a 0.2 kBq/ml threshold ($IC_{0.2}$), which is approximately twice the parathyroidal background value, made it possible to include 91% (41/45) patients. However, as this lead to volume overestimations, a mathematical correction of the results was necessary. The mathematical fitting procedure used here shows that the activity within the $IC_{1.0}$ contour is a significant, independent influencing variable. This is not the case for $IC_{0.2}$, although it is not clear whether this relationship is possibly just masked by significant offset influence. Furthermore, large thyroid glands could not be included in $IC_{1.0}$ analysis as it limits direct comparison of the two methods. However, with median deviations of <10% the two models (Fig. 2b,d), were applicable to the respective patient samples. A user-friendly and time-efficient deployment of these mathematical procedures, in day-to-day clinical

routines, is possible either using templates in standard software, or by direct implementation into specific imaging software. Finally, due to its applicability to >90% patients, it is more sensible to implement $IC_{0.2}$ rather than $IC_{1.0}$.

We believe, only one publication to-date has addressed the issue of ^{124}I-PET-based volumetry for benign thyroid disease (17). In this study, a small patient sample with Graves' disease, and only moderately enlarged thyroid glands, was examined, using comparatively higher-activity ^{124}I (15 MBq), a coincidence camera ("camera PET") and B-mode ultrasound reference. A similar high linear correlation (0.83) was found between the two methods, in agreement with our results. However, a direct comparison of the two studies is not possible, due to large differences in patient composition, techniques employed, and data analysis.

Our method offers numerous advantages for routine clinical use in patients with benign thyroid disorders scheduled for radioiodine therapy, and saves considerable time compared to ldCT (MC). First, MC takes 15 to 20 minutes to complete, and is dependent on organ size, and therefore number of CT slices. In contrast, IC, with mathematical correction, only takes ~3 minutes, and is organ size independent. Second, IC has high observer-independent accuracy, due to the fully computer-based method execution. Hence, specifically trained mid-level staff can execute the procedure, with only the final judgment, on whether the IC-VOI covers the thyroid volume sufficiently, left to an experienced consultant. Third, per patient cost is moderate due to the use of low-activity (1 MBq) and long half-life, ^{124}I (1). Finally, in pretherapeutic dosimetry overall patient radiation exposure is lower (~6.8mSv) compared to other standard tests with 3 MBq ^{131}I (~33mSv) (18).

A limitation of our study was the low number of patients, since it was a pilot study. Also, median errors of 8.2% ($IC_{1.0}$) and 8.9% ($IC_{0.2}$) were found, despite the applied multi-factorial correction. However, in our institution, errors of up to 10% are acceptable in clinical routine. A "real" gold standard was not available, hence MC volume data served as the clinical standard. The ldCT protocol used in these data-sets led to artefacts, particularly caudally and retrosternally, that made it difficult to visually delineate organ boundaries in some patients (19). The exact contribution of this ldCT error, to the overall error, cannot be estimated. To minimise this, MC measurements were undertaken thrice, and its mean was used as reference. Despite the very low threshold ($IC_{0.2}$), 9% (4/45) patients could not be analysed. However, most commercial PET software solutions have options for manually correcting parts of the isocontour VOI by visually comparing them to the ldCT in a fusion image. Finally, the results and mathematical correlations presented here are dependent on the equipment and imaging protocols used. Transferability of our method to other PET/CT devices, activities, and scan intervals, needs to be determined.

In summary**, we show that IC volumetry is a simple and rapid method for thyroid gland volume calculation, applicable to over 90% patients within a clinically acceptable error rate.** In addition, besides dosimetry, the pre-therapeutic radioiodine test with ^{124}I also allows for superior functional topography, morphological CT correlation, ultrasound image fusion, and time efficient PET-based organ volumetry. However, our approach may not be easily transferrable to other test protocols; hence this needs to be tested in other settings and equipment. Future directions point towards additional prospective studies with larger patient samples, and developing methods to overcome the outlined limitations.

Disclosure of Conflict of interest:

The authors do not have any relevant conflicts of interest to disclose.

References

1. Darr AM, Opfermann T, Niksch T, Driesch D, Marlowe RJ, Freesmeyer M. Low-activity 124I-PET/low-dose CT versus 99mTc-pertechnetate planar scintigraphy or 99mTc-pertechnetate single-photon emission computed tomography of the thyroid: a pilot comparison. Clin Nucl Med. 2013;38(10):770-7.

2. Guehne F, Winkens T, Mothes H, Freesmeyer M. Differential Diagnosis of Thyroid Nodules via Real-time PET/Ultrasound (US) Fusion in a Case of Co-existing Medullary Thyroid Cancer and Adenoma. J Clin Endocr Metab. 2013.

3. Reinartz P, Sabri O, Zimny M, et al. Thyroid volume measurement in patients prior to radioiodine therapy: comparison between three-dimensional magnetic resonance imaging and ultrasonography. Thyroid. 2002;12(8):713-7.

4. van Isselt JW, de Klerk JM, van Rijk PP, et al. Comparison of methods for thyroid volume estimation in patients with Graves' disease. Eur J Nucl Med Mol Imaging. 2003;30(4):525-31.

5. Rago T, Bencivelli W, Scutari M, et al. The newly developed three-dimensional (3D) and two-dimensional (2D) thyroid ultrasound are strongly correlated, but 2D overestimates thyroid volume in the presence of nodules. J Endocrinol Invest. 2006;29(5):423-6

6. Shah PJ, Bright T, Singh SS, et al. Large retrosternal goitre: a diagnostic and management dilemma. Heart Lung Circ. 2006;15(2):151-2.

7. Ozgen A, Erol C, Kaya A, Ozmen MN, Akata D, Akhan O. Interobserver and intraobserver variations in sonographic measurement of thyroid volume in children. Eur J Endocrinol. 1999;140(4):328-31.

8. Nygaard B, Nygaard T, Court-Payen M, et al. Thyroid volume measured by ultrasonography and CT. Acta Radiol. 2002;43(3):269-74.

9. Péria O, Chevalier L, François-Joubert A, Caravel J-P, Dalsoglio S, Lavallée S, et al. Using a 3D Position Sensor for Registration of SPECT and US Images of the Kidney. In: Ayache N, editor. Comput. Vis. Virtual Real. Robot. Med. [Internet]. Springer Berlin Heidelberg; 1995. p. 23–9. Available from: http://dx.doi.org/10.1007/978-3-540-49197-2_3

10. Schlogl S, Werner E, Lassmann M, et al. The use of three-dimensional ultrasound for thyroid volumetry. Thyroid. 2001;11(6):569-74.

11. Kollorz EK, Hahn DA, Linke R, Goecke TW, Hornegger J, Kuwert T. Quantification of thyroid volume using 3-D ultrasound imaging. IEEE Trans Med Imaging. 2008;27(4):457-66.

12. Chen A, Niermann KJ, Deeley MA, Dawant BM. Evaluation of multiple-atlas-based strategies for segmentation of the thyroid gland in head and neck CT images for IMRT. Phys Med Biol. 2012;57(1):93-111.

13. Hofheinz F, Potzsch C, Oehme L, et al. Automatic volume delineation in oncological PET. Evaluation of a dedicated software tool and comparison with manual delineation in clinical data sets. Nuklearmedizin. 2012;51(1):9-16.

14. Prieto E, Lecumberri P, Pagola M, et al. Twelve automated thresholding methods for segmentation of PET images: a phantom study. Phys Med Biol. 2012;57(12):3963-80.

15. Zhang T, Tachiya Y, Sakaguchi Y, et al. Phantom study on three-dimensional target volume delineation by PET/CT-based auto-contouring. Fukuoka igaku zasshi. 2010;101(11):238-46.

16. Jentzen W, Freudenberg L, Bockisch A. Quantitative imaging of (124)I with PET/ CT in pretherapy lesion dosimetry. Effects impairing image quantification and their corrections. Q J Nucl Med Mol Imaging. 2011;55(1):21-43.

17. Crawford DC, Flower MA, Pratt BE, et al. Thyroid volume measurement in thyrotoxic patients: comparison between ultrasonography and iodine-124 positron emission tomography. Eur J Nucl Med. 1997;24(12):1470-8.

18. Summary of Current Radiation Dose Estimates to Humans from 123I, 124I, 125I, 126I, 130I, 131I, and 132I as Sodium Iodide. J Nucl Med. 1975;16(9):857-60.

19. Gnannt R, Winklehner A, Goetti R, Schmidt B, Kollias S, Alkadhi H. Low kilovoltage CT of the neck with 70 kVp: comparison with a standard protocol. AJNR Am J Neuroradiol. 2012;33(6):1014-9.

Table 1 Patients

Paramter	Value	Median (Minimum-Maximum)	Mean ± Standard Deviation OR Percentage
Age, years		69 (44-89)	67.6 ± 8.8
Women, n (%)			32 (71%)
Thyroid disorder, n (%)	Goiter		
	Without nodules		13 (29%)
	One nodule		10 (22%)
	Multiple nodules		22 (49%)
	Toxic*		32 (71%)
Thyroid gland volume MC†, ml		58.7 (25,1-203,5)	66.03 ± 32.83
Administered ^{124}I-acitivity, MBq		1.01 (0.96 - 1.18)	1.02 ± 0.04
Time between ^{124}I administration and PET-Scan, h		30.05 (29.68-32.08)	30.16 ± 0.35
TSH, mIU/l		0.31 (0.01 - 2.71)	0.53 ± 0.64
fT3, pmol/l		4.69 (3.22 - 15.08)	5.03 ± 1.87
fT4, pmol/l		13.28 (10.87 - 28.92)	14.62 ± 3.42

*Thyroid disease was classified as toxic when serum TSH < 0.25 mIU/L

† MC: Manual contour delineation; Volumes shown are derived from the manually extracted ldCT data-sets.

Table 2 Comparison of isocontoured ^{124}I PET based volumetry

Parameter	Value	
	$IC_{0.2}$	**$IC_{1.0}$**
Patients included, n (%)	41 (91%)	32 (71%)
Patients excluded, n (%)	4 (9%)	13 (29%)
Volume Mean ± Std Dev., ml	122.8 ± 39.0	64.0 ± 15.64
Activity Mean ± Std Dev., kBq	242.4 ± 69.1	226.56 ± 117.7
Activity/Volume Mean ± Std Dev., kBq/ml	2.15 ± 0.72	3.65 ± 1.08
Independent variables, order of elimination/p-value*		
Offset	- / 0.0425	1 / 0.7265
Activity (IC)	1 / 0.8756	- / 0.0045
Volume (IC)	- / <0.001	- / <0.001

*p-value at the time point of elimination, or for the inclusion into the final model Figure Captions:

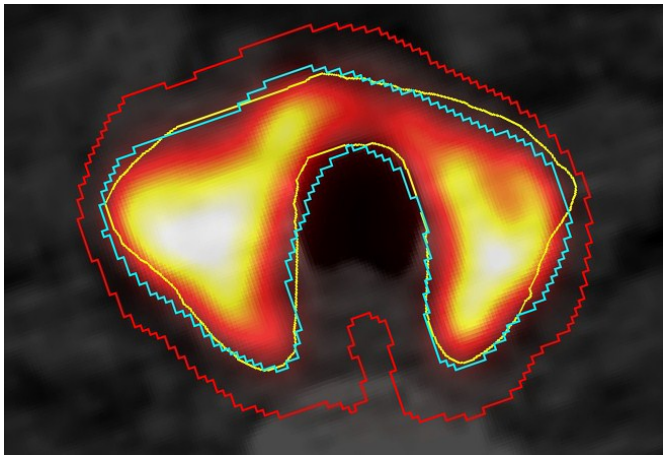

Figure 1: Axial section of a fused ^{124}I-PET/CT image (reconstructed with PMOD Version 3.407), showing $IC_{0.2}$ (red tracing), $IC_{1.0}$ (light blue tracing), and MC (yellow tracing). This shows a clear overestimation of actual volume with low threshold ($IC_{0.2}$). Also seen, is the high degree of match of MC volume (red tracing) with high threshold ($IC_{1.0}$) (light blue tracing).

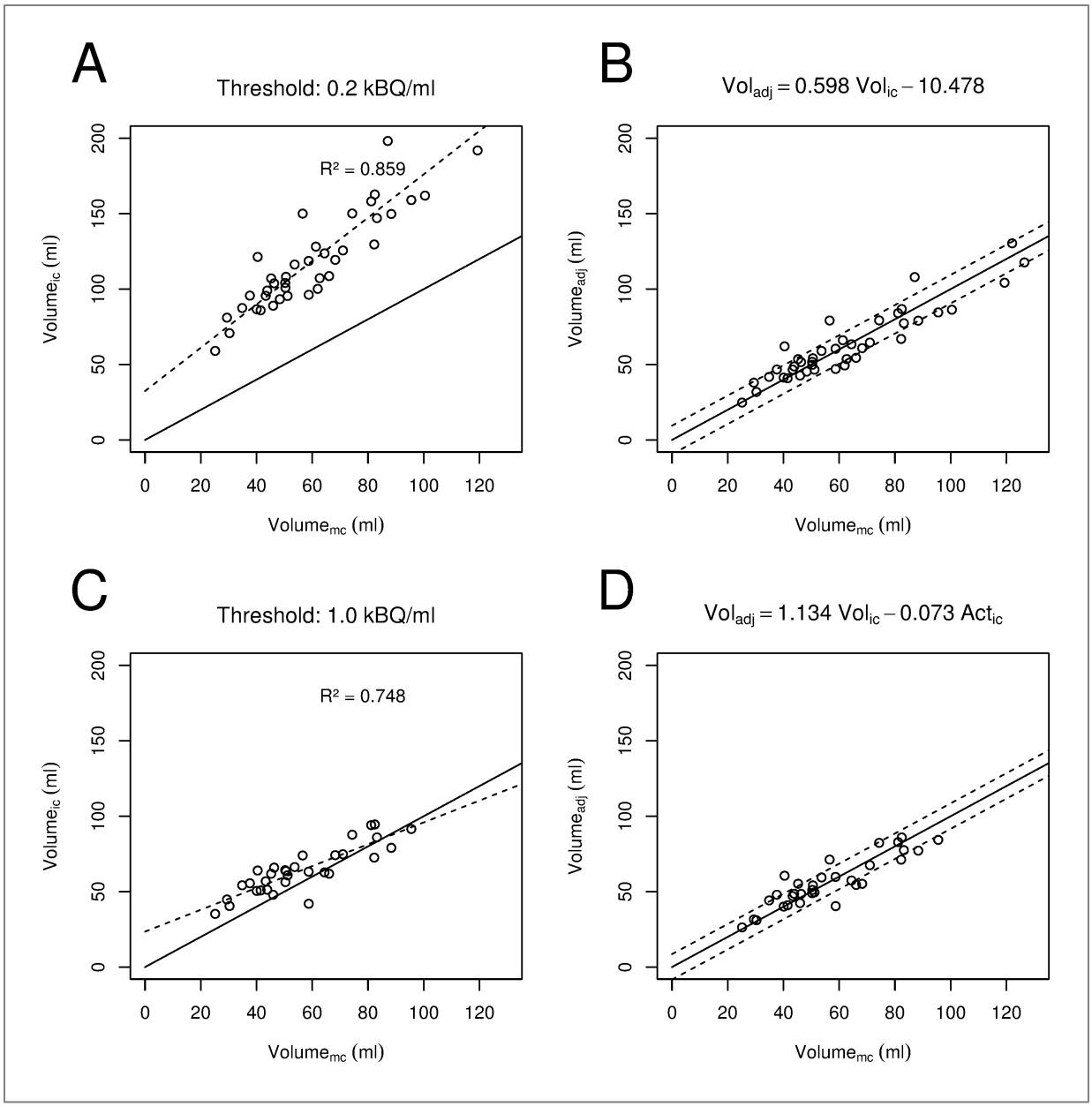

Figure 2: The graphs on the left panel (A, C) show the comparison between reference volume (MC) and the isocontour volume ($IC_{0.2/1.0}$). The solid line represents the fit, and the broken line, the linear regression between the two methods. The correlations are of different strength depending on the threshold. To correct for this, volumes were fitted using multiple linear regression with step-wise parameter elimination. The results of this correction are shown in the graphs on the right panel (B, D); solid line refers to fit, broken lines refer to standard deviation.

3.2. Dreidimensionaler Ultraschall (3D-US)

3.2.1. DICOM-Export und -Archivierung sowie Nachverarbeitung von 3D-US-Daten

3D Ultrasound DICOM Data of the Thyroid Gland.
First Experiences in Exporting, Archiving, Second Reading and 3D Processing

Publikation 2012 in NUKLEARMEDIZIN

Nuklearmedizin 2012; 51: 65–110

E 3145 F
ISSN 0029-5566

NuclearMedicine.

Nuklearmedizin

MOLECULAR IMAGING AND THERAPY

3/12

Kongressausgabe

12. Jahreskongress SGNM
12ème Congrès annuel SSMN
Zürich 2012

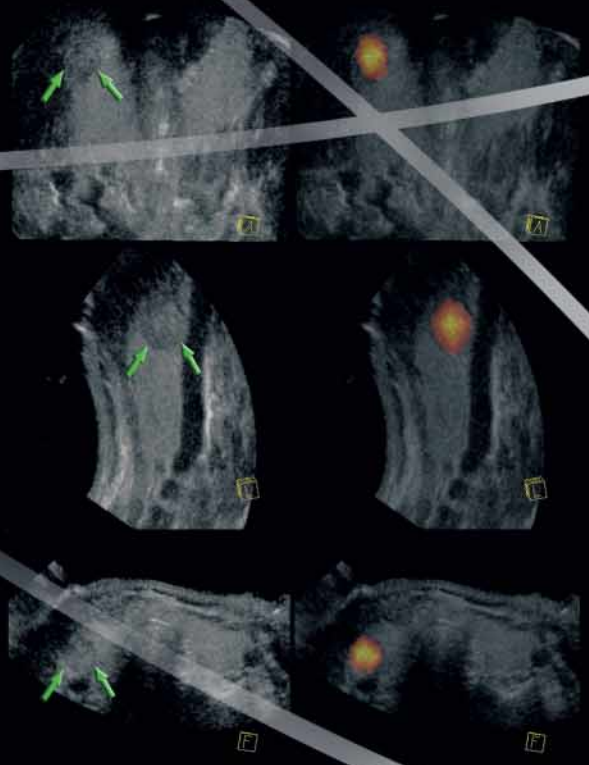

Journal of the German, Austrian and Swiss Societies of Nuclear Medicine

Schattauer

www.schattauer.de
www.nuklearmedizin-online.de

Schattauer GmbH, Postfach 104543, 70040 Stuttgart, Germany

3D ultrasound DICOM data of the thyroid gland

First experiences in exporting, archiving, second reading and 3D processing

M. Freesmeyer[1]; A. Darr[1]; J.-H. Schierz[1]; E. Schleußner[2]; S. Wiegand[1]; T. Opfermann[1]
[1]Clinic of Nuclear Medicine, Jena University Hospital, Jena, Germany;
[2]Clinic of Obstetrics and Gynaecology, Jena University Hospital, Jena, Germany

Keywords
Ultrasound, 3D ultrasound, thyroid gland, DICOM, image fusion

Summary
Purpose: It has recently become possible to generate and archive three-dimensional ultrasound (3D-US) volume data with the DICOM standard Enhanced Ultrasound Volume Storage (EUVS). The objective of this study was to examine the application of the EUVS standard based on the example of thyroid ultrasound. Patients, methods: 32 patients, who were referred for thyroid diagnosis, were given a 3D-US examination of the thyroid gland (GE Voluson E8, convex 3D probe RAB4–8-D). The 3D data sets were exported to EUVS. Necessary additions to DICOM entries and transformation into an established DICOM standard were carried out. The visual assessment and volume measurements were performed by two experts on nuclear medicine using standard software in our hospital. Results: In 24/32 (75%) of the patients, the whole organ was successfully recorded in a single 3D scan; in 8/32 (25%), only part of organ could be covered. In all cases, 3D-US data could be exported and archived. After supplementing the DICOM entry Patient Orientation and transformation into the DICOM PET format, 3D-US data could be displayed in the correct orientation and size at any viewing workstation and any web browser-based PACS viewer. Afterwards, 3D processing such as multiplanar reformation, volumetric measurements and image fusion with data of other cross sectional modalities could be performed. The intraclass correlation of the volume measurements was 0,94 and the interobserver variability was 5.7%. Conclusion: EUVS allows the generation, distribution and archiving of 3D-US data of the thyroid, facilitates a second reading by another physician and creates conditions for advanced 3D processing using routine software

Schlüsselwörter
Ultraschall, 3D-Ultrasschall, Schilddrüse, DICOM, Bildfusion

Zusammenfassung
Seit kurzem ist es möglich, dreidimensionale Ultraschallvolumendaten (3D-US) mittels des DICOM-Standards EUVS (Enhanced Ultrasound Volume Storage) zu erzeugen und zu speichern. Ziel dieser Studie war es, die Anwendbarkeit des EUVS-Standards am Beispiel des Ultraschalls der Schilddrüse zu untersuchen. Patienten, Methoden: Bei 32 Patienten, die zur Diagnostik einer Schilddrüsenerkrankung überwiesen wurden, wurde ein 3D-Ultraschall der Schilddrüse durchgeführt (GE Voluson E8, convex 3D probe RAB4–8-D). Die 3D-Daten wurden im EUVS-Format gespeichert und exportiert. Notwendige DICOM-Einträge sowie die Umwandlung in ein etabliertes DICOM-Format wurden durchgeführt. Die visuelle Beurteilung sowie die Volumen-Messungen wurden durch zwei erfahrene Nuklearmediziner mittels Standard-Software in unserer Klinik durchgeführt. Ergebnisse: Bei 24/32 (75%) Patienten wurde das komplette Organ in einem 3D-Scan vollständig, bei 8/32 (25%) unvollständig erfasst. In allen Fällen konnten die Daten erfolgreich exportiert und archiviert werden. Nachdem der DICOM-Eintrag „Patientenorientierung" hinzugefügt und die Daten in das DICOM-PET-Format umgewandelt wurden, konnten die 3D-US-Daten in korrekter Ausrichtung und Größe auf allen Workstations und mit allen web-basierten PACS-Viewern dargestellt werden. Anschließend konnten 3D-Nachverarbeitungen wie multiplanare Reformatierungen, Volumenbestimmungen und Bildfusionen mit anderen Schnittbildverfahren durchgeführt werden. Die Intraklassenkorrelation der Volumenmessungen betrug 0,94%, die Interobservervariabilität 5,7%. Schlussfolgerung: EUVS erlaubt die Erstellung, Verteilung und Archivierung dreidimensionaler US-Daten der Schilddrüse und ermöglicht die Nachbetrachtung durch einen zweiten Arzt sowie die 3D-Nachverarbeitung mit Standard-Software.

Correspondence to:
Dr. Martin G. Freesmeyer
Nuclear Medicine, Jena University Hospital
Bachstr. 18, 07743 Jena, Germany
Tel. +49/(0)36 41/93 32 20, Fax +49/(0)36 41/93 32 44
E-mail: Martin.Freesmeyer@med.uni-jena.de

3D-Ultraschall-DICOM-Daten der Schilddrüse – Erste Erfahrungen mit Export, Archivierung, Nachbetrachtung und 3D-Nachverarbeitung
Nuklearmedizin 2012; 51: 73–78
doi:10.3413/Nukmed-0471-12-01
received: January 26, 2012
accepted in revised form: March 30, 2012
prepublished online: April 16, 2012

Ultrasound imaging (US) is a standard diagnostic procedure in thyroid illness and delivers images of high soft tissue contrast and superior spatial resolution (25). Among patients who had been referred for evaluation of a palpable thyroid abnormality, ultrasonography altered the clinical management in two thirds of cases (10).

Though US is in fact a tomographic imaging technique, today in routine use US image volumes are not recorded and stored in digital hospital archive. In routine diagnostic ultrasound, the application of the DICOM standard and digital archiving has been limited to capturing

- two-dimensional frames of standard organ views,
- target findings and
- measurements (26).

Currently, missed pathological findings are not documented, which may contribute to remarkable interobserver variability, especially in less experienced examiners (1). Subsequent review of the entire examination by another physician to undertake a second reading is not possible, as the complete image information is no longer available. Moreover, later analysis of distances and volumes cannot be carried out and if necessary the examination has to be repeated.

Though a considerable technical advance in the field of three-dimensional ultrasound (3D-US) was reported (19), until now 3D datasets could only be stored and processed at the scanning platform or at connected dedicated workstations. Currently it is impossible to export the 3D-US data from the device in a way that supports PACS archiving, secondary diagnostic reading and 3D processing with common software tools.

Very recently, it has become possible to export, archive and process standardized 3D-US volume data with the DICOM standard Enhanced Ultrasound Volume Storage (EUVS) (5). This study aimed to

- demonstrate the potential of EUVS in the generation and export as well as the distribution and archiving of 3D-US data achieved by a 3D probe, using the example of the thyroid gland,
- find solutions to overcome current limitations in the routine working environment at our hospital,
- create the conditions for an offline second reading by another physician, without the necessity of patient presence and for advanced 3D processing such as
  - multiplanar reformations,
  - offline volume measurements and
  - offline image fusion with data from other cross-sectional imaging modalities.

Patients and methods

32 subsequent patients (23 women, 9 men; 64.1±10.3 years) who were referred for thyroid diagnosis (23/32 toxic goiter, 7/32 nontoxic goiter, 2/32 Graves disease), were given a 3D-US examination of the thyroid gland. Standard ultrasound was performed using a linear transducer at 7 MHz (Logiq 9, GE Healthcare, Chalfont St. Giles, UK).

3D ultrasound was carried out at an obstetric ultrasound platform with an abdominal, convex, multi-frequency 3D transducer (GE Voluson E8, RAB4–8-D, wide sector opening angle 90°×85°, Zipf, Austria). The prevailing scan orientation was transaxial. An aqueous coupling medium was used (130×120×10mm, Sonar Aid, Geistlich Pharma). The 3D-US data sets were generated and exported using the EUVS standard (SOP UID 1.2.840.10008.5.1.4.1.1.6.2).

Changes in DICOM entries were carried out using the software PMOD (version 3.2.07, PMOD Technologies Ltd., Zurich, Switzerland) and the software package DCMTK – DICOM Toolkit (version 3.6.0, OFFIS, Oldenburg). Data were transformed into the established PET DICOM standard (SOP UID 1.2.840.10008.5.1.4.1.1.128 Positron Emission Tomography Image Storage).

After modification, the datasets were archived in the hospital's PACS. Visual assessments of completeness of organ acquisition, volumetric measurements and further processing were performed by two experts on nuclear medicine at a multimodality workstation (syngo MultiModality WORKPLACE 2010b, Siemens, Erlangen).

The mean and standard deviation of thyroid volume measurements of the 24 completely recorded thyroids were given for each examiner. Interobserver variability and intraclass correlation were calculated (7, 27).

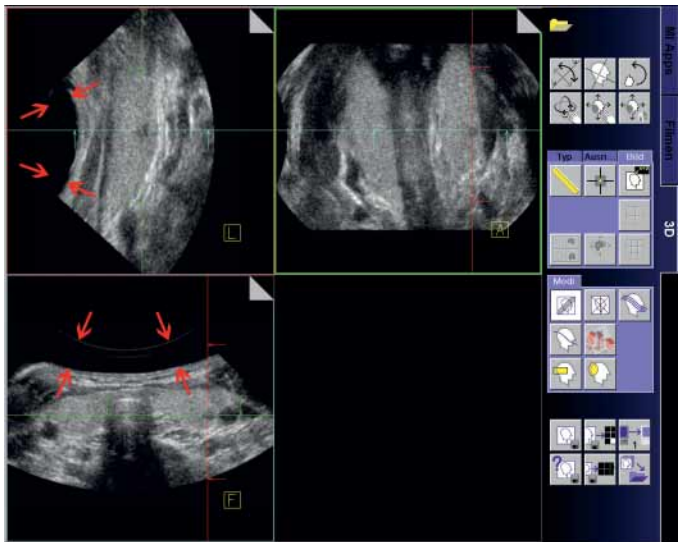

Fig. 1 Routine 3D workplace; display of an ultrasound volume of the thyroid gland in sagittal, coronal and transversal orientation; several workflow buttons for 3D processing (right); aqueous coupling medium (between red arrows): small and slight hypoechoic nodule in the lateral part of the left lobe (cross center)

Results

In all cases, technically the volume of the thyroid could be scanned and 3D-US data could successfully be generated and exported in the EUVS DICOM standard.

The transformation into the established DICOM standard PET was successful in all data sets. The displayed image orientation at the viewing devices depended on the orientation of the probe while scanning,

which was typically transaxial in our study, and sagittal in some additional scans. The respective correct orientation into the DICOM entry Patient Orientation in each data set was done manually without difficulty in all cases.

Afterwards, the data could be displayed in the correct orientation and size at every diagnostic image viewing workstation as well as at any web browser-based PACS viewer in our hospital. The number of images displayed range from 201 to 245. However, the image quality tended to be clearly poorer than the standard examination with 7 MHz.

In 24/32 (75%) patients, the whole organ was successfully recorded by one single 3D scan; in 8/32 (25%), the organ could only be covered incompletely, due to the limited scanning field of view (FOV) of the 3D transducer. In these cases we took additional scans of the missing part after replacing the probe. The complete gland volume was therefore covered by one or two scans in all patients.

Both reading and multiplanar displaying of the modified 3D-US data sets were possible in all cases at an advanced multimodal 3D processing workstation in the standard orientations: transaxial, sagittal and coronar (▶Fig. 1).

Further processing of the data was possible without limitations. For example reformations in free adjustable orientation and slice thickness were easily generated (▶Fig. 2). Moreover, measurements of distances and volumes could be performed in all data sets (▶Fig. 3).

The mean organ volume of the 24 completely recorded thyroids assessed by the two experts was 44.1±21.8ml in examiner 1 and 44.6±20.8ml in examiner 2, while the intraclass correlation was 0.94 and interobserver variability was 5.7% (95% confidence interval 2.5–12.3%).

Furthermore, software image fusion with data from other cross sectional imaging modalities as SPECT could be performed (▶Fig. 4).

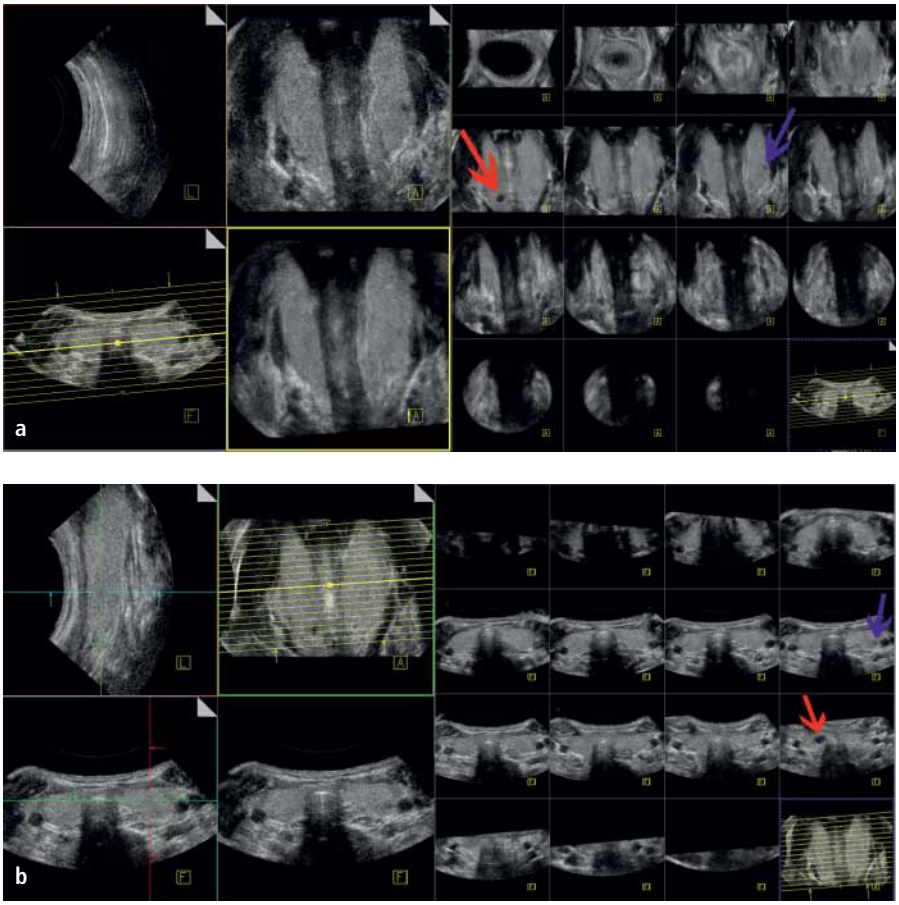

Fig. 2 Multiplanar reformation workflow (left): Generation of a coronar (a) and a transaxial (b) image stack (right) covering the whole thyroid and demonstrating small hypoechoic nodules in the bottom part of the right lobe (red arrow) as well as in the lateral part of the left lobe (blue arrow).

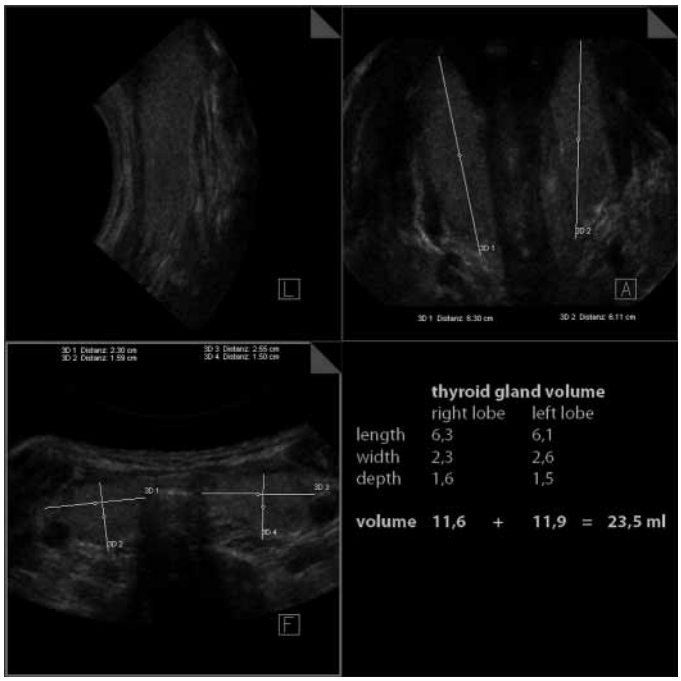

Fig. 3 3D measurement workflow with case example: A woman (age: 53 years) demonstrating slight enlarged thyroid gland

Discussion

Over the last years a considerable technical advance in the field of three-dimensional

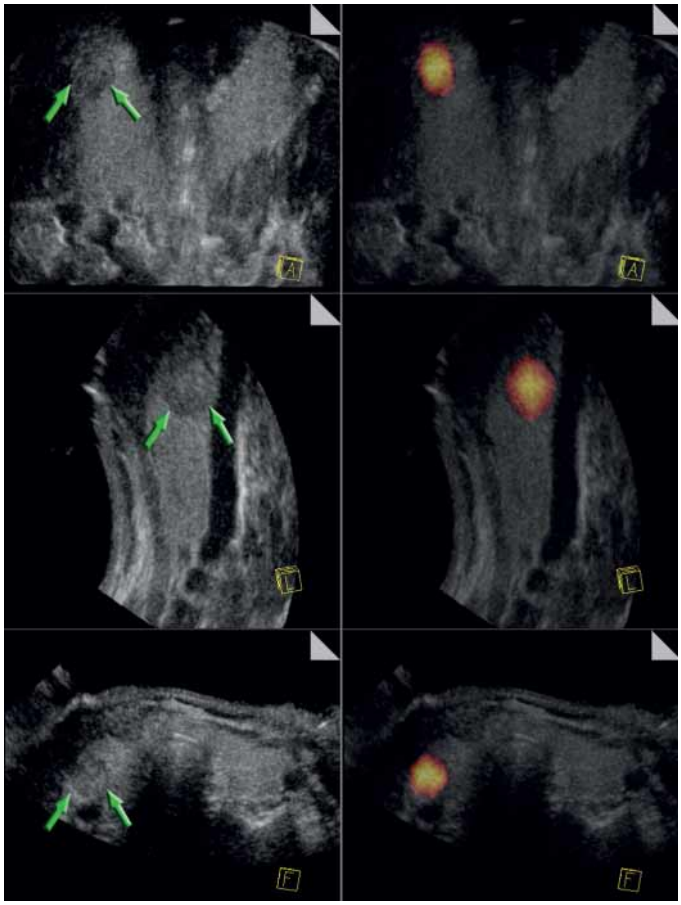

Fig. 4 Image fusion workflow with case example: A woman (age: 58 years) with small thyroid adenoma in the upper part of the right lobe; image fusion of 3D-US volume and $^{99m}TcO_4$-SPECT (green arrows)

ultrasound was reported (19). Several scanning technologies established including static 3D probes (8) as well as free-hand (29) and sensor-navigated (9, 12, 16, 17, 23) 3D transducers. The first and most common type of 3D-US scanner which was used in this study is that based on a mechanically swept array inside the housing through a known trajectory. This allows the acquisition of a pattern of 2D images covering a fixed tissue volume, so the FOV is limited (19).

However, so far as we know there is no way to store recorded 3D-US volumes as cross-sectional image stack in digital clinic archives (PACS). Moreover, it is impossible to review the studies at diagnostic viewing platforms, which are in routine use for CT, MRI, PET and SPECT images.

However, the prerequisite DICOM standard EUVS has recently been established (5), but is still poorly implemented at ultrasound platforms as well as in routine diagnostic viewing and processing software. Hence, we used the dedicated obstetric device GE Voluson E8, for which EUVS became recently available. Recording of the 3D scans was easily achieved and the generation, export and distribution and archiving of 3D-US data were successful in all cases.

Although these first steps were promising, some constraints had been to overcome:

1. The scanning area is bound by the opening angles of the probe, which limits the field of view (FOV) to 90°×85°. If using typical depth adjustments of 4.8 cm and 6.5 cm, the manufacturer indicates total scan volumes of 270 ml and 520 ml, respectively. We optimized the recordable thyroid tissue by using an aqueous coupling medium, which increases the distance between the transducer and the gland. So the organ was displayed in the wider range of the wedge-shaped scanning sector and a greater thyroid part was covered (▶Fig. 1). Thereby the whole organ was completely covered in 75% of the patients by a single scan. Covering the whole thyroid remains a challenge.
2. The recorded data sets could not be processed promptly because information concerning scan orientation in the DICOM header was missing, so we had to manually insert this information into the DICOM entry Patient Orientation. That procedure is technically easy to perform, but time-consuming.
3. Afterwards, the transformation into the established DICOM format PET was necessary because the EUVS standard was not implemented at hospital diagnostic viewing workstations and in 3D processing software.

After these steps data sets could be displayed in the correct orientation and size at every diagnostic image viewing workstation as well as any web browser based PACS viewer in our hospital. Some authors have suggested the potential benefits of making 3D-US familiar for MRI and CT (8).

> The study presented here is the first that facilitated a second reading of 3D-US volumes by any physician at any time, in the patient's absence.

It remains a serious constraint that the convex 3D probe used in this study, which was primarily developed for applications in abdominal and obstetric imaging, delivered poorer image quality compared to standard ultrasound with linear 2D transducers. Although a similar 3D probe with linear array and high frequency was available, its use was not worthwhile, because the scan area was strictly parallel without lateral opening of the FOV. Thus, it allows higher image resolution, but a quite insufficient scanning volume. However, the aim of this study was to prove the principle rather than enhance image quality compared to standard 2D ultrasound. Since the 3D-US volume was composed by processing of sequentially recorded common 2D scans, image characteristics such as calcification shadowing and echo enhancement caused by cysts were completely the same as in 2D standard ultrasound.

We tested reading and advanced 3D processing including multiplanar reforma-

tions subsequent measurements of distances and volumes as well as offline image fusion with data of other modalities and all procedures were easily to perform.

A few studies show the feasibility of volumetric measurements in 3D-US of the thyroid (1, 15, 20, 24, 28, 39) and the presented data support this concept again. The process enables for the first time measurements independent of the 3D-US device itself and on dedicated software platforms. This may considerably improve the availability of this option.

In this study the interobserver variability and intraclass correlation of the volume measurements were low compared to data based on 2D standard thyroid ultrasound (18, 21) and comparable to a first study on 3D ultrasound volumetry in prostate carcinoma (31).

Similar to this, the reconstruction of multiplanar reformations (MPR) is a typical application in 3D-US (36). However, currently this method depends on the presence of the 3D-US device itself or on dedicated software, which limits its potential for widespread use.

Offline fusion of metabolic images with morphological cross-sectional image data remains an important topic in nuclear medicine (14). Fusion imaging of thyroid SPECT with ultrasound may offer the potential of diagnostic improvement. For example, calcification-related absorption may influence metabolic images as described by Eising et al. (6) and overlaying of information from both modalities may help to perceive this phenomenon.

There are few studies concerning image fusion of ultrasound with CT (2, 30, 35, 37, 38), MRI (11, 13, 22), biplane angiography (4) C-arm X-ray (34), SPECT (3, 32, 33), as well as PET (11). In contrast to the concept of offline image fusion ultrasound systems using magnetic sensor tracking are currently emerging in the market which display fused images of CT or MRI and real-time ultrasound simultaneously (9, 12, 16, 17, 23). However, the mentioned techniques depend on specific hard- and software in contrast to our concept which allows offline fusion using routine software.

Limitations

The incomplete recording of large organs and the poor image quality of convex 3D probes are currently limiting factors in 3D-US scanning of the thyroid gland. Moreover, the potential for assessment of retrosternal goiter is probably limited.

Conclusion

The new DICOM standard EUVS allows

- generation and export as well as
- distribution and archiving of 3D-US data.

Despite serious limitations, the procedure was feasible and applicable. Until EUVS becomes more widespread the modification of the DICOM entries and transformation into a more common DICOM format is necessary to facilitate second reading by another physician in the patient's absence and for 3D processing such as

- free adjustable multiplanar reformations,
- subsequent measurements of distances and volumes and
- offline image fusion with data of other modalities.

> The availability of compatible 3D-US datasets will bring the practice of ultrasound examinations into line with CT, MRI, SPECT and PET, as predicted (8).

Advances enabling higher resolution scans of larger tissue volumes are desirable. In addition, the potential role of EUVS standard for diagnostic improvement needs clinical evaluation.

Conflict of interest

The authors declare, that there is no conflict of interest.

References

1. Andermann P, Schlogl S, Mader U et al. Intra- and interobserver variability of thyroid volume measurements in healthy adults by 2D versus 3D ultrasound. Nuklearmedizin 2007; 46: 1–7.
2. Brendel B, Winter S, Rick A et al. Registration of 3D CT and ultrasound datasets of the spine using bone structures. Comput Aided Surg 2002; 7: 146–155.
3. Bucki M, Chassat F, Galdames F et al. Real-Time SPECT and 2D Ultrasound Image Registration. In: Ayache N, Ourselin S, Maeder A (eds). Medical Image Computing and Computer-Assisted Intervention – MICCAI 2007: Berlin, Heidelberg: Springer 2007; 219–226.
4. Cothren RM, Shekhar R, Tuzcu EM et al. Three-dimensional reconstruction of the coronary artery wall by image fusion of intravascular ultrasound and bi-plane angiography. Int J Card Imaging 2000; 16: 69–85.
5. Digital Imaging and Communications in Medicine (DICOM), Supplement 43: Storage of 3D Ultrasound Images. ftp://medicalnemaorg/medical/dicom/final/sup43_ftpdf: National Electrical Manufacturers Association (NEMA) 2008.
6. Eising EG, Jentzen W. Calcification-related absorption in thyroid scintigraphy. Nuklearmedizin 2010; 49: 13–18.
7. Eliasziw M, Young SL, Woodbury MG, Frydayfield K. Statistical methodology for the concurrent assessment of interrater and intrarater reliability – Using goniometric measurements as an example. Phys Ther 1994; 74: 777–788.
8. Elliott ST. Volume ultrasound: the next big thing? Br J Radiol 2008; 81: 8–9.
9. Ewertsen C, Grossjohann HS, Nielsen MB. Image fusion involving ultrasound. Ultraschall Med 2006; 27: 128–129.
10. Hegedus L. Clinical practice. The thyroid nodule. N Engl J Med 2004; 351: 1764–1771.
11. Huang X, Hill NA, Ren J et al. Dynamic 3D ultrasound and MR image registration of the beating heart. Med Image Comput Comput Assist Interv 2005; 8: 171–178.
12. Jung EM, Schreyer AG, Schacherer D et al. New real-time image fusion technique for characterization of tumor vascularisation and tumor perfusion of liver tumors with contrast-enhanced ultrasound, spiral CT or MRI: first results. Clin Hemorheol Microcirc 2009; 43: 57–69.
13. Kaplan I, Oldenburg NE, Meskell P et al. Real time MRI-ultrasound image guided stereotactic prostate biopsy. Magn Reson Imaging 2002; 20: 295–299.
14. Kiefer A, Kuwert T, Hahn D et al. Anatomical accuracy of abdominal lesion localization. Retrospective automatic rigid image registration between FDG-PET and MRI. Nuklearmedizin 2011; 50: 147–154.
15. Lyshchik A, Drozd V, Reiners C. Accuracy of three-dimensional ultrasound for thyroid volume measurement in children and adolescents. Thyroid 2004; 14: 113–120.
16. Minami Y, Kudo M, Chung H et al. Percutaneous radiofrequency ablation of sonographically unidentifiable liver tumors. Feasibility and usefulness of a novel guiding technique with an integrated system of computed tomography and sonographic images. Oncology 2007; 72 (Suppl 1): 111–116.
17. Nakano S, Yorozuya K, Takasugi M et al. Real-time virtual sonography (RVS): a new virtual reality technique for detection of enhancing lesions on contrast-enhanced MR imaging of the breast by using sonography. Nihon Rinsho 2007; 65 (Suppl 6): 304–309.
18. Ozgen A, Erol C, Kaya A et al. Interobserver and intraobserver variations in sonographic measurement of thyroid volume in children. Eur J Endocrinol 1999; 140: 328–331.

19. Prager RW, Ijaz UZ, Gee AH, Treece GM. Three-dimensional ultrasound imaging. Proc Inst Mech Eng H 2010; 224: 193–223.
20. Rago T, Bencivelli W, Scutari M et al. The newly developed three-dimensional (3D) and two-dimensional (2D) thyroid ultrasound are strongly correlated, but 2D overestimates thyroid volume in the presence of nodules. J Endocrinol Invest 2006; 29: 423–426.
21. Reinartz P, Sabri O, Zimny M et al. Thyroid volume measurement in patients prior to radioiodine therapy: comparison between three-dimensional magnetic resonance imaging and ultrasonography. Thyroid 2002; 12: 713–717.
22. Reynier C, Troccaz J, Fourneret P et al. MRI/TRUS data fusion for prostate brachytherapy. Preliminary results. Med Phys 2004; 31: 1568–1575.
23. Sandulescu L, Saftoiu A, Dumitrescu D, Ciurea T. Real-time contrast-enhanced and real-time virtual sonography in the assessment of benign liver lesions. J Gastrointestin Liver Dis 2008; 17: 475–478.
24. Schlogl S, Werner E, Lassmann M et al. The use of three-dimensional ultrasound for thyroid volumetry. Thyroid 2001; 11: 569–574.
25. Sheth S. Role of ultrasonography in thyroid disease. Otolaryngol Clin North Am 2010; 43: 239–255.
26. Sholosh B, Borhani AA. Thyroid ultrasound part 1: technique and diffuse disease. Radiol Clin North Am 2011; 49: 391–416.
27. Shrout PE, Fleiss JL. Intraclass correlations: uses in assessing rater reliability. Psychol Bull 1979; 86: 420–428.
28. Slapa RZ, Jakubowski WS, Slowinska-Srzednicka J, Szopinski KT. Advantages and disadvantages of 3D ultrasound of thyroid nodules including thin slice volume rendering. Thyroid Res 2011; 4: 1.
29. Solberg OV, Lindseth F, Torp H et al. Freehand 3D ultrasound reconstruction algorithms--a review. Ultrasound Med Biol 2007; 33: 991–1009.
30. Steggerda M, Schneider C, van Herk M et al. The applicability of simultaneous TRUS-CT imaging for the evaluation of prostate seed implants. Med Phys 2005; 32: 2262–2270.
31. Tong S, Cardinal HN, McLoughlin RF et al. Intra- and inter-observer variability and reliability of prostate volume measurement via two-dimensional and three-dimensional ultrasound imaging. Ultrasound Med Biol 1998; 24: 673–681.
32. Walimbe V, Jaber WA, Garcia MJ, Shekhar R. Multimodality cardiac stress testing: combining real-time 3-dimensional echocardiography and myocardial perfusion SPECT. J Nucl Med 2009; 50: 226–230.
33. Walimbe V, Zagrodsky V, Raja S et al. Mutual information-based multimodality registration of cardiac ultrasound and SPECT images: a preliminary investigation. Int J Cardiovasc Imaging 2003; 19: 483–494.
34. Wein W, Camus E, John M et al. Towards guidance of electrophysiological procedures with real-time 3D intracardiac echocardiography fusion to C-arm CT. Med Image Comput Comput Assist Interv 2009; 12: 9–16.
35. Wein W, Roper B, Navab N. Automatic registration and fusion of ultrasound with CT for radiotherapy. Med Image Comput Comput Assist Interv 2005; 8: 303–111.
36. Weismann C, Hergan K. Aktueller Stand der 3D-/4D-Volumensonografie der Mamma. Ultraschall Med 2007; 28: 273–282.
37. Winter S, Brendel B, Igel C. Registrierung von Knochen in 3D-Ultraschall- und CT-Daten: Vergleich verschiedener Optimierungsverfahren. In: Meinzer H-P, Handels H, Horsch A, Tolxdorff T (eds). Bildverarbeitung für die Medizin 2005. Heidelberg: Springer 2005; 345–349.
38. Winter S, Brendel B, Rick A et al. Registration of bone surfaces, extracted from CT-datasets, with 3D ultrasound. Biomed Tech (Berl) 2002; 47 (Suppl 1): 57–60.
39. Ying M, Yung DM, Ho KK. Two-dimensional ultrasound measurement of thyroid gland volume: a new equation with higher correlation with 3-D ultrasound measurement. Ultrasound Med Biol 2008; 34: 56–63.

3.2.2. Dreidimensionaler Ultraschall (3D-US)

3.2.2.1. Multimodale Phantomuntersuchungen zur Schilddrüsenvolumetrie

Multimodal Evaluation of 2-Dimensional and 3-Dimensional Ultrasound, Computed Tomography and Magnetic Resonance Imaging in Measurements of the Thyroid Volume Using Universally Applicable Cross-Sectional Imaging Software: A Phantom Study

Publikation in ULTRASOUND IN MEDICINE AND BIOLOGY 2014

Multimodal Evaluation of 2-Dimensional and 3-Dimensional Ultrasound, Computed Tomography and Magnetic Resonance Imaging in Measurements of the Thyroid Volume Using Universally Applicable Cross-Sectional Imaging Software: A Phantom Study

Martin Freesmeyer, Steffen Wiegand, Jan-Henning Schierz, Thomas Winkens, Katharina Licht

from the Clinic of Nuclear Medicine, Jena University Hospital, Jena, Germany

Corresponding author: Dr. Martin Freesmeyer
Clinic of Nuclear Medicine
Jena University Hospital
Bachstrasse. 18
07740 Jena, Germany
Phone: +49-3641-933220, Fax: +49-3641-933244
E-Mail: martin.freesmeyer@med.uni-jena.de

Abstract

Purpose: A precise estimation of the thyroid volume is necessary for adequate therapeutic decision and planning, as well as for monitoring of therapy response. Different methods are available for this purpose. The goal of this study was to compare the precision of different volumetry methods by multimodal evaluation of thyroid phantoms.

Methods: Phantoms with 18 different volumes (range: 10 to 200 ml) and three different shapes (regular, deformed lobes, thickened isthmus) were subjected to volumetry via 2D and 3D ultrasonography (US), computed tomography (CT), and magnetic resonance imaging (MRI). The 3D-US scans were performed using sensor navigated and mechanically swept methods. Volume data sets were obtained and, except for 2D measurements (with volumetry calculated directly at the sonograph), subjected to volumetry calculation with standard cross-sectional imaging software. Two methods were compared for this purpose, i.e., the conventional ellipsoid model and the manually traced method in parallel planes. The reference standards were the measured net volumes of the phantoms.

Results: The manually traced method showed a clear superiority compared to the mathematical calculation via ellipsoid model. Independently of the imaging method used, the discrepancies between the calculated and the reference volumes were significantly smaller when the manually traced method was used. This was particularly evident in the case of deformed phantoms.

Conclusions: This study confirmed the superiority of the manually traced method with CT and MRI volumetry of the thyroid, but extended this knowledge also to the superiority of the 3D-US method, the latter regardless of whether the sensor navigated or the mechanically swept probe was used. A novel aspect was also the successful use of the same universally applicable cross-imaging software for the evaluation of all modalities. The establishment of 3D-US as a cost-effective, radiation-free estimation of the thyroid volume, especially if coupled with high precision and reproducibility, is highly desirable. However, methodology must still be optimized and the time effort further reduced.

Introduction

Pathological changes of the thyroid gland are frequent, mostly depending on the local iodine supply and the prevalence of goiter. In Germany the average prevalence of goiter is 35.9% (Volzke 2003). An exact determination of the thyroid volume and its pathological changes is clinically relevant because therapeutic decisions and monitoring of therapy response are largely based on the thyroid volume (Reinartz 2002, van Isselt 2003).

The primary imaging method of the thyroid is the conventional 2-dimensional B-mode ultrasonography (2D-US) (Lucas 2000, Ying 2008). This method is simple, readily available, inexpensive, free from radiation exposure (Reinartz 2002), and validated in epidemiological studies (Knudsen 1999, Vitti 1994). The conventional 2D-US is based on separate measurements of the two gland lobes. The simplified mathematical model for volumetric calculations assumes that each lobe represents a rotational ellipsoid (Brunn 1981). In the ellipsoid model the volume of each lobe is calculated with the formula $length_{max}$ x $width_{max}$ x $depth_{max}$ x f, and the two volumes are added. Different values have been recommended for the correction factor f (Brunn 1981, Knudsen 1999, Reinartz 2002, Ying 2008), but usually 0.5 is applied in clinical routine. The application of the ellipsoid model, however, is associated to a relatively high intra- and inter-observer variability (Ozgen 1999, Rago 2006). On one hand this is inherent to the tendency of the mathematical model to generate deviations (Ozgen 1999), and on the other hand a nodular goiter can cause lobe deformities and/or thickening of the isthmus, leading to significant imprecisions of the 2D-US volumetry (Rago 2006).

A 3-dimensional sonography (3D-US) has also been developed in the late nineties (Tong 1998). In this case, however, the volume assessment was possible only by means of a dedicated workstation equipped with a special software (Andermann 2007, Kot 2009). Recently, it has become possible to generate universally compatible data in DICOM format (Digital Imaging and Communications in Medicine) that can be subjected to volumetry calculation via a multimodal workstation (Freesmeyer 2012). The advantages of the 3D-US in comparison to the 2D-US include a higher precision (Schlogl 2001) and a clearly reduced intra- and inter-observer variability (Lyshchik 2004, Ng 2004).

In alternative to the ellipsoid model, for 3D data the organ volume in parallel planes can be delimited from the adjacent tissues via the manually traced method. This method is less prone to intra- and inter-operator errors and is considered by some authors as the gold standard (Andermann 2007, Reinartz 2002, van Isselt 2003).
A literature search focused on different scanning and volumetry methods via 3D-US is shown in Table 1. Except for the paper of Kot et al (2009), however, all studies have employed only one 3D-US method, mostly the sensor navigated 3D-US.
The scope of the present phantom study was to compare the volumetric precision of the ellipsoid model and the manually traced method. Several techniques were used for this purpose, i.e., 2D-US, two different 3D-US methods (sensor navigated [3D-sn-US] and mechanically swept [3D-ms-US]), computed tomography (CT), and magnetic resonance imaging (MRI). Two specific aspects were investigated: 1) the influence of the phantom shape; 2) the relative performance of 3D-sn-US and 3D-ms-US. Deformable phantoms compatible with this multimodal approach were developed and scanned, and the data evaluated with a workstation equipped with a standard cross-sectional imaging software.

Material and Methods

Phantoms

Eighteen phantoms with a shape resembling the thyroid gland were developed in 18 predefined volumes (10, 15, 20, 25, 30, 35, 40, 50, 60, 70, 80, 90, 100, 120, 140, 160, 180, and 200 ml) meant to reproduce the range of thyroid volumes typically seen in patients prior to therapeutic interventions. The basic constructs were commercially-available, heart-shaped latex balloons in three original volumes. To maintain the constructs in a water bed, four little pieces of plastic (approx. 2 x 3 mm) were inserted into the phantoms and then ligated with thread from the outside, creating four poles (Fig. 1). The unladen weight (tare) of each empty phantom was measured using a precision scale.

The balloons were filled with a mixture of water and MRI contrast medium (Omniscan 0.5 mmol/ml; GE Healthcare, Oslo, Norway). The water was pre-boiled to minimize the formation of air bubbles via outgassing of dissolved particles. A previously measured dilution ratio of 1 : 99 (contrast medium : water) was applied, on one hand with the goal to reproduce density values basically equivalent to soft tissue for the purpose of CT imaging, and on the other hand to permit an adequate imaging by MRI. The density measurements of the filling mix in comparison to water provided a negligible variability of 0.0015 g/ml, thus a simplified assumption was made that 1 g of phantom content corresponded to 1 ml of volume. The net volumes derived from the weight measurements represented the reference standard for the assessment of the volumetric accuracy of the different methods (see also below). A tubing system with two 3-way stopcocks was used to prevent the entry of air into the phantoms, i.e., one stopcock was used to introduce the contrast mixture and the other to let out any air bubbles. The phantoms were weighed again at the end of the experiments (gross weight), and the subtraction of the previously measured tare provided their net weight and volume.

To reproduce the shapes of the lobes and the typically narrow isthmus of a healthy thyroid, the phantoms were tied as shown in Fig. 1a. For the measurements, the phantoms were placed into a double-walled plastic container (Fig. 1). The four poles of the lobes were fixed with thread to the inner wall of the plastic container, which had been prepared with holes for the insertion and ligation of the thread. The phantoms were then pulled at approx. 2 cm above the bottom of the container and the latter was filled with water until the phantoms were fully immersed (Fig. 1). After completion of the first measurement cycle with normally shaped phantoms, a second cycle was performed with deformed lobes (a model of nodular goiter) (see Fig. 1b for details). In a third cycle, all ties were removed and the model of thickened isthmus was investigated (see details in Fig. 1c). Finally, the phantoms were removed from the container and weighed again to ensure that any leakage occurred during the measurement was detected.

All experiments were carried out within a time frame of 29 days.

Ultrasonography scans

Two different machines were used for US scans. The conventional 2D-US and the 3D sensor navigated sonography (3D-sn-US) were performed using Logiq E9 (GE Medical Systems, Milwaukee, WI, USA) and a linear probe (ML 6-15) in virtual convex mode, with a frequency of 11 MHz and an image depth of 10 cm. A single focus was placed in the middle of the phantom. In the case of 3D-sn-US, the phantom was placed on a stretcher at a distance of approx. 20 cm from a magnetic transmitter (see details in Fig. 2a). Two positional sensors fixed to the probe allowed the recording of position and movement of the ultrasound probe in the magnetic field during the scanning (Fig. 2a). The equipment reconstructed a 3D volume data set on the basis of the coordinates of the probes and of the acquired 2D images.

The 3D mechanically swept sonography (3D-ms-US) was performed using Voluson E8 (GE Medical Systems, Zipf, Austria) and a RAB 6-D convex probe. While in clinical routine this is operated

manually, in these experiments a benchtop tripod was used for fixation (Fig. 2b). The 3D detection was achieved via a mechanically swept array contained in the probe housing. Each scan was performed with a frequency of 6 MHz, depth adjustment of 8.5 cm, field of view of 63°, and volume angle of 85°. The focus was centered in the middle of the phantom. As final step, the equipment reconstructed a 3D volume data set.

The voxel size for both 3D-sn-US and 3D-ms-US was 0.7 x 0.7 x 3.0mm.

Computed tomography (CT)

CT scans were performed with a Biograph mCT (Siemens, Erlangen, Germany) using a low-dose technique (120 kV, 50 mAs). The reconstruction consisted of 3 mm slices with 1.5 mm overlap. The voxel size was 0.7 x 0.7 x 3.0mm.

Magnetic resonance imaging (MRI)

The MRI was performed with a Magnetom Avanto MR B 17 (Siemens) in T1-weighted images and 3 mm slice thickness. The repetition time was 570.0 msec, the echo time 19.0 msec. The resulting voxel size was 0.78 x 0.78 x 3.0mm.

Volumetry

The volumetry of each phantom was assessed for a total of 9 times by an experienced investigator (KL). All imaging techniques were assessed first by means of the ellipsoid formula ($length_{max}$ x $width_{max}$ x $depth_{max}$ x 0.5) (ellipsoid model [em]), with volume acquisitions in two orthogonal planes. The four volume data sets were then assessed by means of the manually traced procedure (mt).

While in the case of the 2D-US the volumes were calculated directly at the sonograph, for all other techniques the calculations were performed with a multimodal workstation (Syngo MultiModality WORKPLACE 2010a, Siemens) with a 3D routine software for cross-sectional imaging (syngoMMWP Version VE40A, CT-Tool VA31A_SP3.5_P17, Siemens). This software allows first to represent the data sets in the three standard planes and then to further evaluate the data.

To obtain the typically missing orientation of the 3D-US data, the DICOM entries were modified by means of the software PMOD (Version 3.4, PMOD Technologies Ltd., Zurich, Switzerland) and the software package Sante DICOM Editor (Version 3.1.21, Santesoft Ltd., Athens, Greece). In this case allslices of the exported 3D-US data (ranging from 0.28-0.34 mm) were merged into one volume and then reconstructed to 3.0 mm slices. This allowed on one hand to limit the effort of the analyses, and on the other hand to guarantee the comparability of the slice thickness with those of the MRI and CT scans (3 mm).

In the case of em, the assessment started from the coronal standard planes, in order to identify the slices with the maximum length. The transversal plane was then oriented perpendicularly to the coronal plane, in order to measure the maximum width and depth.

The mt method was applied in the volumetry software via manual tracing of the phantom contours in parallel slices of transversal planes (Fig. 3 and 4). The calculation of the volumes was automatically performed by the program.

Statistical analysis

The Pearson's correlation coefficient of calculated and reference volumes of the thyroid phantoms was used to demonstrate the suitability of the different scanning methods for volumetric determinations.

Because a correspondence of calculated and reference volumes cannot be fully demonstrated with correlation coefficients, a slightly modified version of the Bland and Altman method (Bland and Altman 1986) was also applied. For this purpose, relative volume differences were calculated for all measurements, i.e., the reference volumes were subtracted from the calculated volumes and the differences divided by the reference volumes. Thus, all relative volume differences were expressed as % values, allowing to calculate the mean discrepancies of each scanning method from the reference. In addition, the methods were compared using the limits of agreement recommended by Bland and Altman (Bland and Altman 1986), which include 95% of all expected values.

To assess systematic errors, the 95% confidence intervals of the means were also calculated. If the confidence intervals did not include the zero value, the corresponding scanning method had a significant systematic error (overestimation or underestimation).

All calculations were performed with the program language R Version 2.15.1 (RDevelopment Core Team, Vienna, Austria).

Results

The mean values, standard deviations, correlation coefficients of calculated versus reference volumes, 95% confidence intervals, and limits of agreement for all five scanning methods (for 3D methods with double assessment via em and mt method), and for all phantom shapes (regular, nodular, thickened isthmus) are presented in Table 2.

The high correlation coefficients (range: 0.984-1.000) found for all methods showed that – irrespectively of the phantom shape – all methods investigated were in principle suitable for volumetric determinations. On the other hand, analyses of the discrepancies between the calculated and the reference volumes provided more differentiated results (Fig. 5). Em, for example, tended to overestimate the volumes (with the exception of MRI of non-deformed phantoms) (Fig. 5). Especially with the sonography methods (except for the 3D-sn-US-em in non-deformed phantoms) the 95% confidence intervals of 2D-em and 3D-ms-US-em remained above the reference line (zero), indicating a systematic overestimation (Fig. 5). Also, the standard deviations of em were relatively large (Table 2) and the relative discrepancies from the reference values were also relatively pronounced, e.g., MRI-em assessments of regular shapes had a mean of -1.8% and a standard deviation of 5.0%, and 3D-ms-US-em of phantoms with thickened isthmus reached a mean of 20.6% with a standard deviation of 12.4% (Table 2).

The deformation of the thyroid phantom was associated – with the exception of CT images – to a significant, systematic overestimation of the volumes (Fig. 5) and to a moderate increase of the standard deviation (Table 2).

In general, the trend to overestimations by em was smallest for the MRI method and largest for the sonography methods.

The mt assessments resulted in more congruent results and smaller standard deviations than observed with em, with almost no differences among the different scanning methods. The mt method showed the smallest deviation (0.1 ± 2.7%) for the 3D-sn-US-mt of the nodular phantom, and the largest deviation (1.9 ± 4.9%) for the 3D-ms-US-mt of phantoms with enlarged isthmus (Table 2).

For the deformed thyroid phantoms, the use of the mt method was associated to very limited differences of means and standard deviations. In this case the calculated volume (with the exception of

the CT) was rather underestimated. On average the standard deviations were fairly similar, although there were individual cases of increases or decreases (range 2.1% to 5.2%) (Table 2).

Nearly all 95% confidence intervals of the mt method included the zero value (Fig. 5), thus a systematic over- or underestimation was negligible. This differed from the results of em, where overestimations of deformed phantoms were observed with 3D-ms-US-em or underestimations of thickened isthmus phantoms were seen with MRI-em (Fig. 5).

Discussion

Several clinical studies have already addressed the issue of volumetric estimation of the thyroid in patients scheduled for surgery of different thyroid diseases (Hermans 1997, Lyshchik 2004). These studies have mostly considered the volume of the excised gland as reference standard, with the limitations that the excision is frequently incomplete and that the ligation of vessels – combined with the mechanical manipulation of the gland – most likely influences the thyroid volume by altering the blood flow and interstitial fluid content (Hermans 1997).

The present multimodal phantom study was undertaken with the aim to develop standards of reference as accurate as possible. Previous phantom studies, indeed, have mostly relied on a single imaging modality, either via ultrasound (Kot 2009, Ng 2004, Pang 2006, Riccabona 1996, Schlogl 2006, Schlogl 2001) or via CT (Shu 2011). A focus of this paper was to compare five different scanning methods, given that all phantoms were subjected to all imaging methods without relevant manipulation. Four of the methods provided volumetric data sets, and all four were fully evaluable. In addition, the present investigations were rather inexpensive (35 Euro per phantom). In particular, the measurement of net weight and volume of each phantom provided an independent and objective method to evaluate the accuracy of the volumetry calculations. At the end of the experiments (29 days in total), only two of the 18 models were found to have undergone weight changes due to leakage, and both were excluded from the analyses. The remaining models had a mean relative change of volume of 0.004%, thus negligible.

A limitation of the present study was that the imaging contrast of the phantoms was unrealistically optimal, allowing a much easier delimitation than ever possible with patients. Due to the sharp contrast between the filling mix and the rubber on the one hand and the rubber and the water on the outside on the other hand, the phantom boundaries were easily identified in each modality,(i.e. US, CT and MRI). On US, the filling was anechoic which does not match physiological appearance of the thyroid gland in vivo, finding the thyroid to exhibit a “salt-and-pepper”-pattern; also, phantom boundaries appeared thicker than they are. On CT, the phantoms were hyperdense with an isodense margin, also in contrast to the in-vivo appearance in a non-contrast-enhanced study, presenting the thyroid to have similar soft-tissue densities as the surrounding muscles, for example. Also, the phantoms were devoid of in vivo artifacts typically caused by arterial pulsation and respiration-related motion. Additionally, 3D-ms-US was performed using a benchtop tripod which represents an ideal situation lacking motion artifacts, not achievable in a clinical setting with the transducer being held by the operator. Therefore, the examined phantoms are clearly different from the thyroid gland as assessed in an in-vivo study, thus direct application of the obtained results to patient care is limited. These pitfalls, on the other hand, were equally present in all scanning modalities, thus the inner validity of the data was not jeopardized, as comparison between modalities was the aim of this study.However, the problem of an unrealistic anechoic filling of the phantoms could be addressed in future studies by using a filling that also produces contrast in US, e.g. corn starch in gelatin.

The data sets were initially available as slices of different thickness. The data acquisition and image reconstruction of CT and MRI occurred primarily in 3 mm slices, whereas the 3D-US data sets consisted of high numbers of slices (up to 400) of very limited thickness (0.28 to 0.34 mm). To optimize the analysis and the comparability of the data, the 3D data sets were reformatted to transversal planes with a slice thickness of 3 mm. After this procedure, the number of slices decreased to a range between 15 (for the 10 ml phantoms) and 40 (for the 200 ml phantoms). Furthermore, the voxel size of the modalities was similar, thus deviations in volume measurements caused by the influence of different modalities was considered negligible.

In addition to the option of delimiting the areas in parallel planes, it is also possible to delimit the target volumes in rotational planes oriented to a predefined longitudinal axis (Andermann 2007, Lyshchik 2004, Schlogl 2006, Schlogl 2001). This technique allows the manual tracing of up to 16 planes (Ng 2004, Pang 2006, Ying and Pang 2009), with the goal to reduce the time effort of the analyses. The mt method chosen in the present study, i.e., the contouring in parallel planes, is analogous to the rotational approach inasmuch as the adaptation of the slice thickness to 3 mm reduces the number of slices and accelerates the measurement process.

The calculation of the correlation coefficients is clearly insufficient for the comparison of different methods because it does not take into account systematic errors. For this reason, the statistical analyses were complemented with the calculation of the limits of agreement of Bland and Altman (Bland and Altman 1986), which correspond to a 1.96-fold standard deviation and include 95% of all expected values.

The conventional 2D-US-em volume calculations showed large discrepancies compared to the reference volumes, particularly for nodular deformation of the phantoms. In this case there was a general overestimation of the volumes, in analogy to other studies (Andermann 2007, Brunn 1981, Schlogl 2006). Other 2D-US studies, on the other hand, showed rather an underestimation of the volumes (Knudsen 1999, Nygaard 2002, Reinartz 2002, van Isselt 2003). The relatively large deviations are attributable to the mathematical formula used (Ozgen 1999), which is associated to a progressively increasing error with increasing extents of gland deformity.

The present data show that the calculations via em resulted more frequently in volume discrepancies for deformed lobes or thickened isthmus than for regularly shaped phantoms. These results are in line with previously published data (Rago 2006, Riccabona 1996).

All 3D methods (3D-ms-US, 3D-sn-US, CT, and MRI) showed significantly smaller discrepancies from the reference volumes when the mt method was used instead of em. Compatibly with other studies (Riccabona 1996), the present study showed that a clear advantage of the mt method consisted in its independence from the shape of the phantom. The novel aspect of this study, however, is that the superiority of the mt method was clearly shown for all four imaging techniques, including two 3D-US methods (Fig. 5). 3D-ms-US-mt and 3D-sn-US-mt were not only comparable to each other, but also in comparison to CT and MRI. Small additional advantages of 3D-sn-US-mt and CT-mt, in turn, were that their 95% confidence intervals included the zero value for all three phantom shapes, whereas the 3D-ms-US-mt showed a small but significant overestimation of the volume of regularly shaped phantoms and the MRI-mt a significant underestimation of the phantoms with thickened isthmus. These discrepancies, on the other hand, were rather limited, with a maximal underestimation of 0.6% and a maximal overestimation of 1.1%. A possible explanation for this small but systematic error is that the investigations were performed by a single operator and that a small operator error was possibly introduced. Additional analyses of intra- and inter-observer variability were not attempted in this study, in analogy to similar studies by other groups (Reinartz 2002, Schlogl 2001), because the results of the mt method were unambiguous.

Depending on the size of the phantom, the time effort of an mt measurement was 10-15 min, whereas em required only 2-4 min per measurement. The available literature mentions similar times (Hermans 1997), but also longer times (30-40 min) (Schlogl 2001, Tong 1998). These measurements are indeed time-consuming, however a possible use of 3D-US for thyroid volumetry in clinical routine does not necessarily require a radiologist. In analogy to the acquisition of CT and MRI data sets, the task can be delegated to specially-trained ultrasound technicians, as already standard of care in many institutions.

The present study indicates that both 3D-sn-US and 3D-ms-US are a possible alternative to the mt volumetry with low-dose CT or MRI. Thus, these results are compatible with those of Kot et al. (2009), who showed that both 3D-sn-US and 3D-ms-US provided precise and reliable results.

A clear advantage of the sonography procedures is that they avoid radiation exposure and circumvent different contraindications, e.g. claustrophobia or pace makers. In addition, a 2-min prolongation of a standard 2D-US for the acquisition of 3D data is altogether less expensive and time-consuming. Current disadvantages include a relatively large time effort in comparison to the 2D–US-em, as well as a limited access to retrosternal goiter (not investigated here). An additional problem is that the technical possibilities are not yet optimal. At present the exporting and processing of sonography data for assessment via commercially available standard software is possible, but relatively elaborate, depending on the availability of standard consoles for the assessment of cross-sectional imaging. The latter, in fact, are established in specialized radiological diagnostic units but are not available in all sonography laboratories (Freesmeyer 2012). It has not been investigated if proprietary volume software of different ultrasound devices are comparable to each other. To avoid this problem, we used the same standard cross-sectional imaging software for all 4 volumetry methods. Nevertheless, the performance of proprietary volume software should be compared to the investigated methods in future studies. The data set modifications performed in this phantom study are conceivably inappropriate for patient data, therefore improvements of the technical possibilities and their implementation in standard imaging software are absolute requisites for a potential clinical application of the present results. Future studies should also evaluate the performance of automated contouring as commonly available software solution in comparison to the investigated methods.

Conclusions

Multimodal-compatible thyroid phantom assessments confirmed the superiority of 3D-US in volumetry calculations, particularly when coupled with the manual traced method. The advantages of the manually traced method compared to the ellipsoid model were evident not only for regularly shaped phantoms, but also for deformed shapes. A novel aspect of this phantom study was the demonstration that 3D-US, CT, and MRI are basically equivalent methods for volumetry estimation. In addition, the data showed that the sensor navigated and the mechanically swept techniques were equally suitable for 3D-US. The analysis of the data by means of a standard workstation for cross-sectional imaging and a routine software did not prove problematic, although data adaptations are still ongoing to optimize the readability and assessability of the data sets. This phantom study was designed to compare different volume assessments and not to exactly represent thyroid diagnostics in vivo. Therefore, studies for in vivo validation of the present results are planned.

Acknowledgements

Dominik Driesch, BioControl Jena GmbH, Jena, Germany, is gratefully acknowledged for his contribution to data analysis, Dr. Ernesta Palombo-Kinne for language and editorial assistance with the manuscript.

Figures

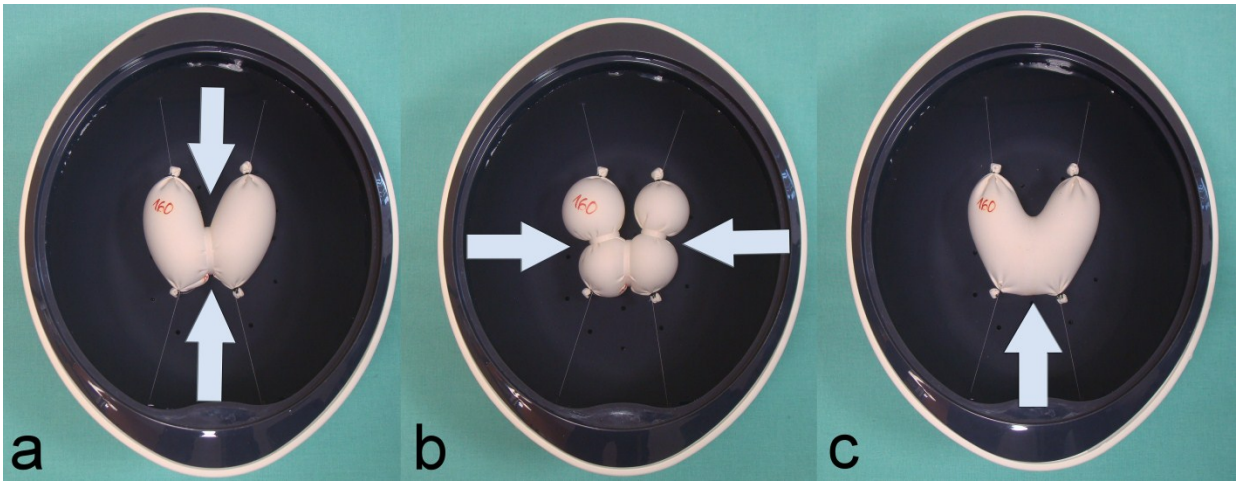

FIG. 1. Shape variants of the thyroid phantom (in this case with a target volume of 160 ml). (**a**) regular shape, with shaping of the isthmus via a cable tie (arrows); (**b**) deformed lobes via additional cable ties (arrows); (**c**) thickened isthmus via removal of all cable ties (arrow).

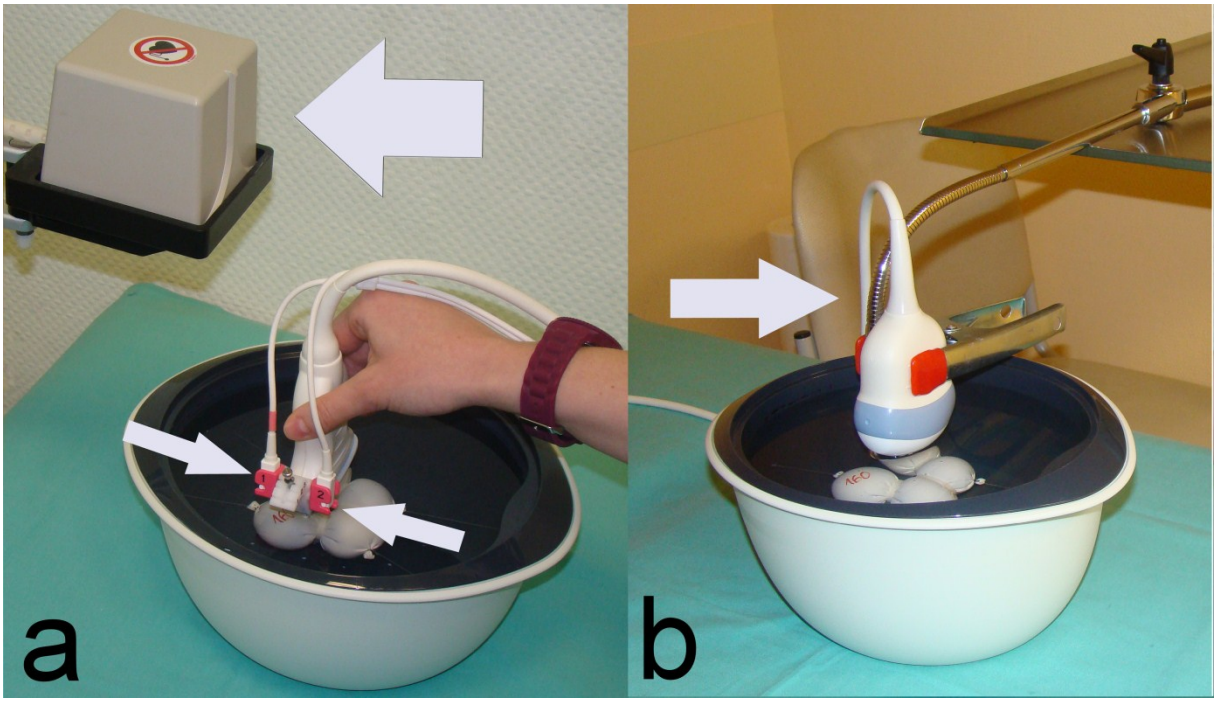

FIG. 2. Scanning set-up of 3D sonography methods: (**a**) sensor navigated (3D-sn-US), position and movement of the probe are recorded by means of positional sensors (small arrows) and an electromagnetic transmitter (large arrow); (**b**) mechanically swept (3D-ms-US), using a probe fixed to a benchtop tripod (arrow), automatic swivel of the array in the housing of the sonography probe.

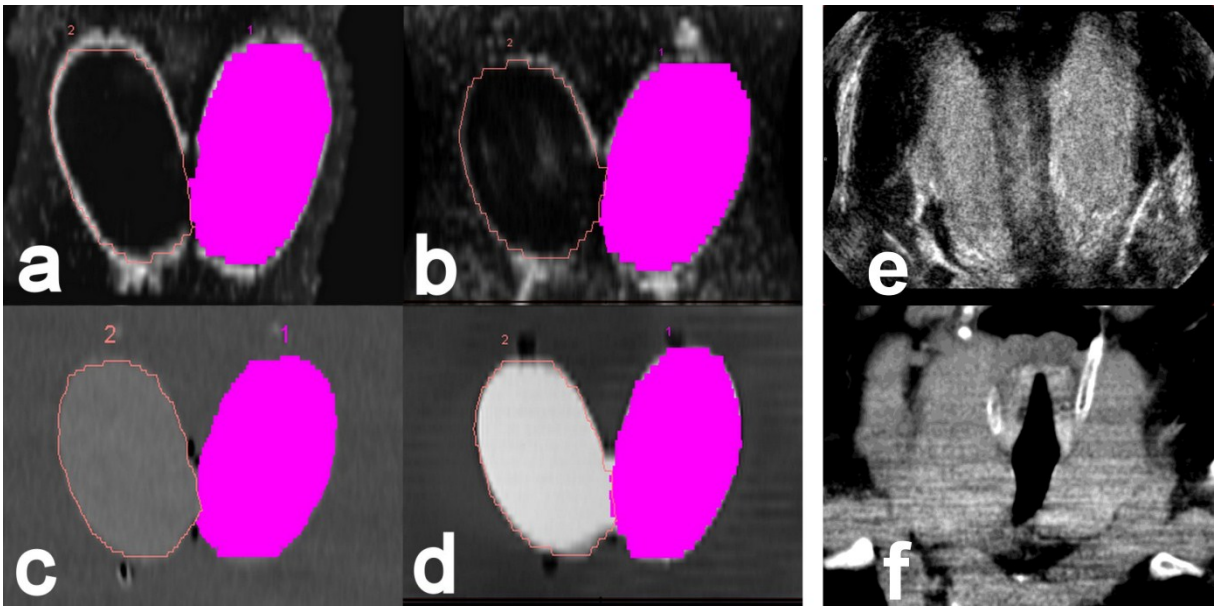

FIG. 3. Coronal slices of a thyroid phantom (in this case with a target volume of 160 ml) for all four 3D scanning methods: (**a**) 3D sensor navigated ultrasonography (3D-sn-US); (**b**) 3D mechanically swept US (3D-ms-US); (**c**) computed tomography (CT); (**d**) magnetic resonance imaging (MRI). Examples of manual tracing of the left lobe (magenta areas). (**e**) 3D-ms-US of a thyroid in vivo; (**f**) low dose CT of a thyroid in vivo.

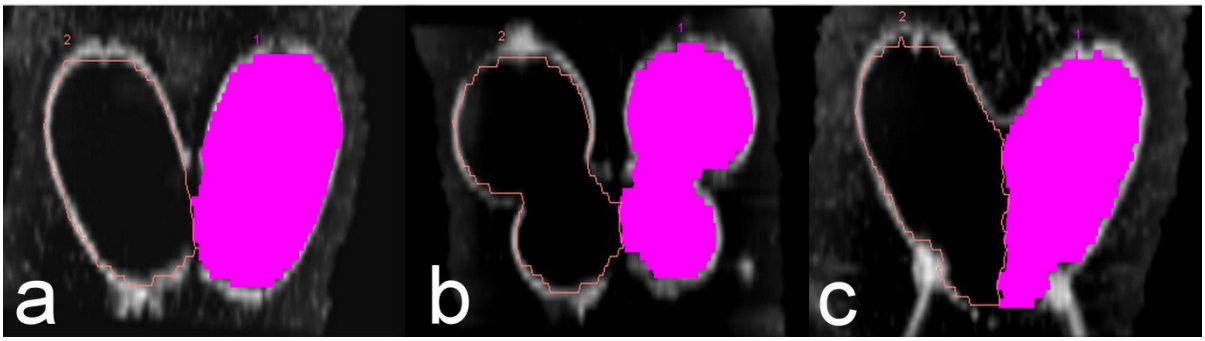

FIG. 4. Manual tracing of the three shape variants of thyroid phantoms via 3D sensor navigated ultrasonography (3D-sn-US): (**a**) regular shape; (**b**) deformed lobes; (**c**) thickened isthmus.

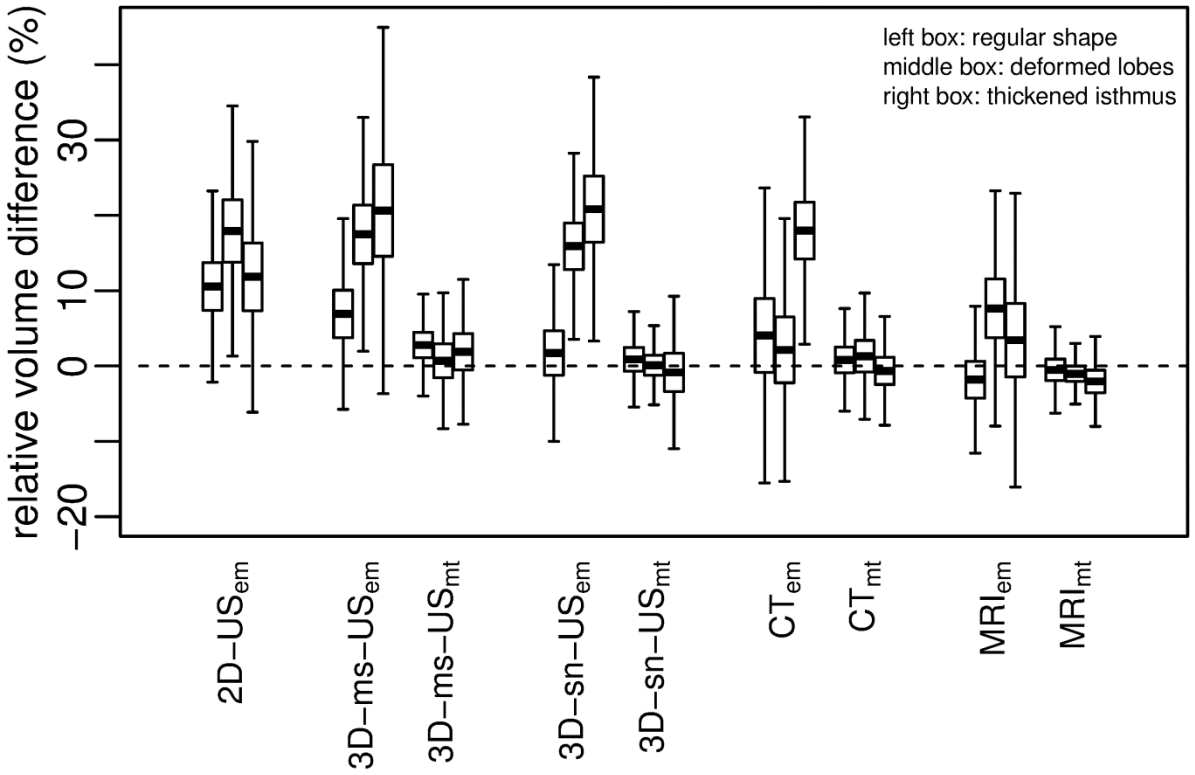

FIG. 5. Volume discrepancies between calculated and reference volumes of the thyroid phantoms. Volumes were quantified for three shape variants (regular shape, deformed lobes, thickened isthmus) using four different imaging methodologies: 2D- and 3D-ultrasonography (US); computed tomography (CT); and magnetic resonance imaging (MRI). Boxplots represent means and 95% confidence intervals of mean relative volume differences; whiskers represent the limits of agreement (1.96-fold standard deviation) according to Bland and Altman (Bland and Altman 1986). The zero line represents the standard of reference, i.e., the volumes derived from the measured net weight of the phantoms. Boxes above the zero line indicate a significant overestimation of the phantom volume, boxes below the zero line a significant underestimation.

em: ellipsoid model, sn: sensor navigated, mt: manually traced, ms: mechanically swept

Tables

TABLE 1. LITERATURE SELECTION OF DIFFERENT SCANNING AND VOLUMETRIC METHODS, WITH SPECIAL FOCUS ON THYROID VOLUMETRY AND 3D ULTRASONOGRAPHY

Reference	*Focus*		*Imaging Modality*					*Objects*		*3D-US Volumetry Method*		*3D-US Volumetry Software*		*Standard of Reference*			
	Thyroid	Non Thyroid	2D-US	3D-sn-US	3D-ms-US	CT	MRI	Phantom	In vivo	Ellipsoid Model	Manually Traced Method	Dedicated to 3D-US	Universally Applicable to Cross-sectional Imaging	Phantom	Surgery	Post Mortem	Imaging Modality
Brunn et al, 1981	X		X						X		X					X	
Riccabona et al, 1996		X	X		X			X			X	X		X			
Hermanns et al, 1997	X					X			X						X		
Tong et al, 1998		X	X		X				X	X	X	X					3D-sn-US
Özgen et al, 1999	X		X						X								2D-US
Schlögl et al, 2001	X		X	X				X	X		X	X		X		X	
Reinartz et al, 2002	X		X				X		X								MRI
Nygaard et al, 2002	X		X			X			X								CT
Ng et al, 2004	X			X				X	X		X	X		X			
van Isselt et al, 2003	X		X				X		X								MRI
Lyshchik et al, 2004	X		X	X					X	X	X	X			X		
Pang et al, 2006		X		X				X			X	X		X			
Rago et al, 2006	X		X	X					X		X	X					3D-sn-US
Schlögl et al, 2006	X		X	X				X			X	X		X			
Andermann et al, 2007	X		X	X					X		X	X					3D-sn-US
Ying et al, 2009		X		X					X	X	X	X				X	
Kot et al, 2009		X		X	X			X			X	X		X			
Shu et al, 2011	X					X		X	X					X			
Present study	X		X	X	X	X	X	X		X	X		X	X			

US: ultrasound, sn: sensor navigated, ms: mechanically swept, CT: computed tomography, MRI: magnetic resonance imaging

TABLE 2. STATISTICAL ANALYSES OF VOLUME MEASUREMENTS BY DIFFERENT SCANNING METHODS

Method	*Phantom Shape*	*Correlation Coefficient*[a]	*Summary Statistics*			*95% Confidence Intervals (CI)*		*Limits of Agreement (LA)*	
			Mean	*Median*	*SD*	*Lower CI*	*Upper CI*	*Lower LA*	*Upper LA*
2D-US (em)	regular	0.997	0.105	0.110	0.065	0.074	0.137	-0.021	0.232
	deformed lobes	0.992	0.179	0.176	0.085	0.138	0.221	0.013	0.345
	thickened isthmus	0.984	0.118	0.133	0.092	0.073	0.163	-0.061	0.298
3D-sn-US (em)	regular	0.996	0.017	-0.001	0.060	-0.012	0.047	-0.100	0.135
	deformed lobes	0.998	0.159	0.151	0.063	0.128	0.190	0.035	0.282
	thickened isthmus	0.993	0.208	0.240	0.089	0.164	0.252	0.033	0.383
3D-sn-US (mt)	regular	0.999	0.009	0.016	0.032	-0.007	0.025	-0.055	0.072
	deformed lobes	0.999	0.001	0.001	0.027	-0.012	0.014	-0.052	0.054
	thickened isthmus	0.999	-0.009	-0.003	0.052	-0.034	0.017	-0.110	0.093
3D-ms-US (em)	regular	0.996	0.069	0.071	0.065	0.037	0.101	-0.058	0.196
	deformed lobes	0.997	0.175	0.154	0.079	0.136	0.213	0.019	0.330
	thickened isthmus	0.993	0.206	0.210	0.124	0.146	0.267	-0.037	0.450
3D-ms-US (mt)	regular	1.000	0.028	0.041	0.034	0.011	0.045	-0.040	0.095
	deformed lobes	0.998	0.007	0.022	0.046	-0.016	0.029	-0.083	0.097
	thickened isthmus	0.999	0.019	0.032	0.049	-0.005	0.043	-0.077	0.115
CT (em)	regular	0.999	0.040	0.029	0.100	-0.008	0.089	-0.155	0.236
	deformed lobes	0.993	0.021	0.035	0.089	-0.022	0.065	-0.153	0.196
	thickened isthmus	0.995	0.180	0.172	0.077	0.142	0.217	0.029	0.330
CT (mt)	regular	0.999	0.008	0.017	0.035	-0.009	0.025	-0.060	0.076
	deformed lobes	0.997	0.013	0.024	0.043	-0.008	0.034	-0.071	0.097
	thickened isthmus	0.999	-0.006	-0.010	0.037	-0.025	0.012	-0.079	0.066
MRI (em)	regular	0.998	-0.018	-0.032	0.050	-0.042	0.006	-0.116	0.079
	deformed lobes	0.993	0.076	0.071	0.080	0.037	0.115	-0.080	0.233
	thickened isthmus	0.990	0.034	0.031	0.099	-0.015	0.083	-0.161	0.229
MRI (mt)	regular	0.999	-0.005	-0.004	0.029	-0.020	0.009	-0.063	0.052
	deformed lobes	1.000	-0.010	-0.005	0.021	-0.020	0.000	-0.051	0.030
	thickened isthmus	0.999	-0.020	-0.025	0.030	-0.035	-0.006	-0.080	0.039

[a] all correlations statistically significant

US: ultrasound, em: ellipsoid model, sn: sensor navigated, mt: manually traced, ms: mechanically swept, CT: computed tomography, MRI: magnetic resonance imaging, SD: standard deviation.

References

Andermann P, Schlogl S, Mader U, Luster M, Lassmann M, Reiners C, (2007) Intra- and interobserver variability of thyroid volume measurements in healthy adults by 2D versus 3D ultrasound. Nuklearmedizin 46:1-7.

Bland JM, Altman DG, (1986) Statistical methods for assessing agreement between two methods of clinical measurement. Lancet 1:307-10.

Brunn J, Block U, Ruf G, Bos I, Kunze WP, Scriba PC, (1981) [Volumetric analysis of thyroid lobes by real-time ultrasound (author's transl)]. Dtsch Med Wochenschr 106:1338-40.

Freesmeyer M, Darr A, Schierz JH, Schleussner E, Wiegand S, Opfermann T, (2012) 3D ultrasound DICOM data of the thyroid gland. First experiences in exporting, archiving, second reading and 3D processing. Nuklearmedizin 51:73-8.

Hermans R, Bouillon R, Laga K, Delaere PR, Foer BD, Marchal G, Baert AL, (1997) Estimation of thyroid gland volume by spiral computed tomography. Eur Radiol 7:214-6.

Knudsen N, Bols B, Bulow I, Jorgensen T, Perrild H, Ovesen L, Laurberg P, (1999) Validation of ultrasonography of the thyroid gland for epidemiological purposes. Thyroid 9:1069-74.

Kot BC, Sin DM, Ying M, (2009) Evaluation of the accuracy and reliability of two 3-dimensional sonography methods in volume measurement of small structures: an in vitro phantom study. J Clin Ultrasound 37:82-8.

Lucas KJ, (2000) Use of thyroid ultrasound volume in calculating radioactive iodine dose in hyperthyroidism. Thyroid 10:151-5.

Lyshchik A, Drozd V, Reiners C, (2004) Accuracy of three-dimensional ultrasound for thyroid volume measurement in children and adolescents. Thyroid 14:113-20.

Ng E, Chen T, Lam R, Sin D, Ying M, (2004) Three-dimensional ultrasound measurement of thyroid volume in asymptomatic male Chinese. Ultrasound Med Biol 30:1427-33.

Nygaard B, Nygaard T, Court-Payen M, Jensen LI, Soe-Jensen P, Gerhard Nielsen K, Fugl M, Hegedus L, (2002) Thyroid volume measured by ultrasonography and CT. Acta Radiol 43:269-74.

Ozgen A, Erol C, Kaya A, Ozmen MN, Akata D, Akhan O, (1999) Interobserver and intraobserver variations in sonographic measurement of thyroid volume in children. European journal of endocrinology / European Federation of Endocrine Societies 140:328-31.

Pang BS, Kot BC, Ying M, (2006) Three-dimensional ultrasound volumetric measurements: is the largest number of image planes necessary for outlining the region-of-interest? Ultrasound Med Biol 32:1193-202.

Rago T, Bencivelli W, Scutari M, Di Cosmo C, Rizzo C, Berti P, Miccoli P, Pinchera A, Vitti P, (2006) The newly developed three-dimensional (3D) and two-dimensional (2D) thyroid ultrasound are strongly correlated, but 2D overestimates thyroid volume in the presence of nodules. J Endocrinol Invest 29:423-6

Reinartz P, Sabri O, Zimny M, Nowak B, Cremerius U, Setani K, Bull U, (2002) Thyroid volume measurement in patients prior to radioiodine therapy: comparison between three-dimensional magnetic resonance imaging and ultrasonography. Thyroid 12:713-7.

Riccabona M, Nelson TR, Pretorius DH, (1996) Three-dimensional ultrasound: accuracy of distance and volume measurements. Ultrasound in obstetrics & gynecology : the official journal of the International Society of Ultrasound in Obstetrics and Gynecology 7:429-34.

Schlogl S, Andermann P, Luster M, Reiners C, Lassmann M, (2006) A novel thyroid phantom for ultrasound volumetry: determination of intraobserver and interobserver variability. Thyroid 16:41-6.

Schlogl S, Werner E, Lassmann M, Terekhova J, Muffert S, Seybold S, Reiners C, (2001) The use of three-dimensional ultrasound for thyroid volumetry. Thyroid 11:569-74.

Shu J, Zhao J, Guo D, Luo Y, Zhong W, Xie W, (2011) Accuracy and reliability of thyroid volumetry using spiral CT and thyroid volume in a healthy, non-iodine-deficient Chinese adult population. Eur J Radiol 77:274-80.

Tong S, Cardinal HN, McLoughlin RF, Downey DB, Fenster A, (1998) Intra- and inter-observer variability and reliability of prostate volume measurement via two-dimensional and three-dimensional ultrasound imaging. Ultrasound Med Biol 24:673-81.

van Isselt JW, de Klerk JM, van Rijk PP, van Gils AP, Polman LJ, Kamphuis C, Meijer R, Beekman FJ, (2003) Comparison of methods for thyroid volume estimation in patients with Graves' disease. Eur J Nucl Med Mol Imaging 30:525-31.

Vitti P, Martino E, Aghini-Lombardi F, Rago T, Antonangeli L, Maccherini D, Nanni P, Loviselli A, Balestrieri A, Araneo G, et al., (1994) Thyroid volume measurement by ultrasound in children as a tool for the assessment of mild iodine deficiency. J Clin Endocrinol Metab 79:600-3 (abstract).

Volzke H, Ludemann J, Robinson DM, Spieker KW, Schwahn C, Kramer A, John U, Meng W, (2003) The prevalence of undiagnosed thyroid disorders in a previously iodine-deficient area. Thyroid 13:803-10 (abstract).

Ying M, Pang BS, (2009) Three-dimensional ultrasound measurement of cervical lymph node volume. Br J Radiol 82:617-25.

Ying M, Yung DM, Ho KK, (2008) Two-dimensional ultrasound measurement of thyroid gland volume: a new equation with higher correlation with 3-D ultrasound measurement. Ultrasound Med Biol 34:56-63 (abstract).

3.2.2. Dreidimensionaler Ultraschall (3D-US)

3.2.2.2. Klinische Untersuchungen zur Schilddrüsenvolumetrie - 3D-US versus ldCT

3-D Ultrasonography is as Accurate as Low-dose CT in Thyroid Volumetry

Publikation 2013 in NUKLEARMEDIZIN

3D ultrasonography is as accurate as low-dose CT in thyroid volumetry

K. Licht; A. Darr; T. Opfermann; T. Winkens; M. Freesmeyer

Clinic of Nuclear Medicine, Jena University Hospital, Germany

Keywords

Thyroid gland volume, thyroid gland ultrasonography, thyroid gland computed tomography, thyroid gland three-dimensional imaging, volumetry methods

Summary

Aim: The purpose of this study was to compare thyroid volumetry by three-dimensional mechanically swept ultrasonography (3DmsUS) and low-dose computed tomography (ldCT). Patients, methods: 30 subjects referred for radioiodine therapy of benign thyroid diseases were subjected to 3DmsUS and ldCT. A prerequisite of 3DmsUS analyses was that the scans had to capture the entire thyroid, excluding therefore cases with a very large volume or retrosternal portions. The 3DmsUS data were transformed into a DICOM format, and volumetry calculations were performed via a multimodal workstation equipped with standard software for cross-sectional imaging. Volume was calculated applying both the ellipsoid model and a manually tracing method. Statistical analyses included 95% confidence intervals (CI) of the means and limits of agreement according to Bland and Altman, the latter including 95% of all expected values. Results: Volumetric measurements by 3DmsUS and ldCT resulted in very high, significant correlation coefficients, r = 0.997 using the ellipsoid model and r = 0.993 with the manually tracing method. The mean relative differences of the two imaging modalities proved very small (–1.2±4.0% [95% CI –2.62; 0.28] using the ellipsoid model; –1.1±5.2% [95% CI –2.93; 0.80] using the manually tracing method) and the limits of agreement sufficiently narrow (–9.1% to 6.8%; –11.3% to 9.2%, respectively). Conclusion: For moderately enlarged thyroids, volumetry with 3DmsUS proved comparable to that of ldCT, irrespective of whether the ellipsoid model or the manually tracing method was applied. Thus, 3DmsUS qualifies as a potential alternative to ldCT, provided that the organ is completely accessible. The use of a standard workstation for cross-sectional imaging with routine software did not prove problematic.

Schlüsselwörter

Schilddrüsenvolumen, Schilddrüsen-Ultraschall, Schilddrüsen-CT, dreidimensionale Bildgebung, Volumetrie

Zusammenfassung

Ziel dieser Studie ist der Vergleich der Schilddrüsenvolumetrie mittels dreidimensionalem mechanisch geschwenktem Ultraschall (3DmsUS) und Niedrigdosis-Computertomographie (ldCT). Patienten, Methoden: Bei 30 Patienten, die aufgrund einer gutartigen Schilddrüsenerkrankung eine Radioiodtherapie erhielten, wurde zusätzlich 3DmsUS und ldCT durchgeführt. Voraussetzung für den 3DmsUS war, dass die komplette Schilddrüse erfasst werden konnte. Die 3DmsUS-Daten wurden in ein DICOM-Format umgewandelt und anschließend die Volumenberechnungen mit einer Standardsoftware für Schnittbildgebung ausgeführt. Das Volumen wurde mit der Ellipsoidformel und einer manuellen Konturierungsmethode ermittelt. Die Statistik wurde mit 95%-Konfidenzintervallen der Mittelwerte und den „limits of agreement" nach Bland und Altmann durchgeführt. Ergebnisse: Der Vergleich der beiden Volumetriemethoden (3DmsUS und ldCT) ergab eine positive, signifikante Korrelation für die Ellipsoidformel (r = 0.997) und die manuelle Konturierungsmethode (r = 0.993). Die durchschnittlichen relativen Differenzen zwischen den Volumetriemethoden waren niedrig (Ellipsoidformel: –1.2±4.0% [95% CI –2.62; 0.28]; manuelle Konturierungsmethode: –1.1±5.2% [95% CI –2.93; 0.80]). Die „limits of agreement" waren ausreichend eng (Ellipsoidformel: –9.1% bis 6.8%; manuelle Konturierungsmethode: –11.3% bis 9.2%). Schlussfolgerung: 3DmsUS und ldCT liefern bei moderat vergrößerten Schilddrüsen vergleichbare Volumina, unabhängig davon, ob die Ellipsoidformel oder die manuelle Konturierungsmethode angewandt wird. Daher stellt der 3DmsUS eine potenzielle Alternative zur ldCT dar, vorausgesetzt, dass das Organ vollständig abgebildet werden kann. Der Einsatz einer Standardsoftware für Schnittbildgebung zur Volumenberechnung war unproblematisch.

Correspondence to:
Martin Freesmeyer, MD
Clinic of Nuclear Medicine, Jena University Hospital
Bachstraße 18, 07743 Jena, Germany
Tel. +49/(0)36 41/93 32 20, Fax +49/(0)36 41/93 32 44
E-mail: martin.freesmeyer@med.uni-jena.de

Volumetrie der Schilddrüse mit 3D-Ultraschall ist so exakt wie CT-Volumetrie
Nuklearmedizin 2014; 0: ••–••
DOI:10.3413/Nukmed-0615-13-08
received: August 19, 2013
accepted in revised form: November 12, 2013
prepublished online: November 26, 2013

Pathological changes of the thyroid gland are frequent, mostly depending on local availability of iodine and prevalence of goiter (24). An exact determination of the thyroid volume and its pathological changes is clinically relevant because therapeutic decisions and monitoring of therapy response largely depend on thyroid volume (16, 23).

The most frequently used volumetry method is based on the assumption that each lobe represents a rotational ellipsoid (3). The volume of each lobe is calculated with the formula $length_{max} \times width_{max} \times depth_{max} \times f$, and the two volumes are added. Different values have been proposed for the correction factor f (3, 7, 16, 26), but usually 0.5 is applied in clinical routine. The ellipsoid model, however, is subject to a relatively high intra- and inter-observer variability (13). Also, a nodular goiter can cause lobe deformities and/or thickening of the isthmus that may result in significant imprecisions of the measurements (15). In alternative, for 3-dimensional (3D) data sets it is also possible to delimit the thyroid gland in parallel planes using the manually tracing method. This method is less operator-dependent and some authors consider it a gold standard (16, 23).

In clinical routine, computed tomography (CT) is an established imaging technique for thyroid volumetry (12, 21), particularly in case of severely enlarged or deformed lobes. Both the ellipsoid and the manually tracing methods are applicable in CT. Imaging via 3-dimensional sonography (3D-US) is also possible (22), but volumetric assessments have been possible only using a dedicated workstation equipped with a special software (1, 8). Recently, however, it has become possible to generate universally compatible data in DICOM format (Digital Imaging and Communications in Medicine). These data can be subjected to volumetry calculation via a multimodal workstation (5).

The focus of this paper was to investigate whether 3D mechanically swept US (3DmsUS) is comparable to low-dose CT (ldCT) for the purpose of thyroid volumetry. The two imaging modalities were compared using clinical data sets assessed with a multimodal cross-sectional workstation equipped with standard software used in clinical routine. Comparisons were performed also after the application of the ellipsoid model and the manually tracing method.

Fig. 1 Set-up of 3D ultrasonography of the thyroid, using a GE Voluson E8 ultrasound platform and a mechanically swept probe RAB 6-D with convex array; multiplanar display in the three standard orientations (transversal, sagittal, coronal)

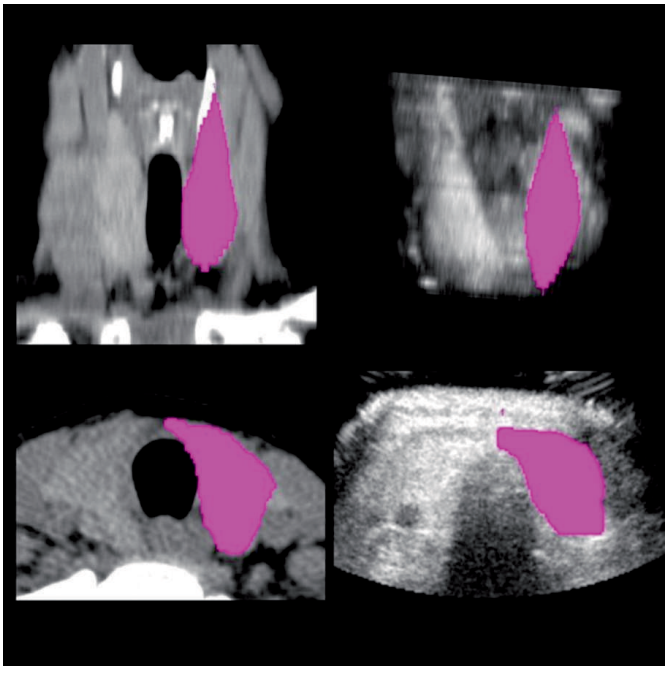

Fig. 2 Left thyroid lobe after manual contouring on a standard assessment console: comparison of low-dose computed tomography (ldCT; left) and 3D-mechanically swept ultrasonography (3DmsUS) assessment (right) in coronal (upper panel) and transversal planes (lower panel)

Patients, material, methods

Patients

This study included 30 consecutive adult patients (20 women, 10 men; mean age 66.8 years, range 44 to 88 years, median 68 years) with benign thyroid diseases, referred to the clinic for radioiodine therapy. The patients had already been included in a separate dosimetry study with ldCT acquisitions (submitted for publication). Written informed consent and ethic committee's approval were obtained. The patients were not exposed to additional radiation. An inclusion criterion for the present analysis was that the thyroid had to be fully depicted by the 3DmsUS scan. Accordingly, 4 additional patients could not be included in the analyses because their thyroid

was very large and/or had retrosternal extensions not fully captured by the field of view of the 3D scan.

Imaging

3DmsUS

The three-dimensional mechanically swept ultrasonography (3DmsUS) was performed using Voluson E8 (GE Medical Systems, Zipf, Austria) and a RAB 6-D convex probe (▶Fig. 1). The 3D acquisition was achieved via a mechanically swept array contained in the probe housing. Each scan was performed with a frequency of 6 MHz, field of view of 63°, and volume angle of 85°. The focus was centered in the middle of the thyroid. As final step, the equipment reconstructed a 3D volume data set.

ldCT

CT scans were performed with a Biograph mCT 40 (Siemens, Erlangen, Germany) using a low-dose technique (120 kV, 50 mAs), the low-dose computed tomography (ldCT). The reconstruction consisted of 3 mm slices with 1.5 mm overlap.

Volumetry

The volumetry assessments were performed by an experienced investigator. The images of both 3DmsUS and ldCT were assessed with the ellipsoid formula [$length_{max} \times width_{max} \times height_{max} \times 0.5$], with volume acquisitions in two orthogonal planes, as well as with the manually tracing method.

The calculations were performed with a multimodal workstation (Syngo MultiModality WORKPLACE 2010a, Siemens, Erlangen, Germany) equipped with a 3D routine software for cross-sectional imaging (syngoMMWP Version VE40A, CT-Tool VA31A_SP3.5_P17, Siemens, Erlangen, Germany). This software allows first to represent the data sets in the three standard planes and then to further evaluate the data.

To obtain the typically missing orientation of the 3D-US data, the DICOM entries were modified by means of the software PMOD (Version 3.4, PMOD Technologies Ltd., Zurich, Switzerland) and the software package Sante DICOM Editor (Version 3.1.21, Santesoft Ltd., Athens, Greece). The orientation was fixed according to a reference phantom with markers. Subsequently, all patients were scanned with the same transducer orientation. The slice thickness of the exported 3D-US data was adapted from 0.28–0.34 mm to 3.0 mm. This allowed on one hand to limit the time efforts of the analyses, and on the other hand to guarantee the comparability of the slice thickness to that of the CT scans (3 mm).

In the case of the ellipsoid model, the assessment started with determining the maximum length of the lobe by angulating the dataset until the plane of maximum length was displayed. The transversal plane was then oriented perpendicularly to the coronal plane, in order to measure the maximum width and depth.

The manually tracing method was applied in the volumetry software via manual tracing of the thyroid contours in parallel slices of transversal planes. The volume calculations were automatically performed by the program.

Tab. 1 Thyroid volumes (ml) as assessed by 3DmsUS and ldCT, using the ellipsoid model and the manually tracing method

	ellipsoid model		manually traced method	
	3DmsUS	ldCT	3DmsUS	ldCT
mean	52.3	53.4	56.5	57.1
median	47.3	47.5	52.1	56.0
standard deviation	23.7	25.0	22.1	22.1

3DmsUS: 3D-mechanically swept ultrasonography; ldCT: low-dose computed tomography

Tab. 2 Statistical analyses of relative volume differences in the comparison between 3D-mechanically swept ultrasonography (3DmsUS) and low-dose computed tomography (ldCT), using the ellipsoid model (em) and the manually tracing method (mt)

		$3DmsUS_{em}$ versus $ldCT_{em}$	$3DmsUS_{mt}$ versus $ldCT_{mt}$
mean (%)		–1.17	–1.07
median (%)		–1.40	–1.20
standard deviation (%)		±4.05	±5.21
95% CI (%)	lower limit	–2.62	–2.93
	upper limit	0.28	0.80
agreement (%)	lower limit	–9.10	–11.28
	upper limit	6.76	9.15
correlation coefficient		0.997	0.993
p value		$< 2.2*10^{-16}$	$< 2.2*10^{-16}$

Statistical analysis

The Pearson's correlation coefficient was used to compare the thyroid volumes as determined by 3DmsUS and ldCT. The Bland and Altman method (2) was also applied to compare the volumetry methods. For this purpose, relative volume differences (%) were calculated for all measurements, i.e., the difference between the volumes measured by either method was divided by the mean of the two values. In addition, the methods were compared using the limits of agreement recommended by Bland and Altman (2), which correspond to 1.96-fold standard deviations and include 95% of all expected values. To assess systematic errors, the 95% confidence intervals of the means were also calculated.

All calculations were performed with the program language R Version 2.15.1 (RDevelopment Core Team, 2012).

Results

The results of the thyroid volumes are shown (▶Tab. 1). The mean volumes ranged between 52.3 and 53.4 ml after assessment via ellipsoid formula, and be-

Tab. 3 Literature selection of different scanning and volumetry assessments, with focus on thyroid volumetry and 3D ultrasonography

first author, year	focus		imaging modality					objects		3D-US volumetry method		3D-US volumetry software		standard of reference			
	thyroid	non thyroid	2D-US	3DsnUS	3DmsUS	CT	MRI	phan-tom	human	ellipsoid model	contouring method	dedicated to 3D-US	universally applicable*	phan-tom	surgery	post mortem	imaging modality
Riccabona, 1996		X	X		X			X			X	X		X			
Tong, 1998		X			X				X	X	X	X					3DmsUS
Schlögl, 2001	X		X	X				X	X		X	X		X		X	
Ng, 2004	X			X				X	X		X	X		X			
Lyshchik, 2004	X		X	X					X	X	X	X			X		
Pang, 2006		X		X				X			X	X		X			
Rago, 2006	X		X	X					X		X	X					3DsnUS
Schlögl, 2006	X		X	X				X			X	X		X			
Andermann, 2007	X		X	X					X		X	X					3DsnUS
Malago, 2008	X		X		X				X		X	X			X		
Ying, 2009		X		X					X	X	X	X				X	
Kot, 2009		X		X	X			X			X	X		X			
present study	**X**				**X**	**X**			**X**	**X**	**X**		**X**				**CT**

*to cross-sectional imaging; US: ultrasonography; sn: sensor navigated; ms: mechanically swept; CT: computed tomography; MRI: magnetic resonance imaging

tween 56.5 and 57.1 ml after assessment with the manually tracing method. The means and medians obtained with the ellipsoid formula tended to be lower than those obtained with the manually tracing method. The range of the measured volumes was 15.0 to 111.2 ml.

The results of the comparisons between the imaging modalities and volumetry methods are shown (▶Tab. 2). Using the ellipsoid model, there was a high (r = 0.997), significant correlation between 3DmsUS and ldCT (relative mean difference –1.2%, median –1.4%). The pronounced correlation was confirmed by the narrow range of the limits of agreement (–9.1% to 6.8%) (▶Tab. 2). The use of the manually tracing method provided similar results, including a high correlation coefficient (r = 0.993) between 3DmsUS and ldCT. In addition, the relative mean and median differences were very small (–1.1% and –1.2%, respectively), and the range of the limits of agreement sufficiently narrow (–11.3% to 9.1%) (▶Tab. 2).

Discussion

Several studies have indicated a potential application of 3D-US in the volumetry of thyroid and other organs (10, 17, 19). An overview on different imaging and volumetry methods via 3D-US is shown (▶Tab. 3). An important aspect of 3D-US in thyroid volumetry is that not only the ellipsoid model, with its partial limitations (9, 25), but also the manually tracing method can be applied in this imaging modality (1, 19). As a matter of fact the field of view in established 3D-US is still limited, therefore large organs cannot be completely imaged (5).

Particularly in case of severely enlarged and/or deformed thyroid glands, with standard 2D B-mode ultrasound reaching its limits, thyroid volumetry based on CT is a commonly accepted procedure (4, 6, 12, 21), with the advantage that both the ellipsoid model and the manually tracing method can be applied. Moreover, the ldCT images may allow evaluation of adjacent structures, e.g., the trachea and oesophagus (20). The ldCT, however, is associated with a certain degree of radiation

exposure, if only limited. Also, claustrophobic patients can only be imaged after sedation. At least in problematic cases, therefore, it would be useful to recur to an alternative option.

The present study compared for the first time the suitability of 3D-US for thyroid volumetry in comparison to ldCT, using two different methods, the ellipsoid model and the manually tracing method.

The contouring in parallel planes with the adaptation of the slice thickness to 3 mm, as chosen in the present study, was performed to reduce the time efforts of the assessments. Concerning the expenditure of time, the manually tracing method seems comparable to the method of delimiting the target volumes in rotational planes oriented to a predefined longitudinal axis, as described by several authors (1, 9, 18, 19). This technique allows manual tracing of up to 16 planes, depending on the study (11, 14, 25).

The present volumetry study was performed in a nuclear medicine setup, therefore the resulting data did not reflect actual volumes. Other studies, in turn, have used surgical or autoptic thyroid samples as reference (6, 19). Since this study was aimed at establishing a principle comparability of 3DmsUS and ldCT, an external reference was considered dispensable at this stage. Nevertheless, the applicability and accuracy of CT for measuring the volume of the thyroid gland has been shown by Hermans et al., comparing the volume as assessed by CT with post-thyroidectomy weight of the thyroid gland, thus providing a valid reference for the present study (6).

The high correlation coefficients obtained in the comparison between the different strategies showed that 3DmsUS and ldCT provided very similar volumetry results (▶Tab. 2). Because the correlation coefficients do not exclude a systematic error, the 95% confidence intervals and the limits of agreement proposed by Bland and Altman (2) were also calculated.

The present results showed a high comparability of 3DmsUS and ldCT, irrespective of whether the ellipsoid model or the manually tracing method was used. This was shown not only by the small relative differences, but also by the sufficiently tight range of the limits of agreement. The differences were assessed as reasonably acceptable, since the tightness of the limit of agreement (approximately ± 10%) is compatible with commonly accepted practices for clinical routine in Germany. Regarding radioiodine therapy, for example, a ±10% difference between calculated and administered dosage is usually considered acceptable.

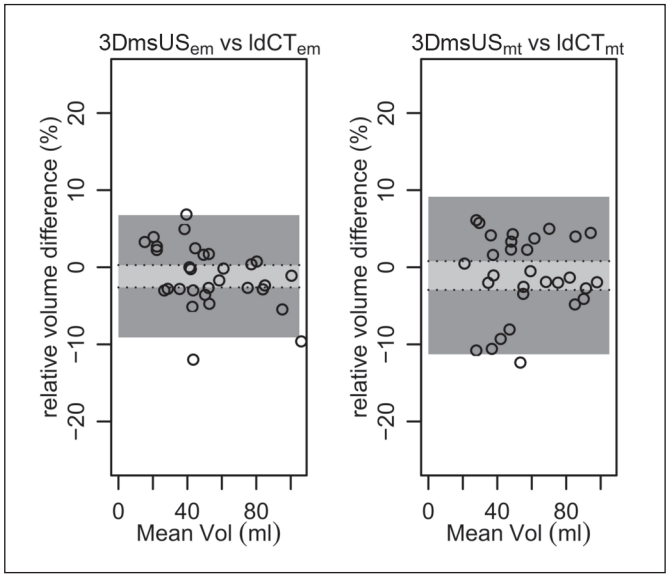

Fig. 3 Bland and Altmann plot of the relative volume differences in volumetry assessments by 3D-mechanically swept ultrasonography (3DmsUS) and low-dose computed tomography (ldCT), both with the ellipsoid model (em) and the manually tracing method (mt). Light grey areas represent confidence intervals (CI) of the means and dark grey areas the range of the limits of agreement.

Application of the ellipsoid model resulted in slightly lower values than the manually tracing method, irrespective of whether the 3DmsUS or the ldCT was used (▶Tab. 1). The literature reports both overestimations (1, 3, 18) and underestimations (7, 12, 16, 23) of the ellipsoid model in conventional ultrasonography.

In terms of volumetric assessment of the acquired images, the time efforts proved similar for both 3DmsUS and ldCT. Depending on the size of the thyroid, the manually tracing measurements required approximately 8–10 minutes, whereas the use of the ellipsoid formula required only 2–3 minutes.

- The potential advantages of 3DmsUS in thyroid volumetry reside mainly in the avoidance of radiation exposure and in the management of patients with contraindications, most notably claustrophobia. In addition, a prolongation of routine 2D-US by approximately 2 minutes – as necessary to obtain a 3D scan – adds only limited costs and time efforts.
- Disadvantages of the 3DmsUS consist in the difficulty of scanning retrosternal or intrathoracic goiter extensions, or large goiters at all, given the limited field of view of the scanner (5). Indeed, four patients had to be excluded from the present analyses because of these limitations. Thus, a clinical application of 3DmsUS is not realistic for thyroid volumes exceeding 100 ml. For large or extended thyroids the method of choice remains the ldCT.

Technical developments are therefore necessary, including probes able to scan large volumes and to provide high local resolution. A possible method to increase the field of view and maintain appropriate spatial resolution is the sensor navigated ultrasonography (8, 9, 11, 15, 19).

Limitations

Important limitations are also the suboptimal technical possibilities regarding medical sonography data. At present, data export and processing into a commercially available standard software is possible but comparably elaborate, depending on the availability of consoles for cross-sectional imaging. The latter is established in diagnostic radiology, however, not in all sonography centers (5). Recently the DICOM standard has been introduced for 3D-US data, however this is not yet ubiquitously

implemented in sonography machines and processing workstations (5). The data adaptations used in the present study are clearly premature for clinical routine, therefore further technical developments and implementation in standard imaging software are needed.

Further studies are planned to evaluate the effects of inter- and intra-observer variability, in analogy to Andermann et al. (1). Also, the data must be validated against surgically removed thyroid glands.

Conclusions

Our data show that the accuracy of thyroid volumetry with 3DmsUS is comparable to that of ldCT, at least for moderately enlarged thyroids. For the first time it was demonstrated that – in as much as the thyroid is fully captured by the 3DmsUS scan – the ldCT can be avoided, reducing the burden of radiation exposure. The volumetric accuracy of 3DmsUS was demonstrated with both the ellipsoid model and the manually tracing method. The evaluation without the need of a dedicated 3D-US software, using instead a standard workstation for cross-sectional imaging and a routine software, proved feasible and in fact not problematic. Nevertheless, adaptations of the 3D-US data sets are still necessary to allow legibility and assessment of the data. The use of 3 mm thick sections and a uniform software for both ldCT and 3D-US resulted in practically identical time efforts for volumetry assessments. Technical developments, including new hardware and software optimized for volumetry purposes, are still required, as well as a wider implementation of the required DICOM standards. Validation of the present data is planned in a study that includes surgically removed thyroid glands.

Acknowledgements

Dominik Driesch, BioControl Jena GmbH, Jena, Germany, is gratefully acknowledged for his contribution to data analysis, Dr. Ernesta Palombo-Kinne for language and editorial assistance with the manuscript.

Conflict of interest

The authors declare that they have no conflict of interest.

References

1. Andermann P, Schlogl S, Mader U et al. Intra- and interobserver variability of thyroid volume measurements in healthy adults by 2D versus 3D ultrasound. Nuklearmedizin 2007; 46: 1–7.
2. Bland JM, Altman DG. Statistical methods for assessing agreement between two methods of clinical measurement. Lancet 1986; 1: 307–310.
3. Brunn J, Block U, Ruf G et al. Volumetric analysis of thyroid lobes by real-time ultrasound. Dtsch Med Wochenschr 1981; 106: 1338–1340.
4. Darr AM, Opfermann T, Niksch T et al. Low-activity ^{124}I-PET/low-dose CT versus ^{99m}Tc-pertechnetate planar scintigraphy or ^{99m}Tc-pertechnetate single-photon emission computed tomography of the thyroid: A pilot comparison. Clin Nucl Med 2013; 38: 770–777.
5. Freesmeyer M, Darr A, Schierz JH et al. 3D ultrasound DICOM data of the thyroid gland. First experiences in exporting, archiving, second reading and 3D processing. Nuklearmedizin 2012; 51: 73–78.
6. Hermans R, Bouillon R, Laga K et al. Estimation of thyroid gland volume by spiral computed tomography. Eur Radiol 1997; 7: 214–216.
7. Knudsen N, Bols B, Bulow I et al. Validation of ultrasonography of the thyroid gland for epidemiological purposes. Thyroid 1999; 9: 1069–1074.
8. Kot BC, Sin DM, Ying M. Evaluation of the accuracy and reliability of two 3-dimensional sonography methods in volume measurement of small structures: an in vitro phantom study. J Clin Ultrasound 2009; 37: 82–88.
9. Lyshchik A, Drozd V, Reiners C. Accuracy of three-dimensional ultrasound for thyroid volume measurement in children and adolescents. Thyroid 2004; 14: 113–120.
10. Malago R, D'Onofrio M, Ferdeghini M et al. Thyroid volumetric quantification: comparative evaluation between conventional and volumetric ultrasonography. J Ultrasound Med 2008; 27: 1727–1733.
11. Ng E, Chen T, Lam R et al. Three-dimensional ultrasound measurement of thyroid volume in asymptomatic male Chinese. Ultrasound Med Biol 2004; 30: 1427–1433.
12. Nygaard B, Nygaard T, Court-Payen M et al. Thyroid volume measured by ultrasonography and CT. Acta Radiol 2002; 43: 269–274.
13. Ozgen A, Erol C, Kaya A et al. Interobserver and intraobserver variations in sonographic measurement of thyroid volume in children. Eur J Endocrinol 1999; 140: 328–331.
14. Pang BS, Kot BC, Ying M. Three-dimensional ultrasound volumetric measurements: is the largest number of image planes necessary for outlining the region-of-interest? Ultrasound Med Biol 2006; 32: 1193–1202.
15. Rago T, Bencivelli W, Scutari M et al. The newly developed three-dimensional (3D) and two-dimensional (2D) thyroid ultrasound are strongly correlated, but 2D overestimates thyroid volume in the presence of nodules. J Endocrinol Invest 2006; 29: 423–426
16. Reinartz P, Sabri O, Zimny M et al. Thyroid volume measurement in patients prior to radioiodine therapy: comparison between three-dimensional magnetic resonance imaging and ultrasonography. Thyroid 2002; 12: 713–717.
17. Riccabona M, Nelson TR, Pretorius DH. Three-dimensional ultrasound: accuracy of distance and volume measurements. Ultrasound Obst Gyn 1996; 7: 429–434.
18. Schlogl S, Andermann P, Luster M et al. A novel thyroid phantom for ultrasound volumetry: determination of intraobserver and interobserver variability. Thyroid 2006; 16: 41–46.
19. Schlogl S, Werner E, Lassmann M et al. The use of three-dimensional ultrasound for thyroid volumetry. Thyroid 2001; 11: 569–574.
20. Shin JJ, Grillo HC, Mathisen D et al. The surgical management of goiter: Part I. Preoperative evaluation. Laryngoscope 2011; 121: 60–67.
21. Shu J, Zhao J, Guo D et al. Accuracy and reliability of thyroid volumetry using spiral CT and thyroid volume in a healthy, non-iodine-deficient Chinese adult population. Eur J Radiol 2011; 77: 274–280.
22. Tong S, Cardinal HN, McLoughlin RF et al. Intra- and inter-observer variability and reliability of prostate volume measurement via two-dimensional and three-dimensional ultrasound imaging. Ultrasound Med Biol 1998; 24: 673–681.
23. Van Isselt JW, de Klerk JM, van Rijk PP et al. Comparison of methods for thyroid volume estimation in patients with Graves' disease. Eur J Nucl Med Mol Imaging 2003; 30: 525–531.
24. Volzke H, Ludemann J, Robinson DM et al. The prevalence of undiagnosed thyroid disorders in a previously iodine-deficient area. Thyroid 2003; 13: 803–810.
25. Ying M, Pang BS. Three-dimensional ultrasound measurement of cervical lymph node volume. Br J Radiol 2009; 82: 617–625.
26. Ying M, Yung DM, Ho KK. Two-dimensional ultrasound measurement of thyroid gland volume: a new equation with higher correlation with 3-D ultrasound measurement. Ultrasound Med Biol 2008; 34: 56–63.

3.3. Nuklearmedizinisch-sonographische Fusionsbildgebung

3.3.1. Softwarebasierte (offline) Fusionsbildgebung

Offline Fusion of 3-Dimensional Ultrasound and $^{99m}TcO_4$-SPECT in Focal Thyroid Adenoma. First Experiences

Posterpräsentation, 50. Jahrestagung der Deutschen Gesellschaft für Nuklearmedizin (DGN) 2012, Bremen

Offline Fusion of 3-Dimensional Ultrasound (3D-US) and $^{99m}TcO_4$-SPECT in Focal Thyroid Adenoma. First Experience

M.Freesmeyer[1], S.Wiegand[1], A.Darr[1], J.Steenbeck[1], E.Schleussner[2], T.Opfermann[1]

Clinic of Nuclear Medicine, Jena University Hospital
Clinic of Obstetrics and Gynaecology, Jena University Hospital

Universitätsklinikum Jena

Klinik für Nuklearmedizin
CA Dr. Martin Freesmeyer
phone +49 3641 9 33927 - fax +49 3641 9 33244
www.nuklearmedizin.uniklinik-jena.de

Purpose/Objective(s):

To prove the feasibility of software fusion of 3-dimensional ultrasound (3D-US) image data and $^{99m}TcO_4$-Single Photon Emission Tomography (SPECT), and to collect first clinical experience on thyroid adenomas.

Methods:

25 patients, referred for radioiodine therapy planning of unifocal, bifocal or multifocal thyroid adenomas, underwent 3D-US examination of the thyroid gland (GE Voluson E8, wobbler probe RAB4-8-D), in addition to standard ultrasound examination (GE Logiq L9, linear probe 7L). The 3D-US data sets were exported in the Enhanced US Volume Storage standard and archived in the hospital's PACS. Additionally SPECT of the thyroid was performed (Siemens, Symbia E). Subsequently, offline fusion of 3D-US and SPECT datasets was done at a multimodal workstation (Siemens, syngo MultiModality Workplace 2010B). The visual assessment and the comparison with the standard US examination regarding organ acquisition and matching of nodes were performed by 2 experienced nuclear medicine physicians.

Results:

In total 38 focal adenomas in 25 patients could be identified at SPECT. Software image fusion and manual co-registration were successful in all patients. All focal SPECT findings could be matched to nodules at US. However, in 8 findings a minor spatial mismatch occurred because of slight deformation of the thyroid due to moderate pressure of the US transducer to the cervical soft tissue during the 3D-US. Moreover, in small and/or isoechoic lesions the visibility at 3D-US was limited because of the convex array of the 3D-US transducer. Therefore, we thoroughly compared the 3D-US volumes side by side with the standard US images (linear array transducer at 7 MHz).

Conclusions:

The recently introduced Enhanced US Volume Storage standard allows not only the generation, distribution and archiving of 3D-US data of the thyroid, but also the subsequent offline image fusion with SPECT data in thyroid adenomas. In a few cases of small findings and/or poor image contrast the visibility of nodules was limited compared to standard US examination. The development of 3D-US transducers with higher resolution and wide scanning range is necessary.

Fig. 1: Ultrasound workplace

3D-Ultrasound examination using GE Voluson Expert E8 with an obstetric 3D-US transducer (volume probe).

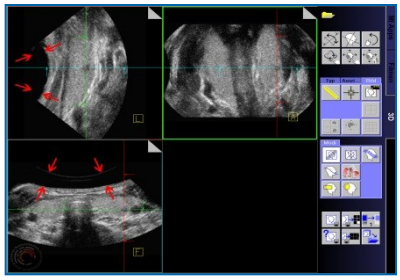

Fig. 2: 3D-US scan results

Routine 3D workplace; display of US volume of the thyroid gland in sagittal, coronal and transversal orientation; aqueous coupling medium (between red arrows): small and slightly hypoechoic nodule in the lateral part of the left lobe (cross center); several workflow buttons for 3D processing (right)

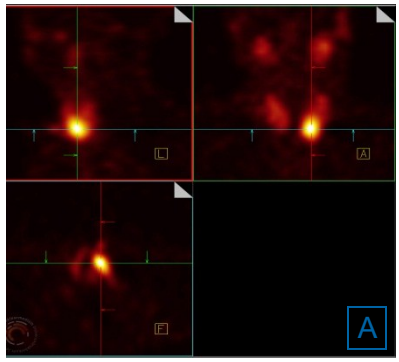

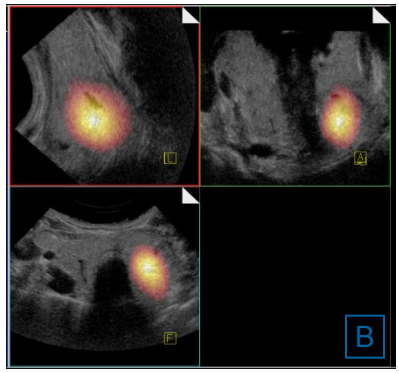

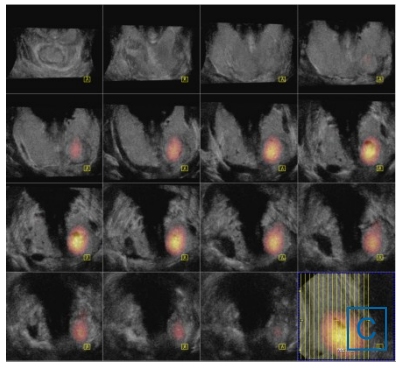

Fig. 3: Case example

Male, 64 years, TSH < 0.1 mU/l

[A]

Routine 3D workplace; display of a $^{99m}TcO_4$-SPECT dataset in sagittal, coronal and transversal orientation. Thyroid adenoma in the inferior part of the left lobe.

[B]

Ultrasound/SPECT Image fusion. Focal $^{99m}TcO_4$-storage fits isoechoic nodule in the inferior part of the left thyroid lobe; display in sagittal, coronal and transversal orientation.

[C]

Multiplanar reformation: Generation of a coronal image stack covering the whole thyroid gland including the thyroid adenoma.

3.3.2. Sensornavigierte Fusionsbildgebung

3.3.2.1. Differentialdiagnose unklarer ^{18}F-FDG-PET/CT-Befunde mit sensornavigierter PET/US-Fusion

PET/US Fusion Technique in Patients with Malignant Melanoma

Manuskript (Pictorial Essay), im November 2013 zur Veröffentlichung in der Zeitschrift EUROPEAN JOURNAL OF ULTRASOUND eingereicht

PET/US Fusion as a Problem-Solving Tool in Oncology Imaging Differentiation of Hernia Repair Mesh Plugs from Malignancy Suspected on PET/CT

Publikation (Interesting Image) 2014 in CLINICAL NUCLEAR MEDICINE

Avoidance of False-Positive Findings on ^{18}F-FDG-PET/CT Using PET/Ultrasound-Fusion: Displaced Laryngeal Silicone Implant Versus Recurrent Cancer

Publikation (Image of the Month) 2014 in JAPANESE JOURNAL OF CLINICAL ONCOLOGY

PET/ultrasound fusion for differentiation of Vox implant silicone particles from recurrent cancer

Publikation (Case Report) 2013 in NUKLEARMEDIZIN

PET/US Fusion Technique in Patients with Malignant Melanoma

M. Freesmeyer[1], S. Sell[2], S. Götze[2], M. Kaatz[3], P. Elsner[2], Th. Winkens[1]

[1] Clinic of Nuclear Medicine, Jena University Hospital, Jena, Germany

[2] Clinic of Dermatology and Allergology, Jena University Hospital

[3] Clinic of Dermatology and Allergology, SRH Hospital Gera

Deutscher Titel: PET/US Fusion bei Patienten mit malignem Melanom

Corresponding author and reprint requests:

Martin Freesmeyer, M.D.

Clinic of Nuclear Medicine

Jena University Hospital

Bachstraße 18, 07743 Jena, Germany

Telephone: +49-3641-9-33220

Fax: +49-3641-9-33244

E-mail: martin.freesmeyer@med.uni-jena.de

All authors have no conflicts of interest.

Prof. Dr. U. Teichgräber is gratefully acknowledged for providing access to GE Logiq E9 device.

Introduction

Multimodal imaging represents a valuable tool in follow-up diagnostic of malignant melanoma (MM). ^{18}F-fluorodeoxyglucose positron emission tomography/computed tomography (FDG-PET/CT) is commonly used to assess for tumor recurrence in high-risk patients (C. Etchebehere et al. Nucl Med Commun 2010; 31: 925-930) and its diagnostic accuracy is regarded to be superior to CT alone (Li Q et al. Onkologie 2012; 35: 522-526). However, due to its limited soft-tissue contrast, CT is not the best option to depict muscles and lymph nodes, considering that other imaging methods with better performance are available. Ultrasound (US) is far more suitable than CT in examining skin, muscles and lymph nodes. However, in contrast to PET/CT, metabolic information is missing.

The approach of combining different modalities (CT, MRI, PET) and US has been used for a few years, first reported by Ewertsen et al. (C. Ewertsen et al. Dan Med Bull 2010; 57: B4172). Also, PET/US fusion has been described to be useful as a “third opinion” on unclear PET/CT findings (R. Drescher et al. Clin Nucl Med 2013 epub ahead of print. doi:10.1097/RLU.0b013e31828164a4). The procedure is performed as follows: 1) Acquisition of a regular PET/CT dataset (Fig. 1a). 2) Transferal of the co-registrated PET and CT data onto the US device (Logiq E9, GE Healthcare, Milwaukee, WI, USA) (Fig. 1b). PET, CT and US images can be displayed on the US device in real-time in any combination in an overlapping, fused format (Fig 1c). 3) Aligning and co-registration of CT (without display of PET information) and US images. 4) Change from CT/US to PET/US fusion display. 5) Actual real-time image fusion examination starts with centering the region of interest on US. Using electromagnetic tracking (VNav, GE Healthcare), the position of the transducer and therefore the image position are detected by a sensor (Fig 1b). PET and CT images track in real-time while the transducer is moved 6) Alignment can be verified during examination using commonly visible structures on US and CT, for example bone as landmarks.

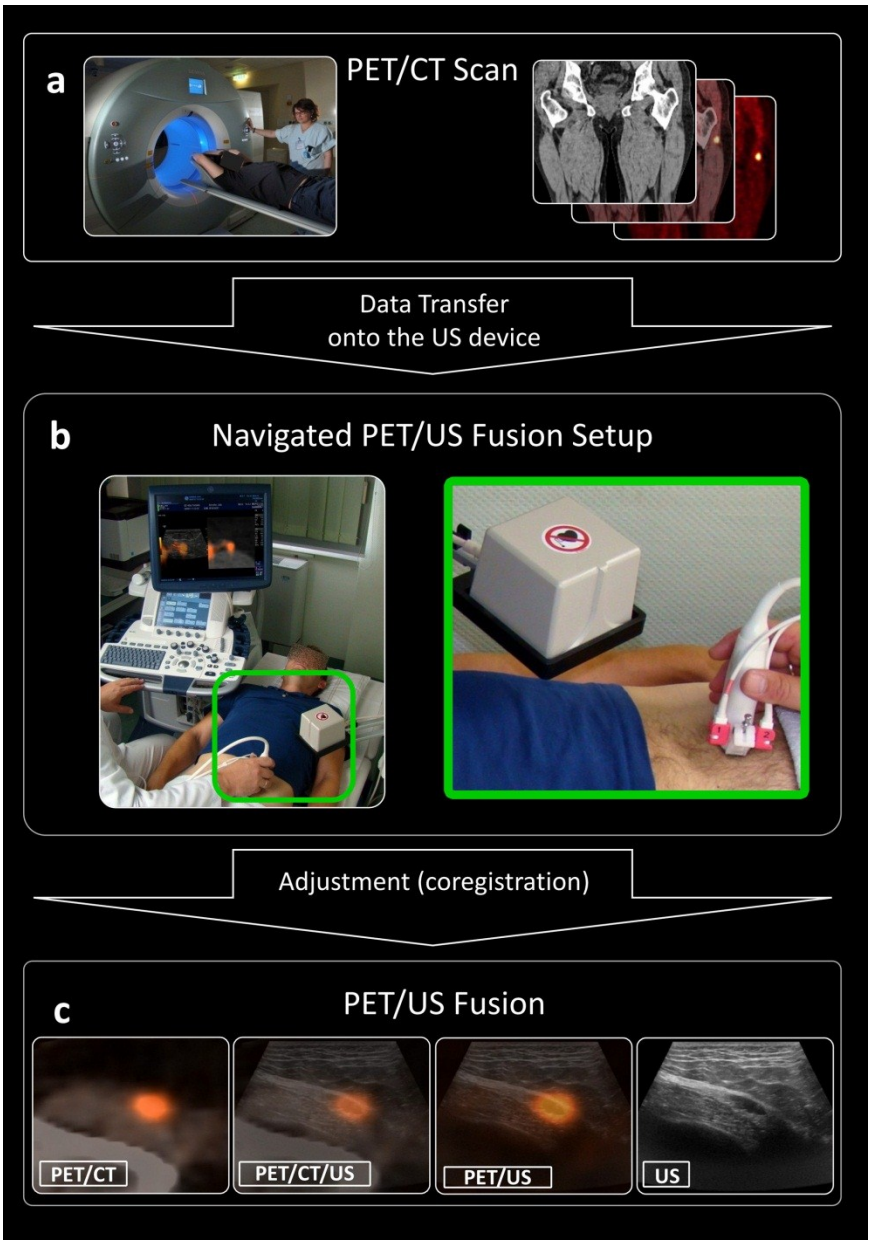

Fig. 1 PET/US fusion procedure. a) A regular PET/CT scan is acquired (Biograph mCT40, Siemens, Erlangen, Germany). The PET/CT data is loaded onto the US device (Logiq E9, GE Healthcare, Milwaukee, WI, USA). b) Co-registration of PET/CT data and US images is enabled using an electromagnetic tracking system (VNav, GE Healthcare), consisting of a magnet transmitter located near the patient and sensors attached to the transducer (green box). c) Following alignment and co-registration, PET/CT/US images are displayed to the user in any combination.

Abb. 1 Setup der PET/US Fusionsuntersuchung. a) Zunächst wird die PET/CT Untersuchung durchgeführt (Biograph mCT40, Siemens, Erlangen, Germany). Anschließend werden die PET/CT Daten auf das Ultraschallgerät (Logiq E9, GE Healthcare, Milwaukee, WI, USA) transferiert. b) Die Koregistrierung der PET/CT-Daten und Ultraschallbilder wird durch ein elektromagnetisches Tracking (VNav, GE Healthcare), bestehend aus einem Transmitter und Sensoren am Schallkopf ermöglicht (grüner Kasten). c) Nach Ausrichtung und Koregistrierung können die PET/CT/US Bilder in jeder Kombination auf dem Ultraschallgerät angezeigt werden.

Case description

Four Patients with unclear PET/CT soft tissue findings were selected and subjected to PET/US (Fig. 2-5). All patients provided informed consent of the procedures.

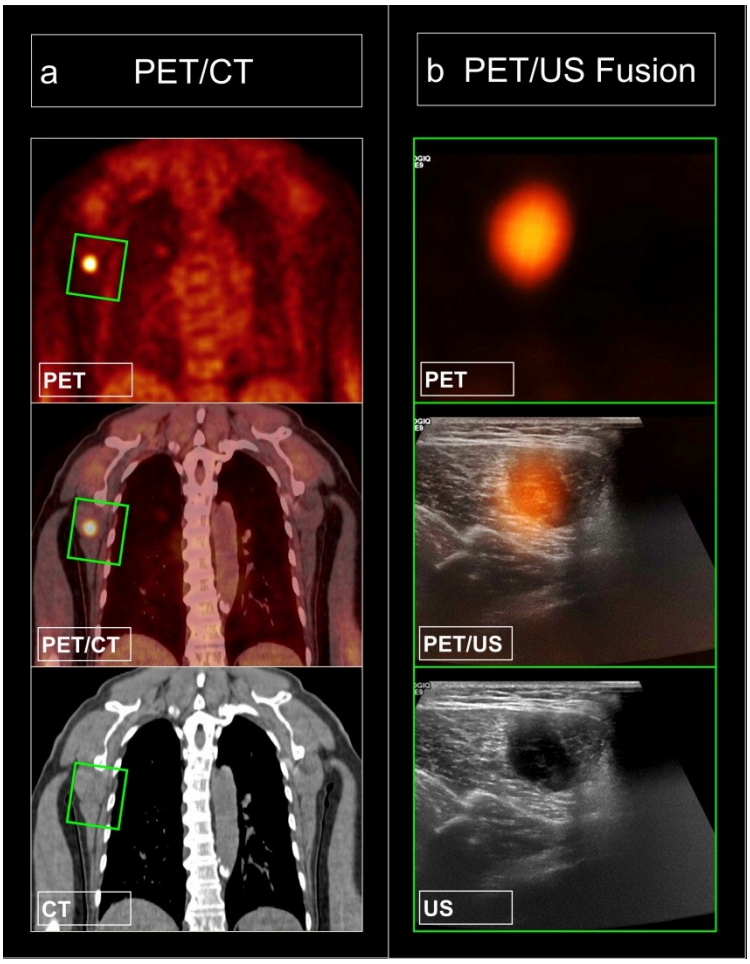

Fig. 2 73-year old female with ^{18}F-FDG-PET/CT, four years after initial diagnosis of a high risk MM of the left heel (pTxN3M1). The current PET/CT scan was performed to exclude metastatic spread prior to resection of a suspected cutaneous metastasis of the lower leg. Current anti-proliferative therapy: none. **a:** Coronal views of (from top to bottom) PET, PET/CT and CT of the thorax, depicting a hypermetabolic focus in the right M. serratus anterior (SUV_{max} 7.8). Low-dose non-contrast-enhanced CT did not show a pathological mass at the site of FDG-uptake. **b:** green section of a, shown as PET/US fusion with (from top to bottom) PET, PET/US and US. Using PET/US fusion technique, the source of glucose accumulation is revealed as being located within muscle tissue, presenting as a hypoechoic and inhomogeneous structure with irregular margins. Note the slight misregistration between the PET and US images. The patient underwent chemotherapy; a follow-up PET/CT scan was not performed.

Abb. 2 ^{18}F-FDG-PET/CT Untersuchung einer 73-jährigen Patientin, vier Jahre nach der Erstdiagnose eines malignen Melanoms der linken Ferse (pTxN3M1). Die aktuelle PET/CT Untersuchung erfolgte zum Ausschluss einer weiteren Metastasierung bei hochgradigem Verdacht auf eine Hautmetastase des Unterschenkels und deren geplanter Resektion. Aktuelle antineoplastische Therapie: keine. **a:** Koronare Darstellung des Thorax mit (von oben nach unten) PET, PET/CT und CT, die einen hypermetabolen Fokus im rechten M. serratus anterior zeigen (SUV_{max} 7.8). Das Nativ-CT zeigt kein pathomorphologisches Korrelat des FDG-Uptakes. **b:** PET/US Fusion des grünen Bildausschnittes aus a mit (von oben nach unten) PET, PET/US und US. Durch die Ultraschallfusionsdarstellung lässt sich der Fokus gesteigerter Stoffwechselaktivität zweifelsfrei einer in der Muskulatur gelegenen Struktur zuordnen. Diese stellt sich im Ultraschall echoarm und inhomogen mit unregelmäßiger Randbegrenzung dar. Dennoch ist eine minimale Abweichung der PET- und US Bilder erkennen. Die Patientin unterzog sich einer Chemotherapie. Eine Kontrolluntersuchung mittels PET/CT fand nicht statt.

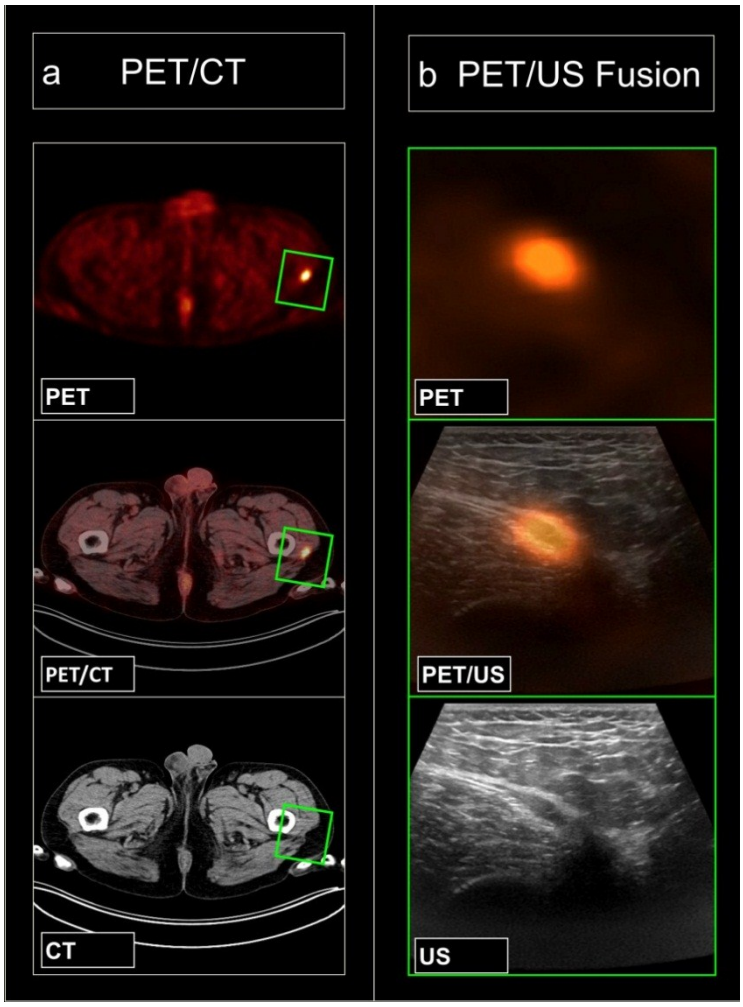

Fig. 3 50-year old male with follow-up ^{18}F-FDG-PET/CT, three years after initial diagnosis of MM of the right forearm (pT3aN0M0). During the past three years, lymph node metastases and cutaneous metastases had occurred and had been resected. The current PET/CT scan was performed to assess the status after temozolomid-chemotherapy. **a:** Transversal views of (from top to bottom) PET, PET/CT and CT of the proximal femora, revealing focal FDG-uptake in the left M. glutaeus medius (SUV_{max} 13.8). On low-dose non-contrast-enhanced CT, no clear pathological mass was present at the site of hypermetabolism. **b:** green section of a, shown as PET/US fusion with (from top to bottom) PET, PET/US and US. PET/US fusion allows a clear allocation of metabolic and morphologic findings within the affected muscle. The hypermetabolic focus is hypoechoic on US. The patient underwent ipilimumab-therapy. On follow-up three months later, the focus was still present, however, with a reduced SUV_{max} of 9.8.

Abb. 3 ^{18}F-FDG-PET/CT Untersuchung eines 50-jährigen Patienten, drei Jahre nach der Erstdiagnose eines malignen Melanoms des rechten Unterarms (pT3aN0M0) und mehreren Metastasenresektionen cutan und lymphonodulär. Die aktuelle PET/CT Untersuchung erfolgte zur Verlaufskontrolle nach Temozolomid-Therapie. **a:** Transversalschnitte mit (von oben nach unten) PET, PET/CT und CT der proximalen Femora, die einen fokalen FDG-Uptake im linken M. glutaeus medius zeigen (SUV_{max} 13.8). Im Nativ-CT ist kein eindeutiges pathomorphologisches Korrelat der Stoffwechselaktivität zu sehen. **b:** PET/US Fusion des grünen Bildausschnittes aus a mit (von oben nach unten) PET, PET/US und US. Die PET/US-Fusion ermöglicht eine eindeutige räumliche Korrelation des Stoffwechsels mit der Morphologie innerhalb des Muskels. Der Fokus mit gesteigertem Glukosemetabolismus stellt sich im Ultraschall echoarm dar. Der Patient wurde anschließend mit Ipilimumab behandelt. In der PET/CT Verlaufskontrolle nach drei Monaten ist die Läsion regredient (SUVmax 9.8).

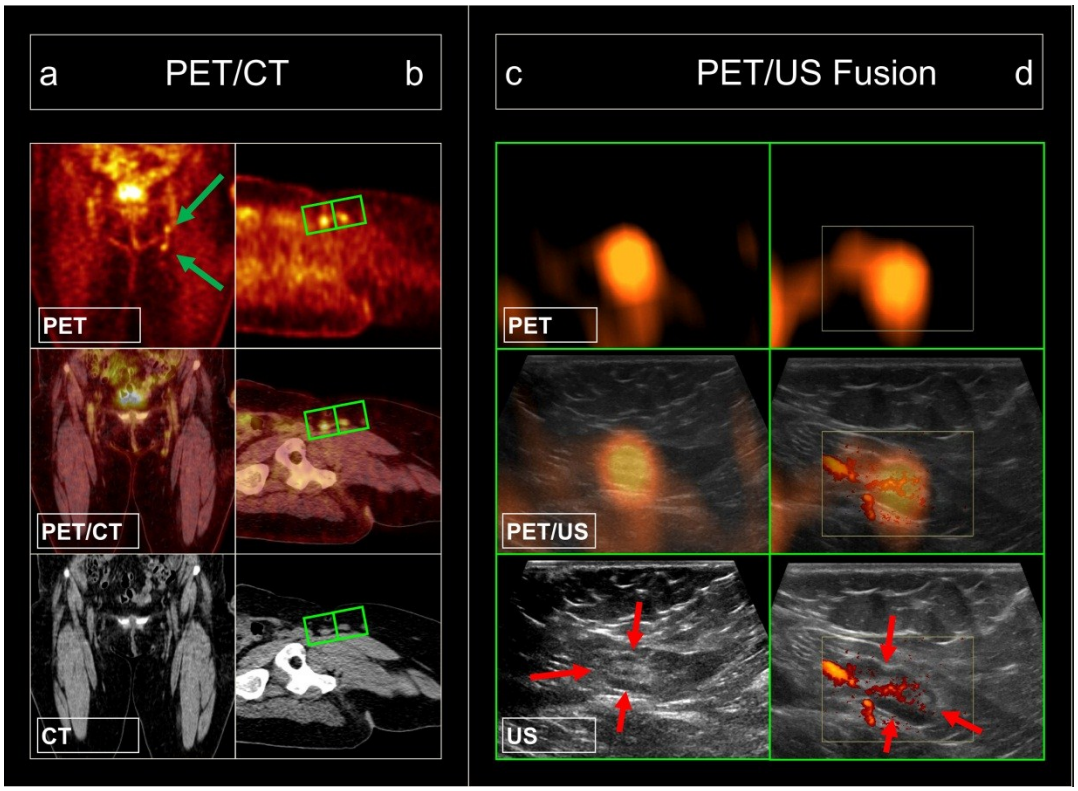

Fig. 4 56-year old female with follow-up 18F-FDG-PET/CT, five years after initial diagnosis of a MM of the right fossa supraclavicularis (pT2aN0M0). The current PET/CT was performed as follow-up three month after resection of a metastasis of the breast. Current anti-proliferative therapy: None. **a+b:** Coronal views (a) and sagittal (b) views of (from top to bottom) PET, PET/CT and CT of the pelvis, depicting two hypermetabolic foci (green arrows) in the left inguinal region (SUV_{max} 3.5). Contrast-enhanced CT showed two round, normal-size lymph nodes. **c+d**: Green section of b, shown as PET/US fusion with (from top to bottom) PET, PET/US and US of the upper (c) and lower (d) lymph node. PET/US fusion clearly depicts the exact localization of increased glucose metabolism. The corresponding lymph nodes (red arrows) are identified via US as lacking signs of malignancy, showing a distinct fat hilum (c+d) and hilum vascularization (d). On follow-up PET/CT scan after six months, the lymph nodes did not exhibit increased glucose metabolism.

Abb. 4 ^{18}F-FDG-PET/CT Untersuchung einer 56-jährigen Patientin, fünf Jahre nach der Erstdiagnose eines malignen Melanoms der rechten Fossa supraclavicularis (pT2aN0M0). Die aktuelle PET/CT Untersuchung wurde als Verlaufskontrolle drei Monate nach partieller Mammaresektion aufgrund einer intramammären Metastase durchgeführt. Aktuelle systemische antiproliferative Therapie: keine. **a+b:** Koronare (a) und sagittale (b) Darstellung der Beckenregion mit (von oben nach unten) PET, PET/CT und CT, die zwei übereinanderliegende, mäßig hypermetabole Foci in der linken Inguinalregion zeigen (SUV_{max} 3.5). Im Kontrastmittel-CT sind zwei rundlich konfigurierte, nicht vergrößerte Lymphknoten sichtbar. **c+d:** PET/US Fusion des grünen Bildausschnittes aus **b** mit (von oben nach unten) PET, PET/US und US des oberen (c) und unteren (d) Lymphknotens. Die PET/US Untersuchung zeigt exakt zwei Lymphknoten als Quelle des FDG-Uptakes. Im Ultraschall weisen diese Lymphknoten aufgrund ihres Fetthilus (c+d) und der hilären Perfusion (d) keine Malignitätszeichen auf. In der Verlaufskontrolle mittels PET/CT nach sechs Monaten zeigten die Lymphknoten keinen gesteigerten Stoffwechsel.

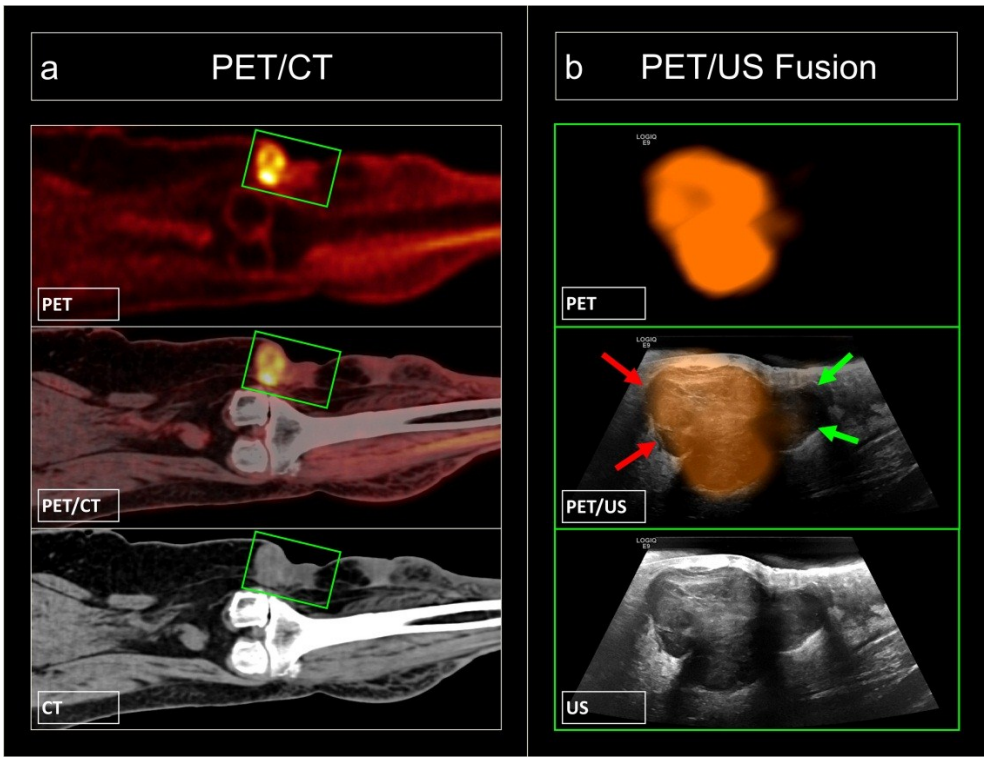

Fig. 5 73-year old female with follow-up ^{18}F-FDG-PET/CT, eight years after initial diagnosis of MM of the left lower leg (pT3bN3cM1a) and cutaneous and lymph node metastases, having received several surgeries for removal of metastases. The current PET/CT scan was performed to exclude further metastatic spread prior to a resection of a subcutaneous metastasis located at the left knee. Current anti-proliferative therapy: none. **a:** coronal views of (from top to bottom) PET, PET/CT and CT of the left knee. Note the intense hypermetabolic cutaneous/sub-cutaneous focus medially of the knee (SUV_{max} 12.2), corresponding well with a nodular mass of soft-tissue densities within sub-cutaneous fat. **b:** green section of a, shown as PET/US fusion with (from top to bottom) PET, PET/US and US. Note the polycyclic, inhomogeneous hypoechoic mass, providing a good match with the hypermetabolic focus. The cranial part of the mass shows vitality as indicated by increased glucose metabolism (red arrows), whereas the green arrows point at the caudal part of the lesion without metabolism, suggesting tumor necrosis. The patient underwent surgical resection. On follow-up PET/CT six months later the soft-tissue metastasis was not detectable anymore.

Abb 5. ^{18}F-FDG-PET/CT Untersuchung einer 73-jährigen Patientin, acht Jahre nach Erstdiagnose eines malignen Melanoms des linken Unterschenkels (pT3bN3cM1a) und Haut- und Lymphknotenmetastasen im Verlauf und mehrfachen Metastasenresektionen. Die aktuelle PET/CT Untersuchung erfolgte zum Ausschluss weiterer Metastasen bei geplanter Resektion einer Weichteilmetastase des linken Knies. Aktuelle antineoplastische Therapie: keine. **a:** Koronare Schichten (von oben nach unten) von PET, PET/CT und CT des linken Kniegelenkes mit einer intensiv hypermetabolen weichteildichten Raumforderung im subkutanen Fettgewebe medial des Kniegelenks (SUV_{max} 12.2). **b:** PET/US Fusion des grünen Bildausschnittes aus a mit (von oben nach unten) PET, PET/US und US. Die suspekte Läsion stellt sich im Ultraschall polyzyklisch, inhomogen und echoarm dar. Die FDG-Anreicherung korreliert gut mit dem sonomorphologisch auffälligen Fokus. Der craniale Anteil der Läsion repräsentiert vitales Tumorgewebe, erkennbar am starken Glukosemetabolismus (rote Pfeile). Im Gegensatz dazu ist der caudale Metastasenanteil (grüne Pfeile) aufgrund der fehlenden Stoffwechselaktivität als Tumornekrose einzuschätzen. Anschließend wurde die Metastase operativ entfernt. Die PET/CT-Kontrolluntersuchung nach sechs Monaten zeigte keinen Hinweis auf eine residuelle Metastase.

Discussion

For therapy decisions in patients with malignant melanoma, it is essential to know the extent of disease. Local recurrence or single metastases are subjected to surgical resection, thus reducing tumor load and prolonging overall survival (D. Ollila et al. J Surg Oncol 1999; 71: 209-213). PET/CT is useful to detect tumor dissemination as it has been described to be more accurate than CT alone (Li Q et al. Onkologie 2012; 35: 522-526). However, unclear findings can occur: On the one hand, CT may provide false-negative results due to its limitations in depicting muscle lesions and lymph node pathologies; on the other hand, PET often shows unspecific, non-malignant increased glucose metabolism due to muscle tonicity and lymphadenitis. The presented cases of Fig. 2 and 3 showed hypermetabolic muscle lesions without a correlate on CT (false-negative on CT). Lymph nodes with increased glucose metabolism were seen in Fig. 4 with reactive lymphadenopathy and metastases as differential diagnoses. In all cases, additional US examination was helpful to obtain morphologic information about the affected structures which were not or only with limited interpretation seen on CT. In Fig. 2 and 3, hypoechoic, inhomogeneous structures were revealed as the cause of increased glucose metabolism. In Fig. 4, two lymph nodes were identified as lacking signs of malignancy on US. PET/US fusion was necessary to exactly allocate the hypermetabolic focus to its corresponding morphological structure. Although hypothetic, in Fig. 5 PET/US fusion could have provide a solid basis to perform a biopsy – aiming at the upper part with increased metabolism would have resulted in a reliable histology whereas the lower part without glucose metabolism would have probably shown necrosis.

Furthermore, PET/US fusion technique allows identifying the exact anatomic structure of the hypermetabolic focus. Usually, US and PET/CT are evaluated side-by-side which may result in an imprecise allocation of findings, even if performed by an experienced physician. It also provides comprehensible images especially useful for residents in training and physicians not

familiar with nuclear medicine procedures and ultrasound. Additionally, perfusion of the focus can be assessed using power mode.

Of course, there are some disadvantages and limitations regarding the PET/US fusion technique: First, it is a rather elaborate procedure which is time consuming and needs an experienced physician. Second, only tissue accessible via US can be examined: Lesions within the lung or bone marrow are not available for PET/US fusion. Third, slight misregistrations as seen for example in Fig. 2 occur due to tissue deformation caused by the pressure applied by the transducer and moving the patient from the PET/CT scanner to the US stretcher.

The procedure of PET/US fusion in malignant melanoma could be improved further, for example using contrast enhanced ultrasound, adding more information to the US examination.

In conclusion, we present four cases of ^{18}F-FDG-PET/US fusion in patients with malignant melanoma. This additional examination proved helpful in these patients, revealing false-negative CT findings to correlate with a metastasis on US and proving false-positive PET findings to be reactive lymphadenopathy.

PET/US Fusion as a Problem-Solving Tool in Oncology Imaging

Differentiation of Hernia Repair Mesh Plugs From Malignancy Suspected on PET/CT

Robert Drescher, MD, MA and Martin Freesmeyer, MD

Abstract: PET/CT is an established modality for evaluation of malignant disease. However, in many cases, specificity is impaired by false-positive findings. Recognition of these cases is crucial for correct diagnosis and subsequent patient management. In the presented case, malignant disease was suspected in a young man because of a history of B symptoms. ^{18}F-FDG PET/CT showed hypermetabolic foci in both inguinal regions initially classified as possible lymphoma. Using a novel technique for PET/US fusion, ultrasound and PET were coregistered to clarify that PET hypermetabolism was due to a foreign body reaction after plug hernioplasty performed several years earlier.

Key Words: PET/US fusion, image fusion, PET/CT, false-positive finding, mesh plug, hernia

(*Clin Nucl Med* 2014;39: e75–e77)

REFERENCES

1. Tessonnier L, Fakhry N, Taïeb D, et al. False-positive finding on FDG-PET/CT after injectable elastomere implant (Vox implant) for vocal cord paralysis. *Otolaryngol Head Neck Surg*. 2008;139:738–739.
2. Jung CH, Kim BY, Kim JW, et al. False-positive F-18 FDG PET/CT from foreign body reaction on anterior chest wall after endoscopic total thyroidectomy via axillo-breast approach for thyroid cancer: two case reports. *Clin Nucl Med*. 2011;36:1036–1038.
3. Adejolu M, Huo L, Rohren E, et al. False-positive lesions mimicking breast cancer on FDG PET and PET/CT. *AJR Am J Roentgenol*. 2012;198: W304–W314.
4. Hsu CH, Lee CM, Lin SY. Inflammatory pseudotumor resulting from foreign body in abdominal cavity detected by FDG PET. *Clin Nucl Med*. 2003;28: 842–844.
5. Vento JA, Karak PK, Henken EM. Gossypiboma as an incidentaloma. *Clin Nucl Med*. 2006;31:176–177.
6. Rutkow IM. The PerFix plug repair for groin hernias. *Surg Clin North Am*. 2003;83:1079–1098.
7. Millikan KW, Doolas A. A long-term evaluation of the modified mesh-plug hernioplasty in over 2000 patients. *Hernia*. 2008;12:257–260.
8. Rettenmaier MA, Heinemann S, Truong H, et al. Marlex mesh mimicking an adnexal malignancy. *Hernia*. 2009;13:221–223.
9. Yilmaz M, Sevinc A, Aybasti N, et al. FDG uptake in abdominal mesh implant on FDG PET/CT. *Clin Nucl Med*. 2008;33:351–352.
10. Koljevic-Markovic A, Orcurto MV, Doenz F, et al. Persistent FDG uptake around an inguinal mesh prosthesis 25 years after implantation. *Clin Nucl Med*. 2007;32:242–243.
11. Nakano S, Yoshida M, Fujii K, et al. Fusion of MRI and sonography image for breast cancer evaluation using real-time virtual sonography with magnetic navigation: first experience. *Jpn J Clin Oncol*. 2009;39:552–559.
12. Ewertsen C, Henriksen BM, Torp-Pedersen S, et al. Characterization by biopsy or CEUS of liver lesions guided by image fusion between ultrasonography and CT, PET/CT or MRI. *Ultraschall Med*. 2011;32:191–197.
13. Venkatesan AM, Kadoury S, Abi-Jaoudeh N, et al. Real-time FDG PET guidance during biopsies and radiofrequency ablation using multimodality fusion with electromagnetic navigation. *Radiology*. 2011;260:848–856.

Received for publication July 10, 2012; accepted November 18, 2012.
From the Clinic of Nuclear Medicine, Jena University Hospital, Jena, Germany.
Conflicts of interest and sources of funding: none declared.
Reprints: Robert Drescher, MD, MA, Clinic of Nuclear Medicine, Jena University Hospital, 07743 Jena, Germany. E-mail: robert.drescher@uni-jena.de.

ISSN: 0363-9762/14/3901–0e75

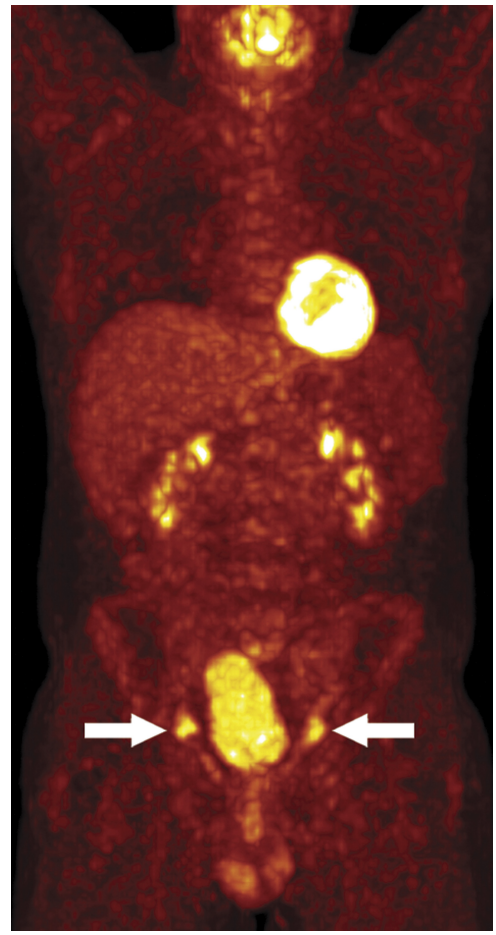

FIGURE 1. PET/CT is an established modality for primary staging and follow-up of malignant diseases. Specificity is impaired by false-positive findings, which were reported for a variety of foreign body reactions, including Teflon implants, hemostatic sponges, gossypibomas, and breast silicone injections.[1–5] Recognition of these cases is crucial for correct diagnosis and patient management.

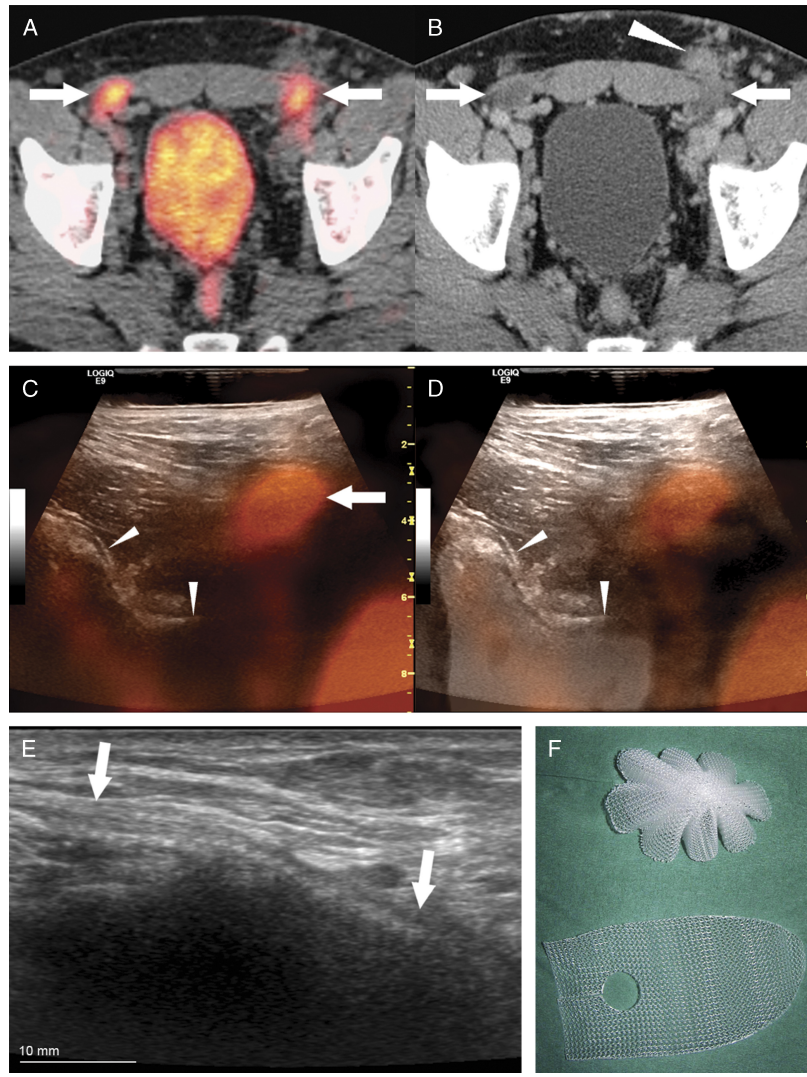

FIGURE 2. The clinical history of the 39-year-old included abdominal pain, weight loss, night sweats, and recurrent deep vein thrombosis. CT, MRI, and endoscopy did not provide a conclusive diagnosis. Initially, the patient denied any history of surgery. A whole-body ^{18}F-FDG PET/CT was performed (Biograph mCT40 scanner; Siemens, Erlangen, Germany; injected activity 233 MBq/6.3 mCi, acquisition delay 75 min). Two focal areas of hypermetabolism at the anterior pelvic peritoneum with nearly symmetric location and metabolism were identified: SUVmax 5.0 and 4.8, respectively (A, arrows). CT showed ovoid soft tissue structures with moderate contrast enhancement, which were regarded as suspicious for enlarged lymph nodes (B, arrows). Anterior to the left-sided lesion, subcutaneous soft tissue densities without hypermetabolism could be seen (B, arrowhead). Ultrasound and PET/US fusion was performed with the VNav° system on a Logic9 scanner with a 9-MHz transducer (GE, Milwaukee, WI). PET/US fusion images localized the hypermetabolic foci to the proximal parts of the inguinal canals (C, arrow). Fusion of PET, CT, and US data in one image confirmed correct positioning of the US probe (D). The margins of the iliac bones were used as anatomical landmarks for exact alignment of the PET dataset with the live US images (C, D, arrowheads). After fading out the PET/CT information from the hybrid display, B-Mode US revealed reticular structures following the inguinal canals (E). Research into the surgical history of the patient confirmed that he underwent hernioplasty procedures 7 years ago, which were performed using Perfix Plugs (Davol/Bard, Warwick, RI). It can be assumed that the focal hypermetabolism and mass effect is caused by foreign body reaction with chronic inflammation and soft tissue swelling. No diagnosis of malignancy was established in the presented patient. Plug hernioplasty is an established surgical hernioplasty method and has been introduced as an alternative to open patch procedures.[6,7] The Perfix plug-and-patch, made of a polypropylene mesh, involves a cone-shaped preformed plug for closure of the abdominal wall defect and a supplementary patch (F). Mimicking of malignancy on PET/CT due to mesh implants has been reported.[8–10] Live fusion of US with other imaging modalities has been introduced by some vendors. As MR/US and CT/US fusion, it is used in breast, liver, and prostate imaging for diagnosis and intervention guidance.[11–13] On the VNav° system, PET/CT data of the desired region are first uploaded to the US platform. After initial manual coregistration by anatomical landmarks, spatial orientation of magnets attached to the US probe are tracked by sensors, allowing automatic image realignment and fusion. The images illustrate that PET/US fusion can be a useful technique to solve diagnostic dilemmas in oncology PET imaging.

JJCO Japanese Journal of Clinical Oncology

Jpn J Clin Oncol 2013

Image of the Month

Avoidance of False-Positive Findings on ^{18}F-FDG-PET/CT Using PET/Ultrasound-Fusion: Displaced Laryngeal Silicone Implant Versus Recurrent Cancer

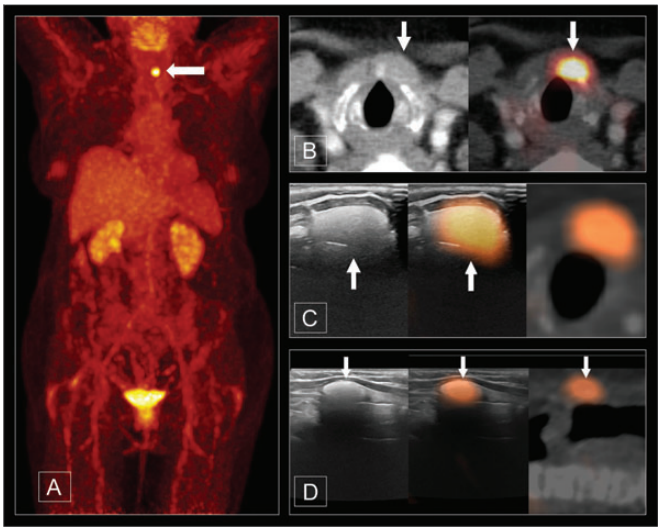

Figure 1.

Figure 2.

A 71-year-old female was diagnosed with non-small-cell lung cancer (NSCLC) with infiltration of the left lateral mediastinum. The squamous cell carcinoma was resected with microscopic residuals (R1 resection). One year after surgery, an ^{18}F-FDG PET/CT was performed to assess for tumor recurrence as this is used for routine check-up in high-risk patients in our institution. A hypermetabolic focus adjacent to the cricoid cartilage was found (Fig. 1A; maximum intensity projection: standardized uptake value [SUV] 13.3), exhibiting a moderate thickening at soft-tissue density values on CT (Fig. 1B). Initially, the finding was suspected to be malignant.

An additional real-time navigated PET/US fusion examination was then performed using an electromagnetic navigation system (Volume Navigation, General Electrics, Milwaukee, WI, USA). Real-time fusion of the PET dataset and US images were obtained and demonstrated a well-defined, diffuse hyperechoic structure in transversal (Fig. 1C, left) and sagittal (Fig. 1D, left) orientation, correlating well with the hypermetabolic focus (Fig. 1C and D, mid images). The US appearance was atypical for tumor tissue, usually being hypoechoic with irregular margins. A review of the patient's medical history revealed that an irreversible vocal cord paralysis had occurred after resection of the NSCLC. A silicone elastomer implant (Fig. 2; Vox® Implants, Bard, Warwick, RI, USA) had been injected to augment the left vocal cord and reduce the glottic gap.

Thus, the benign, artificial appearance of the PET/US fusion images was compatible with migration and displacement of the silicone implants, therefore inducing a foreign body reaction. Accordingly, the presence of malignant tissue as a cause of the hypermetabolic focus seen on PET/CT could be ruled out. The patient underwent surveillance. In this case, US alone could have identified the artificial aspect of the lesion if performed by an experienced physician familiar with ultrasound and nuclear medicine as well, allocating the hypermetabolic focus to ultrasound findings in his mind. The method of PET/US, however, provides clear and comprehensible images, useful for physicians who do not use nuclear medicine techniques and ultrasound on a daily basis. Furthermore, PET/US images can be archived and reviewed at later times, too.

Martin Freesmeyer, Thomas Winkens and Robert Drescher
Clinic of Nuclear Medicine, Jena University Hospital, Jena, Germany
doi:10.1093/jjco/hyt177

Acknowledgement

Dr. Ernesta Palombo-Kinne is gratefully acknowledged for language assistance with the manuscript.

PET/ultrasound fusion for differentiation of Vox implant silicone particles from recurrent cancer

PET/CT is an established modality for evaluation of poorly differentiated thyroid malignancies. However, in some cases specificity is impaired by false-positive findings. False-positive findings on oncologic PET/CT have been reported for a variety of foreign bodies, including teflon implants, haemostatic sponges, gossypibomas, suture granulomas, talc pleurodesis, and breast silicone injections. These cause chronic tissue inflammation and thus focal glucose hypermetabolism. Recognition of these cases is crucial for correct diagnosis and subsequent patient management. Live fusion of ultrasound (US) with other imaging modalities has been introduced by some vendors. As magnetical resonance (MR)/US and CT/US fusion, it is used in breast, liver and prostate imaging for diagnosis and intervention guidance.

In the case presented, tumour recurrence was suspected in a patient with previously treated papillary thyroid cancer. By using a PET/US fusion technique and correlation with the surgical history of the patient, the PET/CT findings could be attributed to a foreign body reaction.

A man with thyroid cancer

Three years ago, the then 57-year-old man was diagnosed with papillary thyroid cancer. The primary tumour located in the isthmus had a diameter of 3.5 cm and infiltrated the thyroid and cricoid cartilages. Staging examinations revealed small pulmonary nodules at least suspicious for metastases. Surgery included partial cricothyroidectomy, resection of the cranial tracheal rings, and airway reconstruction by fixation of the trachea to the thyroid cartilage. Tumour stage was pT4a Nx Mx R0 L1 V1.

Because of a slow progression of the pulmonary nodules seen on CT after two years, the patient was referred to our department. Two radioiodine therapies (RIT) were performed (7.25 and 4.5 GBq ^{131}I). The initial stimulated thyreoglobulin (Tg) level was 85.0 ng/ml (TSH > 30 mU/l). ^{123}I whole body scintigraphy was negative after the RITs, however, the stimulated Tg level remained at 41.3 ng/ml.

To identify poorly differentiated tumour, an additional ^{18}F-FDG PET/CT was performed. Imaging parameters: injected dose 244.5 MBq ^{18}F-FDG, acquisition delay 90 min, non-contrast CT, Biograph mCT 40 scanner (Siemens, Erlangen, Germany). The PET/CT revealed two hypermetabolic foci in the thyroid region with standardized uptake values (SUVs) of 6.5 and 6.1, which were initially classified as malignant and consistent with local recurrence (▶Fig. 1A–C). No further evidence of tumour recurrence or metastases was noted.

Since repeated neck surgery in this patient would have been very difficult, further non-invasive evaluation was necessary. US showed two relatively well-defined, hyperechoic, mass-like structures atypical for tumour tissue adjacent to the thyroid cartilage (▶Fig. 1D). Using a novel magnetic navigation system (VNav°, GE, Milwaukee, WI, USA), live fusion of the PET dataset and US images was performed, correlating these findings with the hypermetabolic foci (▶Fig. 1E). The VNav° system consists of magnetic sensors which are attached to the ultrasound probe, and a fixed magnetic field generator, which is positioned close to the scanning area and detects the spatial orientation of the probe to reconstruct it's position and motion during scanning. Initially, PET/CT data are loaded, and a manual alignment of US and 3D PET and/or CT images is done using anatomical

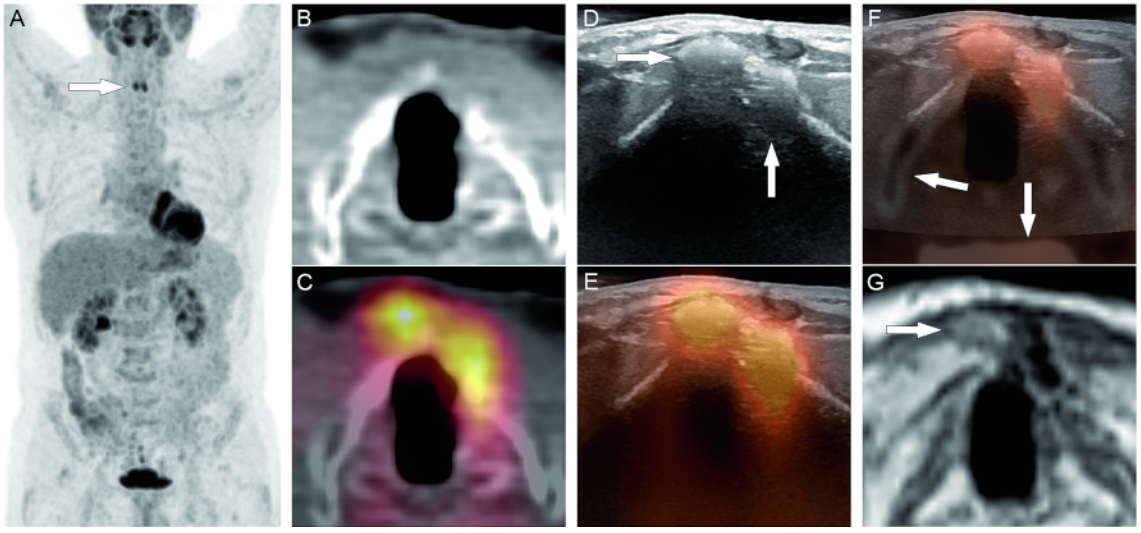

Fig. 1 PET/CT revealed two hypermetabolic foci (A, arrow) anterior and lateral to the thyroid cartilage (B, C). Ultrasound showed two relatively well-defined, hyperechoic, mass-like structures (D) correlating with the hypermetabolic foci on live PET/US fusion (E). Navigated fusion of PET, US and CT images confirmed the correct co-registration (F, arrows: calcified thyroid cartilage and spine). On MR imaging, areas of low Gd-DTPA enhancement were seen (G).

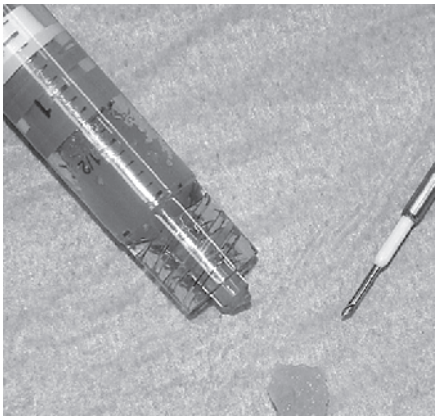

Fig. 2 The Vox Implant kit contains the ready-to-use injectable silicone elastomere in a syringe and a long shapeable needle in a trocar.

landmarks (spine, thyroid cartilage, sternum). 3D images are then automatically reoriented and fused to the live US images according to the position of the probe. To avoid misalignment, tissue deformation due to probe pressure was avoided during US scanning. Patient position was the same as on the PET/CT scanner. For confirmation, fusion of the modalities PET, CT and US into one image was done manually (►Fig. 1F). MR images showed areas of low Gd-DTPA enhancement in this region (►Fig. 1G).

Further research into the patient's history revealed that a second laryngeal intervention was performed eight months after tumour diagnosis to treat post-surgical severe dysphonia. Injectable silicone elastomere implants (Vox Implants, Bard, Warwick, RI, USA) (►Fig. 2) were applied to augment the vocal cords and reduce the glottic gap. During the procedure, Vox Implant injection was compromised due to the extensive scarring from previous surgery. It was suspected that some injected silicone elastomere displaced from the vocal cords into the surrounding tissues after partial thyroid cartilage resection, but this could not be proven immediately.

By PET/US fusion, the presence of malignant tissue structures as the cause of the hypermetabolic foci seen on PET/CT could therefore be ruled out. The patient underwent surveillance.

Discussion

Thyroplasty is performed in patients with vocal cord paralysis and is aimed at medialisation of the vocal cord to facilitate better glottic function and improve vocalisation. Treatment of vocal cord paralysis by injectable implants, including teflon, hydroxyl apatite, and silicone elastomere, is an alternative to external surgery. Medialisation of cord is achieved by the local mass effect of the injected substance. In the EU, silicone elastomeres were approved for vocal cord augmentation in 2001 and have a high success and low complication rate (1). However, chronic inflammatory reactions and particle migrations may occur.

One case of a false-positive PET/CT finding due to a vocal cord silicone elastomere implant (Vox Implant) has been reported (2). In that case, the patient had an extrathyroideal primary malignancy (lung cancer), and the hypermetabolism was seen in the vocal cord as expected after Vox implantation. Therefore, the differential diagnosis was muscle activity, a secondary laryngeal malignancy, or a rare local metastasis. In our case of a patient with metastating thyroid cancer, the degree of expanctancy of a thyroideal finding was much higher, and the hypermetabolic focus was not seen at the expected localization of a Vox Implant. MR imaging was not conclusive; the findings seen may have been easily attributed to post-surgical changes without knowledge of the PET/US results. It is evident that FDG hypermetabolism is particularly misleading in patients with a history of thyroid cancer, and differentiation from inflammation may be impossible without tissue sampling or surgery.

Live fusion of US images with MR images has been used for evaluation of breast tumour extent, for percutaneous intervention guidance at the liver, prostate, and soft tissue masses. In the breast, fusion images determined tumour size more accurately than US; in the prostate, it was possible to target lesions which were only seen on MRI and not on US. Experimentally, live transoesophageal US has been used as an intermediate to co-register the actual catheter position with preprocedural cardiac MR during heart catheterisation. Live PET/US fusion combined with other modalities has been applied predominantly for liver biopsy guidance. In these studies image fusion was a robust and reproducible method and improved characterisation of lesions. Focusing on the area of interest could be based solely on the PET findings if lesions were not or not easily seen on morphological imaging (3, 4).

EVUS (enhanced ultrasound volume storage) allows to save 3D US datasets in a standardized DICOM (digital imaging and communications in medicine) format. This will promote the introduction of these fusion techniques into the clinical practice. The combination of the 3D standard with the possibility of spatial correlation of datasets allows online fusion of modalities like PET, US, CT and MRI (5). Furthermore, it would facilitate offline fusion of the volume data of US, PET and CT data for better visualisation of pathologic findings and intervention planning.

> This case illustrates that PET/US fusion can be a useful technique to solve diagnostic dilemmas in oncology PET imaging.

In the future, it would be even more useful if it is readily available at PET/CT centres, and if the logistical and staff resources are available to routinely conduct such additional investigations.

References

1. Sittel C: Larynx: Implantate und Stents. Laryngo Rhino Otol 2009; 88: S119-S124.
2. Tessonnier L, Fakhry N, Taïeb D et al. False-positive finding on FDG-PET/CT after injectable elastomere implant (Vox implant) for vocal cord paralysis. Otolaryngol Head Neck Surg 2008; 139: 738–739.
3. Ewertsen C, Henriksen BM, Torp-Pedersen S et al. Characterization by biopsy or CEUS of liver lesions guided by image fusion between ultrasonography and CT, PET/CT or MRI. Ultraschall Med 2011; 32: 191–197.
4. Venkatesan AM, Kadoury S, Abi-Jaoudeh N et al. Real-time FDG PET guidance during biopsies and radiofrequency ablation using multimodality fusion with electromagnetic navigation. Radiology 2011; 260: 848–856.
5. Kotzerke J, Luster M, Freesmeyer M. Gebt mir einen festen Punkt im All, und ich hebe die Welt aus den Angeln. Nuklearmedizin 2012; 51: 65–66.

Received: December 12, 2012
Accepted in revised form: March 19, 2013

R. Drescher[1]; A. Müller[2]; T. Lesser[3]; M. Freesmeyer[1]

[1]Clinic of Nuclear Medicine, University Hospital, Jena, Germany; [2]ENT Department, SRH Hospital Gera, Germany; [3]Department of Thoracic and Vascular Surgery and Angiology, SRH Hospital Gera, Germany

3.3.2.2. Sensornavigierte PET/US-Fusionsbildgebung bei Schilddrüsenerkrankungen

Differential Diagnosis of Thyroid Nodules via Real-Time PET/Ultrasound (US) Fusion in a Case of Co-existing Medullary Thyroid Cancer and Adenoma

Cover Image und Publikation (Image in Endocrinology) 2013 im JOURNAL OF CLINICAL ENDOCRINOLOGY AND METABOLISM

Diagnosis of Small Medullary Thyroid Carcinoma via PET/Ultrasound (US) Fusion

Publikation (Image of the Month) 2014 in JAPANESE JOURNAL OF CLINICAL ONCOLOGY

Diagnosis of Struma Ovarii in a Patient with Papillary Thyroid Carcinoma – Verification via ^{124}I-PET/US Fusion

Manuskript (Fallbericht) in EUROPEAN JOURNAL OF ULTRASOUND 2014

JCEM
THE JOURNAL OF CLINICAL ENDOCRINOLOGY & METABOLISM
NOVEMBER 2013 • VOLUME 98 • NUMBER 11

2012 Impact Factor 6.430

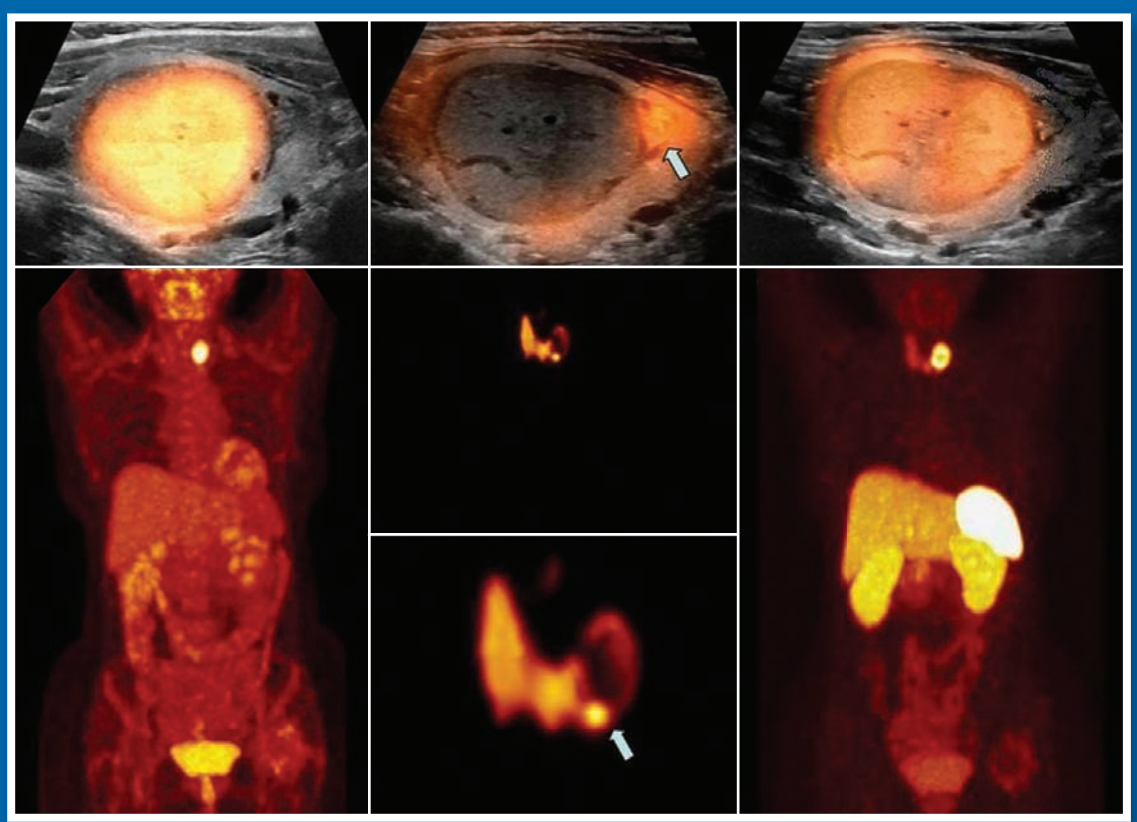

THE ENDOCRINE SOCIETY®
www.endo-society.org

Differential Diagnosis of Thyroid Nodules via Real-Time PET/Ultrasound (US) Fusion in a Case of Co-existing Medullary Thyroid Cancer and Adenoma

Falk Gühne, Thomas Winkens, Henning Mothes, and Martin Freesmeyer

Clinics of Nuclear Medicine (F.G., T.W., M.F.) and General, Visceral, and Vascular Surgery (H.M.), Jena University Hospital, 07743 Jena, Germany

A 52-year-old woman presented with apparent carcinoid syndrome. Gallium 68 (^{68}Ga)-DOTATOC positron emission tomography (PET)/computed tomography (CT) found a 2.5-cm somatostatin receptor (SR)-positive nodule in the left thyroid lobe. Basal serum calcitonin was 5184 ng/L, TSH was 0.63 mU/L, and free T_4 was 16.98 pmol/L, so medullary thyroid cancer was suspected. Ultrasonography (Figure 1, A and B), ^{18}F-fluorodeoxyglucose (FDG) PET/CT, and iodine 124 (^{124}I) PET/CT, performed to allocate thyroid nodules to ^{68}Ga-DOTATOC PET findings and exclude metastases, revealed an adjacent nodule <1 cm (Figures 1 and 2), believed to be adenoma. The patient provided informed consent for all procedures.

To unambiguously characterize the nodules, we used a magnetic navigation system (VNav; GE Healthcare) to perform live fusion of metabolic/functional images acquired through PET and morphological images obtained with ultrasound (PET/ultrasonography) (1). Live fusion recently was reported to be a problem-solving tool in cases of unclear PET findings (2); although CT shows anatomical landmarks facilitating PET image interpretation, ultrasonography offers superior soft-tissue resolution to that of CT. Moreover, real-time coregistration allows immediate, interactive investigation. PET/CT data are acquired according to standard protocol, then loaded onto an ultrasonography system located in a separate room; images are aligned using anatomical landmarks, and three-dimensional PET/CT views are then automatically reoriented and fused to live ultrasonographic images according to ultrasound probe positioning (3) (Figure 2, A–C, and Movie 1).

After thyroidectomy, histology confirmed our hypothesis regarding the lesions. Real-time fusion of PET/ultrasonography images thus differentiated an ^{18}F-FDG-positive, ^{124}I-negative, and SR-positive thyroid nodule, which proved to be medullary thyroid cancer, from an adjacent ^{18}F-FDG-negative, ^{124}I-positive, and SR-negative nodule, which turned out to be a compensated autonomous adenoma (Figure 2).

Acknowledgments

Robert Marlowe edited the manuscript.

Address all correspondence and requests for reprints to: Martin Freesmeyer, MD, Clinic of Nuclear Medicine, Jena University Hospital, Bachstrasse 18, 07743 Jena, Germany. E-mail: martin.freesmeyer@med.uni-jena.de.

Disclosure Summary: The authors have nothing to disclose.

References

1. **Ewertsen C, Henriksen BM, Torp-Pedersen S, Bachmann Nielsen M.** Characterization by biopsy or CEUS of liver lesions guided by image fusion between ultrasonography and CT, PET/CT or MRI. *Ultraschall Med*. 2011;32:191–197.
2. **Drescher R, Freesmeyer M.** PET/US fusion as a problem-solving tool in oncology imaging: differentiation of hernia repair mesh plugs from malignancy suspected on PET/CT [published online ahead of print April 10, 2013]. *Clin Nucl Med*. doi:10.1097/RLU.0b013e31828164a4.
3. **Drescher R, Müller A, Lesser T, Freesmeyer M.** PET/ultrasound fusion for differentiation of Vox implant silicone particles from recurrent cancer. *Nuklearmedizin*. 2013;52:N29–N30.

ISSN Print 0021-972X ISSN Online 1945-7197
Printed in U.S.A.

Received June 18, 2013. Accepted August 13, 2013.
First Published Online September 3, 2013

Abbreviations: CT, computed tomography; FDG, ^{18}F-fluorodeoxyglucose; ^{68}Ga, gallium 68; ^{124}I, iodine 124; PET, positron emission tomography; SR, somatostatin receptor.

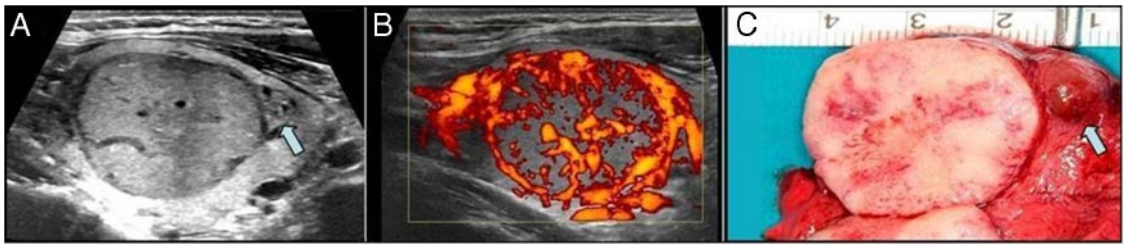

Figure 1. Left thyroid lobe nodule showing a regular margin, faint hypoechogenicity, and no microcalcification, ie, no typical signs of malignancy, on B-mode ultrasonography (A), and hyperperfusion on power-mode ultrasonography (B). C, This nodule proved to be a medullary thyroid cancer adjoining a smaller autonomous adenoma (arrow).

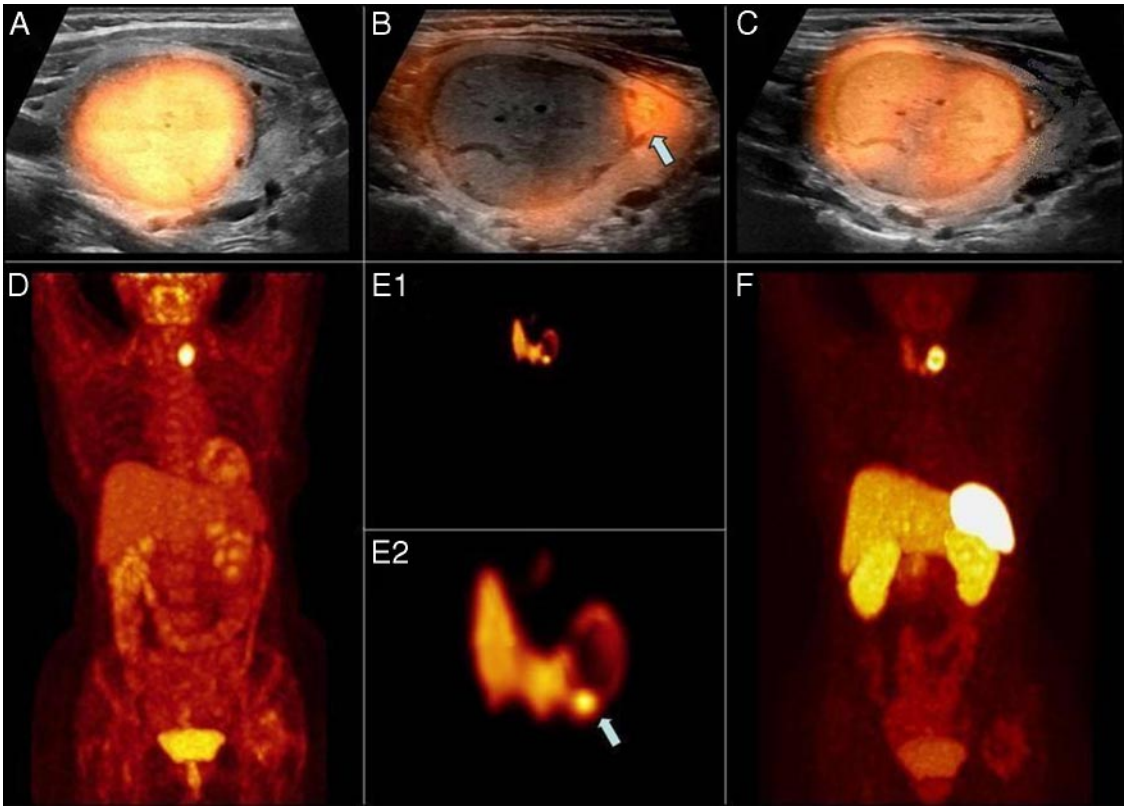

Figure 2. PET/ultrasonography fusion images (top row) and maximum intensity projection PET images (bottom row) using ^{18}F-FDG (A and D), ^{124}I (B and E), and ^{68}Ga-DOTATOC (C and F). A and D, ^{18}F-FDG-positivity of the larger thyroid nodule; B and E, ^{124}I-negativity of that nodule and ^{124}I-positivity of a smaller, adjacent nodule (arrow); C and F, SR-positivity of the larger nodule.

JJCO Japanese Journal of Clinical Oncology

Jpn J Clin Oncol 2013

Image of the Month

Diagnosis of Small Medullary Thyroid Carcinoma via PET/Ultrasound (US) Fusion

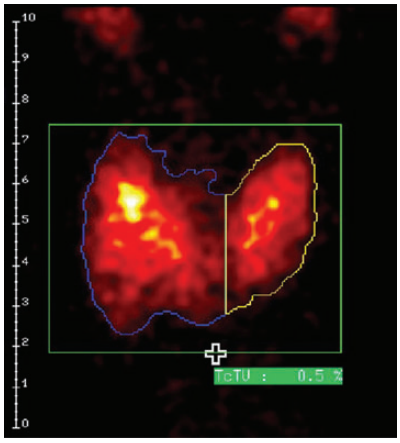

Figure 1.

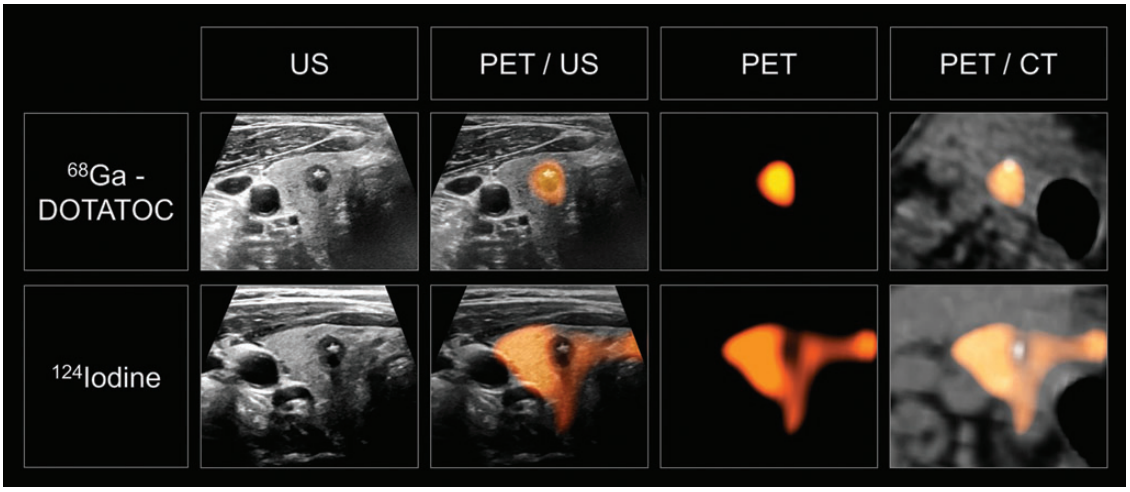

Figure 2.

An euthyroid 72-year-old woman (TSH 1.1 mU/l) was referred to our institution for second-reading diagnostics. A small (max. diameter 9 mm), hypoechoic nodule with central macrocalcification had been incidentally found within the thyroid. ^{99m}Tc-PT scintigraphy had shown normal uptake with moderate maxima (right > left) in the upper parts of both thyroid lobes but no sign of hypofunctionality (Fig. 1). The basal calcitonin level, however, was 123.0 pg/ml and therefore a medullary thyroid cancer was suspected.

We performed a ^{124}I-PET/CT to assess the functional state of the thyroid incidentaloma and found that the nodule was clearly hypofunctional. We also performed a ^{68}Ga-DOTATOC-PET/CT to assess the somatostatin receptor (SSTR) status and exclude metastatic spread, with findings of moderate SSTR positivity in the nodule, but absence of pathologic expression within the body. Nonetheless, the exact localization of metabolic findings was hindered due to the poor spatial resolution and soft-tissue contrast of the CT; therefore, PET/ultrasound fusion imaging was performed.

To allocate the metabolic findings within the thyroid, we used a magnetic navigation system (VNav, GE Healthcare, Milwaukee, WI, USA) to perform live fusion of metabolic/functional images acquired through PET and morphologic images obtained with ultrasound (PET/US) (Fig. 2). Fusion images of PET, US and CT clearly depicted the thyroid nodule as ^{68}Ga-DOTATOC-positive (top row) and ^{124}I-negative (bottom row) (Fig. 2: transversal sectional images from left to right: Ultrasound, PET/US fusion, PET and PET/CT). Post-thyroidectomy and simultaneous neck dissection histology proved that the thyroid incidentaloma was a medullary thyroid cancer. Following total thyroidectomy, the calcitonin levels fell below the limits of detection.

In summary, we were able to (1) exactly spatially correlate the ultrasonographic findings with PET and CT and (2) unambiguously characterize the intrathyroidal incidentaloma as lacking thyroid metabolism (which was not seen on standard ^{99m}Tc-PT scintigraphy) and presenting somatostatin receptors using PET/US fusion technique.

Dr. Ernesta Palombo-Kinne is gratefully acknowledged for language assistance with the manuscript.

Martin Freesmeyer[1], *Henning Dralle*[2] *and Thomas Winkens*[1]
[1]*Clinic of Nuclear Medicine, Jena University Hospital, Jena*
[2]*Clinic of General, Visceral and Vascular Surgery, Halle University Hospital, Halle/Saale, Germany*
doi:10.1093/jjco/hyt175

Diagnosis of Struma Ovarii in a Patient with Papillary Thyroid Carcinoma – Verification via ^{124}I-PET/US Fusion

Eine Patientin mit papillärem Schilddrüsenkarzinom und Struma ovarii – Diagnose durch ^{124}I-PET/US Fusion

Introduction

Struma ovarii is an extremely rare and mostly benign germ-cell tumor containing predominantly differentiated thyrocytes. Simultaneous presentation of thyroid cancer and benign struma ovarii is rare; only sporadic case reports have been published (C. Ghander et al. Gynecol Oncol 2006; 102: 378 – 380 and A. Jammah et al. Arq Bras Endocrinol Metabol 2011; 55: 490 – 493 and W. Macdonald et al. Clin Nucl Med 2007; 32: 380 – 382). We describe a case of an incidentally detected struma ovarii in a patient with papillary thyroid cancer (PTC), with verification by ^{124}I-positron emission tomography/computed tomography (PET/CT). ^{124}I-PET/CT has been extensively described for patients with metastatic thyroid cancer, and a few studies report also on its role in benign thyroid diseases (Freudenberg et al. Eur Radiol 2004; 14: 2092 – 2098 and Darr et al. Clin Nucl Med 2013, [epub ahead of print]). However, due to its limited spatial resolution and soft-tissue contrast, CT has disadvantages in the detection of small structures or lesions in the pelvis, where soft-tissue contrast is poor. Therefore, ultrasound (US) is more suitable for depicting pathological structures located in soft tissue.

Case description

A 48-year-old female with newly diagnosed PTC (1.1 cm) was referred to our institution for ^{131}I radioiodine ablation after surgical resection. In addition to residual thyroid tissue in the neck, the pre-therapeutic whole-body scintigraphy using ^{123}I revealed a focus in the right lower abdomen, with suspicion of a struma ovarii (not displayed). To detect the source of iodine accumulation, ^{124}I-PET/CT was performed (**Fig. 1a, b**) after obtaining informed consent from the patient. However, the exact anatomical origin of emitted radiation could not be clearly identified on CT, presumably due to limited soft-tissue contrast. Therefore, US and subsequent PET/US fusion were carried out to allocate the iodine accumulation. US scanning was performed using an electromagnetic navigation system (VNav, LOGIQ E9, GE Healthcare, Milwaukee, WI, USA), enabling the tracking of the transducer and thus the image position. Previously acquired PET/CT data were loaded onto the US device and then manually aligned by the examiner using anatomical landmarks that are visible on CT and US (**Fig. 1c**). At least three common points have to be identified in order to achieve correct registration between both modal-

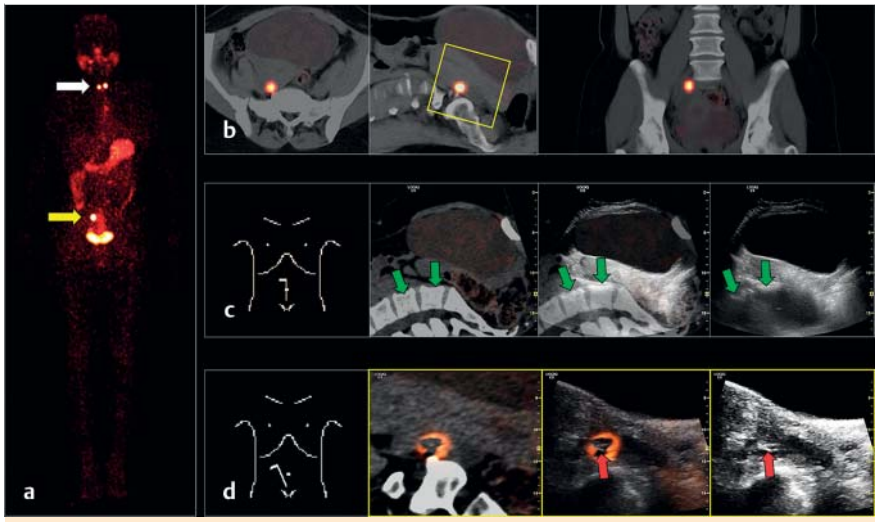

Fig. 1 **a** Pre-therapeutic ^{124}I-PET maximum intensity projection (MIP) with residual thyroid tissue (white arrow) and suspected struma ovarii (yellow arrow). **b** ^{124}I-PET/CT images; from left to right: transverse, sagittal, coronal plane. **c** From left to right: a pictogram showing transducer's strict sagittal position; PET/CT images with little ^{124}I activity within the bladder; PET/CT/US image; US image. The green arrows indicate the front edges of lumbar vertebrae, visible on CT as well as on US by means of the reflecting bone contours. As seen on the PET/CT/US image, the modalities provide an exact match. d: Detailed section of b (yellow frame) with, from left to right: a pictogram showing transducer's right parasagittal position; PET/CT image with a ^{124}I-focus near a lumbar vertebra and the uterus; PET/US image, clearly linking the focus to the ovary and identifying a homogeneous hyperechoic structure within the right ovary as the source of radiation without signs of malignancy, e. g. no hypoechogenicity, no irregular margins (red arrow); US image. The missing display of ^{124}I-activity in the center of the focus represents an artifact generated by display of above-threshold radiation levels to be a "zero-value" (typical for ^{124}I studies in our setup). In fact, the highest activity was present in the center of the lesion.

Abb. 1 **a** Prätherapeutische ^{124}I-PET Maximum-Intensitätsprojektion mit Darstellung von residuellem Schilddrüsengewebe (weißer Pfeil) und vermuteter Struma ovarii (gelber Pfeil). **b** ^{124}I-PET/CT-Bilder mit (von links nach rechts) transversalen, sagittalen und koronaren Schnittbildern. **c** Von links nach rechts: Piktogramm mit streng sagittaler Schallkopfausrichtung; PET/CT-Schnittbild mit geringer ^{124}I-Aktivität in der Blase; PET/CT/US-Schnittbild; Ultraschallbild. Die grünen Pfeile zeigen auf die Vorderkanten der lumbalen Wirbelkörper, die sowohl im CT als auch im Ultraschall (anhand der Konturen infolge Totalreflektion) sichtbar sind. Wie aus dem PET/CT/US-Bild ersichtlich, stimmen die verschiedenen Bildmodalitäten exakt überein. **d** Bildausschnitt aus „b" (gelber Rahmen) mit (von links nach rechts): einem Piktogramm mit rechts parasagittaler Ausrichtung des Schallkopfes; PET/CT-Schnittbild mit einem ^{124}I- Fokus in unmittelbarer Nachbarschaft des Uterus und eines Lendenwirbelkörpers; PET/US-Schnittbild mit sicherer Zuordnung des Prozesses zum Ovar, wobei sich als Korrelat der fokalen Jodanreicherung eine homogen echoreiche Struktur ohne Hinweis auf Malignität (d. h. keine Hypoechogenität, keine unscharfe Abgrenzbarkeit zur Umgebung) zeigt (roter Pfeil); Ultraschallbild. Das „Loch" innerhalb der angezeigten ^{124}I-Aktivität ist ein Artefakt, das dadurch zustande kommt, dass Werte oberhalb eines Schwellenwertes als Nullwert angezeigt werden (Dies ist in unserem Fusions-Setup üblich). Die Aktivität war innerhalb des „Lochs" am höchsten.

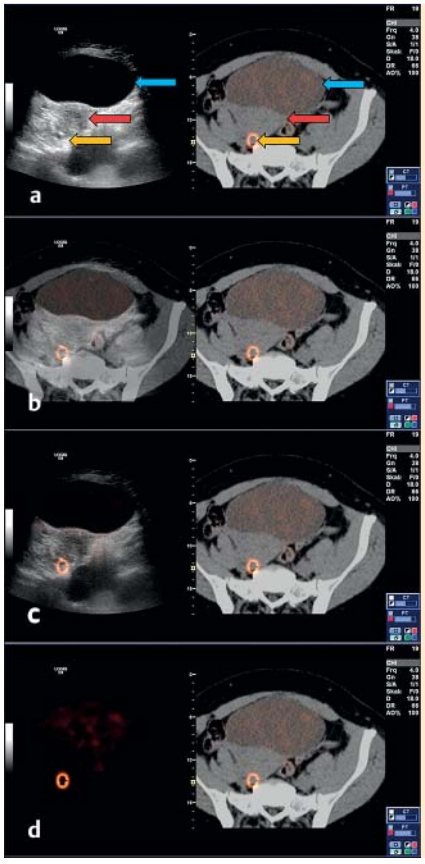

Fig. 2 Fusion imaging as seen on US display. All images: transverse plane of the pelvis, showing the bladder (blue arrow), uterus (red arrow) and right ovary posterior to the uterus (orange arrow). Switching modalities on the "active" display on the left side enables interchanging and overlaying modalities in any combination of PET/CT/US. The right display shows the corresponding PET/CT images as a reference, changing with movement of the US transducer. **a** US (left) and corresponding PET/CT image (right) after co-registration of both modalities. **b** PET/CT/US fusion image (left). Comparing the contour of the bladder, both modalities provide an exact match (as also visible in **Fig. 1**). **c** PET/US fusion image (left). **d** PET image (left). Note the tracer within the bladder, due to the renal excretion of ^{124}I.

Abb. 2 Fusionsbildgebung, entsprechend der Anzeige auf dem Bildschirm des US-Gerätes. Alle Bilder zeigen transversale Schnittbilder des Beckens mit Darstellung der Harnblase (blauer Pfeil), des Uterus (roter Pfeil) und des rechten Ovars, das hinter dem Uterus liegt (oranger Pfeil). Das Wechseln der Modalitäten auf dem linken, „aktiven" Display ermöglicht eine Darstellung und Überlagerung der PET/CT/US-Bilder in jeglicher Kombination. Das rechte Display zeigt das dem Ultraschallbild entsprechende PET/CT-Bild, das sich bei Bewegung des Ultraschallkopfes mitbewegt. **a** US (links) und das dazugehörige PET/CT- Bild (rechts) nach Koregistrierung beider Modalitäten. **b** PET/CT/US-Fusionsbild (links). An der Kontur der Blase in der überlagerten Darstellung kann man erkennen, dass die Registrierung genau übereinstimmt (wie auch in **Abb. 1** ersichtlich). **c** PET/US-Fusionsbild (links). **d** PET Bild (links). In der Blase befindet sich ebenfalls ^{124}I, da dieser Radiotracer überwiegend über die Nieren ausgeschieden wird.

ities (E. M. Jung et al. PLoS One 2012; 7: e33 956). Bony landmarks were chosen because they are not subject to tissue deformation caused by the transducer. Following co-registration of US images and PET/CT data, both datasets were displayed in an overlapping format as well as side-by-side (**Fig. 1 d, 2**). As the transducer was moved within the electromagnetic field, the US image and the PET/CT image were aligned in real-time to allow direct comparison of the findings. PET/US fusion images clearly identified hyperechoic tissue within the right ovary to be the source of radiation. No ovarian mass but rather an ovary of normal shape and size with a hyperechoic area matching the ^{124}I-focus was detectable. Additional endovaginal ultrasound was performed. However, there were no sonographically suspicious structures within the right ovary.

Due to the rarity of struma ovarii, there are no precise guidelines as to how to manage this condition. In our case, the patient declined surgery, thus final histological confirmation was not available. A few differential diagnoses could cause iodine accumulation: metastasis and endometriosis. However, benign struma ovarii was regarded as the most probable cause, based on sonographic findings. On follow-up visit after radioiodine ablation three months later, whole-body scintigraphy with ^{131}I (not displayed) revealed complete regression of the thyroid tissue within the ovary and the cervical foci as well.

Discussion

The role of different imaging methods in struma ovarii has been evaluated before, but with a focus on morphologic imaging (J. Shen et al. Abdom Imaging 2011; 36: 627 – 631). Metabolic imaging – as obtained through iodine or ^{99m}Tc-pertechnetate whole-body scintigraphy – leads to the diagnosis of struma ovarii usually on an incidental basis. ^{99m}Tc-pertechnetate or $^{123/131}$I single photon emission CT (SPECT)/CT has been described to be useful in the diagnosis of unclear whole-body scintigraphy findings (M. Mulazimoglu et al. Clin Nucl Med 2012; 37: 304 – 306). However, SPECT/CT is not available in all institutions, and it is inferior to ^{124}I-PET regarding spatial resolution and inferior to ultrasound regarding soft-tissue contrast and spatial resolution. Therefore, the PET/US fusion imaging technique offers advantages compared to SPECT/CT. The use of PET/US was first described by Ewertsen et al. in 2009 (C. Ewertsen et al. Dan Med Bull 2010; 57: B4172). The US findings of struma ovarii are heterogeneous masses with cysts or fat and solid parts accompanied by central vascularization (K. van de Moortele et al. JBR-BTR 2003; 86: 209 – 210 and Y. Zalel et al. J Ultrasound Med 2000; 19: 857 – 861), which was also the case in our patient. The fusion of PET/CT/US enabled the exact localization of the PET positive focus.

PET/US fusion imaging has some limitations that need to be considered. First, the setup applied in this study was rather elaborate, requiring an additional examination after regular PET/CT scan. Currently, efforts are being made to simplify the protocol to integrate PET/US fusion in the clinical routine. Second, the patient was exposed to additional radiation. However, compared with the radiation exposure resulting from radioiodine therapy using 3.7 GBq ^{131}I, application of 37 MBq ^{124}I can be considered negligible. The US examination could have been improved using contrast-enhanced US.

This case presents the advantages of PET/US as an emerging method of fusion imaging technique. Its application in thyroid

diagnostics using ^{124}I has been previously reported (Darr et al. Clin Nucl Med 2013, [epub ahead of print]). However, this is the first report concerning ^{124}I PET/US in a patient with struma ovarii.

Catchword phrases

▼

In certain cases, ultrasound plays a key role in hybrid imaging when other modalities reach their limitations.

The PET/US fusion technique can be used to verify unclear findings in thyroid cancer diagnostics.

Acknowledgement

▼

Dr. Ernesta Palombo-Kinne is gratefully acknowledged for language assistance.

M. Freesmeyer, E. Schleußner, T. Winkens, Jena

3.3.3. Technische Entwicklungen zur integrierten nuklearmedizinisch-sonographischen Fusionsbildgebung (Hybridbildgebung)

3.3.3.1. Integriert-sequentielles Konzept: Kombination von freehand SPECT (fhSPECT) und sensornavigierter Sonographie

Hybrid Integration of Real-Time Ultrasound and Freehand-SPECT: Proof of Concept in Patients with Thyroid Diseases

Publikation RADIOLOGY 2014

Hybrid Integration of Real-time US and Freehand SPECT: Proof of Concept in Patients with Thyroid Diseases[1]

Martin Freesmeyer, MD
Thomas Opfermann, PhD
Thomas Winkens, MD

Purpose: To report an initial experience regarding the feasibility and applicability of quasi-integrated freehand single photon emission computed tomography (SPECT)/ultrasonography (US) fusion imaging in patients with thyroid disease.

Materials and Methods: Local ethics committee approval was obtained, and 34 patients were examined after giving written informed consent. After intravenous application of 75 MBq of technetium 99m pertechnetate, freehand three-dimensional SPECT was performed. Data were reconstructed and transferred to a US system. The combination of two independent positioning systems enabled real-time fusion of metabolic and morphologic information during US examination. Quality of automatic coregistration was evaluated visually, and deviation was determined by measuring the distance between the center of tracer distribution and the center of the US correlate.

Results: All examinations were technically successful. For 18 of 34 examinations, the automatic coregistration and image fusion exhibited very good agreement, with no deviation. Only minor limitations in fusion offset occurred in 16 patients (mean offset ± standard deviation, 0.67 cm ± 0.3; range, 0.2–1.0 cm). SPECT artifacts occurred even in situations of clear thyroid findings (eg, unifocal autonomy).

Conclusion: The freehand SPECT/US fusion concept proved feasible and applicable; however, technical improvements are necessary.

[1] From the Clinic of Nuclear Medicine, Jena University Hospital, Bachstrasse 18, 07743 Jena, Germany. Received October 16, 2013; revision requested November 8; revision received November 18; accepted December 3; final version accepted December 11. **Address correspondence to** M.F. (e-mail: *martin.freesmeyer@med.uni-jena.de*).

The combination and integration of different imaging modalities have proved to be a highly successful way to overcome the limitations of functional imaging (1,2). Starting in 2000, this hybrid imaging approach has led to the introduction of positron emission tomography (PET)/computed tomography (CT), single photon emission CT (SPECT)/CT, and PET/magnetic resonance (MR) imaging in clinical settings (2–4). Few concepts of linking ultrasonography (US) with nuclear medicine imaging have been presented (5–8). However, no integrated concept (in terms of two modalities in one device, comparable to a PET/CT scanner) is available for linking US with nuclear medicine imaging. A handheld device provides a solid basis for an integrated concept, owing to its compact design and mobility (in comparison to a conventional SPECT scanner). Fused imaging could make a useful contribution to diagnostic tests, specifically with regard to the thyroid.

Technetium 99m pertechnetate ($^{99m}TcO_4$) scintigraphy is indicated in patients with below-normal thyroid-stimulating hormone levels or thyroid nodules larger than 1 cm in diameter (9). In the diagnostic work up for the thyroid, $^{99m}TcO_4$ scintigraphy and US findings are compared and evaluated by means of side-by-side examination.

Limitations in evaluation occur because of the different image characteristics of both methods. US enables unobscured imaging of the thyroid tissue with high spatial resolution and soft-tissue contrast (10). $^{99m}TcO_4$ scintigraphy yields functional data; however, the spatial resolution is on the order of 1 cm. Furthermore, it provides visualization from one projection, whereby adjacent lesions cannot be distinguished from one another. For this reason, it appears to be useful to develop a combined device that will permit the combined use of both methods in one examination.

In recent years, a compact freehand SPECT system (declipseSPECT; SurgicEye, Munich, Germany) has been developed for the intraoperative imaging of sentinel lymph nodes (11–13). Because this involves the visualization of ^{99m}Tc-labeled protein particles in the tissue, the method itself appears to be suitable for detecting the distribution of $^{99m}TcO_4$ within the thyroid.

Concerning US, real-time fused images can already be obtained by combining US (equipped with sensor-based navigation) with other previously recorded data sets, such as MR imaging, CT, PET/CT, and SPECT (6,7,14–16). The registration and alignment of both data sets are based on a US transducer fitted with sensors that are located in an electrical field generated by an electromagnet (17). The goal of this study was to report an initial experience regarding the feasibility and applicability of quasi-integrated freehand SPECT/US fusion imaging in patients with thyroid disease.

Advances in Knowledge

- By using handheld SPECT and US, thyroid metabolic data were successfully coregistered on the US images in real time in 34 patients.
- For 18 of 34 examinations, the automatic coregistration and image fusion exhibited very good agreement with no deviation, and in 16 examinations, the mean deviation was 0.67 cm ± 0.3.

Materials and Methods

Patients

The freehand SPECT system and the US device were provided by SurgicEye and GE Healthcare (Milwaukee, Wis), respectively. The authors had full control of the data submitted for publication. This study was approved by the local ethics committee, and all patients provided written informed consent. In September and October of 2012, 280 patients were referred to our clinic for $^{99m}TcO_4$ scintigraphy and US. Two hundred twelve patients decided to participate in the study. On the basis of the $^{99m}TcO_4$ study and US results, patient selection was performed by a physician (M.F.) experienced in radiology (16 years) and nuclear medicine (9 years), according to the inclusion criteria of either distinct focal thyroid uptake or homogeneous tracer distribution, which were met by 34 patients (mean age ± standard deviation, 62 years ± 10; range, 43–83 years; 25 women and nine men) (Table). Referral indications were hyperthyreosis (26 cases) and/or cervical pressure (12 cases). Exclusion criteria were inhomogeneous thyroid uptake, multifocal uptake, and diverging results of $^{99m}TcO_4$ study and US examination. The patients underwent standard thyroid diagnostic tests (thyroid-stimulating hormone measurement, US, and $^{99m}TcO_4$ scintigraphy) and subsequently underwent a freehand SPECT examination, immediately followed by a sensor-navigated thyroid US study. Thyroid scintigraphy was indicated for all patients, and they were not exposed to any additional radiation. Seventy-five MBq of $^{99m}TcO_4$ was administered intravenously. To demonstrate the technical feasibility of this method, only patients with clear constellations of findings (concordant findings of $^{99m}TcO_4$ scintigraphy and US, such as unifocal autonomy with only one nodule or diffuse homogeneous uptake without nodules) were selected.

Freehand SPECT

Freehand SPECT is a three-dimensional SPECT imaging modality based on data acquisition with a handheld gamma probe that is moved freely around the area of interest (11,18,19). It has initially been developed to visualize sentinel lymph nodes intraoperatively to guide sentinel lymph node removal. According to the manufacturer information, its

Published online before print
10.1148/radiol.14132415 **Content codes:** HN NM US

Radiology 2014; 000:1–6

Author contributions:
Guarantor of integrity of entire study, M.F.; study concepts/study design or data acquisition or data analysis/interpretation, all authors; manuscript drafting or manuscript revision for important intellectual content, all authors; approval of final version of submitted manuscript, all authors; literature research, M.F., T.O.; clinical studies, M.F.; experimental studies, M.F., T.O.; statistical analysis, M.F., T.O.; and manuscript editing, M.F., T.W.

Conflicts of interest are listed at the end of this article.

Patient Characteristics

Characteristic	Datum
No. of patients	34
Mean age (y)	62 ± 10 (43–83)*
No. of men	9/34 (26)
Thyroid disorder	
Unifocal autonomy	16/34 (47)
Graves disease	10/34 (29)
Nontoxic goiter	6/34 (18)
Normal thyroid	2/34 (6)
Offset	
No deviation	18/34 (53)
Minor deviation ≤ 1 cm	16/34 (47)
Mean offset (cm)	0.67 ± 0.3 (0.2–1.0)*
Major deviation > 1 cm	0/34 (0)

Note.—Numbers in parentheses are percentages, unless indicated otherwise.

* Data are mean ± standard deviation. Numbers in parentheses are ranges.

Figure 1

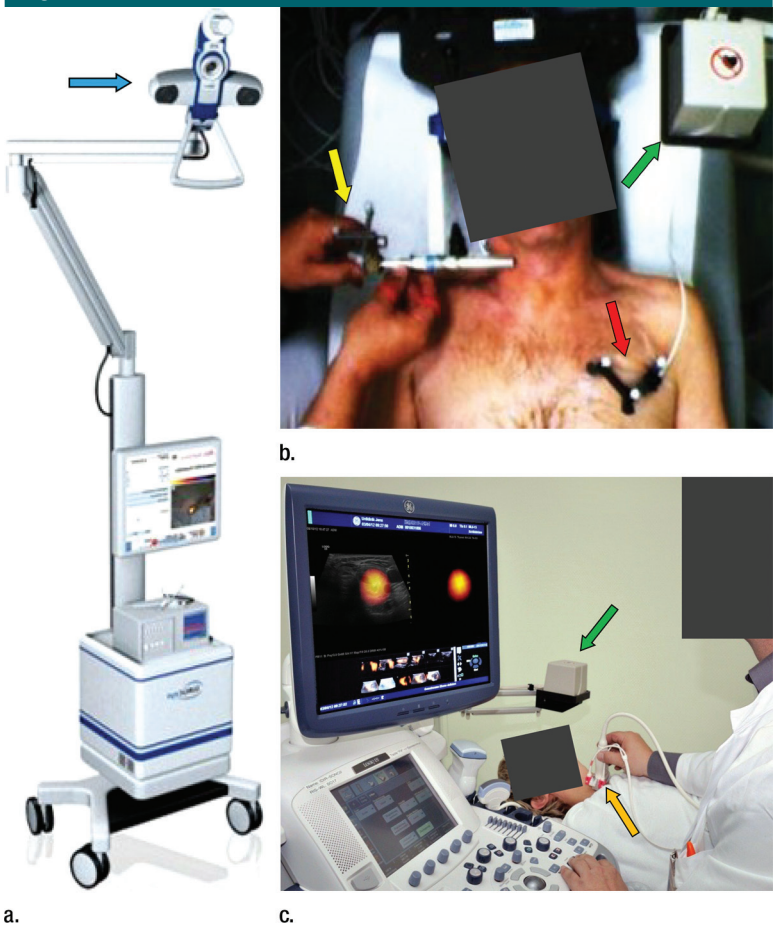

Figure 1: Photographs show study setup. The declipseSPECT system with positioning unit (arrow in **a**) determines the position of the gamma probe, which has optical markers affixed (yellow arrow in **b**). The patient's neck is scanned laterally to ventrally to capture the raw data. Allocation is performed by using an optical localization sensor affixed to the patient (red arrow in **b**). Immediately after the SPECT data have been loaded onto the US machine in Digital Imaging and Communications in Medicine format (by using a USB stick), navigated US is performed (**c**). The orientation of the US transducer is determined by using attached electromagnetic sensors (gold arrow in **c**) in a magnetic field generated by a transmitter (green arrows in **b** and **c**). The optical and electromagnetic tracking systems are linked via a shared sensor that is affixed to the patient.

spatial resolution is 5 mm. The system consists of the following: *(a)* two optical localization sensors (Polaris Vicra; NDI, Waterloo, Ontario, Canada), one affixed to a gamma probe (NucleoProbeMR200; NucleoMed, Rome, Italy) and the other one affixed to the patient; *(b)* a tracking system (optical and positioning camera) located above the patient to detect the sensors; *(c)* a computing unit for data processing; and *(d)* a monitor as the output device, to visualize the tracer distribution within the area of interest.

The optical tracking system detects the position and orientation of the patient and the gamma probe, and thus the tracer distribution within the area of interest. A modified iterative algorithm (maximum-likelihood expectation maximization) for nonuniform limited-angle projections was used for reconstruction. The system generates a three-dimensional SPECT data set and correlates the images in a maximum intensity projection with a live video image of the patient and, thus, the patient's anatomy (11).

Navigated US

US was performed by using a commercially available US system (LOGIQE9; GE Healthcare) configured with Volume Navigation and an ML6–15 US transducer. An electromagnetic transmitter is placed near the imaging area, and a pair of electromagnetic sensors is attached to a bracket that connects to the transducer. The position-sensing equipment allows the US device to track the transducer's position, and therefore the image position, within the electromagnetic field.

Fusion Imaging

To ensure the correct positioning and alignment of both tracking systems, it is essential that the optical sensor (freehand SPECT) and the electromagnetic localization device (US) are merged. Therefore, a combined sensor consisting of the patient's optical sensor and an additional electromagnetic sensor was assembled and placed on the patient's chest (Fig 1).

Figure 2

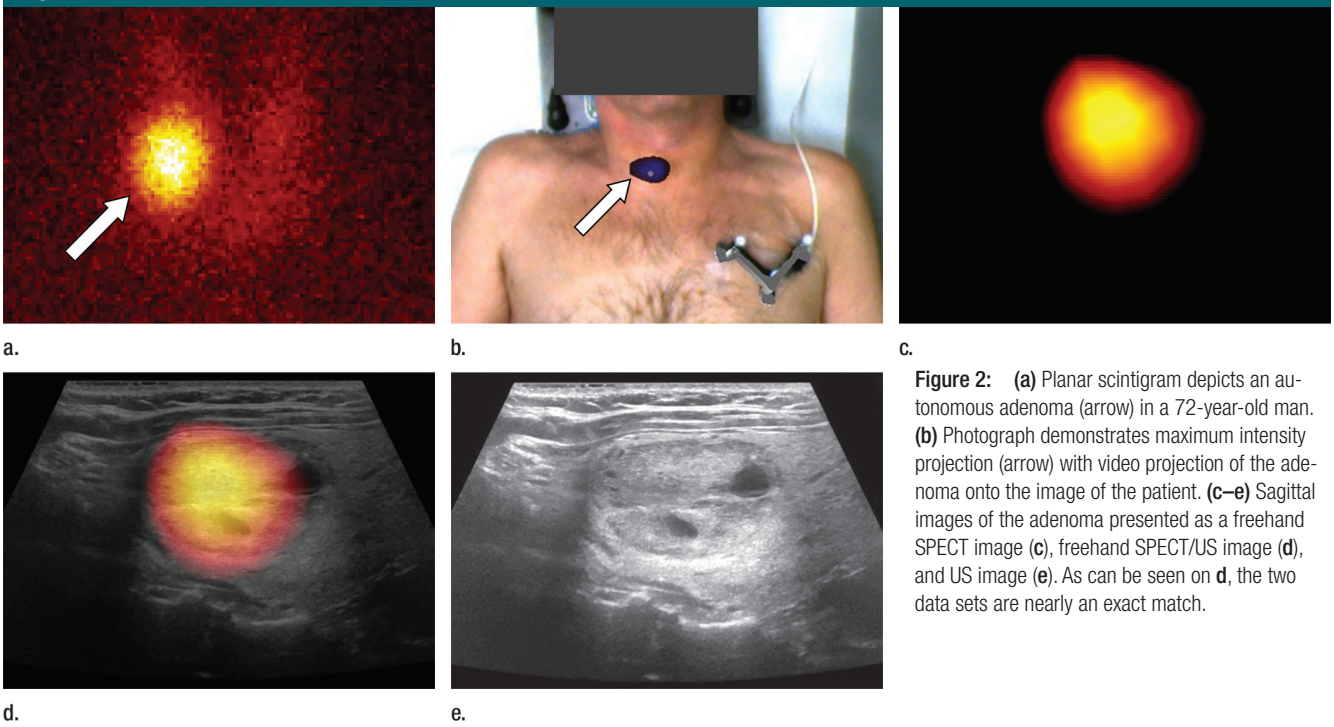

Figure 2: **(a)** Planar scintigram depicts an autonomous adenoma (arrow) in a 72-year-old man. **(b)** Photograph demonstrates maximum intensity projection (arrow) with video projection of the adenoma onto the image of the patient. **(c–e)** Sagittal images of the adenoma presented as a freehand SPECT image (**c**), freehand SPECT/US image (**d**), and US image (**e**). As can be seen on **d**, the two data sets are nearly an exact match.

The combination of two independent tracking systems allows for automatic coregistration of SPECT and US images without the need for point-based registration (eg, using anatomic landmarks). As the US image is moved, the freehand SPECT image tracks in real time. The images are displayed side by side or in blended, overlapping format (Fig 2).

The quality of automatic coregistration of the two data sets was evaluated visually by a physician (M.F.) with longtime experience in nuclear medicine and radiology and was assigned one of three categorizations: *(a)* very good agreement with no deviation; *(b)* minimal, acceptable deviations up to 1 cm; or *(c)* unacceptable deviations larger than 1 cm, error registered.

In hyperfunctional nodules, deviations were measured from the center of maximum activity to the center of the nodule at US and in homogeneous tracer uptake from the center of each lobe as it appeared at freehand SPECT to the center of the lobe as it appeared at US.

Attention was also paid to potential freehand SPECT artifacts that occurred during reconstruction and US examination.

Results

Standard diagnostic tests, including scintigraphy, US, and laboratory results, demonstrated the following disorders: focal thyroid autonomy (n = 16), Graves disease (n = 10), nontoxic goiter (n = 6), and normal findings (n = 2).

The mean examination time for freehand SPECT and US was 19 minutes ± 7 (range, 10–40 minutes).

For 18 of 34 examinations, the automatic coregistration and image fusion exhibited very good agreement, with no deviation. For 16 of 34 examinations, acceptable deviations between freehand SPECT and US were found (0.67 cm ± 0.3; range, 0.2–1.0 cm) (Table). These were not predominantly in one direction or the other.

In some cases, artifacts occurred at freehand SPECT, including *(a)* reconstruction of what appeared to be tracer uptake outside the thyroid, which was not seen at planar scintigraphy (n = 13); *(b)* reconstruction of two points of maximum uptake (right and left lobe), with only one hyperfunctional nodule at planar scintigraphy, and US with a regular-sized thyroid with one 1.7-cm nodule (n = 1); and *(c)* suboptimal imaging of the caudal and dorsal parts of the thyroid (n = 3).

Discussion

Our study demonstrates that automatic coregistration of metabolic freehand SPECT and morphologic US data and presentation as a fused image are technically feasible in the thyroid. About half of the examinations proved the US and freehand SPECT data to be an exact match, directly correlating the center of a focus as seen with freehand SPECT to its corresponding region at US.

The freehand SPECT system was originally created for the detection of sentinel lymph nodes, and it has never been used in a thyroid diagnostic examination before. In a phantom study, its full width at half maximum was found to be 13 mm (20). This spatial resolution is clearly insufficient to distinguish

small thyroid structures with different $^{99m}TcO_4$ uptake. Therefore, only clear constellations of findings were examined, and it was not the goal of our study to evaluate the clinical value or the potential effect on treatment decision making, but rather to demonstrate the feasibility of fusion imaging. However, even in these clear constellations of findings, artifacts occurred, which confirmed the inability of the system to precisely visualize thyroid metabolism.

Freehand SPECT is suitable to develop an integrated concept of nuclear medicine imaging and US because it is a compact, mobile system with the potential of truly being integrated into a US transducer in the future. As a prerequisite to develop such a device, this study shows the feasibility of combining both methods immediately without moving the patient. Compactness and almost simultaneous acquisition are points that differ from similar, previously published concepts. Bucki et al used conventional SPECT data to fuse with live US images (6). Galdames et al combined previously acquired SPECT data and previously acquired US images with a separate workstation (8). Studies in which PET/CT was combined with live US have been performed by Ewertsen (7).

Benefits of the presented quasi-integrated concept lie first in the tomographic imaging of the freehand SPECT, which, unlike conventional $^{99m}TcO_4$ scintigraphy, permits imaging of tracer distribution free of overlapping. Second, the uncertainties of visual coregistration when interpreting findings from scintigraphy and US side by side might be avoided. For example, in $^{99m}TcO_4$ scintigraphy, the caudal thyroid margin can only with difficulty be differentiated from a hypofunctional nodule in that location. Simultaneous presentation of both imaging modalities on the display of the US machine might aid in this assessment. Third, this imaging technique requires no additional radiation exposure, if patients are already being referred for thyroid scintigraphy.

Our study had limitations. First, 34 of 212 patients were selected to participate. This is a large selection bias, which may influence the results. Second, the spatial resolution of freehand SPECT is more limited than that of US, owing to physical factors. The resolution achieved with this setup will presumably be insufficient to distinguish between smaller (<1 cm) lesions that are located adjacent to one another. Therefore, only definitive constellations of findings were examined in this feasibility study. Thus, our results are applicable to this selected set of patients only.

Third, minor spatial deviations between the two modalities occurred in approximately one-half of the cases. The metabolic organ boundaries obviously did not match those detected with US. Possible reasons could be *(a)* minimal patient movements occurring between freehand SPECT data acquisition and US that were not detected by the sensors and *(b)* the slight deformation of the tissue caused by the pressure from the US transducer (as opposed to the freehand SPECT data, which were acquired without any contact). Therefore, a critical evaluation of the fused image is necessary. Potential approaches to solve these problems include establishing better systems to detect patient movements and the use of standoff pads to distribute the pressure more evenly.

Future studies should be conducted to compare performance of freehand SPECT with conventional SPECT, because both methods obtain a three-dimensional tracer distribution. This comparison was not considered in the present study, according to the focus on the goal of proving general feasibility.

In summary, the presented concept of freehand SPECT/US has proved to be easy and quick to perform. The thyroid metabolic data were successfully coregistered on the US images in real time. However, the system configuration used in this study confirmed the assumed low SPECT quality in accurately depicting thyroid lesions. Also, the precision of the image fusion needs to be improved.

This concept might be a further step toward developing an integrated hybrid imaging technique analogous to PET/CT, SPECT/CT, and PET/MR imaging.

Acknowledgments: SurgicEye, Munich, Germany, and GE Healthcare, Milwaukee, Wis, are gratefully acknowledged for providing the hardware to perform this study, free of charge.

Disclosures of Conflicts of Interest: M.F. Financial activities related to the present article: Author is a co-inventor of the SurgicEye system, which provided nonfinancial support in the form of the freehand SPECT system used; and GE Healthcare provided the US device. Financial activities not related to the present article: none to disclose. Other relationships: author has a patent pending. **T.O.** No relevant conflicts of interest to disclose. **T.W.** No relevant conflicts of interest to disclose.

References

1. Seo Y, Mari C, Hasegawa BH. Technological development and advances in single-photon emission computed tomography/computed tomography. Semin Nucl Med 2008;38(3):177–198.
2. Townsend DW. Dual-modality imaging: combining anatomy and function. J Nucl Med 2008;49(6):938–955.
3. Beyer T, Townsend DW, Brun T, et al. A combined PET/CT scanner for clinical oncology. J Nucl Med 2000;41(8):1369–1379.
4. Hasegawa BH, Wong KH, Iwata K, et al. Dual-modality imaging of cancer with SPECT/CT. Technol Cancer Res Treat 2002;1(6):449–458.
5. Péria O, Chevalier L, Francois-Joubert A, et al. Using a 3D position sensor for registration of SPECT and US images of the kidney. In: Proceedings from the First International Conference on Computer Vision, Virtual Reality and Robotics in Medicine; April 3–6, 1995; Nice, France. 1995;905:23-29.
6. Bucki M, Chassat F, Galdames F, Asahi T, Pizarro D, Lobo G. Real-time SPECT and 2D ultrasound image registration. Med Image Comput Comput Assist Interv 2007;10(Pt 2):219–226.
7. Ewertsen C. Image fusion between ultrasonography and CT, MRI or PET/CT for image guidance and intervention—a theoretical and clinical study. Dan Med Bull 2010;57(9):B4172.
8. Galdames FJ, Perez CA, Estévez PA, et al. Registration of renal SPECT and 2.5D US images. Comput Med Imaging Graph 2011;35(4):302–314.
9. Dietlein M, Dressler J, Grunwald F, et al. Guideline for in vivo- and in vitro procedures for thyroid diseases (version 2) [in German]. Nuklearmedizin 2003;42(3):109–115.
10. Lee JH, Anzai Y. Imaging of thyroid and parathyroid glands. Semin Roentgenol 2013;48(1):87–104.

11. Wendler T, Hartl A, Lasser T, et al. Towards intra-operative 3D nuclear imaging: reconstruction of 3D radioactive distributions using tracked gamma probes. Med Image Comput Comput Assist Interv 2007; 10(Pt 2):909–917.

12. Wendler T, Herrmann K, Schnelzer A, et al. First demonstration of 3-D lymphatic mapping in breast cancer using freehand SPECT. Eur J Nucl Med Mol Imaging 2010;37(8):1452–1461.

13. Wiesner S, Dressel P, Friebe M, et al. Registration free SPECT and ultrasound imaging. Presented at the 23rd Conference of the Society for Medical Innovation and Technology (SMIT 2011), Tel Aviv, 2011.

14. Curiel L, Chopra R, Hynynen K. Progress in multimodality imaging: truly simultaneous ultrasound and magnetic resonance imaging. IEEE Trans Med Imaging 2007;26(12):1740–1746.

15. Tang AM, Kacher DF, Lam EY, Brodsky M, Jolesz FA, Yang ES. Multi-modal imaging: simultaneous MRI and ultrasound imaging for carotid arteries visualization. Conf Proc IEEE Eng Med Biol Soc 2007;2007:2603–2606.

16. Rennert J, Georgieva M, Schreyer AG, et al. Image fusion of contrast enhanced ultrasound (CEUS) with computed tomography (CT) or magnetic resonance imaging (MRI) using volume navigation for detection, characterization and planning of therapeutic interventions of liver tumors. Clin Hemorheol Microcirc 2011;49(1-4):67–81.

17. Prager RW, Ijaz UZ, Gee AH, Treece GM. Three-dimensional ultrasound imaging. Proc Inst Mech Eng H 2010;224(2):193–223.

18. Bluemel C, Schnelzer A, Okur A, et al. Freehand SPECT for image-guided sentinel lymph node biopsy in breast cancer. Eur J Nucl Med Mol Imaging 2013;40(11):1656–1661.

19. Mihaljevic AL, Rieger A, Belloni B, et al. Transferring innovative freehand SPECT to the operating room: first experiences with sentinel lymph node biopsy in malignant melanoma. Eur J Surg Oncol 2013 Sep 17. [Epub ahead of print]

20. Krohn T, Verburg FA, Brockmann H, Winz OH, Mottaghy FM, Behrendt FF. A phantom assessment of portable imaging and radioguided surgery systems with technetium-99m and fluorine-18. Nucl Med Commun 2012;33(5):452–458.

3.3.3. Technische Entwicklungen zur integrierten nuklearmedizinisch-sonographischen Fusionsbildgebung (Hybridbildgebung)

3.3.3.2. Integriert-simultanes Konzept: Kombination von real-time handheld Emission Spot Allocator (rthESA) und Sonographie

Real-time Handheld Emission Spot Allocator (rthESA) for Simultaneous Fusion Imaging with Ultrasound

Publikation in Nuklearmedizin 2014

Real-time Handheld Emission Spot Allocator (rthESA) for Simultaneous Fusion Imaging with Ultrasound

Martin Freesmeyer M.D.[1], Thomas Winkens[1], Christian Kühnel[1,2]

[1] Clinic of Nuclear Medicine, Jena University Hospital, Jena, Germany
[2] Ernst-Abbe-University of Applied Sciences, Jena, Germany

Corresponding author and reprint requests:

Martin Freesmeyer, M.D.
Clinic of Nuclear Medicine
Jena University Hospital
Bachstrasse 18
07740 Jena
Germany
Phone: +49-3641-933220
Fax: +49-3641-933244
Email: martin.freesmeyer@med.uni-jena.de

Word count: 1967

Type of Manuscript: Technical Development

Acknowledgments

GF & E GmbH, Seeheim, Germany is gratefully acknowledged for developing the hardware and software by author's commission. We thank Dr. Dominik Driesch for statistical analyses and Dr. Ernesta Palombo-Kinne for assistance with the manuscript.

Funding:
The rthESA system was provided by GF & E GmbH, Seeheim, Germany by commission of M. Freesmeyer.

Advances in Knowledge:

1. The rthESA proved feasible to exactly localize a spot radiation source in a single plane, with additional consideration of the distance from the detector.
2. Spot radiation sources were detected faster when located close to the detector.
3. Real-time allocation and simultaneous overlay to a US image was technically successful.
4. The device still presents clear technical limitations requiring further development; nevertheless it represents a concept of integrated simultaneous hybrid imaging.

Implications for Patient Care:

N/A

Summary statement:

This proof-of-concept paper presents the development of a compact, mobile device able to allocate and visualize a radiation source in real time; after connection to a US transducer, the rthESA enabled the correct allocation of a spot radiation source within a live US image.

Abstract

Purpose: First, to report on initial experiences and technical parameters of a newly developed real-time handheld emission spot allocator (rthESA), and second, to report on the simultaneous acquisition of rthESA and US data as rthESA/US fusion images.

Materials/Methods: The rthESA consisted of five semiconductor-detectors arranged in alternate position in two rows. This design allowed the examination of focal activities in the same plane as US. The signals were interpreted by an ad hoc software and the real-time allocation of spot radiation sources within air- and water phantoms was investigated for ^{99m}Tc, ^{131}I, and ^{18}F. A compact US probe was fixed in plane with the rthESA and connected to a standard US equipment. Experiments with a liver phantom were performed to verify the integration of ^{99m}Tc-rthESA data and US images.

Results: The allocation proved to be successful for all radionuclides. The system showed a noticeable performance latency, most pronounced for positions far from the detector (1cm distance: 0.7±0.5 sec; 4cm distance: 6.1±3.2 sec). Within the liver phantom, the rthESA enabled the correct allocation of a spot radiation source within a live US image.

Conclusion: The rthESA allowed an exact localization of spot radiation sources in single plane, with additional consideration of the distance from the detector, leading to real-time allocation and simultaneous overlay with US images. In spite of clear technical limitations in need of further development, this proof-of-concept study shows that this hybrid detector has the potential to provide integrated simultaneous nuclear medicine and US images.

Introduction

Functional imaging in nuclear medicine is commonly associated with limited spatial resolution and locatability of findings (1). Combining nuclear medicine techniques with morphological imaging has proven highly successful in overcoming these limitations i.e., positron emission tomography/computed tomography (PET/CT), single photon emission computed tomography (SPECT)/CT, and PET/magnetic resonance imaging (MRI) (2-5). A hybrid device of nuclear medicine imaging and ultrasound (US), however, is not yet available, in spite of the high spatial resolution and soft-tissue contrast of sonography.

A few studies have addressed the combination of SPECT and US images (6, 7), however these studies are based on sequential acquisition in two different examinations, the first for functional data and the second for morphological data. The overlay of the two datasets can be performed "live" on US display during examination, or "offline" on separate workstations. To date, however, a simultaneous acquisition has not yet been described.

Combining two devices for simultaneous radiation detection and US imaging requires the development of a device that is able to locate an emission source in plane with sonography, i.e., can depict the distance from the device. Also, visualization has to occur immediately without reconstruction.

The present proof-of-concept, phantom-based study had two goals: 1) To report on initial experiences and technical parameters of a newly developed real-time handheld emission spot allocator (rthESA), and 2) To report on the simultaneous acquisition of rthESA and US data as rthESA/US fusion images.

Materials and Methods

Real-time handheld emission spot allocator (rthESA)

The rthESA consisted of three parts: a detector array, an electronic measuring unit (i.e., high-voltage detector supply, pre-amplifier, pulse-shaping amplifier, discriminator with logic-signal shaping), and a computer-assisted workstation.

The detector array contained five cubic Cd-Zn-Te semiconductor-detectors. These were arranged in alternating order to allow the examination of focal activities in plane with the scan-field-of-view (Figure 1).

The measurable energy spectrum ranged between 100 and 550 keV. The semiconductor-detectors were operated in reverse bias and connected to a 5-fold pre-amplifier (12 V, low-voltage supply). The signals were separately conducted through the electronic measurement unit and processed. Finally, the data were conveyed to a counter board (Meilhaus-Zählerkarte ME1400, Meilhaus, Puchheim, Germany) connected to a computer-assisted workstation (not displayed). The ad hoc developed software (TM1410 and ME1400Server, Marschelke Messtechnik, Reichenau, Germany) analyzed the data of all five detectors and interpreted the signal localization on the basis of background reference data.

The system was initially calibrated to generate reference data. For this purpose, 63 reference points were measured for each of the investigated nuclides, and nuclide-specific results were

incorporated in the database.

Phantoms and radionuclides

For phantom experiments, the rthESA was tested in an air phantom (Figure 2a) and a water phantom (to simulate soft tissue) (Figure 2b). A spot radiation source at the top of a rod was plugged into one of 63 holes placed into a vertical Plexiglas plate. The radiation at each of the measured positions was detected by the detector array, and its position within the phantom grid was defined via the ratio of the values measured at the detectors (Figure 2, Supplement 1).

The rthESA system was calibrated against three radionuclides most commonly used in clinical routine (^{99m}Tc, ^{131}I, and ^{18}F). For air- and water phantom experiments, 1 MBq of each nuclide was used to create the spot radiation source.

The liver phantom consisted of a large piece of cow liver containing a 5-mm capsule filled with 1 MBq ^{99m}Tc solution (Figure 3). This phantom served to verify the feasibility of the hybrid rthESA/US construct in terms of detector integration, data acquisition, and image fusion.

Screen visualization of the rthESA signals

The localization of the radiation source was depicted as a red spot within a coordinate system (Figure 2).

Latency assessment

The *initial* latency of the rthESA in identifying the source location entering the scan-field-of-view was individually assessed for each of the radionuclides investigated. For this purpose five points of the matrix (two close to and two far from the detectors, one in central position) were subjected to five different measurements per position. A spot allocation was assessed as reliable when no changes of position occurred for at least 3 sec.

Hardware and software integration and image fusion of rthESA and US

For liver phantom measurements, the rthESA detector and the US probe were joined in a Plexiglas case (Figures 3 and 4). The US probe was connected to a standard ultrasonography device (Logiq E9, GE Healthcare). The screen display of rthESA and standard US information was combined and visualized in the computer-assisted workstation via a USB frame grabber (DFG/USB2pro, TheImagingSource, Bremen, Germany) (Figure 4). The image superimposition was performed using the same software employed for the visualization of the spot source (Supplement 4). An initial co-registration was necessary to guarantee the spatial image matching of the two imaging modalities (gauging).

Statistical analysis

The results were analyzed by Cox regression using the statistical survival package LanguageR. The significance level was established at $p<0.05$.

Results

For each of the three radionuclides investigated (^{99m}Tc, ^{131}I, and ^{18}F), the use of the rthESA allowed an exact allocation of 63 measurement points in the image matrix, in air phantoms as well as in water phantoms (Supplement 1).

In terms of initial response time, a Cox regression analysis with uncensored data excluded a significant influence of the nuclide type or the phantom type on the response speed, whereas the distance from the detector played a significant role ($p<0.05$). For all nuclides, in fact, the spot radiation sources closer to the detector was localized significantly faster (e.g., 1 cm distance: 0.7 ± 0.5 sec) than the source distant from the detector (4 cm distance: 6.1 ± 3.2 sec) (Table 1).

Considering the different nuclides, the speed of correct allocation (latency) was only moderately different, with ^{18}F showing a longer latency (mean 4.2 ± 4.1 sec) than ^{99m}Tc and ^{131}I (mean 2.9 ± 3.4 sec, 2.9 ± 2.2 sec, respectively) (not significant).

Concerning the liver phantom, the simultaneous scanning with the combined rthESA/US device was also technically successful. Directing the combined device towards the spot source resulted in a source allocation that matched the actual US localization of the capsule (Figure 3). If the source *entered* the scan-field-of-view, the initial localization of the focus required approximately 2 sec (Supplement 2); if the radiation source was moved *within* the scan-field-of-view, the correct re-localization time was approximately 9 sec (Supplement 3).

Discussion

This proof-of-concept paper presents the development of a compact, mobile device able to allocate and visualize a radiation source in real time. After connection to a US transducer, the rthESA enabled the correct allocation of a spot radiation source within a live US image. The software allowed a simultaneous transparent overlay of both imaging modalities, representing a development in the direction of hybrid nuclear medicine/US imaging (Supplement 4). The source allocation proved to be successful for ^{99m}Tc, ^{131}I and ^{18}F and the system showed some response latency.

The presented technology expands on previous approaches of functional/US fusion imaging, for example offline fusion of separately acquired metabolic and 2.5D/3D US data (8, 9) or fusion of PET or SPECT data and US images during live US examination (10-12). However, these methods present certain disadvantages, i.e, imprecise co-registration caused by *sequential* acquisition of data, slight patient movements (even if examinations are performed on the same stretcher), and tissue deformation during US (unlike PET and SPECT data, obtained without physical contact). Thus, simultaneous functional/US scanning and image fusion can be clearly useful in overcoming these disadvantages. Considering these aspects, the present approach of simultaneous rthESA/US fusion imaging is a truly integrated concept of nuclear medicine imaging and US.

Previously developed handheld gamma cameras depict radiotracer distribution in the plane of acquisition, i.e., length and width (13). The distance of a source from the detector usually

cannot be determined unless the scan is performed from multiple directions and a reconstruction takes place after acquisition of raw data. In contrast, the present device was able to determine and display the location of the radiation source by scanning from a single direction.

This investigation has the following strengths: 1) In contrast to established hybrid imaging techniques (PET/CT, SPECT/CT, and PET/MRI), the present is a truly simultaneous technique. To date only special PET/MRIs of the newest generation are simultaneous (14); 2) The presented setting does not require complex tracking systems, since the integration at the hardware level requires only a single initial spatial co-registration; 3) Unlike tomographic methods, the present image acquisition does not require acquisition from different positions and subsequent reconstruction to allow a correct localization. 4) In the current set-up, the activity measurement takes place in plane with the US, i.e., both modalities are simultaneously depicted on the same plane; 5) The presented approach enables the detection of different emission energies (^{99m}Tc in low-energy range, ^{131}I in high-energy range, and ^{18}F in ultrahigh-energy range) without the need of a hardware collimator.

Limitations of the present technology are: 1) The current set-up is limited to the detection of a single focus, thus future studies are warranted for the investigation of multiple foci and two-point discrimination; 2) A clear discrepancy exists between the resolution of the rthESA (63 points) and that of the US (mm or less). Nevertheless, even at the current status the device was sufficiently correct in localizing a focus in a liver phantom; 3) This approach is based on the localization of a source in comparison with reference data acquired via time-consuming calibrations. As a matter of fact, this is not very different from the gauging or constancy tests of a gamma camera with defined radioactive standards; 4) Evaluation of the system's response was mainly focused on the *initial* allocation of a radiation source. Tracing a radiation source was relatively slow, meaning that the device is not suitable for quick scans of larger tissue areas (Supplement 1 and 3); 5) In the current configuration, the device was able to localize a spot source in an environment without activity. As this study did not yet address the influence of background activity, the results are not applicable to complex activity distributions.

Practical Applications

In conclusion, we present a hybrid device with the following characteristics: 1) Exact localization of a spot radiation source in a single plane, with additional consideration of the distance from the detector; and 2) Real-time allocation and simultaneous overlay to a US image. The device still presents clear technical limitations requiring further development; nevertheless it represents a concept of integrated simultaneous hybrid imaging.

References

1. Munley MT, Kagadis GC, McGee KP, Kirov AS, Jang S, Mutic S, et al. An introduction to molecular imaging in radiation oncology: a report by the AAPM Working Group on Molecular Imaging in Radiation Oncology (WGMIR). Med Phys. 2013;40(10):101501.

2. Seo Y, Mari C, Hasegawa BH. Technological development and advances in single-photon emission computed tomography/computed tomography. Seminars in nuclear medicine. 2008;38(3):177-98.

3. Townsend DW. Dual-modality imaging: combining anatomy and function. J Nucl Med. 2008 Jun;49(6):938-55.

4. Beyer T, Townsend DW, Brun T, Kinahan PE, Charron M, Roddy R, et al. A combined PET/CT scanner for clinical oncology. J Nucl Med. 2000;41(8):1369-79.

5. Hasegawa BH, Wong KH, Iwata K, Barber WC, Hwang AB, Sakdinawat AE, et al. Dual-modality imaging of cancer with SPECT/CT. Technology in cancer research & treatment. 2002;1(6):449-58.

6. Bucki M, Chassat F, Galdames F, Asahi T, Pizarro D, Lobo G. Real-Time SPECT and 2D Ultrasound Image Registration. In: Ayache N, Ourselin S, Maeder A, editors. Medical Image Computing and Computer-Assisted Intervention – MICCAI 2007. Lecture Notes in Computer Science. 4792: Springer Berlin / Heidelberg; 2007. p. 219-26.

7. Galdames FJ, Perez CA, Estevez PA, Held CM, Jaillet F, Lobo G, et al. Registration of renal SPECT and 2.5D US images. Comput Med Imaging Graph. 2011;35(4):302-14.

8. Freesmeyer M, Wiegand S, Darr A, Steenbeck J, Schleussner E, Opfermann T. Offline Fusion of 3-dimensional Ultrasound and 99m-TcO4-SPECT in Focal Thyroid Adenoma. First Experiences. Nuklearmedizin. 2012 2012;51(2):A95.

9. Galdames FJ, Perez CA, Estevez PA, Held CM, Jaillet F, Lobo G, et al. Registration of renal SPECT and 2.5D US images. Comput Med Imaging Graph. 2011;35(4):302-14.

10. Ewertsen C. Image fusion between ultrasonography and CT, MRI or PET/CT for image guidance and intervention - a theoretical and clinical study. Dan Med Bull. 2010;57(9):B4172.

11. Jung EM, Friedrich C, Hoffstetter P, Dendl LM, Klebl F, Agha A, et al. Volume Navigation with Contrast Enhanced Ultrasound and Image Fusion for Percutaneous Interventions: First Results. PLoS One. 2012;7(3).

12. Drescher R, Muller A, Lesser T, Freesmeyer M. PET/ultrasound fusion for differentiation of Vox implant silicone particles from recurrent cancer. Nuklearmedizin. 2013;52(3):N29-30.

13. Abe A, Takahashi N, Lee J, Oka T, Shizukuishi K, Kikuchi T, et al. Performance evaluation of a hand-held, semiconductor (CdZnTe)-based gamma camera. Eur J Nucl Med Mol Imaging. 2003;30(6):805-11.

14. Fraioli F, Punwani S. Clinical and research applications of simultaneous Positron Emission Tomography- Magnetic Resonance Imaging (PET-MRI). Br J Radiol. 2013. [epub ahead of print]

		Air phantom					Water phantom				
		Near to detector		Middle	Far from detector		Near to detector		Middle	Far from detector	
Nuclide		Position 1	Position 2	Position 3	Position 4	Position 5	Position 1	Position 2	Position 3	Position 4	Position 5
^{99m}**Tc**	Mean	0.8	0.8	4.4	4.8	4.8	0.6	0.2	2.0	6.4	4.0
	SD	0.4	0.4	4.5	4.8	4.8	0.5	0.4	2.3	3.4	2.0
^{131}**I**	Mean	0.8	0.8	3.6	5.2	4.8	0.8	0.8	3.0	5.2	4.4
	SD	0.4	0.4	1.5	1.3	1.5	0.4	0.4	1.4	2.0	1.1
^{18}**F**	Mean	0.8	0.8	2.0	7.4	6.8	0.2	0.6	3.8	9.0	10.8
	SD	0.4	0.4	0.7	0.5	1.3	0.4	0.5	0.8	2.9	3.9

Table 1: Initial response time (in seconds) of rthESA detector in assigning the exact position of a spot radiation source. Each measurement started on entering of the spot radiation source in the scan-field-of-view. Five measurements per position were performed. A constant display of the position for at least three seconds was considered as positive allocation. Position 1 = uppermost left corner of the phantom (1 cm distance from detector); position 2 = uppermost right corner (1 cm distance from detector); position 3 = middle row, middle column (2.5 cm distance from detector); position 4 = lowermost left corner (4 cm distance from detector); position 5 = lowermost right corner (4 cm distance from detector).

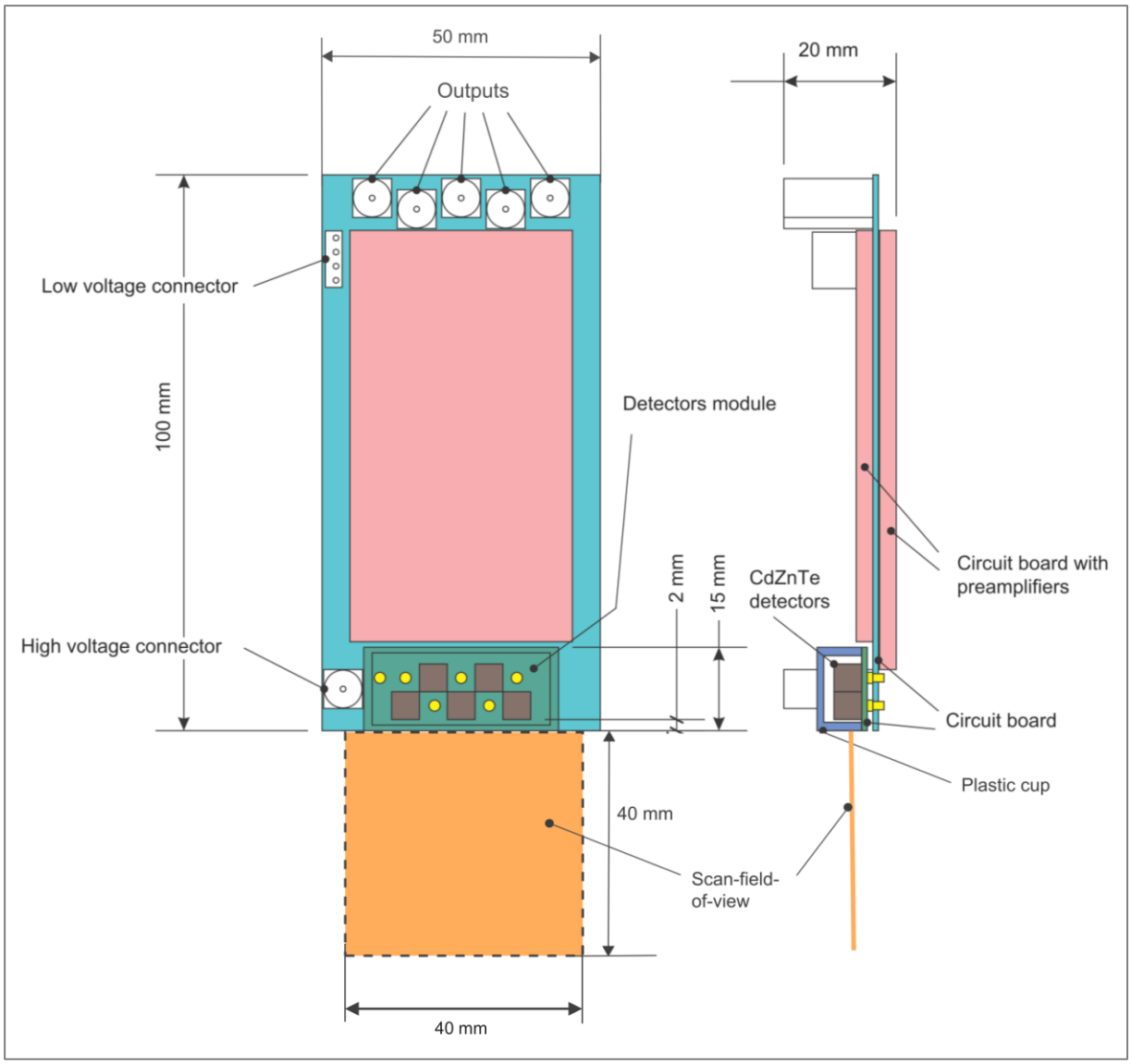

Figure 1: Schematic representation of the detector array of the real-time handheld emission spot allocator (rthESA). This consists of a module containing five cubic 4.8-mm Cd-Zn-Te semiconductor detectors (ZRF Ritec SIA, Riga, Latvia) arranged in alternate order on a single plane, three upfront and two in a second row. This order was designed to allow the examination of focal activities in plane with the scan-field-of-view which had a measuring depth (z axis) of 40 mm and a width (x axis) of 40 mm. The alternating order of the detectors allowed to determine the coordinates (x and z values) of a given spot source. The signals of the five detectors were transmitted to the electronic measuring unit (not displayed) via the circuit board. Soldering points in yellow.

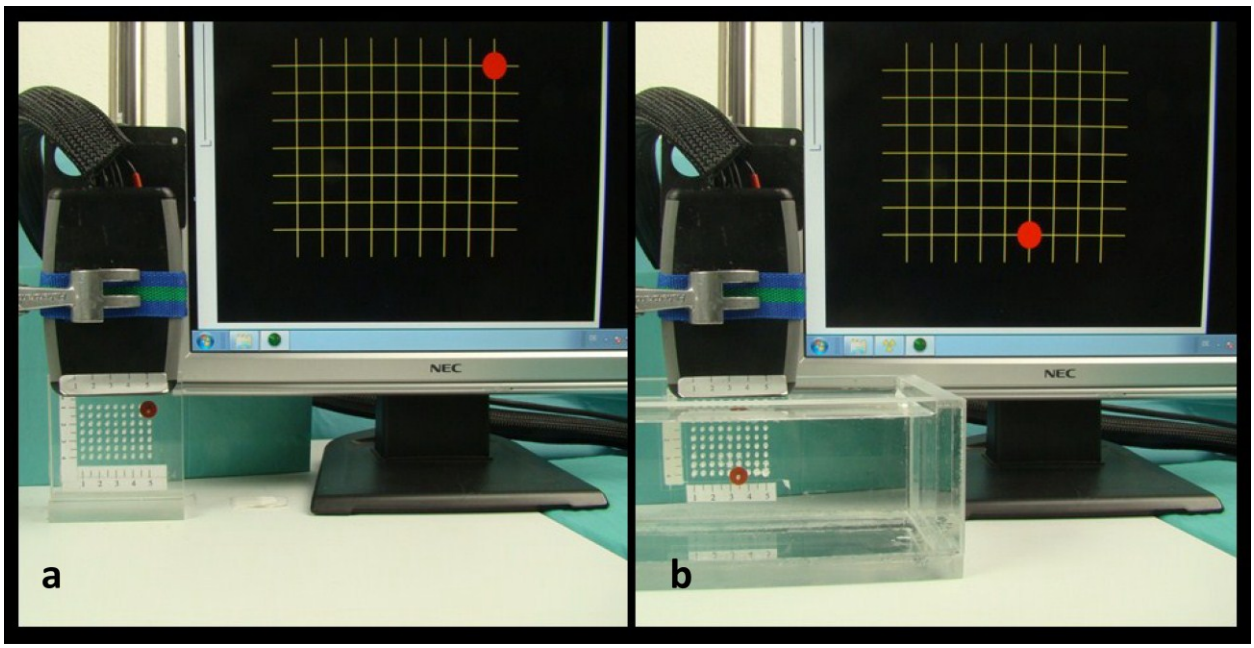

Figure 2:

a) Set-up of air phantom (left, bottom), rthESA device (left, middle; contained in a black housing with a centimeter scale at its bottom, fixed to a benchtop tripod), and display screen. A spot radiation source (in red; left, bottom; consisting of a plastic rod [27 mm long, 2 mm thick] with a spot radiation source sealed at its top and a red disk to visualize the rod) is plugged into a hole of the 9x7 matrix of a vertical Plexiglas phantom, and five rthESA detectors (arranged as shown in Figure 1) measure the radiation emitted. The top row of the phantom is at 1cm distance from the detector. The distance between each hole is 5 mm. The resulting electronic signals are transferred to a computer, and the information is conveyed to a 9x7 matrix on a display screen, with each intersecting point of the grid matching a hole of the phantom. The exact allocation of a spot within the display matrix is visualized as a round red dot (in this experiment at the uppermost right corner).

b) Set-up of water phantom experiments, with same settings as in a). In this case, the spot source is correctly allocated in the bottom row, fourth hole from the right.

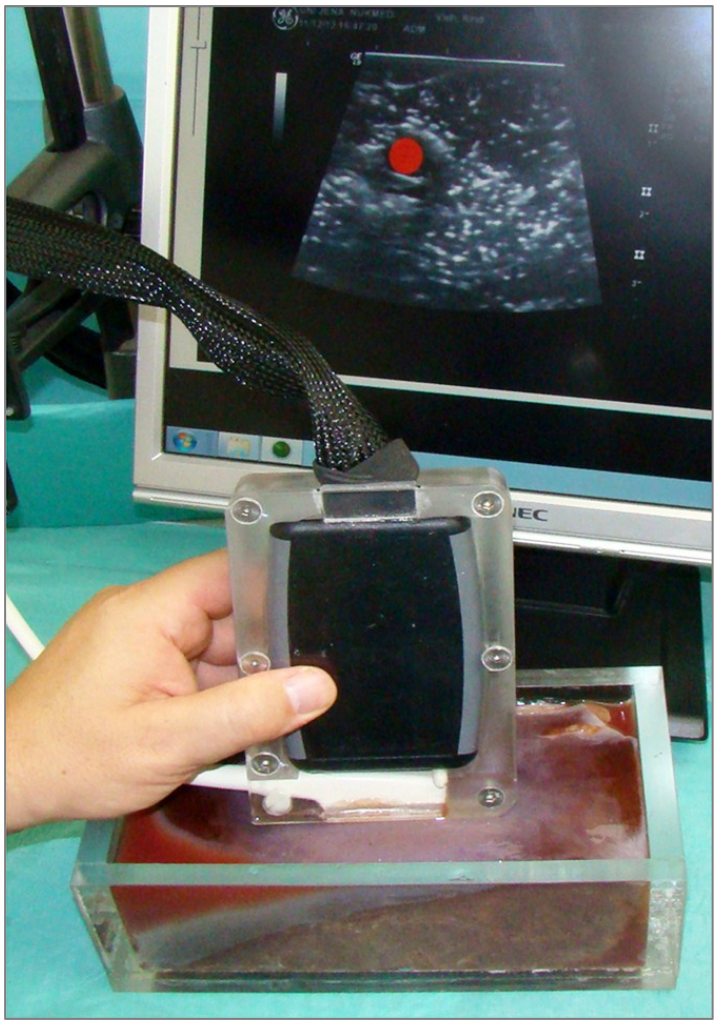

Figure 3:

Set-up of liver phantom experiments. The hybrid detector consists of the rthESA and an ultrasound (US) probe encased in a Plexiglas housing. The intraoperative US probe used for these experiments (i739L, GE Healthcare, Milwaukee, WI, USA) was particularly apt to the scope of this study, owing to its compactness and the lateral exit of the cable. The small size of the US probe allowed a vertical alignment with the rthESA detector, i.e., on the same plane. Thus, the radiation emitted by the phantoms traveled through the US probe to reach the detectors. The piece of cow liver contains a 5-mm plastic capsule filled with 1 MBq ^{99m}Tc. The screen displays both the rthESA information (red dot) and the US image of the sample, with an exact spatial match between the radiation source and the plastic capsule containing the radionuclide.

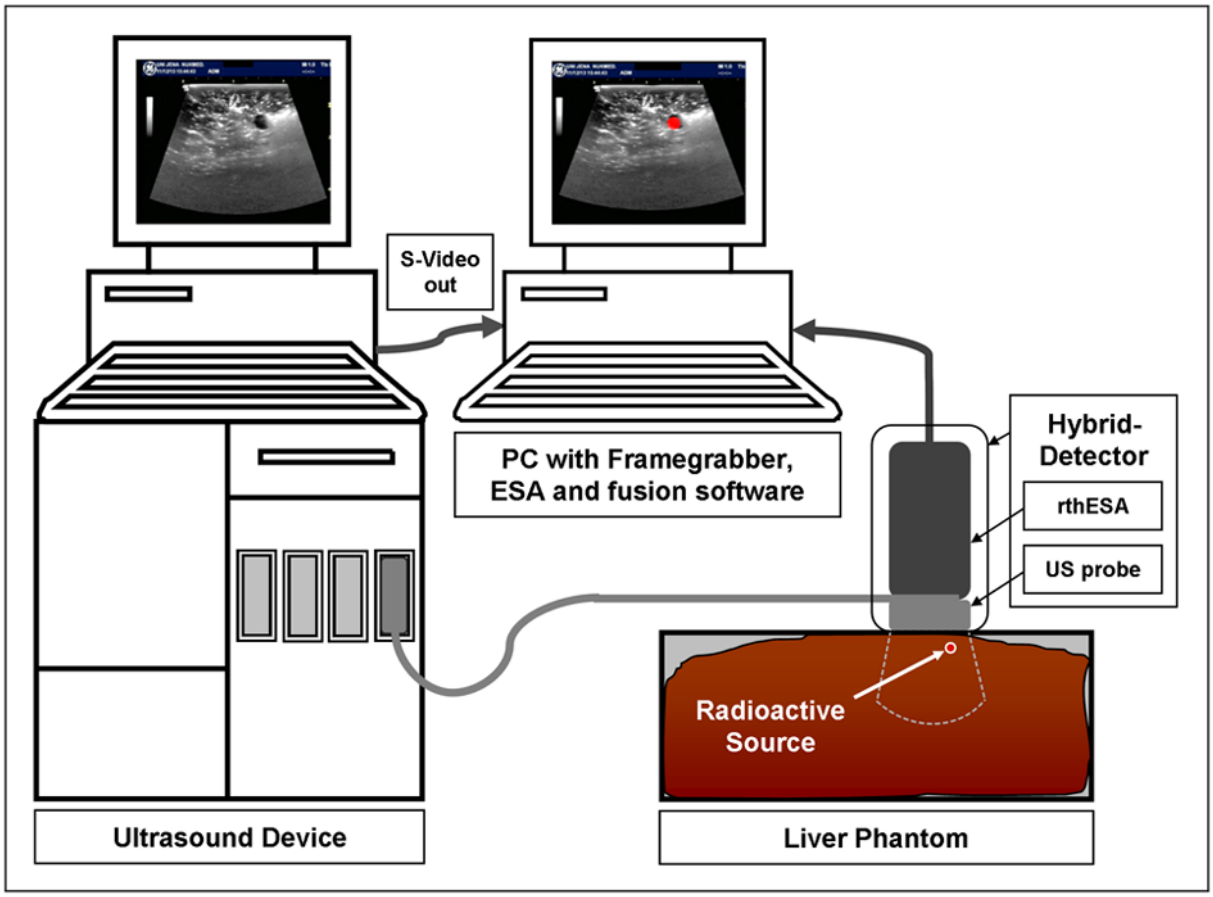

Figure 4:

Schematic representation of rthESA/ultrasound (US) fusion procedure. The hybrid detector (right) consists of rthESA (top) and US probe (bottom) encased in the same housing. The hybrid device correctly detects the position of a radiation source within a US image of a cow liver. The rthESA signals are transferred to a computer equipped with a software specifically programmed to display the radiation source. The US probe is connected to a standard US device and the video signals are transferred to the same computer that processes the rthESA information. A specifically programmed software superimposes both pieces of information.

Supplement 1: Video of rthESA performance, showing the air phantom (left, bottom), rthESA (left, middle), and screen display (right). The spot source (at the top of the rod) is visualized in red. First, the source is plugged into the third leftmost hole from the bottom in the 9x7 matrix of the air phantom and is immediately visualized as a red dot on the 9x7 matrix on the monitor. The radiation source is then moved to the right uppermost hole of the matrix. The correct allocation of the spot requires 17 seconds.

Supplement 2: Video of rthESA performance, showing the liver phantom (left, bottom), hybrid detector (rthESA and US probe) (left, middle), and screen display (right). The liver tissue contains a 5-mm plastic capsule filled with 1 MBq ^{99m}Tc. Initially, the monitor shows the US image only. The liver phantom is then moved in the y axis below the fixed hybrid detector. As the capsule appears on the US screen, the red dot (representing rthESA information) is displayed in real time on the same monitor. After two steps of transient misregistration, the radiation source is then correctly allocated (time required app. 2 seconds).

Supplement 3: Video of rthESA performance, showing the liver phantom (middle, bottom), hybrid detector (rthESA and US probe) (handheld, middle), and screen display (right, background). The liver tissue contains a 5-mm plastic capsule filled with 1 MBq ^{99m}Tc. Initially, the monitor shows the correct overlay of the red dot and the hypoechoic capsule as seen on US. The hybrid detector is then moved in the x axis. The capsule is now displayed on the right side of the display. After several steps of transient misregistration, the radiation source is then correctly allocated at the changed location of the capsule (time required 9 sec).

Supplement 4: Video of rthESA and US modalities as displayed on the monitor. The information of rthESA and US can be overlaid and displayed in real time in a semi-transparent combination. The video starts with US images only, changes to rthESA/US, then switches to rthESA only, changes back to rthESA/US, and finally displays US images only.

4. Darstellung der wichtigsten Ergebnisse und Einordnung in das wissenschaftliche Umfeld

4.1. ^{124}Iod-Niedrigaktivitäts-PET/Niedrigdosis-CT (^{124}Iod-PET/CT)

4.1.1. Funktionstopographie der Schilddrüse mit ^{124}Iod-PET/CT

Diese Studie wurde in der Zeitschrift Clinical Nuclear Medicine publiziert (vgl. 3.1.1., S. 17).
Ziel der vorliegenden Studie ist die Untersuchung der visuellen Vergleichbarkeit von konventioneller Szintigraphie und SPECT unter Anwendung von $^{99m}TcO_4$ mit ^{124}Iod-PET (PET) als Niedrigaktivitäts-PET/Niedrigdosis-CT unter Verwendung von lediglich 1 MBq ^{124}Iod. Geprüft werden sollte, ob (i) alle szintigraphisch diagnostizierten Befunde in der PET gesehen werden können und (ii) ob über die Szintigraphie/SPECT hinaus Zusatzinformationen erhoben werden können.
Einbezogen wurden 21 Patienten mit benignen Veränderungen der Schilddrüse (fokale Autonomien, Struma, Morbus Basedow), bei denen ein Radiojodtest in Vorbereitung auf eine Radiojodtherapie durchgeführt wurde.
Die szintigraphische Untersuchung der Schilddrüse erfolgte entsprechend der geltenden Leitlinien *(Dietlein et al. 2007A)*. Im Anschluss wurden SPECT-Aufnahmen an einer Zweikopf-Gammakamera durchgeführt. Für die PET/CT-Aufnahmen wurde ^{124}Iod peroral verabreicht. Anatomische Koregistrierung und Schwächungskorrektur erfolgten computertomographisch, wobei der minimal verfügbare Röhrenstrom eingestellt wurde (Stromzeitprodukt: 30 mAs), um die Strahlenbelastung so gering wie möglich zu halten. Die durch die CT-Komponente zusätzlich verursachte Strahlenexposition betrug lediglich 0,3 mSv. Bei 10 Patienten wurde die PET/CT Untersuchung am Tag der ^{124}Iod-Applikation (nach ca. 6h), bei 11 weiteren am Folgetag (nach ca. 23h) durchgeführt. Es wurde eine Bettposition von hochzervikal bis zum Aortenbogen über 10 Minuten gemessen.

Alle szintigraphisch bzw. in der SPECT erhobenen Befunde wurden in der PET gesehen. Darüber hinaus ließen sich mit der PET signifikant mehr fokale Mehrspeicherungen im Vergleich zu den herkömmlichen Untersuchungsverfahren abgrenzen (PET 83, SPECT 33, Szintigraphie 25). Hinsichtlich der Minderspeicherungen war dieser Effekt zwar als Trend, jedoch nicht statistisch signifikant nachweisbar (PET 9, SPECT 6, Szintigraphie 5). Die in der PET zusätzlich erfassten Befunde zeigten bei Messungen im Ultraschall signifikant kleinere Volumina und Durchmesser. Unter den Patienten mit fokalen Schilddrüsenautonomien und hyperthyreoter Stoffwechsellage ergab sich bei der PET-basierten Ermittlung des therapeutischen Zielvolumens für die Radiojodtherapie eine Zunahme von 21,9 %.

Weiterhin zeigte die Arbeit die bessere Abgrenzbarkeit anatomischer Details in der ^{124}Iod-PET im Vergleich zu planarer $^{99m}TcO_4$-Szintigraphie und $^{99m}TcO_4$-SPECT am Beispiel des

Lobus pyramidalis. Zudem konnte die signifikant häufigere Detektion eines retrosternalen Anteils durch PET/CT im Vergleich zur planaren $^{99m}TcO_4$-Szintigraphie demonstriert werden.

Die vorliegende Studie befasst sich erstmals mit dem diagnostischen Potential eines ^{124}Iod-Niedrigkaktivitätskonzeptes bei gutartigen Schilddrüsenerkrankungen im Vergleich zur konventionellen Diagnostik. Ausgangspunkt waren die Annahmen, dass (i) mit ^{124}Iod eine höhere Bildgüte durch die überlegene Ortsauflösung und den hohen Bildkontrast der PET möglich wird, dass (ii) durch den hohen spezifischen Uptake sowie die große Messempfindlichkeit der PET sehr geringe Mengen ^{124}Iod für eine adäquate Bildgebung genügen und dass (iii) durch die höhere Energie sowie die CT-Schwächungskorrektur Absorptionseffekte eine im Vergleich zur $^{99m}TcO_4$-Szintigraphie deutlich geringere Rolle spielen.

Da mit der PET alle fokalen Szintigraphie- und SPECT-Befunde reproduzierbar waren, kann die ^{124}Iod-PET hinsichtlich des Auffindens fokaler Befunde als mindestens gleichwertig betrachtet werden. Die Tatsache, dass die mit der PET zusätzlich erfassten fokalen Mehrspeicherungen signifikant kleinere Durchmesser und Volumina zeigten, spricht dafür, dass eine höhere Empfindlichkeit der Methode vorliegt. Diese ist wahrscheinlich auf die bessere Ortsauflösung zurückzuführen. Inwieweit ein höherer Bildkontrast zusätzlich dazu beiträgt, lässt sich anhand der Daten nicht analysieren.

Das Ergebnis, dass in der PET bei den 17 laborchemisch hyperthyreoten Patienten mit fokalen Autonomiebefunden eine Vergrößerung des zu therapierenden Volumens um durchschnittlich 21,9 % auftrat, stellt ein therapeutisch relevantes Ergebnis dar. Da das autonome Volumen linear in die Aktivitätskalkulation mittels Marinelli-Formel *(Marinelli et al. 1948, Eschmann et al. 2002, Dietlein et al. 2007B)* eingeht, wäre die therapeutische Aktivitätsmenge höher kalkuliert worden.

Aufgrund der Strahlenabsorption durch das Sternum und der niedrigen Energie von $^{99m}TcO_4$ kann sich ein retrosternaler Schilddrüsenanteil in der planaren Szintigraphie dem Nachweis entziehen *(Delorme und Hoffner 2003)*. Sonographisch ist die Beurteilbarkeit eines retrosternalen Schilddrüsenanteils ebenfalls erschwert *(Blank und Braun 2007)*. Ein Vorteil der CT-Untersuchung liegt hingegen in der sicheren Detektion von retrosternalem Schilddrüsengewebe *(Kilic et al. 2011)*. Dies konnte im Patientengut aufgrund der signifikant häufigeren Detektion eines retrosternalen Anteils durch PET/CT im Vergleich zur planaren $^{99m}TcO_4$-Szintigraphie bestätigt werden. Dies hat erhebliche therapeutische Relevanz, da im Falle eines ausgedehnten retrosternalen Schilddrüsengewebsanteiles eine chirurgische Therapie erforderlich sein kann *(Machado et al. 2011, Kadhim et al. 2006)*.

In der Regel ist die Darstellbarkeit des Lobus pyramidalis im Szintigramm auf verdickte Befunde begrenzt *(Spencer et al. 1997)*, wobei die vorteilhaften Eigenschaften der PET eine

höhere Detailerkennbarkeit vermuten lassen. In Übereinstimmung hierzu ließ sich im Patientengut der Lobus pyramidalis in der PET statistisch häufiger erkennen als in der Szintigraphie bzw. SPECT. Obwohl diesem Ergebnis aus nuklearmedizinischer Sicht nur geringe therapeutische Relevanz zukommt, ist es geeignet, die überlegene Bildgüte der PET zu illustrieren.

Im Vergleich zur Schilddrüsenszintigraphie mit $^{99m}TcO_4$ (~ 0,8 mSv) verursacht die ^{124}Iod-PET/CT eine höhere Strahlenexposition (~ 6,8 mSv) *(Dietlein et al. 2007A)*. Allerdings relativiert sich diese Belastung im prätherapeutischen Setting durch die nachfolgende Radiojodbehandlung mit ^{131}Iod in therapeutischer Dosierung.

Zusammenfassend zeigt diese Pilotstudie, dass mit der ^{124}Iod-PET/CT im Vergleich zum konventionellen Procedere keine Befunde übersehen werden, jedoch diagnostisch und therapeutisch relevante Zusatzinformationen gewonnen werden. Darüber hinaus ist ein Potential im Zusammenhang mit der navigierten PET/US-Fusionsbildgebung wahrscheinlich (vgl. 3.3.2.2.).

4.1.2. Prätherapeutische Bestimmung der Iodaufnahme mit ^{124}Iod-PET

Die Ergebnisse dieser Studie wurden im Dezember 2013 in der Zeitschrift JOURNAL OF CLINICAL ENDOCRINOLOGY AND METABOLISM überarbeitet zur erneuten Begutachtung eingereicht (vgl. 3.1.2., S. 26).

Ziel dieser Studie ist der Vergleich der prätherapeutischen Uptakemessung mittels ^{124}Iod-Niedrigaktivitäts-PET/Niedrigdosis-CT (^{124}Iod-PET/CT) mit dem etablierten Verfahren an einem Sondenmessplatz unter Verwendung von ^{131}Iod. Untersucht wurden 24 Patienten mit benignen Schilddrüsenerkrankungen, die im Rahmen der Vorbereitung einer Radiojodtherapie in unserer Abteilung behandelt wurden.

Bei den Patienten, die in die Studie eingeschlossen wurden, erfolgte zunächst die konventionelle Uptakemessung mit ^{131}Iod, die 30h nach Applikation von 3 MBq ^{131}Iod stattfand. Die Messung der thyreoidalen Aufnahme von ^{124}Iod erfolgte 7 Tage später ebenfalls 30h nach Applikation von 1 MBq ^{124}Iod. Beide Isotope wurden in gleicher Galenik oral verabreicht. Die ^{124}Iod-PET/CT-Untersuchung des Halses und des oberen Anteils des Thorax erfolgte nach einem etablierten Protokoll (vgl. 3.1.1.).

Die PET- und CT- Datensätze wurden mit der Software PMOD 3.407 (PMOD Technologies Ltd., Zürich, Schweiz) fusioniert und der Uptake quantifiziert. Hierbei wurden drei unterschiedliche VOI-Techniken angewandt:

- VOI der gesamten Halsweichteile (whole neck, WN)
- VOI-Erstellung mittels Isokontur bei einem Schwellwert von 0,2 kBq/ml (IC)
- VOI-Erstellung durch manuell schichtweise Konturierung der Schilddrüse im CT-Datensatz (manually contoured, MC) (3.1.2., Abb. 1)

Aufgrund der unterschiedlichen physikalischen Halbwertszeiten von ^{124}Iod und ^{131}Iod wurde bei beiden Nukliden eine Zerfallskorrektur der gemessenen Aktivitäten durchgeführt.

Der mittlere korrigierte Uptake nach 30h betrug für die ^{131}Iod-Sonden-Messung 30,7 ± 10,3 % und für ^{124}Iod-PET/CT.WN 31,7 ± 8,9 %, wobei eine hohe signifikante, positive Korrelation bestand (3.1.2., Tab. 2, Abb. 2).

Im Vergleich zu den ^{124}Iod-PET.WN-Daten ergibt die Auswertung des ^{124}Iod-PET.IC basierten Uptakes etwas niedrigere Werte (IC 29,8 ± 8,6 % vs. WN 31,7 ± 8,9 %). Die mit manueller Konturierung (^{124}Iod-PET.MC) ermittelten Uptakewerte zeigen eine deutlich stärker ausgeprägte signifikante systematische Abweichung im Vergleich zu ^{124}Iod-PET.WN von 6,2 % (MC 24,5 ± 7,1 % vs. WN 31,7 ± 8,9 %).

Die vorliegende Arbeit ist nach unserer Kenntnis die erste, die sich dem Vergleich des prätherapeutischen Uptakes von ^{124}Iod und ^{131}Iod bei gutartigen Schilddrüsenerkrankungen widmet.

Im untersuchten Patientengut zeigte sich zwischen den beiden Verfahren eine sehr gute Übereinstimmung sowie eine nur moderate Standardabweichung der prozentualen Iodaufnahme. Für die WN-Methode liegt keine systematische Über- oder Unterschätzung vor, sodass der Ersatz der Uptakebestimmung mit ^{131}Iod an einem Sondenmessplatz durch ^{124}Iod-PET möglich erscheint.

Eine vergleichbare Korrelation wurde auch in einer Arbeit über intratherapeutische Dosimetrie mit simultaner Applikation von ^{124}Iod und ^{131}Iod gefunden *(Eschmann et al. 2002)*.

Beim Vergleich der beiden PET/CT-Konturierungsverfahren (^{124}Iod-PET/CT.IC, ^{124}Iod-PET/CT.MC), die Teilvolumina des gesamten Scanvolumens (^{124}Iod-PET/CT.WN) darstellen, zeigen sich erwartungsgemäß systematisch niedrigere Uptakewerte.

Für das ^{124}Iod-PET/CT.IC Verfahren erlaubt die verwendete Software eine schnelle und effektive schwellwertbasierte Isokonturierung von Speicherstrukturen *(Kemerink et al. 2011)*. Dies ermöglicht in unserer Arbeit eine einfache Trennung zwischen intra- und extrathyreoidaler Aktivität, während bei sondenbasierten Messungen benachbarte Strukturen, wie Halsweichteile und Anteile der Speicheldrüsen zwangsläufig mit gemessen werden. Der Vergleich der PET-Ergebnisse lässt erkennen, dass nach 30h ein geringer extrathyreoidaler Anteil messbar ist.

Mit Blick auf einen kompakten Workflow im Rahmen der Auswertung einer ^{124}Iod-PET/CT-Untersuchung erscheint die simultane Bestimmung des Volumens und der thyreoidalen Iod-Aufnahme innerhalb der MC-VOI eine sinnvolle Kombination. Insbesondere bei stark vergrößerten Organen und/oder einem sonographisch unzugänglichen retrosternalen Anteil ist die Volumenbestimmung mit Hilfe der CT sinnvoll *(Hermans et al. 1997)*. Neben der Volumetrie ermöglicht die CT die sichere und einfache Beurteilung der Nachbarstrukturen, insbesondere der Trachea *(Shin et al. 2011)*. Die manuelle Konturierung der morphologischen Organgrenzen in der CT ermöglicht die exakte Bestimmung des Volumens, ist jedoch mit einem vergleichsweise hohen Zeitaufwand für den Untersucher verbunden *(Hermans et al. 1997, Nygaard et al. 2002)*.

Die vorliegenden Daten lassen jedoch die Integration der Uptakebestimmung in einen Volumetrie-Workflow mittels manueller Konturierung (MC) nicht sinnvoll erscheinen, da es zu einer relevanten systematischen Unterschätzung der thyreoidalen Aktivität um ca. ein Fünftel kommt. Als Ursache hierfür muss angenommen werden, dass es bei der PET-Bildgebung durch den „positron range effect“ regelhaft zu einer „Überstrahlung“ der anatomischen

Organgrenzen kommt. Die anatomisch basierte Konturierung führt folglich zu einer randständigen Beschneidung des PET-Datensatzes und verursacht dadurch die Unterschätzung der Iodaufnahme. Mithin erscheint die ^{124}Iod-PET/CT.MC-Auswertung zwar für eine valide Volumenbestimmung, jedoch nicht für die Erfassung des thyreoidalen Uptakes geeignet.

Für einen Einsatz in der klinischen Routine lässt die ^{124}Iod-PET/CT zur prätherapeutischen Uptakebestimmung gegenüber dem herkömmlichen Workflow mittels ^{131}Iod-Sondenmessung potentielle Vorteile erwarten, die über die Quantifizierung der Iodaufnahme noch hinausgehen:

- keine Abstandsabhängigkeit
- Schwächungskorrektur durch die CT *(Kinahan et al. 1998)*.
- intrinsische morphologische Korrelation zu der CT *(Shah et al. 2006, vgl. 3.1.1.)*
- Option der CT-Volumetrie *(Nygaard et al. 2002)*
- Option der Ultraschallfusionsbildgebung (vgl. 3.3.2.)
- geringere Strahlenexposition (~6,8 mSv inklusive Niedrigdosis-CT) im Vergleich zum Standardradiojodtest mit 3 MBq ^{131}Iod (~33 mSv) *(Berman et al. 1975)*

Zugleich ergeben sich für die Anwendung der ^{124}Iod-PET/CT auch begrenzende Faktoren:

- hohe Anschaffungs- und Betriebskosten für PET/CT-Geräte
- limitierte Verbreitung und Verfügbarkeit von PET/CT-Geräten

Die präsentierte Studie weist Limitationen auf, wobei insbesondere die geringe Patientenzahl im Rahmen der Pilotstudie sowie der fehlende Vergleich zur intratherapeutischen Dosimetrie zu nennen sind. Darüber sind durch die einzeitige Messung keine Aussagen zur Radiojodkinetik möglich.

Zusammenfassend demonstrieren die vorliegenden Daten erstmals die Möglichkeit der prätherapeutischen Uptakemessung bei benignen Schilddrüsenerkrankungen unter Verwendung von 1 MBq ^{124}Iod. Für die Ermittlung eines potentiellen Behandlungsvorteils sind jedoch prospektive Studien an größeren Patientengruppen sowie die subtile Korrelation mit der intratherapeutischen Dosimetrie unerlässlich. Über die Möglichkeit der Bestimmung der Iodaufnahme hinaus lässt die Methode eine Reihe von Vorteilen im Rahmen der funktionstopographischen Diagnostik (vgl. 3.1.1.), der Volumetrie bei schwierigen anatomischen Verhältnissen (vgl. 3.1.3.) sowie der navigierten PET/US-Fusionsbildgebung (vgl. 3.3.2.) vermuten.

4.1.3. Schwellwertbasierte Volumetrie der Schilddrüse mit ^{124}Iod-PET

Diese Studie wurde im Januar 2014 in der Zeitschrift THYROID eingereicht (vgl. 3.1.3., S. 40).

Ziel der vorliegenden Studie ist es, auf der Grundlage der ^{124}Iod-PET/CT einen auf möglichst alle Patienten anwendbaren Algorithmus zu entwickeln, um das Schilddrüsenvolumen zeitsparend zu ermitteln. Hierfür wurde der Zusammenhang zwischen der schwellwertbasierten Isokontur-Volumenbestimmung in der ^{124}Iod-PET und der manuell-konturierten Volumenermittlung im Niedrigdosis-(low-dose-)CT (ldCT) ermittelt und als mathematisches Modell formuliert.

Insgesamt wurden PET- sowie CT-Datensätze von 45 konsekutiven Patienten retrospektiv ausgewertet, die im Rahmen der Planung einer Radiojodtherapie einer benignen Schilddrüsenerkrankung an einer Dosimetriestudie teilnahmen (vgl. 3.1.2). Die Durchführung der ^{124}Iod-PET/CT erfolgte exakt 30 Stunden nach Applikation, wobei die Untersuchungsparameter eines etablierten Protokolls verwandt wurden (vgl. 3.1.1.).

Alle Datensätze wurden mit Hilfe der Software PMOD 3.407 (PMOD Technologies Ltd., Zürich, Schweiz) ausgewertet. Zunächst erfolgte die Volumenbestimmung der Schilddrüse im axial rekonstruierten CT-Datensatz durch schichtweise manuelle Konturierung (MC) eines Volume of Interest (VOI). Zur Reduktion der Intraobservervariabilität wurde die MC-Volumetrie drei Mal an unterschiedlichen Tagen ausgeführt und der Mittelwert der Messungen verwendet. Bei der automatischen Konturierung im PET-Datensatz mittels Isokontur-VOI (IC) wurden zwei empirisch ermittelte Schwellwerte angewandt: 0,2 kBq/ml ($IC_{0.2}$) und 1 kBq/ml ($IC_{1.0}$).

Um hypofunktionelle Areale am Rand der Schilddrüsenspeicherfigur erkennen zu können, wurde besonderes Augenmerk darauf gerichtet, ob es zu einer fehlerhaften Konturierung der IC-VOI kam. Hierfür wurde ein subtiler visueller Vergleich der IC-VOI-Form mit den anatomischen Grenzen der Schilddrüse in der ldCT in der PET/CT-Fusionsdarstellung durchgeführt. Als Ausschlusskriterium wurde eine Abweichung (mismatch) zwischen IC-Kontur und morphologischer CT-Form von mehr als 1,0 cm in mindestens einer der drei Standardebenen (coronar, axial, sagittal) definiert.

Die manuell konturierte Bestimmung des Volumens in der CT (MC) ergab ein Volumen von 65,1 ± 32,4 ml. Die somit ermittelten VOIs enthielten eine mittlere Aktivität von 200,2 ± 69,8 kBq (Tab. 1 in 3.1.3.).

Bei 4 ($IC_{0.2}$) bzw. 13 ($IC_{1.0}$) der Patienten (9 % bzw. 29 %) zeigte sich, dass randständige hypofunktionelle Befunde (Kalk, Zysten, Knoten) von der IC-VOI nicht erfasst wurden, sodass sie von der weiteren Auswertung ausgeschlossen wurden. Mithin erfolgte die IC-Auswertung bei 41 ($IC_{0.2}$) bzw. 32 ($IC_{1.0}$) Patienten. Das mittlere Volumen betrug

122,8 ± 39,0 ml ($IC_{0.2}$) bzw. 64,0 ± 15,64 ml ($IC_{1.0}$), wobei sich ein mittlerer Aktivitätsinhalt von 242,4 ± 69,1 kBq ($IC_{0.2}$) respektive 226,56 ± 117,7 kBq ($IC_{1.0}$) ergab (Tab. 2 in 3.1.3.).

Für die Ergebnisse ($IC_{0.2}$ und $IC_{1.0}$) wurden eine multiple lineare Regression und eine schrittweise Eliminierung von nicht-signifikanten Variablen angewandt. In einem ersten Schritt erfolgte die Einbeziehung zweier unabhängiger Variablen (Volumen und Aktivität der jeweiligen IC) bei Möglichkeit eines variablen Schnittpunktes der Y-Achse. Im Anschluss wurden die Volumendaten regressiv angepasst und jeweils die Variable mit dem niedrigsten Signifikanzniveau eliminiert, bis alle übrigen Variablen signifikant ($p<0,05$) waren.

Die IC-Volumina wurden mathematisch auf der Grundlage der MC-Daten angepasst ($mIC_{0.2}$ und $mIC_{1.0}$) (3.1.3., Abb. 2b/d). Bei der Regressionsanalyse der angepassten mIC-Volumina zeigte sich ein R^2 von 0,93 (MC vs. $mIC_{0.2}$) bzw. von 0,96 (MC vs. $mIC_{1.0}$). Der Median der relativen Abweichungen der modifizierten Volumina vom MC-Volumen betrug 9,0 % (MC vs. $mIC_{0.2}$) bzw. 8,2 % (MC vs. $mIC_{1.0}$).

Die PET ermöglicht die automatische Ermittlung des (metabolischen) Volumens von Organen und krankhaften Befunden unter Verwendung von Schwellwerten (Isokonturverfahren) *(Zhang et al. 2010, Jentzen et al. 2011)*. Die Anwendung dieser Technik im Rahmen von ^{124}Iod-PET-Untersuchungen der Schilddrüse erscheint aufgrund der regelhaft hohen Target-Background-Ratio vielversprechend.

Das angewandte Verfahren der automatischen Konturierung bietet im Vergleich zur manuellen Konturierung den Vorteil einer schnellen Durchführbarkeit in der klinischen Routine *(Crawford et al. 1997)*. In der PET kommt es allerdings regelhaft zu einer unscharfen Darstellung der Speicherkontur. Dieses Phänomen ist bei der Anwendung von ^{124}Iod aufgrund der hohen Energie der emittierten Positronen von 1535 und 2138 keV und der großen Positronenreichweite stark ausgeprägt *(Jentzen et al. 2011)*.

Die vorliegenden Resultate zeigen, dass mit einem Isokonturschwellwert von 1,0 kBq/ml ($IC_{1.0}$) primär eine hohe Übereinstimmung der Volumina mit der Referenz (MC) erzielt werden kann. Allerdings ist die Methode auf 29 % der Patienten nicht anwendbar, weil es durch randständige Minderspeicherungen oder Speicherdefekte zu relevanten Abweichungen der PET-$IC_{1.0}$-Isokontur von der CT-morphologischen Form kommen kann.

Um die Methode auf ein möglichst großes Patientenkollektiv anwenden zu können, wurde zusätzlich ein niedrigerer Schwellwert von 0,2 kBq/ml ($IC_{0.2}$) angewandt, der etwa dem Doppelten der parathyreoidalen Aktivität entsprach. Dies ermöglicht zwar die Einbeziehung von 91 % der Patienten, allerdings werden dadurch regelhaft zu große Volumina ermittelt, sodass eine mathematische Korrektur der Ergebnisse notwendig ist.

Die beiden ermittelten Modelle ($mIC_{0.2}$ und $mIC_{1.0}$) (3.1.3., Abb. 2 b/d) sind für das jeweils repräsentierte Patientenkollektiv mit Abweichungen kleiner 10 % anwendbar. Eine einfache und effiziente Nutzung im klinischen Alltag erscheint mit einer Implementierung in PET Standardsoftware möglich. Insgesamt ist hierfür der Ansatz von $mIC_{0.2}$ durch seine Anwendbarkeit auf >90 % der Patienten sinnvoller.

Bisher beschäftigte sich nur eine Arbeit mit der Thematik der ^{124}Iod-PET-basierten Volumetrie bei benignen Schilddrüsenerkrankungen *(Crawford et al. 1997)*. In dieser Studie wurde mit vergleichsweise hoher ^{124}Iod-Aktivität (15 MBq) ein kleines Patientenkollektiv mit Immunthyreopathie vom Typ Morbus Basedow und im Mittel nur moderater Organvergrößerung (28,1 ml) an einer Koinzidenz-Kamera („Kamera-PET“) untersucht, wobei als Referenzmethode der 2D-Ultraschall verwandt wurde. Übereinstimmend mit der vorliegenden Studie zeigte sich mit einem R^2 von 0,83 eine hohe positive Korrelation. Allerdings ist der direkte Vergleich der Studien aufgrund der Abweichungen der Zusammensetzung des Patientengutes, der angewandten Untersuchungstechnik sowie der Auswertemethodik limitiert.

Die IC-Volumetrie zeigt potentielle Vorteile für eine klinische Anwendung:

- geringer Zeitaufwand: ca. 3 min (unabhängig von der Organgröße)
- geringe Untersucherabhängigkeit durch automatische Volumenermittlung
- moderate Radiopharmakakosten pro Patient bei Anwendung von 1 MBq ^{124}Iod (vgl. 3.1.1.)

Zugleich zeigt die vorgelegte Studie auch Limitationen:

- begrenzte Patientenzahl: Pilotcharakter der Studie
- kein Vergleich zu einem „echten“ Goldstandard (Volumetrie von Operationspräparaten), Ersatz durch dreimalige manuelle Konturierung der ldCT-Daten
- trotz niedrigem Schwellenwert ($IC_{0.2}$) keine Anwendbarkeit auf 9 % der Patienten
- Studien-Ergebnisse an Untersuchungsprotokoll gebunden (applizierte Aktivität, Messzeitpunkt etc.): limitierte Übertragbarkeit auf andere Protokolle

Zusammenfassend lässt sich feststellen, dass die IC-Volumetrie in der PET ein einfach und schnell auf über 90 % der Patienten anwendbares Verfahren der Bestimmung des Schilddrüsenvolumens bei klinisch akzeptablen Abweichungen < 10 % darstellt. Der prätherapeutische Radiojodtest mit ^{124}Iod liefert folglich neben der Dosimetrie, der überlegenen Funktionstopographie, der CT-Korrelation sowie der Option des Fusionsultraschalls auch die Möglichkeit einer zeiteffizienten PET-basierten Organvolumetrie. Allerdings sind die Ergebnisse auf abweichende Test-Protokolle nicht einfach übertragbar. Darüber hinaus sind prospektive Untersuchungen mit höheren Patientenzahlen wünschenswert.

4.2. Dreidimensionaler Ultraschall (3D-US)

4.2.1. DICOM-Export und -Archivierung sowie Nachverarbeitung von 3D-US-Daten

Diese Studie wurde 2012 in der Zeitschrift NUKLEARMEDIZIN publiziert (vgl. 3.2.1., S. 52).

Ziel der Studie ist die Untersuchung des Potentials des DICOM-Standards EUVS (SOP UID 1.2.840.10008.5.1.4.1.1.6.2) hinsichtlich der Erzeugung, des Exports sowie der digitalen Verteilung und Archivierung von 3D-US-Daten der Schilddrüse.

Es wurden 32 konsekutive Patienten untersucht, die wegen einer Erkrankung der Schilddrüse zur Diagnostik überwiesen wurden. Die Patienten erhielten eine 3D-US-Untersuchung der Schilddrüse an einem für die Geburtshilfe optimierten Gerät (GE Voluson E8). Dabei wurde ein mechanisch geschwenkter konvexer 3D-Schallkopf mit einem Öffnungswinkel von 90° x 85° und eine Bandbreite von 2 bis 8 MHz verwendet (Volumensonde RAB4-8-D). Während des automatischen mechanischen Schwenks des Arrays innerhalb des Gehäuses erfolgte die manuelle Fixierung der Sonde. Aus den sequentiell während des Schwenks generierten Einzelbildern wurde der 3D-US-Datensatz erzeugt.

Nach der Erzeugung und dem Export der 3D-US-Daten im EUVS-Standard waren aufgrund der fehlenden Angaben zur Position des Patienten zunächst manuelle Einträge im DICOM-Header mit Hilfe der Software PMOD (Version 3.2.07, PMOD Technologies Ltd., Zürich, Schweiz) und dem Softwarepaket DCMTK - DICOM Toolkit (Version 3.6.0, OFFIS, Oldenburg) notwendig. Darüber hinaus erfolgte die Umwandlung in einen etablierten DICOM-Standard (willkürliche Auswahl des PET-Standards) und die Archivierung im Klinik-PACS. Die Nachverarbeitung wurde auf einer multimodalen Workstation (syngo MultiModality WORKPLACE 2010b, Siemens, Erlangen) ausgeführt.

In allen Fällen waren sowohl die 3D-US-Aufnahme als auch die Erzeugung und der Export des EUVS-DICOM-Standards erfolgreich durchführbar. Nach der Eintragung der Patientenorientierung in den DICOM-Header konnten die Daten in korrekter Orientierung auf den in unserer Klinik verfügbaren Workstations und mit webbrowser-basierten PACS Viewern betrachtet werden. Die Bildqualität war aufgrund der konvexen Geometrie der 3D-US-Sonde und der Optimierung für geburtshilfliche Fragestellungen tendenziell schlechter als mit einer 7,5-MHz-Linearsonde. Bei 24 von 32 (75 %) Patienten konnte das gesamte Organ mit einem 3D-US-Scan vollständig aufgezeichnet werden. Bei 8 von 32 (25 %) wurde die Schilddrüse mit der 3D-US-Sonde inkomplett erfasst.

In den letzten Jahren ist es zu bedeutenden technischen Fortschritten auf dem Gebiet des 3D-US gekommen *(Prager et al. 2010)*. In der vorliegenden Studie wurde mit einer Volumensonde die am weitesten verbreitete 3D-US-Technologie verwendet.

Die Archivierung in digitalen Praxis- oder Klinikarchiven sowie die Nachbetrachtung und Nachverarbeitung kompletter Untersuchungsvolumina ist klinischer Standard in der CT-, MRT-, PET- und SPECT- Diagnostik. Voraussetzung hierfür ist ein ubiquitär verfügbarer und kompatibler DICOM-Standard.

Der DICOM-Standard EUVS für 3D-US-Daten ist erst vor einigen Jahren vorgestellt worden *(National Electrical Manufacturers Association 2008)*, hat allerdings bisher auf Ultraschallgeräten und diagnostischen Workstations nur geringe Verbreitung gefunden. Aus diesem Grund wurde in der vorliegenden Studie ein für die Geburtshilfe optimiertes Ultraschallgerät verwendet, auf dem der EUVS bereits implementiert ist.

Die Aufnahme von 3D-US-Daten der Schilddrüse sowie deren Export, digitale Verteilung und Archivierung haben sich als anwendbar und durchführbar erwiesen. Hierdurch wird die Umsetzung für die klinische Routine vielversprechender Aspekte möglich:

- Nachbefundung (second reading) zu jeder Zeit ohne die Präsenz des Patienten
- multiplanare Rekonstruktionen mit frei wählbarer Orientierung und Schichtdicke (3.2.1., Abb. 2/3)
- nachträgliche Messungen von Distanzen und Volumina (3.2.1., Abb. 4)
- softwarebasierte Bildfusion mit Daten anderer Schnittbildverfahren (3.2.1., Abb. 5)

Neben dem Potential haben sich bei den Untersuchungen bedeutende Limitationen gezeigt:

- Begrenzung des Scanbereiches durch den Öffnungswinkel der Ultraschallsonde
- beschränkte Bildqualität
- mangelnde Verfügbarkeit von 3D-US-Sonden, die sowohl eine hohe Bildqualität (hoher Frequenzbereich) als auch eine hohe Volumenabdeckung realisieren
- Notwendigkeit der Ergänzung von Daten über die Patientenposition im DICOM Header
- begrenzte Verbreitung/mangelnde Implementierung des EUSV: Umwandlung in gebräuchliches DICOM-Format notwendig
- eingeschränkter Zugang zu retrosternalen Schilddrüsenanteilen

Zusammenfassend lässt sich feststellen, dass der neue DICOM-Standard EUVS Generierung, Export, Verteilung und Archivierung von 3D-US-Daten der Schilddrüse erlaubt. Ungeachtet bedeutender Limitationen hat sich das Verfahren als anwendbar erwiesen. Die Anwendung des EUSV scheint geeignet, die Modalität Ultraschall gegenüber anderen tomographischen Verfahren wie CT, MRT, SPECT und PET aufzuwerten *(Elliott 2008)*.

4.2.1. Volumetrie mit 3D-Ultraschall (3D-US)

4.2.1.1. Untersuchungen zur Volumenbestimmung am Schilddrüsenphantom

Die Ergebnisse dieser Studie wurden im Dezember 2013 in der Zeitschrift ULTRASOUND IN MEDICINE AND BIOLOGY überarbeitet neu eingereicht (vgl. 3.2.2.1., S. 60).

Ziel der vorliegenden Phantom-Studie ist es, anhand von 2D-US, zwei unterschiedlichen 3D-US sowie CT- und MR-Scans (i) die Genauigkeit der auf dem Ellipsoidmodell (em) basierenden Volumenberechnung im Vergleich zur manuellen Konturierung (manual tracing, mt) zu untersuchen. Dabei sollte (ii) der Einfluss der Schilddrüsenform auf die Ergebnisse ermittelt sowie (iii) die zwei 3D-US-Verfahren verglichen werden.

Dazu wurden annähernd schilddrüsenförmige, US-, CT- und MRT-kompatible Phantome in 18 Volumenabstufungen von 10 bis 200 ml mit Hilfe flüssigkeitsgefüllter Luftballons hergestellt, wobei der Isthmus durch eine Einschnürung mit einem Kabelbinder simuliert wurde (3.2.2.1, Abb. 1a). Nach Abschluss des ersten Messzyklus wurden die Seitenlappen der Modelle mit je einem weiteren Kabelbinder deformiert (3.2.2.1, Abb. 1b). In einem dritten Untersuchungsdurchgang erfolgte die Entfernung aller Kabelbinder, sodass sich ein modellhaft verdickter Isthmus ergab (3.2.2.1, Abb. 1).

Für die sonographischen Verfahren wurden zwei unterschiedliche Geräte verwendet. Der mechanische 3D-US (mechanically swept, 3D-ms-US) erfolgte mit dem Modell Voluson E8 unter Verwendung der RAB6-D-Konvex-Volumensonde mit 6 MHz (GE Medical Systems, Zipf, Österreich). Der konventionelle 2D-US und der sensornavigierte 3D-US (3D-sn-US) wurden bei einer Frequenz von 11 MHz mit Linear-Sonde ML6-15 am Modell Logiq E9 (GE Medical Systems, Milwaukee, USA) durchgeführt. Die DICOM-Einträge zur räumlichen Orientierung der 3D-Ultraschalldaten wurden ergänzt (vgl. 3.2.1.). Der CT-Scan erfolgte mit einem Biograph mCT 40 in low dose-Technik (120 kV, 50 mAs), der MRT-Scan an einem Magnetom Avanto MR B 17 in T1-Wichtung (beide Geräte: Siemens, Erlangen, Deutschland). Mit allen Verfahren wurden Schichtdicken von 3 mm erzeugt.

Die Daten aller 5 Bildgebungstechniken wurden mittels em-Methode ($Länge_{max}$ x $Breite_{max}$ x $Höhe_{max}$ x 0,5) ausgewertet. Darüber hinaus wurden die 4 Volumendatensätze mittels mt-Volumetrie auf einer multimodalen Workstation (syngo MultiModality WORKPLACE 2010a, Siemens, Erlangen, Deutschland) mit 3D-Routine-Software für Schnittbilddaten vermessen (syngoMMWP Version VE40A, CT-Tool VA31A_SP3.5_P17, Siemens, Erlangen, Deutschland).

Nach der Berechnung der Pearson-Korrelationskoeffizienten zwischen den bestimmten und den realen Volumina wurde die Über- bzw. Unterschätzung des Referenzvolumens mit Hilfe der Limits of Agreement nach Bland und Altman beurteilt *(Bland et Altmann 1986).*

Je nach Größe des Phantoms betrug in der vorliegenden Arbeit der Zeitaufwand für eine mt-Messung 10 - 15 min, wohingegen bei der em-Volumetrie mit 2 - 4 min pro Messung ein wesentlich geringerer zeitlicher Aufwand erforderlich war.

Bei der em-Auswertung bestand ein Trend zur Überschätzung des tatsächlichen Volumens. Vor allem bei den sonographischen Verfahren lag eine signifikante systematische Überschätzung vor. Darüber hinaus traten hohe Standardabweichungen auf. Durch die Verformung des Schilddrüsenphantoms kam es zu einer Zunahme der signifikanten, systematischen Überschätzung der realen Volumina und einer moderaten Vergrößerung der Standardabweichungen.

Die mt-Auswertungen hingegen zeigten für alle Scanverfahren eine deutlich stärkere Übereinstimmung des Mittelwertes zur Referenz sowie eine kleinere Standardabweichung im Vergleich zu den korrespondierenden em-Volumetrie-Ergebnissen. Durch die Verformung der Schilddrüsenphantome kam es bei Anwendung der mt-Methode nur zu sehr geringen Änderungen der Mittelwerte und Standardabweichungen. Darüber hinaus waren (bei fast allen Untersuchungen) weder eine Über- noch eine Unterschätzung feststellbar. Die Überschätzung, die beim 3D-ms-US des normal geformten Phantoms auftrat, respektive die Unterschätzung der MRT beim Modell mit verdicktem Isthmus, waren mit 1,1 % bzw. 0,6 % sehr gering.

Um eine besonders genaue Referenz zu gewährleisten (Goldstandard), wurde in der vorliegenden Arbeit der Ansatz einer Phantomstudie gewählt. Durch das Wiegen der Phantome am Anfang und am Ende der Studie waren einerseits die Ermittlung des Netto-Gewichtes, respektive -volumens und andererseits die Überprüfung der Dichtigkeit möglich. Von anderen Autoren wurden Operationspräparate als Referenz genutzt *(Lyshchik et al. 2004, Hermans et al. 1997)*. Limitierend bei dieser Verfahrensweise ist, dass das Gewebe bei einem chirurgischen Eingriff in der Regel nicht vollständig entfernt wird und sich möglicherweise die Blutfülle sowie der Flüssigkeitsgehalt und damit das Volumen durch die Ligatur von Blutgefäßen und die mechanische Alteration im Rahmen der Operation ändern *(Hermans et al. 1997)*.

In der präsentierten Studie wird ein einfaches Konzept zum Bau preiswerter, multimodal kompatibler (US, CT und MRT) und hinsichtlich der Form einfach modifizierbarer Phantome entwickelt und angewandt. Von anderen Autoren wurden Phantome für nur ein bestimmtes bildgebendes Verfahren ausgelegt, z.B. für den Ultraschall *(Kot et al. 2009, Schlögl et al. 2001, Ng et al. 2004, Riccabona et al. 1996, Pang et al. 2006, Schlögl et al. 2006)* oder für die CT *(Shu et al. 2011)*.

Die konventionelle 2D-Sonografie zeigt unter der Verwendung des em-Modells eine große Abweichung vom realen Volumen, insbesondere bei den deformierten Schilddrüsen-

phantomen. Dabei wurde das reale Volumen in Analogie zu anderen Studien *(Brunn et al. 1981, Andermann et al. 2007)* überschätzt. Andere Veröffentlichungen fanden hingegen bei der Anwendung des 2D-US eine Unterschätzung des tatsächlichen Volumens *(van Isselt et al. 2003, Reinartz et al.2002, Knudsen et al. 1999, Nygaard et al. 2002)***.** Die Daten zeigen weiterhin, dass bei der Kalkulation mit der em-Methode die Abweichungen der Volumina bei Verformung der Seitenlappen oder Verdickung des Isthmus in der Regel größer sind als bei normal geformten Schilddrüsenphantomen. Auch dieses Ergebnis bestätigt die Resultate vorangegangener Studien *(Rago et al. 2006, Riccabona et al. 1996)*.

Alle Volumendatensätze (3D-ms-US, 3D-sn-US, CT und MRT) zeigen bei der Volumetrie mittels mt-Methode signifikant kleinere Abweichungen vom realen Volumen als bei der Ermittlung mittels em-Methode. In Übereinstimmung mit anderen Autoren *(Riccabona et al. 1996)* konnte erneut demonstriert werden, dass die mt-Methode auch bei Verformungen der Schilddrüsenphantome eine hohe Genauigkeit aufweist. Erstmals wurde dies allerdings für 4 verschiedene bildgebende Verfahren gezeigt (3.2.2.1., Tab. 2). Die vorliegende Studie lässt beide 3D-US-Verfahren (3D-ms-US, 3D-sn-US) als mögliche Alternativen zur mt-Volumenbestimmung mit CT oder MR erscheinen, was die Ergebnisse anderer Autoren bestätigt *(Kot et al. 2009)*.

Die angewandte mt-Methode hat jedoch potentielle Limitationen:

- hoher Auswerte-Zeitbedarf der mt-Methode im Vergleich zur em-Volumetrie im 2D-US
- mangelnder Zugang zu retrosternalen Strumaanteilen im Vergleich zu CT und MRT
- nicht ausgereifte technische Voraussetzungen
    - 3D-US-Export/-Modifizierung noch aufwendig
    - Auswertung an Routinesoftware für Auswertung von Schnittdaten gebunden (Ultraschallabteilungen begrenzt verfügbar)

Zusammenfassend zeigt die Untersuchung anhand multimodal kompatibler Schilddrüsenphantome die Vorteile des 3D-Ultraschalls bei der Volumenbestimmung, insbesondere bei Nutzung der mt-Methode. Die Vorzüge im Vergleich zur em-Methode kommen sowohl bei normal geformten Schilddrüsenphantomen, insbesondere jedoch bei abnormer Gestalt zum Tragen. Erstmals wird die weitgehende Gleichwertigkeit von CT, MR und den beiden 3D-US-Verfahren anhand von Phantomen demonstriert. Die Auswertung mit einer Standard-Workstation für Schnittbildgebung und Routinesoftware ist unproblematisch möglich. Allerdings sind derzeit noch Anpassungen der 3D-US-Datensätze notwendig, um Lesbarkeit und Auswertbarkeit zu realisieren. Die Überprüfung der Daten im Rahmen einer in-vivo-Studie ist geplant.

4.2.2.2. Klinische Untersuchungen zur Schilddrüsenvolumetrie - 3D-US versus ldCT

Diese Studie wurde in der Zeitschrift NUKLEARMEDIZIN publiziert (vgl. 3.2.3., S. 75).

Ziel dieser Studie ist der Vergleich zwischen dreidimensionalem mechanisch-geschwenktem Ultraschall mit einer sogenannten Volumensonde (3D-ms-US) und Niedrigdosis-CT (ldCT) hinsichtlich der Übereinstimmung der Ergebnisse der Schilddrüsenvolumetrie.

Bei 30 Patienten, die aufgrund einer gutartigen Schilddrüsenerkrankung eine Radiojodtherapie erhielten, wurden zusätzlich ein 3D-ms-US durchgeführt (Voluson E8, RAB 6-D Konvexsonde, 6 MHz, GE, Austria) (3.2.2.2., Abb. 1). Darüber hinaus erfolgte im Rahmen einer Dosimetriestudie (hier nicht berichtet) ein ldCT (120 kV/50 mAs, Biograph mCT40, Siemens, Deutschland). Einbezogen wurden Patienten, bei denen die Schilddrüse mit 3D-ms-US vollständig erfasst wurde. Die 3D-ms-US-Daten wurden exportiert und nachbearbeitet (vgl. 3.2.1.). Die Auswertungen erfolgten auf einer Workstation mit Standardsoftware für Schnittbildgebung (vgl. 3.2.2.1.). Das Volumen wurde jeweils mit dem Ellipsoidmodell (em, $Länge_{max}$ x $Breite_{max}$ x $Höhe_{max}$ x 0,5) und der manuellen Konturierung der Schilddrüsengrenzen (manually traced, mt) ermittelt. Die statistische Auswertung umfasste die Ermittlung der relativen Differenzen, der Korrelationskoeffizienten, der 95 %-Konfidenzintervalle der Mittelwerte und der Limits of Agreement *(Bland et Altmann 1986)* (vgl. 3.2.1., 3.2.2.1.).

Die Mittelwerte der Volumina betrugen 52,3 ml (3D-ms-US) und 53,4 ml (ldCT) mit der em-Methode sowie 56,5 ml (3D-ms-US) und 57,1 ml (ldCT) mit der mt-Volumetrie. Die Mittelwerte und Mediane waren für die em-Methode tendenziell niedriger als für die mt-Methode (3.2.2.2., Tab. 1). Der Vergleich der Modalitäten ergab eine starke, positive und signifikante Korrelation (em: 0,997; mt: 0,993). Die durchschnittlichen relativen Differenzen zwischen den Volumetriemethoden waren niedrig (em: -1,2 ± 4,0 % [95 % CI 2,62; 0,28]; mt: -1,1 ± 5,2 % [95 % CI 2,93; 0,80]). Die „Limits of Agreement“ zeigten nur eine geringe Abweichung
(em: -9,1 % bis 6,8 %; mt: -11,3 % bis 9,2 %) und es lag keine signifikante Über- oder Unterschätzung vor (3.2.2.2., Tab. 2).

Die vorliegende Studie ist die erste, die 3D-US mit ldCT in der Schilddrüsenvolumetrie direkt vergleicht. Dabei werden sowohl die em- als auch die mt-Methode berücksichtigt.

Eine Reihe von Studien hat sich der Volumetrie mittels 3D-US gewidmet *(z.B. Malago et al. 2008, Riccabona et al. 1996, Schögl et al. 2001)* (3.2.2.2., Tab. 2). Ein bedeutender Vorteil des 3D-US im Vergleich zur 2D-Technik ist, dass sich zusätzlich zur begrenzt genauen em-Methode *(Lyshchik et al. 2004, Ying et al. 2009)* auch die mt-Volumetrie anwenden lässt *(Andermann et al. 2007, Schögl et al. 2001)*.

Die Wertigkeit der CT bei der Bestimmung des Schilddrüsenvolumens wurde in mehreren Arbeiten thematisiert, wobei sie in der Praxis vor allem bei stark vergrößerten und/oder deformierten Schilddrüsen angewandt wird, wenn der 2D-US besonders schlecht einsetzbar ist *(Hermans et al. 1997, Nygaard et al. 2002, Shu et al. 2011)*. Neben der Volumenbestimmung erlaubt die CT die Beurteilung der Beziehung der Schilddrüse zu Nachbarstrukturen wie Trachea und Ösophagus *(Shin et al. 2011)*. Die unvermeidliche Strahlenexposition lässt sich im Rahmen von Niedrigdosis-Protokollen begrenzen und erscheint angesichts der Fülle an Informationen gerechtfertigt.

Es wird eine hohe Übereinstimmung zwischen ermittelten Volumina (3D-ms-US vs. ldCT) sowohl für die em-Methode als auch für die mt-Volumetrie anhand der kleinen relativen Differenzen einerseits und der geringen Spanne der Limits of Agreement andererseits gezeigt. In der klinischen Praxis werden im Rahmen der Radiojodtherapie prozedurale Abweichungen bis 10 % gewöhnlich toleriert, z.B. zwischen kalkulierter und verabreichter Aktivität. In diesem Kontext erscheinen die in der vorliegenden Studie ermittelten Volumenabweichungen akzeptabel klein.

Das Potential des 3D-US in der klinischen Routine liegt darin, dass die höhere Genauigkeit der mt-Volumetrie ohne Strahlenexposition nutzbar gemacht werden kann. Daneben bietet der 3D-US Vorteile hinsichtlich Archivierbarkeit, Nachbefundung und Nachverarbeitung (vgl. 3.2.1.). Aber auch Patienten mit Klaustrophobie, denen eine CT-Untersuchung nicht zugemutet werden kann, könnten profitieren.

Hinsichtlich einer Routineanwendung der Methode existieren relevante Limitationen. Da das erfassbare Volumen durch die Öffnungswinkel der Volumensonde begrenzt ist, können stark vergrößerte Schilddrüsen derzeit nicht vollständig untersucht werden (vgl. 3.2.1.). Außerdem ist die sichere Erfassung potentiell relevanter Nachbarstrukturen (Trachea, Ösophagus) nicht in dem Maße gewährleistet, wie es bei der CT der Fall ist. Technische Entwicklungen sollten die Erfassung möglichst großer Scanvolumina mit hoher räumlicher Auflösung ermöglichen.

Zusammenfassend lässt sich feststellen, dass 3D-ms-US und ldCT bei moderat vergrößerten Schilddrüsen vergleichbare Ergebnisse liefern, unabhängig davon, ob die Ellipsoidformel oder die manuelle Konturierungsmethode angewandt wird. Vorausgesetzt, dass das Organ vollständig abgebildet werden kann, stellt der 3D-ms-US eine potentielle Alternative zur ldCT dar. Der Einsatz einer Standardsoftware für Schnittbildgebung zur Volumenberechnung ist unproblematisch möglich, sodass eine dedizierte 3D-US-Workstation oder eine spezielle 3D-US-Software entbehrlich sind. Allerdings sind die Optimierung von Hard- und Software sowie die ubiquitäre Verbreitung des 3D-US-DICOM-Formats notwendig. Darüber hinaus sind weitere Studien hinsichtlich der Inter- und Intraobservervariabilität sowie der Validierung des 3D-ms-US im Vergleich zu Volumenbestimmungen an Thyreoidektomiepräparaten sinnvoll.

4.3. Nuklearmedizinisch-sonographische Fusionsbildgebung

4.3.1. Softwarebasierte (offline) Fusionsbildgebung

Die Ergebnisse dieser Studie wurden auf der 50. Jahrestagung der Deutschen Gesellschaft für Nuklearmedizin (DGN) in Bremen präsentiert und im Kongressheft der Zeitschrift NUKLEARMEDIZIN publiziert *(vgl. 3.3.1., S. 82).*

Ziel der Studie ist die Überprüfung der Anwendbarkeit der softwarebasierten Bildfusion von mechanisch geschwenktem 3D-US und $^{99m}TcO_4$-SPECT am Beispiel autonomer Adenome der Schilddrüse.

Bei 25 Patienten, die im Rahmen der Planung einer Radiojodtherapie wegen uni-, bi- oder multifokaler Autonomie untersucht wurden, erfolgten zusätzlich zur Standarddiagnostik eine mechanische 3D-US-Untersuchung (vgl. 1.2.; Voluson E8, Volumensonde RAB4-8-D, GE Medical Systems, Zipf, Österreich) und eine SPECT (Symbia E, Siemens, Erlangen, Deutschland) der Schilddrüse. Im Anschluss erfolgte die softwarebasierte Fusion beider Datensätze mit Hilfe einer multimodalen Workstation (syngo MultiModality Workplace 2010B, Siemens, Deutschland). Bei allen Patienten konnten die Datensätze erfolgreich manuell koregistriert und fusioniert werden. Bei 30 von 38 in der SPECT diagnostizierten Adenomen war eine optimale räumliche Übereinstimmung möglich. Lediglich bei 8 Befunden traten leichte räumliche Abweichungen auf, die am ehesten auf die geringe Deformierung des zervikalen Weichgewebes durch den Kontakt zur 3D-US-Sonde zurückzuführen waren. Aufgrund des konvexen Charakters der verwendeten 3D-US-Sonde war die Bildqualität nicht optimal, sodass sich echogleiche und sehr kleine Befunde schwierig abgrenzen ließen.

Die Studie zeigt anhand eines selektierten Patientengutes mit optimalen Voraussetzungen für die SPECT-Bildgebung, dass eine softwarebasierte SPECT/3D-US-Fusionsbildgebung (offline Fusion) mit Hilfe multimodaler Workstations möglich ist. Faktisch stehen in der SPECT - neben den Adenomen selbst - nur die Speicheldrüsen und die Schilddrüsenkontur (bei residualer $^{99m}TcO_4$-Aufnahme in das nicht autonome Gewebe) als Landmarken zur Verfügung. Bei geringem Uptake und/oder nur dezenten Speichermaxima sind erhebliche Unsicherheiten hinsichtlich einer korrekten Koregistrierung zu erwarten. Die Anwendung von SPECT- und ultraschallkompatiblen Markern ist aufgrund der kleinen Kontaktfläche der 3D-US-Volumensonde nicht möglich. Erfolgversprechender wäre das Marker-Konzept bei Anwendung des sensornavigierten 3D-US, da hier großflächige Scans ausgeführt und ausreichend voneinander entfernte Marker einbezogen werden können.

4.3.2. Sensornavigierte nuklearmedizinisch-sonographische Fusionsbildgebung

4.3.2.1. Differentialdiagnose unklarer ^{18}F-FDG-PET/CT-Befunde mit sensornavigierter PET/US-Fusion

Die Arbeit wurde im November 2013 als Pictorial Essay zur Veröffentlichung in der Zeitschrift EUROPEAN JOURNAL OF ULTRASOUND eingereicht (vgl. 3.3.2.1., S. 84).

Ziel dieses Manuskriptes ist es, erste Erfahrungen in der Anwendung der sensornavigierten PET/US-Fusionstechnik (Volume Navigation, Logiq E9, GE, Milwaukee, WI, USA) (vgl. 1.1.) als diagnostische Ergänzung einer ^{18}F-FDG-PET/CT-Untersuchung bei Patienten mit malignem Melanom zu berichten.

Zwei der Kasuistiken (Abb. 2 und 3) beschreiben die sichere Identifizierung von ^{18}F-FDG-positiven Muskelmetastasen im PET/US-Fusionsbild. Bei diesen, in der CT nicht erkennbaren (falsch-negativen) Läsionen fanden sich als Korrelat der PET-Information hochsuspekte, echoarm-inhomogene Ultraschallbefunde. Bei einem dieser Fälle (Abb. 2) war die Überlagerung der Befunde jedoch nicht völlig deckungsgleich (geringe Fehlregistrierung).

In einem dritten Fall (Abb. 4) gelang die sichere Zuordnung von zwei moderaten fokalen ^{18}F-FDG-Anreicherungen zu inguinalen Lymphknoten, die keinerlei sonographische Malignitätszeichen aufwiesen.

Darüber hinaus demonstriert eine vierte Kasuistik (Abb. 5) die funktionstopographische Zuordnung des heterogenen Binnenstoffwechsels innerhalb einer großen Weichteilmetastase. Obwohl sonographisch innerhalb des Gesamtbefundes nicht zu separieren, erwies sich der kaudale Anteil als nahezu stoffwechselfrei (avital), während die kraniale Partition eine ausgeprägte Glukoseaufnahme zeigte.

Die folgenden Kasuistiken wurden 2013 in CLINICAL NUCLEAR MEDICINE, JAPANESE JOURNAL OF CLINICAL ONCOLOGY und NUKLEARMEDIZIN publiziert oder zur Publikation akzeptiert (vgl. 3.3.2.1., S. 84)

Ziel dieser Publikationen ist es, erste Erfahrungen mit der sensornavigierten PET/US-Fusion in der Differentialdiagnose unklarer ^{18}F-FDG-Anreicherungen infolge von eingebrachtem Fremdmaterial zu berichten.

In einem Fall (Clinical Nuclear Medicine 2013) wurde ein Patient wegen Bauchschmerzen, Gewichtsverlust, Nachtschweiß und rezidivierenden Thrombosen stationär behandelt. Die Ergebnisse der klinischen und laborchemischen Untersuchungen sowie der CT, der MRT und endoskopischer Untersuchungen erbrachten keine konklusive Diagnose. Im Aufnahmegespräch hatte der Patient die Frage nach einer chirurgischen Maßnahme verneint. Im Rahmen einer ^{18}F-FDG-PET/CT wurden symmetrische fokale Befunde mit erhöhtem Zuckerstoffwechsel an der ventralen Bauchwand kurz oberhalb der Leistenregion detektiert, die in der CT unscheinbaren ovalen Strukturen entsprachen und zunächst als

pathologisch veränderte Lymphknoten angesehen wurden (Abb. 2B). Ein pathophysiologischer Zusammenhang des PET/CT-Befundes mit den geschilderten Krankheitssymptomen wurde in Erwägung gezogen. Die ergänzende sensornavigierte PET/US-Untersuchung erlaubte die sichere Zuordnung der Befunde zum Eingang des Leistenkanals (Abb. 2C). Nach dem Ausblenden der PET- und der CT-Bildinformation im Hybridbild ließ sich im US eine unscheinbare netzartige Struktur abgrenzen (Abb. 2E). Die erneute gezielte Befragung des Patienten ergab, dass er sich sieben Jahre zuvor einer beidseitigen minimal-invasiven Hernioplastie unterzogen hatte, bei der der Eingang des Leistenkanals mit Hilfe von Netzen aus Polypropylen (Perfix Plug, Davol/Bard, Warwick, RI, USA) verstärkt worden war. Folglich ließ sich der erhöhte Glukosestoffwechsel auf eine chronische Fremdkörperreaktion zurückzuführen.

Zwei weitere Kasuistiken widmen sich einer 71-jährigen Frau mit nichtkleinzelligem Lungenkarzinom (Japanese Journal of Clinical Oncology 2014) und einem 51-jährigen Mann mit lokal fortgeschrittenem papillärem Schilddrüsenkarzinom (pT4a) (Nuklearmedizin 2013). Beide Patienten wurden in kurativer Intention chirurgisch versorgt. Aufgrund eines mikroskopischen Tumorrestes bzw. des primär fortgeschrittenen Stadiums bestand jedoch ein hohes Risiko für das Auftreten eines Tumorrezidivs, sodass im Intervall von einem bzw. zwei Jahren nach der Primärtherapie eine ^{18}F-FDG-PET/CT-Untersuchung erfolgte. Bei beiden Patienten zeigten sich fokale Befunde mit gesteigertem Glukosestoffwechsel ventral des Kehlkopfes, wobei sich in der CT kein morphologisches Korrelat fand, respektive lediglich eine marginale Weichteilverdickung erkennen ließ. Die Befunde wurden als hochgradig verdächtig hinsichtlich des Vorhandenseins von Tumorrezidivgewebe bewertet. In der ergänzend durchgeführten sensornavigierten PET/US-Untersuchung konnten die Befunde jedoch zweifelsfrei gut abgrenzbaren, diffus-echoreichen Strukturen zugeordnet werden, die keinerlei sonographische Malignitätskriterien aufwiesen. Eine erneute subtile Analyse der Krankengeschichte ergab, dass bei beiden Patienten postoperativ eine irreversible Stimmbandlähmung aufgetreten war. Zur Verbesserung des Glottisschlusses und der Vokalisation erfolgte die Injektion von Silikonelastomer (Vox Implant, Bard, Warwick, RI, USA) in die Stimmlippen. Im weiteren Verlauf war es zu einer Migration und prälaryngealen Deposition des eingebrachten Materials mit konsekutiver chronischer Fremdkörperreaktion gekommen.

Die ^{18}F-FDG-PET ist eine etablierte Methode in der onkologischen Bildgebung. Allerdings wird die Spezifität und der positive prädiktive Wert durch falsch-positive Befunde limitiert *(Adejolu et al. 2012)*. Diese werden z.B. durch fokal erhöhten Muskeltonus, Aktivität im braunen Fettgewebe, stoffwechselaktive gutartige Tumore, septische und aseptische Entzündungen, vorangegangene medizinische Interventionen sowie eingebrachtes Fremdmaterial hervorgerufen. Zur Vermeidung falscher Diagnosen kommt - neben der subtilen Recherche

anamnestischer Daten - der korrelierenden Bewertung der PET-Befunde mit morphologisch orientierten Bildgebungsverfahren große Bedeutung zu *(Strauss 1996)*. Naturgemäß erfolgt dies bei PET/CT-Untersuchungen zunächst mit Hilfe der CT *(Beyer et al. 2000)*. Bezüglich der Bewertung kleiner Befunde und von Strukturen mit geringen Absorptionsunterschieden ist die Aussagekraft der CT jedoch limitiert. Gerade in diesen Bereichen liegt die Stärke der Ultraschalldiagnostik. In Fällen, in denen mit PET und CT keine konklusive Bewertung möglich ist, wird in der Klinik für Nuklearmedizin am Universitätsklinikum Jena eine ergänzende sensornavigierte PET/US-Untersuchung durchgeführt.

Bei der bisher üblichen, gezielten sonographischen Nachuntersuchung unklarer PET/CT-Befunde (side-by-side Betrachtung) kann es selbst bei erfahrenen Untersuchern zur versehentlich falschen räumlichen Verknüpfung der Befunde kommen. Die PET/US-Fusionsbildgebung ermöglicht jedoch die zweifelsfreie Korrelation der Methoden. Darüber hinaus ist eine instruktive und plausible Dokumentation der Befunde als Fusionsdarstellung möglich. Diese können ausgedruckt oder digital gespeichert werden. So kann das Verständnis bei fachfremden Ärzten, Ärzten in Weiterbildung und Studenten gefördert werden.

Bisher wurde die sensornavigierte PET/US-Fusion nur im Kontext bildgeführter Interventionen (in der Regel Biopsien) angewandt (vgl. 1.1.). Unsere ersten Erfahrungen zeigen jedoch, dass sie ein erfolgreich anwendbares Verfahren ist, mit dem sich bei unklaren ^{18}F-FDG-PET/CT-Befunden eine eindeutige Zuordnung zwischen PET- und US-Information treffen lässt. Auch wenn eine systematische, prospektive Untersuchung mit angemessenen Patientenzahlen noch aussteht, legen die Fallbeispiele nahe, dass die Methode geeignet ist, diagnostische Unklarheiten der ^{18}F-FDG-PET/CT zu überwinden.

Allerdings bestehen hinsichtlich des Einsatzes in der klinischen Routine Limitationen. Erstens handelt es sich um eine zeitaufwendige Zusatzuntersuchung, deren Durchführung profunde Erfahrung im Ultraschall und in der PET/CT-Bewertung voraussetzt. Zweitens sind unklare ossäre und pulmonale Befunde der Methode nicht zugänglich, sodass klinische Vorteile auf die Untersuchung von Weichteilen und parenchymatöse Organen beschränkt bleiben werden. Drittens können geringe Fehlregistrierungen durch schallkopfbedingte Weichteilverformungen, respektive durch abweichende Lagerung zwischen PET/CT und PET/US sowie Bewegungen des Patienten während der PET/US-Untersuchung hervorgerufen werden.

Bei Patienten mit malignem Melanom ist die genaue Kenntnis der Krankheitsausbreitung für die Festlegung von Therapieentscheidungen von herausragender Bedeutung, da die Identifizierung von Lokalrezidiven und solitärer Metastasen sowie deren gezielte chirurgische Entfernung zu einer Verlängerung des Gesamtüberlebens führen können *(Ollila et al. 1999)*. Die ^{18}F-FDG-PET/CT ist eine etablierte Methode in der bildgebenden Diagnostik bei Hochrisiko-

Patienten mit malignem Melanom *(Freudenberg et al. 2004B, Etchebehere et al. 2010)*. Nicht selten führen jedoch unspezifische ^{18}F-FDG-Anreicherungen zu erheblichen Unsicherheiten in der Bewertung und zu Folgen für das weitere Management *(Keu et Iagaru 2014)*.
Wie die Beispiele der Patienten mit malignem Melanom (Abb. 2 bis 4) zeigen, ist die CT hinsichtlich der Bewertung von Befunden im Muskelgewebe und von Lymphknoten limitiert. Da beim malignen Melanom Muskel- und Lymphknoten-Metastasen häufig auftreten, allerdings fokale Glukosespeicherungen auch durch vermehrte Muskelaktivität und entzündete Lymphknoten auftreten können, erscheint die nähere Charakterisierung mittels sensornavigierter PET/US-Fusion insbesondere bei dieser Erkrankung sinnvoll.
Im Rahmen der Gewinnung von Gewebe für die feingewebliche Untersuchung ist der Ort der Entnahme von großer Bedeutung, insbesondere, wenn Teile des Tumors nekrotisch sind. Obwohl im konkreten Fall keine Biopsie notwendig war, illustriert die vierte Kasuistik (Abb. 5), dass die PET/US Fusion im Kontext der Wahl eines aussichtsreichen Biopsieortes einen wichtigen Beitrag leisten kann, um die Entnahme aus einem avitalen bzw. nekrotischen Bereich zu vermeiden. Besonders interessant ist dieser Aspekt, da Biopsien oft ultraschallgestützt ausgeführt werden.

Fremdmaterial, das im Rahmen medizinischer Eingriffe in den Körper eingebracht wird, stellt eine Herausforderung für die moderne Bildgebung dar und kann auch nach vielen Jahren in situ krankhafte Befunde vortäuschen *(Jung et al. 2011)*. In der ^{18}F-FDG-PET führen z.B. Teflon-Implantate, Fadengranulome, Talkumpleurodesen und Silikon aus Brustimplantaten zu falsch-positiven Befunden *(Hsu et al. 2003, Adejolu et al. 2012)*.
Die geschilderten Fälle zeigen die Schwierigkeiten, die durch Fremdkörper im PET entstehen können exemplarisch am Beispiel von implantiertem Polypropylen-Netz im Rahmen einer Herniotomie und injiziertem Silikonelastomer nach Stimmbandlähmung. Das eingebrachte Fremdmaterial verursacht einen dauerhaften Entzündungsreiz, der mit einem erhöhten Zuckerstoffwechsel einhergeht. Deutlich wird auch, dass Silikonelastomer besonders trügerisch sein kann, da eine Migration möglich ist, sodass ein auffälliger PET-Befund auch entfernt vom Ort der Einbringung auftreten kann. Die sensornavigierte PET/US-Untersuchung half in den geschilderten Fällen, Malignität als Ursache des PET-Befundes auszuschließen. Allerdings unterstreichen die Erfahrungen auch erneut die Notwendigkeit einer subtilen Anamneseerhebung im Vorfeld einer ^{18}F-FDG-PET/CT-Untersuchung.

Zusammenfassend lässt sich feststellen, dass die sensornavigierte PET/US-Fusion eine vielversprechende Methode ist, um in der onkologischen Bildgebung unklare ^{18}F-FDG-PET/CT-Befunde differentialdiagnostisch zu verifizieren bzw. zu falsifizieren. Einerseits können Verdachtsdiagnosen erhärtet, andererseits falsch-positive Befunde vermieden werden. Prospektive Studien sind notwendig.

4.3.2.1. Sensornavigierte PET/US-Fusionsbildgebung bei Schilddrüsenerkrankungen

Die Kasuistiken wurden 2013 in JAPANESE JOURNAL OF CLINICAL ONCOLOGY, JOURNAL OF CLINICAL ENDOCRINOLOGY AND METABOLISM und EUROPEAN JOURNAL OF ULTRASOUND publiziert bzw. zur Publikation akzeptiert (vgl. 3.3.2.2., S. 101).

Ziel dieser Arbeiten ist die Darstellung erster Erfahrungen in der Anwendung der sensornavigierten PET/US-Fusionsbildgebung als Ergänzung zur konventionellen Diagnostik von Schilddrüsenerkrankungen bzw. von extrathyreoidalen Iodspeicherungen.

Die erste Patientin (*JAPANESE JOURNAL OF CLINICAL ONCOLOGY)* wurde zur Zweitbeurteilung vorgestellt, da ein 9 mm großer, echoarmer Schilddrüsenknoten im Ultraschall diagnostiziert worden war. Die in einer anderen Einrichtung vorab durchgeführte $^{99m}TcO_4$-Szintigraphie zeigte eine normale Aktivitätsverteilung ohne fokale Minderspeicherung (Abb. 1). Der basale Calcitioninspiegel allerdings war leicht erhöht, sodass ein medulläres Schilddrüsenkarzinom vermutet wurde. In einer ergänzend durchgeführten ^{124}Iod-PET/CT zeigte sich eine umschriebene fokale Hypofunktionalität. Zum Ausschluss von Fernmetastasen wurde die Patientin einer ergänzenden ^{68}Ga-DOTATOC-PET/CT unterzogen, in der sich eine fokal vermehrte Dichte von Somatostatin-Rezeptoren zeigte. Die sensornavigierte PET/US-Fusionsuntersuchung ermöglichte die Zuordnung sowohl des ^{124}Iod- als auch des ^{68}Ga-DOTATOC-PET-Befundes zum sonographisch diagnostizierten kleinen Schilddrüsenknoten (Abb. 2). Die Verdachtsdiagnose eines medullären Schilddrüsenkarzinoms wurde im Rahmen der sich anschließenden Thyreoidektomie bestätigt.

Bei einer zweiten Patientin (*JOURNAL OF CLINICAL ENDOCRINOLOGY AND METABOLISM)* wurden zur Abklärung eines Karzinoidsyndroms eine ^{68}Ga-DOTATOC- und eine ^{18}F-FDG-PET/CT durchgeführt, bei der sich ein fokaler Befund mit hoher Somatostatinrezeptordichte und gesteigertem Glukosestoffwechsel im linken Schilddrüsenlappen zeigte. Die gezielte Sonographie ergab allerdings zwei eng benachbarte, scharf begrenzte Knoten mit vermehrter Perfusion und Durchmessern von 2,5 cm respektive knapp 1 cm. Der daraufhin bestimmte Calcitonin-Spiegel zeigte sich deutlich erhöht, sodass ein medulläres Schilddrüsenkarzinom vermutet wurde. Ergänzend erfolgte eine ^{124}Iod-PET/CT, bei der sich ein Befund ohne Iodstoffwechsel und ein Areal mit erhöhter Iodaffinität zeigten (Suppl. 1 auf dem beiliegenden Datenträger). Um die Knoten unzweifelhaft zuordnen und charakterisieren zu können, wurde eine sensornavigierte PET/US-Fusionsuntersuchung unter Berücksichtigung aller drei Tracer durchgeführt (vgl. 1.1.). Der größere Knoten zeigte sich glukosestoffwechselaktiv, jodnegativ und somatostatinrezeptorpositiv und wurde mithin als das vermutete medulläre Karzinom suspiziert, während der kleinere Befund aufgrund des erhöhten Iodstoffwechsels, des geringen Glukosemetabolismus und der marginalen

Somatostatinrezeptordichte als kompensiertes Schilddrüsenadenom bewertet wurde. Beide Diagnosen wurden histologisch bestätigt.
Eine dritte Patientin (EUROPEAN JOURNAL OF ULTRASOUND) wurde nach der operativen Versorgung eines papillären Schilddrüsenkarzinoms zur Vorbereitung einer Radiojodtherapie vorgestellt. Im prätherapeutischen ^{123}Iod-Ganzkörperszintigramm fand sich eine fokale Mehranreicherung im Becken paramedian rechts (Abb. 1a). Um deren Ursprung zu identifizieren, wurde eine ergänzende ^{124}Iod-PET/CT durchgeführt, in der sich zwar die jodaffine Struktur dorsal des Uterus lokalisieren, allerdings in der CT keine eindeutige anatomische Struktur abgrenzbar ließ (Abb. 1b). Die anschließend durchgeführte sensornavigierte PET/US-Untersuchung zeigte als Korrelat der vermehrten Iodaufnahme ein sehr kleines echoreiches Areal innerhalb des normal großen und unauffällig geformten rechten Ovars. Da die Patientin eine operative Sicherung abgelehnt hatte, waren die Erkenntnisse von besonderer Relevanz. Die Abwesenheit eines sonographisch erfassbaren Tumors unterstützte die Bewertung als benigne Struma ovarii.

In den geschilderten Fällen war die sichere Zuordnung der PET- und der US-Information sowohl innerhalb der Schilddrüse als auch im Becken problemlos möglich. Aufgrund der überlegenen Abbildungseigenschaften der PET (vgl. 3.1.1.) konnten auch Befunde < 1 cm sicher beurteilt werden, die sich szintigraphisch - wie im Fall der ersten Patientin - dem Nachweis entziehen können. Dies ist insofern klinisch bedeutsam, dass durch die rasante Entwicklung der Ultraschalltechnik in den letzten Jahren immer mehr und immer kleinere Schilddrüsenknoten entdeckt werden *(Hegedüs 2004, Aspinall et al. 2013)*. Zwar wird bei Knoten < 1 cm gewöhnlich keine Szintigraphie durchgeführt, allerdings werden diese häufig als koinzidente Befunde im Rahmen der Bewertung größerer Nodi diagnostiziert und führen zu Interpretationsschwierigkeiten in der Szintigraphie. Zwar ist die klinische Relevanz kleiner Schilddrüsenknoten statistisch betrachtet niedrig *(Jin et McHenry 2012)*, aber die geschilderten Kasuistiken zeigen, dass sie im Einzelfall vorhanden ist.

Dem offenkundigen Potential der Methode stehen begrenzende Faktoren hinsichtlich Zeitaufwand, Registrierungsgenauigkeit und fehlendem Anwendbarkeit des Ultraschalls bei verkalkten, respektive gashaltigen Strukturen gegenüber (vgl. 3.3.2.1.).

Zusammenfassend lässt sich feststellen, dass die sensornavigierte PET/US-Fusion ein anwendbares Verfahren sowohl zur Diagnostik von Schilddrüsenerkrankungen als auch in der Differentialdiagnose extrathyreoidaler Iodspeicherungen ist. Mindestens für zweifelhafte Fälle im Rahmen der konventionellen Diagnostik und bei therapeutischer Relevanz kann die Methode angewandt werden. Prospektive Studien zur Beurteilung des Stellenwertes in der klinischen Routine sind notwendig.

4.3.3. Integrierte Konzepte

4.3.3.1. Integriert sequentielles Konzept

Die Ergebnisse dieser Studie sind in der Zeitschrift RADIOLOGY zur Veröffentlichung akzeptiert (vgl. 3.3.3.1., S. 110).

Ziel dieser Arbeit ist es, erste klinische Erfahrungen hinsichtlich der Durchführbarkeit und Anwendbarkeit eines integrierten hybriden Bildgebungskonzeptes aus fhSPECT und Ultraschall bei Patienten mit Schilddrüsenerkrankungen zu berichten (Proof of Concept).

34 Patienten, die sich einer $^{99m}TcO_4$-Szintigraphie und einer Ultraschalluntersuchung der Schilddrüse unterzogen hatten, erhielten zusätzlich eine fhSPECT-Untersuchung, direkt gefolgt von einer sensornavigierten fhSPECT/US-Fusionsuntersuchung der Schilddrüse.

Für die Studie wurde eine Kombination eines fhSPECT-Systems (declipseSPECT, SurgicEye, München, Deutschland) mit magnetisch sensornavigiertem Ultraschall (Volume Navigation, Logic9, ML6-15 Sonde, GE, Milwaukee, WI, USA) verwendet. Dabei ermöglichte die digitale Verknüpfung von zwei unabhängigen Tracking-Systemen (optisches Tracking für fhSPECT und elektromagnetisches Tracking für Ultraschall) die Koregistrierung der fhSPECT/Ultraschall-Bilder ohne manuelle Koregistrierung mittels anatomischer Landmarken.

Bei der fhSPECT-Untersuchung werden dreidimensionale SPECT-Daten durch optisches Tracking einer handgeführten Gammasonde erzeugt *(Wendler et al. 2007, Wendler et al. 2009, Wiesner et al. 2011)*. Das System besteht erstens aus zwei optischen Sensoren (Polaris Vicra, NDI, Waterloo, Ontario, Canada), von denen einer an der Szintillationssonde (NucleoProbe MR200, NucleoMed, Rom, Italy) und der andere am Patienten befestigt ist, zweitens einer Videokamera, die über dem Patienten platziert wird, um die optischen Marker detektieren zu können, drittens einer Computereinheit für die Datenverarbeitung und viertens einem Monitor zur Visualisierung der Aktivitätsverteilung innerhalb der Untersuchungsregion.

Alle 34 Untersuchungen waren technisch erfolgreich, d.h. es konnte ein fhSPECT-Datensatz erzeugt und im Rahmen der sensornavigierten sonographischen Bildgebung in Echtzeit überlagert werden (3.3.3.1., Abb. 2). Bei 18/34 Untersuchungen zeigte die automatische Koregistrierung und Fusionierung eine sehr gute Übereinstimmung ohne Abweichung. Bei 16/34 fanden sich zwischen fhSPECT und Ultraschall akzeptable Abweichungen, wobei diese keine Richtungspräferenz zeigten. Bei keinem der 34 Patienten war eine inakzeptable Abweichung > 1 cm vorhanden.

In einigen Fällen traten jedoch Artefakte in der fhSPECT auf:

- scheinbare Aktivitätsanreicherung außerhalb der Schilddrüse dorsal des Isthmus (n=13)

- Rekonstruktion von zwei Maxima (rechter und linker Lappen) bei nur einem hyperfunktionellen Knoten in der planaren Szintigraphie (n=1)
- Suboptimale Darstellung kaudaler und dorsaler Organanteile (n=2)

Die vorliegende Studie stellt erstmals ein integriertes Hybridbildgebungskonzept für die Schilddrüsendiagnostik mit SPECT und Ultraschall vor, das eine bettseitige Untersuchung in einer Sitzung und auf der gleichen Untersuchungsliege erlaubt. Es konnte gezeigt werden, dass die räumliche Verknüpfung von metabolischen und morphologischen Informationen sowie deren Darstellung als Fusionsbild technisch machbar und anwendbar sind.

Die technischen Parameter des für die Detektion radioaktiv markierter Wächterlymphknoten optimierten fhSPECT-Systems *(Wendler et al. 2007, Wendler et al. 2009, Wiesner et al. 2011)* ließen ein qualitativ ausreichendes Scanergebnis bei szintigraphischen Grenzbefunden zweifelhaft erscheinen. Deshalb war es nicht das vorrangige Ziel, die klinische Wertigkeit oder gar einen möglichen Einfluss auf die Therapieentscheidung zu überprüfen.

Potentielle Vorteile dieses integrierten Konzeptes im Vergleich zur konventionellen Diagnostik sind:

- überlagerungsfreie Darstellung der Aktivitätsverteilung durch fhSPECT
- bessere räumliche Zuordnung szintigraphischer und sonographischer Befunde im Vergleich zur separaten Befundung (side-by-side)
- Keine zusätzliche Strahlenbelastung

Folgende Limitationen müssen bedacht werden:

- begrenzte Ortsauflösung der fhSPECT, derzeit noch unzureichend zur Beurteilung bzw. Differenzierung kleiner, unmittelbar nebeneinander liegender Befunde
- geringe Fehlregistrierungen durch
    - minimale Patientenbewegungen zwischen fhSPECT-Datenerhebung und Ultraschalluntersuchung, die vom Trackingsystem nicht erfasst werden (z.B. durch inadäquate Positionierung des Sensors, komplexe Körperbewegungen)
    - geringe Verformung des Gewebes durch den Kontakt zur Ultraschallsonde (im Gegensatz zur berührungsfreien Erhebung der fhSPECT Daten)

Zusammenfassend erweist sich das vorgestellte Konzept als einfach und schnell anwendbar sowie als technisch erfolgreich durchführbar. Die metabolischen Informationen der fhSPECT konnten während der Bewegung des Ultraschallkopfes in Echtzeit den sonographischen Bildern überlagert werden. Allerdings zeigen sich in der hier angewandten Systemkonfiguration noch erhebliche technische Limitationen hinsichtlich der SPECT-Qualität und der Genauigkeit der Fusion. Vorbehaltlich einer technischen Optimierung ist jedoch ein sinnvoller Beitrag zur Schilddrüsendiagnostik möglich.

4.3.3.2. Integriert simultanes Konzept

Die Ergebnisse dieser Studie wurden im Januar 2014 in der Zeitschrift RADIOLOGY zur Veröffentlichung eingereicht (vgl. 3.3.3.2., S. 117).

Diese Machbarkeitsstudie (Proof of Concept) verfolgt zwei Ziele:

1. Ein neu entwickelter, kompakter Detektor zur Ortung einer radioaktiven Punktquelle in Echtzeit (real-time handheld Emission Spot Allocator - rthESA) soll mit Hilfe eines Luft- und eines Wasser-Phantoms getestet werden.
2. Die simultane Datenakquisition mit rthESA und US in einem kombinierten hybriden Detektor sowie die Echtzeit-Überlagerung als rthESA/US-Fusionsbild sollen an einem Leberphantom demonstriert werden.

Das rthESA-System besteht aus drei Teilen: dem Detektorarray, einer elektronischen Messeinheit sowie einem PC mit speziell entwickelter Software. Das Detektorarray ist aus fünf kubischen Kadmium-Zink-Tellurid (Cd-Zn-Te) Halbleiterdetektoren aufgebaut, die alternierend räumlich versetzt angeordnet sind (3.3.2.2., Abb. 1). Durch diese Anordnung kann die Tiefen- und Längenposition eine Strahlenquelle in Echtzeit bestimmt werden. Die durch die Gamma-Strahlung erzeugten Messdaten werden durch die elektronische Messeinheit mit der Software analysiert (Marschelke Messtechnik, Reichenau, Deutschland). Die Signalortung erfolgt auf der Grundlage charakteristischer Verhältnisse der Messwerte der Detektoren.

Die Tests im Luft- und Wasserphantom (3.3.2.2., Abb. 2a/b) wurden mit Punktquellen der drei klinisch häufig angewandten Nuklide ^{99m}Tc, ^{131}Iod und ^{18}F durchgeführt, wobei die Visualisierung der georteten Quelle als roter Punkt auf einem Bildschirm erfolgte (3.3.2.2., Abb. 2, Suppl. 1 auf beiliegender CD). Für das Leberphantom wurde eine ultraschallkompatible Kapsel (5 mm Durchmesser) mit 1 MBq $^{99m}TcO_4$ in eine Rinderleber eingebracht (3.3.2.2., Abb. 3).

Der Einbau des rthESA-Detektors und einer kompakten, für den intraoperativen Gebrauch optimierten US-Sonde erfolgte hintereinander in ein Plexiglasgehäuse im Sinne eines Hybriddetektors (3.3.2.2., Abb. 3 und 4). Für die Darstellung als Fusionsbild wurden rthESA- und US-Informationen mittels eines Framegrabbers (DFG/USB2pro, TheImagingSource, Bremen, Deutschland) (3.3.2.2., Abb. 4) auf einem PC zusammengeführt und die Bildüberlagerung mit Hilfe einer Software realisiert (Suppl. 4 auf beiliegender CD). Eine einmalige initiale Kallibierung war notwendig, um die räumliche Integrität der beiden Modalitäten zu garantieren.

Für jedes der untersuchten Radionuklide ^{99m}Tc, ^{131}Iod und ^{18}F war die exakte Lokalisierung der Punktquellen sowohl im Luft- als auch im Wasserphantom möglich (Suppl. 1 auf beiliegender CD). Die initiale Anzeige durch das rthESA-System erfolgte bei detektornaher Platzierung signifikant schneller als bei detektorferner Positionierung der Punktquelle (3.3.2.2., Tab. 1).

Im Leberphantom war die simultane Datenakquisition mit dem rthESA/US-Hybriddetektor erfolgreich durchführbar. Wenn sich die Quelle im Messfeld des Hybriddetektors befand, war die Anzeige des Spots im rthESA/US-Fusionsbild räumlich übereinstimmend (3.3.2.2., Abb. 3). Beim ersten Aufsuchen trat eine kürzere Latenz bis zur korrekten Anzeige auf (Suppl. 2 auf beiliegender CD) als bei einer Verschiebung des Schallkopfes und einer Nachverfolgung der Quelle (Suppl. 3 auf beiliegender CD).

Alle bisher bekannten Studien zur sonographisch-nuklearmedizinischen Fusionsbildgebung wurden sequentiell durchgeführt *(Bucki et al. 2007, Galdames et al. 2011, Ewertsen 2010, Ewertsen et al. 2011, Venkatesan et al. 2011, Di Mauro et al. 2013, Futamura et al. 2013)*. Fehl-registrierungen können hierbei insbesondere durch die schallkopfbedingte Gewebeverformung sowie durch die abweichende Lagerung respektive Patientenbewegung auftreten. Die simultane Akquisition beider Informationen in Echtzeit mit einem handgehaltenen, integrierten Detektor wäre geeignet, diese Limitationen zu überwinden. Um eine simultane Fusionsbildgebung zu ermöglichen ist es notwendig, die Aktivitätsverteilung (nahezu) in Echtzeit in der Ebene des Ultraschallbildes zu messen und darzustellen. Eine besondere Herausforderung stellt dabei die Bestimmung der Tiefe (Entfernung vom Detektor) einer radioaktiven Quelle dar. Bisher publizierte Arbeiten mit einer kompakten Gammakamera und simultaner Bildanzeige messen die eintreffende Strahlung in einer Ebene, d.h. es werden lediglich die Längen- und Breitenposition berücksichtigt *(Abe et al. 2003)*. Bei den etablierten emissionstomographischen Techniken werden Rohdaten aus mehreren Richtungen (in der Regel 360°) aufgezeichnet und erst zeitlich versetzt rekonstruiert, was eine simultane Bildgebung unmöglich macht.

Diese phantombasierte Machbarkeitsstudie zeigt, dass durch die räumlich versetzt angeordneten Einzeldetektoren im Array des rthESA-Detektors die korrekte Lokalisierung und Visualisierung einer radioaktiven Quelle möglich ist. Da für ^{99m}Tc, ^{131}Iod und ^{18}F kein Hardware-Kollimator notwendig war, besteht offenbar keine relevante Abhängigkeit vom Energiebereich.

Die Integration des kompakten und mobilen rthESA und einer US-Sonde in einem gemeinsamen Gehäuse im Sinne eines Hybriddetektors ermöglicht die simultane Erzeugung des Ultraschallbildes und die Ortung der radioaktiven Quelle in einer Ebene des Lebergewebes sowie die halbtransparente Überlagerung beider Bildinformationen (Suppl. 4 auf beiliegender CD).

Die vorliegende Studie zeigt Vorteile des Konzeptes:

- simultane Akquisition (im Gegensatz zu den meisten etablierten Hybridgeräten)
- Ortung und Visualisierung (nahezu) in Echtzeit
- räumliche Zuordnung ohne Scan aus verschiedenen Raumrichtungen

- Hardwareintegration des Detektors
    - kein Tracking-System (Sensornavigation) erforderlich
    - Akquisition beider Informationen in *einer* Ebene
- Reduktion von Fehlregistrierungen
    - Verformung des Gewebes beeinflusst beide Modalitäten gleichsinnig
    - Kein Einfluss von Patientenbewegungen, da simultane Akquisition
- Kompatibilität ohne Hardware-Kollimation
    - mit gebräuchlichen Nukliden: ^{99m}Tc, ^{131}Iod, ^{18}F
    - großes Energiespektrum (Niedrig- bis Hochenergie)

Die Studie zeigt jedoch auch noch profunde Limitationen:

- Visualisierung lediglich *eines* Fokus, keine Darstellbarkeit einer Aktivitätsverteilung
- Untersuchungen ohne Hintergrundaktivität, keine Übertragbarkeit der Ergebnisse auf komplexe Aktivitätsverteilungen
- Trägheit des rthESA
    - relative schnelle initiale Ortung der Quelle
    - bei Positionsänderung des Detektors relative langsame “Verfolgung” (Tracing) (Suppl. 1 und 3 auf beiliegender CD)

Zusammenfassend zeigt diese Machbarkeitsstudie, dass eine simultane nuklearmedizinisch-sonographische Fusionsbildgebung praktikabel ist. Der rthESA-Detektor ermöglicht (i) die exakte Lokalisierung einer radioaktiven Quelle in einer Schicht, wobei insbesondere die sichere Darstellung der Entfernung vom Detektor (Tiefe) hervorzuheben ist, und die (ii) simultane Überlagerung mit dem Ultraschallbild. Es bestehen technische Limitationen, die eine Weiterentwicklung für den klinischen Einsatz unabdingbar machen.

5. Zusammenfassung und Ausblick

Die Entwicklung und Erforschung neuer Methoden und Technologien für die medizinische Diagnostik ist insbesondere in Bereichen von Bedeutung, in denen objektive Limitationen mit klinischer Relevanz bestehen. Auch in der etablierten Schilddrüsenbildgebung existieren trotz des bereits hohen Standards begrenzende Faktoren. Methodische und technische Neuerungen erscheinen mithin sinnvoll und geboten.

Die vorliegende Habilitationsschrift stellt die Entwicklung und Erprobung neuer Konzepte der Schilddrüsendiagnostik in drei Teilgebieten vor, wobei verschiedene Limitationen (vgl. 1.3.) adressiert können werden (siehe Übersicht auf S. 160).

- In den Arbeiten über die ^{124}Iod-Niedrigaktivitäts-PET/Niedrigdosis-CT konnten verschiedene neue positive Aspekte für die Schilddrüsendiagnostik aufgezeigt werden. Durch diese Untersuchungstechnik wird (i) die Ortsauflösung der herkömmlichen Szintigraphie übertroffen und konsekutiv die Detektierbarkeit kleinerer Strukturen sowie anatomischer Details verbessert. Durch den parallel akquirierten CT-Datensatz können (ii) sinnvolle zusätzliche Erkenntnisse zur Größe und Morphologie der Schilddrüse sowie deren Beziehung zu Nachbarorganen gewonnen werden. Darüber hinaus sind (iii) im Rahmen der Vorbereitung von Radiojodtherapien prätherapeutische Uptake-Messungen möglich, wobei (iv) zwischen dem intrathyreoidalen und extrathyreoidalen Anteil unterschieden werden kann. Durch das isokonturbasierte PET-Volumetrieverfahren kann (v) eine einfache, schnelle und weitgehend untersucherunabhängige Bestimmung des Schilddrüsenvolumens erfolgen. Die gewonnenen PET/CT-Bilder sind (vi) in besonderer Weise für die Nutzung im Rahmen der navigierten PET/US-Fusionsbildgebung geeignet. Die radiopharmakonbedingten Kosten pro Patient können aufgrund der geringen verabreichten Aktivität bei entsprechender Planung im Vergleich zu etablierten PET-Tracern vergleichsweise moderat gestaltet werden. Limitierend für eine Einführung in die Routinediagnostik wirken die höhere Strahlenexposition (6-fach vs. $^{99m}TcO_4$-Szintigraphie), das lange Zeitintervall zwischen Applikation und Scan und die begrenzte Verfügbarkeit von PET/CT-Geräten.
- Auch in den Arbeiten über die 3D-Sonographie wurde das Potential für die Verbesserung der Schilddrüsendiagnostik demonstriert. Mit Hilfe des neuen DICOM-Standards EUSV ist (i) ein einfacher Datenexport in einem kompatiblen Format und (ii) die Speicherung im Praxis- oder Klinik-Bildarchiv möglich, über das die Daten (iii) auf jeder mit dem PACS vernetzten Workstation einer Einrichtung betrachtet und nachverarbeitet werden können. Der 3D-US ermöglicht (iv), sofern das Organ vollständig dem Ultraschall zugänglich ist, den lückenlosen Scan der Schilddrüse und

Gebiet	Limitation	betroffene Modalität	Teilaspekte	Lösungen bzw. Lösungsansätze	Kapitel	kommerziell verfügbar
Informations-technologie	**Lückenhafte Dokumentation / mangelnde Archivierbarkeit des vollständigen Untersuchungs-volumens**	Sonographie	Archivierung in Praxis- oder Klinik-PACS	DICOM-Standard EUSV	3.2.1. 3.2.2. 3.2.3. 3.3.1.	Ja
			Verfügbarkeit in medizinischen Netzwerken			
			Nachbefundung (Second Reading)	3D-US DICOM-Standard EUSV		Ja
			Nachverarbeitung (z.B. Volumetrie, offline Fusion)			
Bildgebung			lückenloser Scan des kompletten Organs	3D-US		Ja
	Ortsauflösung	Szintigraphie	Knotendetektion Darstellung anatomischer Details	^{124}Jod-PET	3.1.1.	Ja
	Retrosternales / intra-thorakales Gewebe	Sonographie Szintigraphie	Totalreflexion / Auslöschung begrenzte Penetration des Sternum (Absorption)	Niedrigdosis-CT ^{124}Jod-PET/CT		Ja
	Kalk- oder gashaltige Nachbarstrukturen	Sonographie Szintigraphie	Totalreflexion / Auslöschung / Bildartefakte Absorption			
	Korrelation zwischen Anatomie und Funktion	Sonographie Szintigraphie	intrathyreoidal	^{99m}Tc-SPECT/US-Fusion (offline) ^{124}Jod-PET/US-Fusion (sensornavigiert) ^{99m}Tc-fhSPECT/US-Fusion rthESA/US-Fusion	3.3.1. 3.3.2.2. 3.3.3.1. 3.3.3.2.	Ja Ja Nein Nein
			zwischen Schilddrüse und Nachbarorganen	^{124}Jod-PET/CT ^{124}Jod-PET/US-Fusion	3.1.1. 3.3.2.2.	Ja
			Integration von nuklearmedizinischer und sonographischer Modalität	^{99m}Tc-fhSPECT/US-Fusion rthESA/US-Fusion	3.3.3.1 3.3.3.2	Nein Nein
			Fehlregistrierung bei Bildfusion durch: - sequentielle (nicht simultane) Bilderzeugung - abweichende Lagerung - Patientenbewegung - Weichteildeformierung durch die US-Sonde	rthESA/US-Fusion	3.3.3.2	Nein
			Präsentation als überlagertes Fusionsbild	^{99m}Tc-SPECT/US-Fusion (offline) ^{124}Jod-PET/US-Fusion (navigiert) ^{99m}Tc-fhSPECT/US-Fusion ^{99m}Tc-/ ^{131}Jod-/ ^{18}F-rthESA/US-Fusion	3.3.1. 3.3.2.2. 3.3.3.1. 3.3.3.2.	Ja Ja Nein Nein
Quantifizierung	**Uptakemessung Dosimetrie**	Kamera- oder Sondenmessungen	Einbeziehung retrostrenaler Anteile, Integration in bildgebendes Verfahren	^{124}Jod-PET/CT	3.1.2.	Ja
	Volumetrie	Sonographie	Ungenauigkeit des etablierten Ellipsoid-Modells bei Formabweichungen der Schilddrüse	manuelle Konturierung (CT oder 3D-US) ^{124}Jod-PET-Isokontur-Volumetrie	3.2.2. 3.1.3.	Ja
			Zeitbedarf	^{124}Jod-PET-Isokontur-Volumetrie	3.1.3.	Ja
			Observervariabilität			

Übersicht der Limitationen der konventionellen Schilddrüsendiagnostik, der Lösungen bzw. Lösungsansätze und der korrespondierenden Kapitel

(v) die vollständige digitale Archivierung des Untersuchungsvolumens als Schichtstapel im PACS. Dadurch ergeben sich auf üblichen Schnittbildworkstations die Vorteile (vi) des Second Readings, (vii) des Side-by-Side-Vergleichs mit vorangegangenen 3D-US-Studien und anderen Schnittbildverfahren. Darüber hinaus kann (viii) eine nachträgliche Datenverarbeitung (Processing) erfolgen, z.B. zur Bestimmung von Distanzen, zur Volumetrie unter Einbeziehung von Konturierungsverfahren sowie (ix) zur softwarebasierten Bildfusion. Hinsichtlich der Volumetrie konnte (x) die Gleichwertigkeit des 3D-US zu anderen Schnittbildverfahren und (xi) die Überlegenheit der manuell-konturierten Volumetrie gegenüber dem Ellipsoid-Modell am Phantom nachgewiesen werden. Limitierend wirken der derzeit noch geringe Verbreitungsgrad des EUSV-DICOM-Standards, die Notwendigkeit ergänzender Eintragungen im DICOM-Header der exportierten Datensätze, die begrenzte Bildqualität und/oder die begrenzte Größe des erfassbaren Volumens. Darüber hinaus ist die DICOM-Export-Option für Volumendaten nach unserer Kenntnis derzeit nur für die mechanisch-geschwenkten 3D-US-Volumen-Sonden und nicht für die anderen 3D-US-Verfahren verfügbar.

- Die Entwicklungen und Untersuchungen zur Einbeziehung des Ultraschalls in das Konzept der Fusions- bzw. Hybridbildgebung haben gezeigt, dass die räumliche Verknüpfung und bildliche Überlagerung der morphologisch-sonographischen Informationen mit den nuklearmedizinisch-funktionellen Bilddaten mit verschiedenen technischen Lösungen möglich ist.
- Es konnte die sequentielle, dreistufige Herangehensweise der softwarebasierten (offline) Fusion mit SPECT-Datensätzen mit gebräuchlicher Schnittbildsoftware demonstriert werden. Obwohl das Prinzip grundsätzlich anwendbar ist, wirkt der eklatante Mangel an anatomischen Landmarken limitierend. Navigations- bzw. Trackingsysteme zur Verknüpfung von Zweikopf-SPECT-Kameras mit Ultraschallgeräten haben sich in Studien als überaus aufwendig und wenig praktikabel erwiesen. Durch die erneute Lagerung des Patienten sowie die Deformierung des Weichgewebes durch den Kontakt mit der Ultraschallsonde kann es darüber hinaus zu Fehlregistrierungen kommen.
- Eine potentielle Lösung bietet die in zwei Arbeitsschritten durchführbare, sensornavigierte Ultraschallfusion mit PET/CT, bei der die CT als anatomische Referenz genutzt wird.
    - Die ersten Erfahrungen in der Differentialdiagnose unklarer Weichteil-Befunde in der ^{18}F-FDG-PET/CT bei Patienten mit Malignem Melanom legen nahe, dass in der Rolle der „third opinion“ zu PET und CT ein bedeutender klinischer Stellenwert liegen könnte. Bekräftigt wird dies durch Untersuchungen, die

zeigen, dass auch bei Fremdkörpern und Implantaten, die einen erhöhten Glukosestoffwechsel verursachen, jedoch im CT nicht visualisierbar sind, die Vermeidung falsch positiver Befunde durch PET/US-Fusion möglich ist.

- Besonders großes Potential für die klinische Anwendung der Methode scheint in der Kombination mit ^{124}Iod-PET/CT zu liegen, da hierbei die Vorteile der PET mit der sicheren räumlichen Korrelation zum Ultraschall verknüpft werden können. Diese Vorteile lassen sich selbst bei sehr kleinen Befunden innerhalb der Schilddrüse und auch bei ektoper Iodspeicherung zeigen.

Trotz des vielversprechenden Potentials der kommerziell verfügbaren Systeme stellt der sequentielle, zweizeitige Charakter ein relevantes Problem dar, da es nicht nur zu einem zusätzlichen Zeitaufwand für Arzt und Patient, sondern durch die erneute (oft gering abweichende) Lagerung des Patienten sowie die Deformierung des Weichgewebes im Rahmen des Kontaktes mit der Ultraschallsonde zu Fehlregistrierungen kommen kann.

- Aus diesem Grund wurde die neue, zweistufige Technik der fhSPECT/US-Fusion anhand von Schilddrüsenbefunden erprobt. Diese ohne erneute Lagerung des Patienten, unmittelbar sequentiell durchgeführte Methode ist einfach anwendbar. Limitierend wirken die derzeit noch begrenzte Ortsauflösung sowie Artefakte des fhSPECT. Daneben sind Fehlregistrierungen durch geringe, unwillkürliche Patientenbewegungen sowie den Druck der Ultraschallsonde auf das Gewebe möglich.
- In einer weiteren Studie wurde die Entwicklung eines hybriden Detektors vorgestellt und dessen Funktionstüchtigkeit in einer Phantomstudie anhand typischer in der Heilkunde eingesetzter Nuklide erfolgreich demonstriert. Durch die Hardwareintegration von US-Sonde und nuklearmedizinischem Detektor sowie die simultane Messung der Emission in der Ebene des Ultraschallbildes können die Limitationen der vorgenannten Methoden überwunden werden. Im klinischen Einsatz würde das Konzept eine Zeitersparnis und eine weitgehende Unabhängigkeit von der Lagerung bzw. Bewegung des Patienten erlauben. Dieses Konzept erlaubt aktuell jedoch nur die Lokalisation eines einzelnen umschriebenen radioaktiven Fokus im Gewebe. Die Darstellung komplexer Radioaktivitätsverteilungen wurde nicht erprobt.

Aus dem klinischen Potential der vorgestellten Methoden einerseits, sowie den geschilderten Limitationen andererseits ergeben sich Implikationen für die Zukunft. Zunächst sind die apparativ-technische Weiterentwicklung der Methoden sowie eine Optimierung der informationstechnischen Einbindung notwendig. Darüber hinaus muss eine Entwicklung hin

zu einer zeitsparenden und einfachen Anwendbarkeit erfolgen, um einen rationellen klinischen Workflow zu ermöglichen und personelle Ressourcen zu schonen. Die mittelfristige Umsetzung notwendiger technischer Optimierungen erscheint angesichts der in den letzten Jahren stattgehabten aufwendigen und komplexen Entwicklungen wie PET/MRT realistisch.

Die Einführung neuer Methoden in der medizinischen Routine der Schilddrüsenbildgebung ist folglich möglich. Allerdings sind bei einer breiten unkritischen klinischen Anwendung auch neue Herausforderungen zu bedenken.

So kann die verbesserte Darstellung kleiner und kleinster Schilddrüsenbefunde durch die ^{124}Iod-PET das bereits aus der 2D-Sonographie bekannte Phänomen der Überdiagnostik klinisch wenig relevanter Strukturen noch verstärken *(Brito et al. 2013)*. Die Weiterentwicklung diagnostischer Behandlungspfade hin zu einem immer differenzierteren, risikoadaptierten Vorgehen wird dann noch vordringlicher werden, um das Potential der neuen Methoden zum Nutzen der Patienten ausschöpfen zu können, ohne unangemessenen Aufwand, Kosten und Morbidität zu verursachen. In diesem Kontext könnte sich die PET/US-Fusionsbildgebung zu einer wichtigen Voraussetzung entwickeln, um durch die sichere räumliche Zuordnung auch kleiner Befunde die korrelierende nuklearmedizinisch-sonographische Charakterisierung zu ermöglichen.

Eine methodische Parallele kann in der Diagnostik von Lungenrundherden gesehen werden, die seit der Einführung der CT und der Multislice-CT sprungartig häufiger diagnostiziert werden. Letztlich hat dies zu zurückhaltenden Behandlungspfaden mit subtiler Risikobewertung und differenzierter Behandlungsstrategie geführt *(Johnson et al. 2012, Blagev et al. 2013)*. Erste Anregungen für ein differenziert-zurückhaltendes Management kleiner Schilddrüsenknoten liegen bereits vor *(Brito et al. 2013, Ito et al. 2010)*.

Abschließend sei festgestellt, dass sich auf der Grundlage der hier vorgestellten Entwicklungen und Untersuchungen trotz der vielversprechenden Ergebnisse vorerst nur das Potential, nicht jedoch die Evidenz einer Verbesserung der Schilddrüsendiagnostik ableiten lässt. Parallel zu der notwendigen Weiterentwicklung hinsichtlich Apparation, Informationstechnik und rationeller Anwendbarkeit sind weitere klinische Studien erforderlich. Mit Hilfe eines Teils der vorgestellten Methoden (^{124}Iod-PET/CT, prätherapeutische Uptakemessung und PET-Isokontur-Volumetrie, navigierte Fusion) ergeben sich bereits jetzt Ansatzpunkte für prospektive Studien unter Einbeziehung größerer Patientengruppen. Der andere Teil der präsentierten Verfahren (3D-US, fhSPECT/US, rthESA/US) muss jedoch zunächst technischen Weiterentwicklungen unterzogen werden, um die für klinische Studien notwendige Leistungsfähigkeit zu realisieren.

6. Literaturverzeichnis

Abe A, Takahashi N, Lee J, Oka T, Shizukuishi K, Kikuchi T, Inoue T, Jimbo M, Ryuo H, Bickel C. 2003. Performance evaluation of a hand-held, semiconductor (CdZnTe)-based gamma camera. Eur J Nucl Med Mol Imaging, 30 (6):805-811.

Adejolu M, Huo L, Rohren E, Santiago L, Yang WT. 2012. False-positive lesions mimicking breast cancer on FDG PET and PET/CT. AJR Am J Roentgenol, 198 (3):W304-314.

Aghini-Lombardi F, Antonangeli L, Martino E, Vitti P, Maccherini D, Leoli F, Rago T, Grasso L, Valeriano R, Balestrieri A, Pinchera A. 1999. The spectrum of thyroid disorders in an iodine-deficient community: the Pescopagano survey. J Clin Endocrinol Metab, 84 (2):561-566.

Andermann P, Schlogl S, Mader U, Luster M, Lassmann M, Reiners C. 2007. Intra- and interobserver variability of thyroid volume measurements in healthy adults by 2D versus 3D ultrasound. Nuklearmedizin Nuclear medicine, 46 (1):1-7.

Anders HJ. 1998. Compression syndromes caused by substernal goitres. Postgrad Med J, 74 (872):327-329.

Aspinall SR, Ong SG, Wilson MS, Lennard TW. 2013. How shall we manage the incidentally found thyroid nodule? Surgeon, 11 (2):96-104.

Atkins HL. 1971. Technetium-99m pertechnetate uptake and scanning in the evaluation of thyroid function. Semin Nucl Med, 1 (3):345-355.

Berman MB, L.E.; Burke, J. et al. (MIRD Committee). 1975. Summary of Current Radiation Dose Estimates to Humans from 123I, 124I, 125I, 126I, 130I, 131I, and 132I as Sodium Iodide. Journal of Nuclear Medicine, 16 (9):857-860.

Beyer T, Townsend DW, Brun T, Kinahan PE, Charron M, Roddy R, Jerin J, Young J, Byars L, Nutt R. 2000. A combined PET/CT scanner for clinical oncology. J Nucl Med, 41 (8):1369-1379.

Blagev DP, Lloyd JF, Conner K, Dickerson J, Adams D, Stevens SM, Woller SC, Evans RS, Elliott CG. 2013. Follow-Up of Incidental Pulmonary Nodules and the Radiology Report. J Am Coll Radiol. pii: S1546-1440(13)00481-X. doi:10.1016/j.jacr.2013.08.003. [Epub ahead of print]

Bland JM, Altman DG. 1986. Statistical methods for assessing agreement between two methods of clinical measurement. Lancet, 1 (8476):307-310.

Blank W, Braun B. 2007. Sonography of the thyroid--Part 1. Ultraschall Med, 28 (6):554-568; quiz 570-554.

Brito JP, Morris JC, Montori VM. 2013. Thyroid cancer: zealous imaging has increased detection and treatment of low risk tumours. BMJ, 347:f4706.

Brodmann M, Lipp RW, Passath A, Seinost G, Pabst E, Pilger E. 2004. The role of 2-18F-fluoro-2-deoxy-D-glucose positron emission tomography in the diagnosis of giant cell arteritis of the temporal arteries. Rheumatology (Oxford), 43 (2):241-242.

Brunn J, Block U, Ruf G, Bos I, Kunze WP, Scriba PC. 1981. [Volumetric analysis of thyroid lobes by real-time ultrasound (author's transl)]. Dtsch Med Wochenschr, 106 (41):1338-1340.

Bucki M, Chassat F, Galdames F, Asahi T, Pizarro D, Lobo G. 2007. Real-Time SPECT and 2D Ultrasound Image Registration. In: Ayache N, Ourselin S, Maeder A, Hrsg. Medical Image Computing and Computer-Assisted Intervention – MICCAI 2007. Springer Berlin / Heidelberg, 219-226.

Cantisani V, Lodise P, Grazhdani H, Mancuso E, Maggini E, Di Rocco G, D'Ambrosio F, Calliada F, Redler A, Ricci P, Catalano C. 2013. Ultrasound elastography in the evaluation of thyroid pathology. Current status. Eur J Radiol. pii: S0720-048X(13)00253-2. doi: 10.1016/j.ejrad.2013.05.008. [Epub ahead of print]

Clevert DA, Paprottka PM, Helck A, Reiser M, Trumm CG. 2012. Image fusion in the management of thermal tumor ablation of the liver. Clin Hemorheol Microcirc, 52 (2-4):205-216.

Crawford DC, Flower MA, Pratt BE, Hill C, Zweit J, McCready VR, Harmer CL. 1997. Thyroid volume measurement in thyrotoxic patients: comparison between ultrasonography and iodine-124 positron emission tomography. Eur J Nucl Med, 24 (12):1470-1478.

Crocetti L, Lencioni R, Debeni S, See TC, Pina CD, Bartolozzi C. 2008. Targeting liver lesions for radiofrequency ablation: an experimental feasibility study using a CT-US fusion imaging system. Investigative radiology, 43 (1):33-39.

Delorme S, Hoffner S. 2003. [Diagnosis of thyroid disease. Part 2: thyroid gland nodes, diagnosis and treatment of thyroid carcinoma]. Radiologe, 43 (2):179-194.

Dietlein M, Dressler J, Eschner W, Leisner B, Reiners C, Schicha H, Deutsche Gesellschaft fur N, Deutsche Gesellschaft fur Medizinische P. 2007A. [Procedure guideline for thyroid scintigraphy (version 3)]. Nuklearmedizin, 46 (5):203-205.

Dietlein M, Dressler J, Grunwald F, Leisner B, Moser E, Reiners C, Schicha H, Schneider P, Schober O. 2007B. [Guideline for radioiodine therapy for benign thyroid diseases (version 4)]. Nuklearmedizin, 46 (5):220-223.

Di Mauro E, Solbiati M, De Beni S, Forzoni L, D'Onofrio S, Solbiati L. 2013. Virtual navigator real-time ultrasound fusion imaging with positron emission tomography for liver interventions. Conf Proc IEEE Eng Med Biol Soc, 2013:1406-1409

Drzezga A, Souvatzoglou M, Eiber M, Beer AJ, Furst S, Martinez-Moller A, Nekolla SG, Ziegler S, Ganter C, Rummeny EJ, Schwaiger M. 2012. First clinical experience with integrated whole-body PET/MR: comparison to PET/CT in patients with oncologic diagnoses. J Nucl Med, 53 (6):845-855

Duric N, Littrup P, Babkin A, Chambers D, Azevedo S, Pevzner R, Tokarev M, Holsapple E, Rama O, Duncan R. 2005. Development of ultrasound tomography for breast imaging: technical assessment. Med Phys, 32 (5):1375-1386.

Duric N, Littrup P, Poulo L, Babkin A, Pevzner R, Holsapple E, Rama O, Glide C. 2007. Detection of breast cancer with ultrasound tomography: first results with the Computed Ultrasound Risk Evaluation (CURE) prototype. Med Phys, 34 (2):773-785.

Duric N, Boyd N, Littrup P, Sak M, Myc L, Li C, West E, Minkin S, Martin L, Yaffe M, Schmidt S, Faiz M, Shen J, Melnichouk O, Li Q, Albrecht T. 2013. Breast density measurements with ultrasound tomography: a comparison with film and digital mammography. Med Phys, 40 (1):013501 doi: 10.1118/1.4772057

Elliott ST. 2008. Volume ultrasound: the next big thing? The British journal of radiology, 81 (961):8-9.

Eschmann SM, Reischl G, Bilger K, Kupferschlager J, Thelen MH, Dohmen BM, Besenfelder H, Bares R. 2002. Evaluation of dosimetry of radioiodine therapy in benign and malignant thyroid disorders by means of iodine-124 and PET. Eur J Nucl Med Mol Imaging, 29 (6):760-767.

Etchebehere EC, Romanato JS, Santos AO, Buzaid AC, Camargo EE. 2010. Impact of [F-18] FDG-PET/CT in the restaging and management of patients with malignant melanoma. Nucl Med Commun, 31 (11):925-930.

Ewertsen C. 2010. Image fusion between ultrasonography and CT, MRI or PET/CT for image guidance and intervention - a theoretical and clinical study. Dan Med Bull, 57 (9):B4172.

Ewertsen C, Rue Nielsen K, Bachmann Nielsen M. 2011. Freehand Biopsy Guided by Electromagnetic Needle Tracking: A Phantom Study. Ultraschall in der Medizin, 32 (6):614-618.

Franken PR, Guglielmi J, Vanhove C, Koulibaly M, Defrise M, Darcourt J, Pourcher T. 2010. Distribution and dynamics of (99m)Tc-pertechnetate uptake in the thyroid and other organs assessed by single-photon emission computed tomography in living mice. Thyroid, 20 (5):519-526.

Freudenberg LS, Antoch G, Jentzen W, Pink R, Knust J, Gorges R, Muller SP, Bockisch A, Debatin JF, Brandau W. 2004A. Value of (124)I-PET/CT in staging of patients with differentiated thyroid cancer. Eur Radiol, 14 (11):2092-2098.

Freudenberg LS, Schueler AO, Beyer T, Antoch G, Kuhl H, Bornfeld N, Bockisch A, Egelhof T. 2004B. Whole-body fluorine-18 fluordeoxyglucose positron emission tomography/computed tomography (FDG-PET/CT) in staging of advanced uveal melanoma. Surv Ophthalmol, 49 (5):537-540.

Freudenberg LS, Jentzen W, Marlowe RJ, Koska WW, Luster M, Bockisch A. 2007A. 124-iodine positron emission tomography/computed tomography dosimetry in pediatric patients with differentiated thyroid cancer. Experimental and clinical endocrinology & diabetes : official journal, German Society of Endocrinology [and] German Diabetes Association, 115 (10):690-693.

Freudenberg LS, Jentzen W, Gorges R, Petrich T, Marlowe RJ, Knust J, Bockisch A. 2007B. 124I-PET dosimetry in advanced differentiated thyroid cancer: therapeutic impact. Nuklearmedizin Nuclear medicine, 46 (4):121-128.

Freudenberg LS, Jentzen W, Petrich T, Fromke C, Marlowe RJ, Heusner T, Brandau W, Knapp WH, Bockisch A. 2010A. Lesion dose in differentiated thyroid carcinoma metastases after rhTSH or thyroid hormone withdrawal: 124I PET/CT dosimetric comparisons. European journal of nuclear medicine and molecular imaging, 37 (12):2267-2276.

Freudenberg LS, Fromke C, Petrich T, Marlowe RJ, Koska WW, Brandau W, Eising EG, Knust EJ, Bockisch A, Jentzen W. 2010B. Thyroid remnant dose: 124I-PET/CT dosimetric comparison of rhTSH versus thyroid hormone withholding before radioiodine remnant ablation in differentiated thyroid cancer. Experimental and clinical endocrinology & diabetes : official journal, German Society of Endocrinology [and] German Diabetes Association, 118 (7):393-399.

Futamura M, Morimitsu K, Nawa M, Kanematsu M, Gotoh N, Yoshida K. 2013. Novel navigation surgery using image fusion of PET/CT and sonography for axillary neoplasm: First experience. Int J Surg Case Rep, 4 (8):719-722.

Galdames FJ, Perez CA, Estevez PA, Held CM, Jaillet F, Lobo G, Donoso G, Coll C. 2011. Registration of renal SPECT and 2.5D US images. Comput Med Imaging Graph, 35 (4):302-314.

Hadaschik BA, Kuru TH, Tulea C, Rieker P, Popeneciu IV, Simpfendorfer T, Huber J, Zogal P, Teber D, Pahernik S, Roethke M, Zamecnik P, Roth W, Sakas G, Schlemmer HP, Hohenfellner M. 2011. A novel stereotactic prostate biopsy system integrating pre-interventional magnetic resonance imaging and live ultrasound fusion. The Journal of urology, 186 (6):2214-2220.

Hakime A, Deschamps F, De Carvalho EGM, Teriitehau C, Auperin A, De Baere T. 2010. Clinical Evaluation of Spatial Accuracy of a Fusion Imaging Technique Combining Previously Acquired Computed Tomography and Real-Time Ultrasound for Imaging of Liver Metastases. Cardiovascular and Interventional Radiology, 34 (2):338-344.

Hegedus L. 2004. Clinical practice. The thyroid nodule. N Engl J Med, 351 (17):1764-1771.

Hermans R, Bouillon R, Laga K, Delaere PR, Foer BD, Marchal G, Baert AL. 1997. Estimation of thyroid gland volume by spiral computed tomography. European radiology, 7 (2):214-216.

Herzog H, Tellman L, Qaim SM, Spellerberg S, Schmid A, Coenen HH. 2002. PET quantitation and imaging of the non-pure positron-emitting iodine isotope 124I. Appl Radiat Isot, 56 (5):673-679.

Hoang JK, Branstetter BF, Gafton AR, Lee WK, Glastonbury CM. 2013. Imaging of thyroid carcinoma with CT and MRI: approaches to common scenarios. Cancer Imaging, 13:128-139.

Hobbs RF, Wahl RL, Lodge MA, Javadi MS, Cho SY, Chien DT, Ewertz ME, Esaias CE, Ladenson PW, Sgouros G. 2009. 124I PET-based 3D-RD dosimetry for a pediatric thyroid cancer patient: real-time treatment planning and methodologic comparison. J Nucl Med, 50 (11):1844-1847.

Hotze LA, Schumm-Draeger PM. 2003. Schilddrüsenkrankheiten: Diagnostik und Therapie.

Hsu CH, Lee CM, Lin SY. 2003. Inflammatory pseudotumor resulting from foreign body in abdominal cavity detected by FDG PET. Clin Nucl Med, 28 (10):842-844.

Ito Y, Miyauchi A, Inoue H, Fukushima M, Kihara M, Higashiyama T, Tomoda C, Takamura Y, Kobayashi K, Miya A. 2010. An observational trial for papillary thyroid microcarcinoma in Japanese patients. World J Surg, 34 (1):28-35.

Jentzen W, Freudenberg L, Eising EG, Sonnenschein W, Knust J, Bockisch A. 2008A. Optimized 124I PET dosimetry protocol for radioiodine therapy of differentiated thyroid cancer. Journal of nuclear medicine : official publication, Society of Nuclear Medicine, 49 (6):1017-1023.

Jentzen W, Weise R, Kupferschlager J, Freudenberg L, Brandau W, Bares R, Burchert W, Bockisch A. 2008B. Iodine-124 PET dosimetry in differentiated thyroid cancer: recovery coefficient in 2D and 3D modes for PET(/CT) systems. Eur J Nucl Med Mol Imaging, 35 (3):611-623.

Jentzen W, Hobbs RF, Stahl A, Knust J, Sgouros G, Bockisch A. 2010. Pre-therapeutic (124)I PET(/CT) dosimetry confirms low average absorbed doses per administered (131)I activity to the salivary glands in radioiodine therapy of differentiated thyroid cancer. Eur J Nucl Med Mol Imaging, 37 (5):884-895.

Jentzen W, Freudenberg L, Bockisch A. 2011. Quantitative imaging of (124)I with PET/ CT in pretherapy lesion dosimetry. Effects impairing image quantification and their corrections. Q J Nucl Med Mol Imaging, 55 (1):21-43.

Jin J, McHenry CR. 2012. Thyroid incidentaloma. Best Pract Res Clin Endocrinol Metab, 26 (1):83-96.

Johnson DB, Powers MA, Wu S, Huang YC. 2012. Follow-up recommendations for chest CT scan reports of incidental pulmonary nodules. Chest, 141 (1):280-281.

Judenhofer MS, Wehrl HF, Newport DF, Catana C, Siegel SB, Becker M, Thielscher A, Kneilling M, Lichy MP, Eichner M, Klingel K, Reischl G, Widmaier S, Rocken M, Nutt RE, Machulla HJ, Uludag K, Cherry SR, Claussen CD, Pichler BJ. 2008. Simultaneous PET-MRI: a new approach for functional and morphological imaging. Nat Med, 14 (4):459-465.

Jung CH, Kim BY, Kim JW, Lee SW, Kwak JJ, Mok JO, Kim CH, Hong HS, Kang SK, Park JM. 2011. False-positive F-18 FDG PET/CT from foreign body reaction on anterior chest wall after endoscopic total thyroidectomy via axillo-breast approach for thyroid cancer: two case reports. Clin Nucl Med, 36 (11):1036-1038.

Jung EM, Schreyer AG, Schacherer D, Menzel C, Farkas S, Loss M, Feuerbach S, Zorger N, Fellner C. 2009. New real-time image fusion technique for characterization of tumor vascularisation and tumor perfusion of liver

tumors with contrast-enhanced ultrasound, spiral CT or MRI: first results. Clinical hemorheology and microcirculation, 43 (1):57-69.

Kadhim AL, Sheahan P, Timon C. 2006. Management of life-threatening airway obstruction caused by benign thyroid disease. J Laryngol Otol, 120 (12):1038-1041.

Kaplan I, Oldenburg NE, Meskell P, Blake M, Church P, Holupka EJ. 2002. Real time MRI-ultrasound image guided stereotactic prostate biopsy. Magn Reson Imaging, 20 (3):295-299.

Kemerink GJ, Visser MG, Franssen R, Beijer E, Zamburlini M, Halders SG, Brans B, Mottaghy FM, Teule GJ. 2011. Effect of the positron range of 18F, 68Ga and 124I on PET/CT in lung-equivalent materials. Eur J Nucl Med Mol Imaging, 38 (5):940-948.

Keu KV, Iagaru AH. 2014. The clinical use of PET/CT in the evaluation of melanoma. Methods Mol Biol, 1102:553-580.

Kilic D, Findikcioglu A, Ekici Y, Alemdaroglu U, Hekimoglu K, Hatipoglu A. 2011. When is transthoracic approach indicated in retrosternal goiters? Ann Thorac Cardiovasc Surg, 17 (3):250-253.

Kinahan PE, Townsend DW, Beyer T, Sashin D. 1998. Attenuation correction for a combined 3D PET/CT scanner. Med Phys, 25 (10):2046-2053.

Knudsen N, Bols B, Bulow I, Jorgensen T, Perrild H, Ovesen L, Laurberg P. 1999. Validation of ultrasonography of the thyroid gland for epidemiological purposes. Thyroid : official journal of the American Thyroid Association, 9 (11):1069-1074.

Knust EJ, Dutschka K, Weinreich R. 2000. Preparation of 124I solutions after thermodistillation of irradiated 124TeO2 targets. Appl Radiat Isot, 52 (2):181-184.

Koc M, Ersoz HO, Akpinar I, Gogas-Yavuz D, Deyneli O, Akalin S. 2002. Effect of low- and high-dose levothyroxine on thyroid nodule volume: a crossover placebo-controlled trial. Clin Endocrinol (Oxf), 57 (5):621-628.

Kolbert KS, Pentlow KS, Pearson JR, Sheikh A, Finn RD, Humm JL, Larson SM. 2007. Prediction of absorbed dose to normal organs in thyroid cancer patients treated with 131I by use of 124I PET and 3-dimensional internal dosimetry software. J Nucl Med, 48 (1):143-149.

Kot BC, Sin DM, Ying M. 2009. Evaluation of the accuracy and reliability of two 3-dimensional sonography methods in volume measurement of small structures: an in vitro phantom study. J Clin Ultrasound, 37 (2):82-88.

Lubberink M, Abdul Fatah S, Brans B, Hoekstra OS, Teule GJ. 2008. The role of (124)I-PET in diagnosis and treatment of thyroid carcinoma. Q J Nucl Med Mol Imaging, 52 (1):30-36.

Lucas KJ. 2000. Use of thyroid ultrasound volume in calculating radioactive iodine dose in hyperthyroidism. Thyroid, 10 (2):151-155.

Luster M, Verburg FA, Scheidhauer K. 2010. Diagnostic imaging work up in multi-nodular goiter. Minerva Endocrinol, 35 (3):153-159.

Lyshchik A, Drozd V, Reiners C. 2004. Accuracy of three-dimensional ultrasound for thyroid volume measurement in children and adolescents. Thyroid : official journal of the American Thyroid Association, 14 (2):113-120.

Machado NO, Grant CS, Sharma AK, al Sabti HA, Kolidyan SV. 2011. Large posterior mediastinal retrosternal goiter managed by a transcervical and lateral thoracotomy approach. Gen Thorac Cardiovasc Surg, 59 (7):507-511.

Mahlstedt J, Bähre M, Börner W, Joseph K, Montz R, Reiners C, Schicha H. 1989. Indikationen zur Schilddrüsenszintigraphie. Nuklearmediziner, 12:223-228.

Malago R, D'Onofrio M, Ferdeghini M, Mantovani W, Colato C, Brazzarola P, Motton M, Mucelli RP. 2008. Thyroid volumetric quantification: comparative evaluation between conventional and volumetric ultrasonography. J Ultrasound Med, 27 (12):1727-1733.

Marinelli LD, Quimby EH, Hine GJ. 1948. Dosage determination with radioactive isotopes; practical considerations in therapy and protection. Am J Roentgenol Radium Ther, 59 (2):260-281.

Minami Y, Kudo M, Chung H, Inoue T, Takahashi S, Hatanaka K, Ueda T, Hagiwara H, Kitai S, Ueshima K, Fukunaga T, Shiozaki H. 2007. Percutaneous radiofrequency ablation of sonographically unidentifiable liver tumors. Feasibility and usefulness of a novel guiding technique with an integrated system of computed tomography and sonographic images. Oncology, 72 Suppl 1:111-116.

Miyagawa T, Ishikawa S, Kimura T, Suetomi T, Tsutsumi M, Irie T, Kondoh M, Mitake T. 2010. Real-time Virtual Sonography for navigation during targeted prostate biopsy using magnetic resonance imaging data. Int J Urol, 17 (10):855-860.

Munoz A, Bernal J. 1997. Biological activities of thyroid hormone receptors. Eur J Endocrinol, 137 (5):433-445.

Natarajan S, Marks LS, Margolis DJ, Huang J, Macairan ML, Lieu P, Fenster A. 2011. Clinical application of a 3D ultrasound-guided prostate biopsy system. Urologic oncology, 29 (3):334-342.

National Electrical Manufacturers Association. 2008. Digital Imaging and Communications in Medicine (DICOM), Supplement 43: Storage of 3D Ultrasound Images. Available from the NEMA DICOM web site ftp://medical.nema.org/medical/dicom/final/sup43_ft.pdf: National Electrical Manufacturers Association (NEMA)

Ng E, Chen T, Lam R, Sin D, Ying M. 2004. Three-dimensional ultrasound measurement of thyroid volume in asymptomatic male Chinese. Ultrasound Med Biol, 30 (11):1427-1433.

Nygaard B, Nygaard T, Court-Payen M, Jensen LI, Soe-Jensen P, Gerhard Nielsen K, Fugl M, Hegedus L. 2002. Thyroid volume measured by ultrasonography and CT. Acta Radiol, 43 (3):269-274.

Ollila DW, Hsueh EC, Stern SL, Morton DL. 1999. Metastasectomy for recurrent stage IV melanoma. J Surg Oncol, 71 (4):209-213.

Ozgen A, Erol C, Kaya A, Ozmen MN, Akata D, Akhan O. 1999. Interobserver and intraobserver variations in sonographic measurement of thyroid volume in children. Eur J Endocrinol, 140 (4):328-331.

Pang BS, Kot BC, Ying M. 2006. Three-dimensional ultrasound volumetric measurements: is the largest number of image planes necessary for outlining the region-of-interest? Ultrasound Med Biol, 32 (8):1193-1202.

Paschke R, Ludgate M. 1997. The thyrotropin receptor in thyroid diseases. N Engl J Med, 337 (23):1675-1681.

Pentlow KS, Graham MC, Lambrecht RM, Cheung NKV, Larson SM. 1991. Quantitative Imaging of I-124 Using Positron Emission Tomography with Applications to Radioimmunodiagnosis and Radioimmunotherapy. Medical Physics, 18 (3):357-366.

Pichler BJ, Judenhofer MS, Wehrl HF. 2008. PET/MRI hybrid imaging: devices and initial results. Eur Radiol, 18 (6):1077-1086.

Platzek I, Beuthien-Baumann B, Schneider M, Gudziol V, Langner J, Schramm G, Laniado M, Kotzerke J, van den Hoff J. 2013. PET/MRI in head and neck cancer: initial experience. Eur J Nucl Med Mol Imaging, 40 (1):6-11.

Polyzos SA, Kita M, Efstathiadou Z, Poulakos P, Slavakis A, Sofianou D, Flaris N, Leontsini M, Kourtis A, Avramidis A. 2008. Serum thyrotropin concentration as a biochemical predictor of thyroid malignancy in patients presenting with thyroid nodules. J Cancer Res Clin Oncol, 134 (9):953-960.

Prager RW, Ijaz UZ, Gee AH, Treece GM. 2010. Three-dimensional ultrasound imaging. Proc Inst Mech Eng H, 224 (2):193-223.

Quick HH, von Gall C, Zeilinger M, Wiesmuller M, Braun H, Ziegler S, Kuwert T, Uder M, Dorfler A, Kalender WA, Lell M. 2013. Integrated whole-body PET/MR hybrid imaging: clinical experience. Invest Radiol, 48 (5):280-289.

Rago T, Bencivelli W, Scutari M, Di Cosmo C, Rizzo C, Berti P, Miccoli P, Pinchera A, Vitti P. 2006. The newly developed three-dimensional (3D) and two-dimensional (2D) thyroid ultrasound are strongly correlated, but 2D overestimates thyroid volume in the presence of nodules. J Endocrinol Invest, 29 (5):423-426.

Reinartz P, Sabri O, Zimny M, Nowak B, Cremerius U, Setani K, Bull U. 2002. Thyroid volume measurement in patients prior to radioiodine therapy: comparison between three-dimensional magnetic resonance imaging and ultrasonography. Thyroid, 12 (8):713-717.

Rennert J, Georgieva M, Schreyer AG, Jung W, Ross C, Stroszczynski C, Jung EM. 2011. Image fusion of contrast enhanced ultrasound (CEUS) with computed tomography (CT) or magnetic resonance imaging (MRI) using volume navigation for detection, characterization and planning of therapeutic interventions of liver tumors. Clin Hemorheol Microcirc, 49 (1-4):67-81.

Riccabona M, Nelson TR, Pretorius DH. 1996. Three-dimensional ultrasound: accuracy of distance and volume measurements. Ultrasound Obstet Gynecol, 7 (6):429-434.

Robinson S, Julyan PJ, Hastings DL, Zweit J. 2004. Performance of a block detector PET scanner in imaging non-pure positron emitters--modelling and experimental validation with 124I. Phys Med Biol, 49 (24):5505-5528.

Schicha H, Schober O. 2013. Nuklearmedizin: Basiswissen und Klinische Anwendung. 7. überarbeitete und aktualisierte Auflage. Schattauer. Stuttgart, New York.

Schlemmer HP, Pichler BJ, Schmand M, Burbar Z, Michel C, Ladebeck R, Jattke K, Townsend D, Nahmias C, Jacob PK, Heiss WD, Claussen CD. 2008. Simultaneous MR/PET imaging of the human brain: feasibility study. Radiology, 248 (3):1028-1035.

Schlogl S, Andermann P, Luster M, Reiners C, Lassmann M. 2006. A novel thyroid phantom for ultrasound volumetry: determination of intraobserver and interobserver variability. Thyroid, 16 (1):41-46.

Schlogl S, Werner E, Lassmann M, Terekhova J, Muffert S, Seybold S, Reiners C. 2001. The use of three-dimensional ultrasound for thyroid volumetry. Thyroid, 11 (6):569-574.

Sgouros G, Kolbert KS, Sheikh A, Pentlow KS, Mun EF, Barth A, Robbins RJ, Larson SM. 2004. Patient-specific dosimetry for 131I thyroid cancer therapy using 124I PET and 3-dimensional-internal dosimetry (3D-ID) software. J Nucl Med, 45 (8):1366-1372.

Shah PJ, Bright T, Singh SS, Lang CM, Pyragius MD, Malycha P, Edwards JR. 2006. Large retrosternal goitre: a diagnostic and management dilemma. Heart Lung Circ, 15 (2):151-152.

Sheth S. 2010. Role of ultrasonography in thyroid disease. Otolaryngol Clin North Am, 43 (2):239-255, vii.

Sholosh B, Borhani AA. 2011. Thyroid ultrasound part 1: technique and diffuse disease. Radiologic clinics of North America, 49 (3):391-416, v.

Shu J, Zhao J, Guo D, Luo Y, Zhong W, Xie W. 2011. Accuracy and reliability of thyroid volumetry using spiral CT and thyroid volume in a healthy, non-iodine-deficient Chinese adult population. Eur J Radiol, 77 (2):274-280.

Shin JJ, Grillo HC, Mathisen D, Katlic MR, Zurakowski D, Kamani D, Randolph GW. 2011. The surgical management of goiter: Part I. Preoperative evaluation. Laryngoscope, 121 (1):60-67.

Singh AK, Kruecker J, Xu S, Glossop N, Guion P, Ullman K, Choyke PL, Wood BJ. 2008. Initial clinical experience with real-time transrectal ultrasonography-magnetic resonance imaging fusion-guided prostate biopsy. BJU Int, 101 (7):841-845.

Spencer RP, Scholl RJ, Erbay N. 1997. Tc-99m pertechnetate thyroid images in hyperthyroidism. Size, distribution, and presence of a pyramidal lobe. Clin Nucl Med, 22 (8):519-522.

Spitzweg C, Morris JC. 2002. Sodium iodide symporter (NIS) and thyroid. Hormones (Athens), 1 (1):22-34.

Stalla GK. 2007. Therapielexikon Endokrinologie und Stoffwechselkrankheiten. Springer. Heidelberg

Strauss LG. 1996. Fluorine-18 deoxyglucose and false-positive results: a major problem in the diagnostics of oncological patients. Eur J Nucl Med, 23 (10):1409-1415.

Struve C. 1982. Ultraschalltomographie des Abdomens. Urban & Schwarzenberg, München-Wien-Baltimore; Auflage: 2. neubearbeitete und erweiterte Auflage.

Taylor S, Stewart FS. 1951. Distribution of radio-iodine in human thyroid gland. Lancet, 2 (6676):232-235.

Thorwarth D, Henke G, Muller AC, Reimold M, Beyer T, Boss A, Kolb A, Pichler B, Pfannenberg C. 2011. Simultaneous 68Ga-DOTATOC-PET/MRI for IMRT treatment planning for meningioma: first experience. Int J Radiat Oncol Biol Phys, 81 (1):277-283.

Tong S, Cardinal HN, McLoughlin RF, Downey DB, Fenster A. 1998. Intra- and inter-observer variability and reliability of prostate volume measurement via two-dimensional and three-dimensional ultrasound imaging. Ultrasound Med Biol, 24 (5):673-681.

Townsend DW. 2008. Dual-modality imaging: combining anatomy and function. J Nucl Med, 49 (6):938-955.

Tuschy U. 2004. Latente Hyperthyreosen. UNI-MED-Verl. 2. Aufl. Bremen

Ukimura O. 2010. Image-guided surgery in minimally invasive urology. Curr Opin Urol, 20 (2):136-140.

van Isselt JW, de Klerk JM, van Rijk PP, van Gils AP, Polman LJ, Kamphuis C, Meijer R, Beekman FJ. 2003. Comparison of methods for thyroid volume estimation in patients with Graves' disease. Eur J Nucl Med Mol Imaging, 30 (4):525-531.

Venkatesan AM, Kadoury S, Abi-Jaoudeh N, Levy EB, Maass-Moreno R, Krücker J, Dalal S, Xu S, Glossop N, Wood BJ. 2011. Real-time FDG PET Guidance during Biopsies and Radiofrequency Ablation Using Multimodality Fusion with Electromagnetic Navigation. Radiology, 260 (3):848-856.

Weber AL, Randolph G, Aksoy FG. 2000. The thyroid and parathyroid glands. CT and MR imaging and correlation with pathology and clinical findings. Radiol Clin North Am, 38 (5):1105-1129.

Wein W, Khamene A, Clevert DA, Kutter O, Navab N. 2007. Simulation and fully automatic multimodal registration of medical ultrasound. Med Image Comput Comput Assist Interv, 10 (Pt 1):136-143.

Wein W, Brunke S, Khamene A, Callstrom MR, Navab N. 2008. Automatic CT-ultrasound registration for diagnostic imaging and image-guided intervention. Med Image Anal, 12 (5):577-585.

Wendler T, Hartl A, Lasser T, Traub J, Daghighian F, Ziegler SI, Navab N. 2007. Towards intra-operative 3D nuclear imaging: reconstruction of 3D radioactive distributions using tracked gamma probes. Med Image Comput Comput Assist Interv, 10 (Pt 2):909-917.

Wendler T, Herrmann K, Schnelzer A, Lasser T, Traub J, Kutter O, Ehlerding A, Scheidhauer K, Schuster T, Kiechle M, Schwaiger M, Navab N, Ziegler SI, Buck AK. 2010. First demonstration of 3-D lymphatic mapping in breast cancer using freehand SPECT. Eur J Nucl Med Mol Imaging, 37 (8):1452-1461.

Wiesner S, Dressel P, Friebe M, Freesmeyer M, Navab N, Wendler T, Traub J. 2011. Registration Free SPECT and Ultrasound Imaging [Abstract].

Wolff J. 1998. Perchlorate and the thyroid gland. Pharmacol Rev, 50 (1):89-105.

Woo, J. From wired frames to 3D, a short history of Kretztechnik AG, Zipf, Austria, http://www.ob-ultrasound.net/kretztechnik.html. Stand Dezember 2013

Xu S, Kruecker J, Turkbey B, Glossop N, Singh AK, Choyke P, Pinto P, Wood BJ. 2008. Real-time MRI-TRUS fusion for guidance of targeted prostate biopsies. Comput Aided Surg, 13 (5):255-264.

Ying M, Yung DM, Ho KK. 2008. Two-dimensional ultrasound measurement of thyroid gland volume: a new equation with higher correlation with 3-D ultrasound measurement. Ultrasound Med Biol, 34 (1):56-63.[Abstract]

Ying M, Pang BS. 2009. Three-dimensional ultrasound measurement of cervical lymph node volume. Br J Radiol, 82 (980):617-625.

Zaidi H. 1996. Comparative methods for quantifying thyroid volume using planar imaging and SPECT. J Nucl Med, 37 (8):1421-1426.

Zhang T, Tachiya Y, Sakaguchi Y, Mitsumoto K, Mitsumoto T, Ohya N, Sasaki M. 2010. Phantom study on three-dimensional target volume delineation by PET/CT-based auto-contouring. Fukuoka Igaku Zasshi, 101 (11):238-246.

Danksagung

Für die wissenschaftliche und von dieser nicht zu trennende klinische Tätigkeit in der Klinik für Nuklearmedizin am Universitätsklinikum Jena war die menschliche und fachliche Unterstützung zahlreicher, im Folgenden genannter Berufsgruppen und Personen maßgeblich, denen ich für die Unterstützung bei der Durchführung der Studien und bei der Auswertung der Daten sowie für die Mitwirkung bei der Erstellung der Manuskripte herzlich danken möchte:

- dem ehemaligen Direktor der Klinik für Nuklearmedizin Professor Dr. med. Dietmar Gottschild für seine stetige und freundliche Unterstützung und Beratung
- den ärztlichen Kollegen und ehemaligen Doktoranden der Klinik für Nuklearmedizin, insbesondere Dr. med. Thomas Winkens, Dr. med. Andreas Darr, Dr. med. Jan-Henning Schierz
- den Doktoranden Katharina Licht und Julian Westphal
- den Medizinphysikexperten der Klinik für Nuklearmedizin Dr. rer. nat. Thomas Opfermann und Dipl. Ing. (FH) Steffen Wiegand
- dem Radiopharmazeuten der Klinik für Nuklearmedizin Dr. rer. nat. Tobias Niksch
- dem Bachelor-Studenten Christian Kühnel (Medizintechnik, FH Ernst-Abbe, Jena)
- dem Mechaniker der Klinik für Nuklearmedizin Herrn Steffen Schrott
- dem Strahlenschutzbevollmächtigten des Universitätsklinikums Jena Dr. rer. nat. Marcel Scheithauer
- den MTRAs der Klinik für Nuklearmedizin unter der Leitung von Frau Petra Katzemann
- Herrn Dominik Driesch für die freundliche und kompetente Assistenz bei Statistik, Biometrie und der Erarbeitung graphischer Darstellungen
- Frau Dr. Ernesta Palombo-Kinne und Herrn Robert J. Marlowe für die geduldige und kompetente Durchsicht englischer Manuskripte
- Prof. Dr. med. Ekkehard Schleußner und Mitarbeitern für die Möglichkeit der Nutzung des Ultraschallgerätes GE Voluson E8 im Arbeitsbereich Pränataldiagnostik der Klinik für Frauenheilkunde und Geburtshilfe am Universitätsklinikum Jena
- Prof. Dr. med. Ulf Teichgräber und Mitarbeitern für die zeitweise Möglichkeit der Nutzung des Ultraschallgerätes GE Logiq E9 in der Abteilung Gynäkologische Diagnostik des IDIR II am Universitätsklinikum Jena
- Prof. Dr. rer. nat. med. habil. Jürgen Reichenbach und den MTRA der MRT-Abteilung des IDIR I am Universitätsklinikum Jena für Unterstützung bei Phantommessungen
- allen nicht näher genannten Personen (Kollegen, Freunden), die mein persönliches und fachliches Umfeld in positiver Weise prägten

Ganz besonders möchte ich meiner Ehefrau Daniela Freesmeyer und meinen Kindern Leonore, Magnus und Elisabeth danken, die meine mangelnde häusliche Präsenz geduldig ertrugen.

Dank gebührt jedoch auch allen Patientinnen und Patienten, ohne deren Mitwirkung diese Arbeiten nicht möglich gewesen wären und an deren verbesserter Versorgung sich alle klinische Wissenschaft messen lassen muss.

Ehrenwörtliche Erklärung

Ich erkläre hiermit, dass mir die Habilitationsordnung der Friedrich-Schiller-Universität Jena vom 07.10.1997 bekannt ist.
Ferner erkläre ich, dass ich die vorliegende Arbeit ohne unzulässige Hilfe Dritter und ohne Benutzung anderer als der angegebenen Hilfsmittel angefertigt habe. Die aus anderen Quellen direkt oder indirekt übernommenen Daten und Konzepte sind unter Angabe der Quelle gekennzeichnet.

Bei der Auswahl und Auswertung folgenden Materials haben mir die nachstehend aufgeführten Personen in der jeweils beschriebenen Weise entgeltlich/unentgeltlich geholfen:

- Unentgeltlich: Koautoren der enthaltenden Publikationen und Manuskripte sowie beteiligte gegenwärtige und ehemalige Doktoranden, insbesondere
    - Herr Thomas Winkens
    - Herr Dr. med. Andreas Darr
    - Herr Dr. rer. nat. Thomas Opfermann
    - Frau Katharina Licht
    - Herr Julian Westphal
- Entgeltlich:
    - Durchsicht und Bearbeitung englischer Manuskripte: Frau Dr. Ernesta Palombo-Kinne und Herr Robert J. Marlowe
    - Statistische Beratung und Anfertigung von graphischen Darstellungen: Herr Dominik Driesch

Weitere Personen waren an der inhaltlich-materiellen Erstellung der Arbeit nicht beteiligt. Insbesondere habe ich hierfür nicht die entgeltliche Hilfe von Vermittlungs- bzw. Beratungsdiensten in Anspruch genommen. Niemand hat von mir unmittelbar oder mittelbar geldwerte Leistungen für Arbeiten erhalten, die im Zusammenhang mit dem Inhalt der vorgelegten Arbeit stehen.
Die Arbeit wurde bisher weder im In- noch Ausland in gleicher oder ähnlicher Form einer anderen Prüfungsbehörde vorgelegt.
Ich versichere, dass ich nach bestem Wissen die reine Wahrheit gesagt und nichts verschwiegen habe.

Jena, den 29. Januar 2014

Lebenslauf

Name:	Freesmeyer
Vorname:	Martin
Titel:	Dr. med.
Geburtsdatum/-ort:	10.10.1969 in Jena
Familienstand:	verheiratet, 3 Kinder
Staatsangehörigkeit:	deutsch
Bekenntnis:	evangelisch-lutherisch

Studium

01.10.1990 - 17.09.1996	Studium der Humanmedizin an der FSU Jena
01.10.1995 - 06.09.1996	Praktisches Jahr (PJ), Wahlfach Strahlentherapie, FSU Jena
20.09.1996	Erlaubnis zur Tätigkeit als AiP
01.05.1998	Approbation als Arzt

Beruflicher Werdegang

01.09.1988 - 30.09.1990	Klinik für f. Anästhesiologie und Intensivtherapie, FSU Jena, Hilfspfleger
unterbrochen durch	
01.10.1988 - 31.01.1990	Sanitätsdienst, NVA
01.11.1996 - 31.03.1997	Institut für Pathologie, FSU Jena, AiP
01.04.1997 - 30.04.1998	Klinik für Anästhesiologie und Intensivtherapie, FSU Jena, AiP
01.05.1998 - 31.12.2003	Institut für Diagnostische und Interventionelle Radiologie, FSU Jena, Weiterbildungsassistent
ab 13.02.2003	als Facharzt für Diagnostische Radiologie / Oberarztvertreter
01.01.2004 - 30.04.2007	Klinik für Nuklearmedizin, Martin-Luther-Universität Halle, Weiterbildungsassistent
seit 26.01.2007	Facharzt für Nuklearmedizin
seit 01.05.2007	Klinik für Nuklearmedizin, Universitätsklinikum Jena, Chefarzt/Leiter

Wissenschaftlicher Werdegang

03.05.1999	Promotion zum Dr. med., summa cum laude, an der Medizinischen Fakultät der FSU Jena *Comparison of peripheral bone and body axis skeleton in a rat model of mild-to-moderate renal failure in the presence of physiological serum levels of calcitropic hormones*. publiziert in BONE 2001

Publikationen:	Peer reviewed	53
	- Originalarbeiten	32
	- Kasuistiken	21
	Vorträge/Präsentationen (publiziert)	67
	Leitlinie/Guideline	1
	Editorial	1
	Reviews	2
	Letter to the Editor	1
	Vorträge (eingeladen)	ca. 145

Lehre: Lehrauftrag Nuklearmedizin seit dem WS 2007 (13 Semester)
„Kliniker des Jahres“, 01/2009, Wahl durch das 9. Semester
„Auszeichnung für engagierte Lehre“, 01/2014, Wahl durch das 9.Semester

Sonstiges:

Gastherausgeberschaft „Der Nuklearmediziner“ 2013 Band 36, Heft 3
Mitglied im wissenschaftlichen Beirat „Der Nuklearmediziner**“**

Jena, den 29.01.2014